Copyright Warning & Restrictions

The copyright law of the United States (Title 17, United States Code) governs the making of photocopies or other reproductions of copyrighted material.

Under certain conditions specified in the law, libraries and archives are authorized to furnish a photocopy or other reproduction. One of these specified conditions is that the photocopy or reproduction is not to be "used for any purpose other than private study, scholarship, or research." If a, user makes a request for, or later uses, a photocopy or reproduction for purposes in excess of "fair use" that user may be liable for copyright infringement,

This institution reserves the right to refuse to accept a copying order if, in its judgment, fulfillment of the order would involve violation of copyright law.

Please Note: The author retains the copyright while the New Jersey Institute of Technology reserves the right to distribute this thesis or dissertation

Printing note: If you do not wish to print this page, then select "Pages from: first page # to: last page #" on the print dialog screen

ABSTRACT

OPTIMUM DESIGN AND MACHINING PARAMETERS OF A PERMANENT MAGNET BRUSHLESS DC LINEAR MOTOR AS A CNC FEED DRIVE

by
William Tereshkovich

A new heuristic has been developed to determine optimal operating parameters applied to a permanent magnet brushless DC linear motor (PMBDCLM) as a CNC feed drive. An FEA model has been developed utilizing an electromagnetic postprocessor to provide performance output of a PMBDCLM and DC servomotor. Based on the developed FEA models, velocity results have been utilized to provide feedrate levels for design of experiments (DOE). DOE has been conducted to provide force, tolerance, and surface finish data necessary for the performance comparison of a DC servo motor/ballscrew equipped CNC vertical milling machine and a PMBDCLM equipped CNC vertical milling machine. Based on the DOE, a knowledge base has been developed using force, tolerance, and surface finish data. Relationships between force, and spindle speed and feedrate with tolerance and surface finish indices were determined. A heuristic has been developed which represents a guide of applying a set of decisions through the knowledge base to provide a set of operating parameters that will meet user specified tolerance and surface finish requirements for given surfaces. Application of the developed heuristic to a milled part is illustrated. A PMBDCLM CNC retrofit for a conventional ballscrew feed drive system has also been developed to improve machine performance and cost.

OPTIMUM DESIGN AND MACHINING PARAMETERS OF A PERMANENT MAGNET BRUSHLESS DC LINEAR MOTOR AS A CNC FEED DRIVE

by
William Tereshkovich

A Dissertation
Submitted to the Faculty of
New Jersey Institute of Technology
In Partial Fulfillment of the Requirements for the Degree of
Doctor of Philosophy in Industrial Engineering

Department of Industrial and Manufacturing Engineering

January 2000

APPROVAL PAGE

OPTIMUM DESIGN AND MACHINING PARAMETERS OF A PERMANENT MAGNET BRUSHLESS DC LINEAR MOTOR AS A CNC FEED DRIVE

William Tereshkovich

Dr. George Abdou, P.E. CMfgE., Dissertation Advisor — Date
Associate Professor of Industrial and Manufacturing Engineering, NJIT

Dr. Sanchoy Das, Committee Member — Date
Associate Professor of Industrial and Manufacturing Engineering, NJIT

Dr. One-Jang Jeng, Committee Member — Date
Assistant Professor of Industrial and Manufacturing Engineering, NJIT

Dr. Durgamadhab Misra, Committee Member — Date
Associate Professor of Electrical and Computer Engineering, NJIT

Dr. Stephen Tricamo, Committee Member — Date
Professor of Industrial and Manufacturing Engineering, NJIT

BIOGRAPHICAL SKETCH

Author: William Tereshkovich

Degree: Doctor of Philosophy in Industrial Engineering

Date: January 2000

Undergraduate and Graduate Education:

- Doctor of Philosophy in Industrial Engineering
  New Jersey Institute of Technology, Newark, NJ, 2000

- Master of Science in Manufacturing Systems Engineering
  New Jersey Institute of Technology, Newark, NJ, 1995

- Bachelor of Science in Engineering Technology
  New Jersey Institute of Technology, Newark, NJ, 1994

- Associate in Science in Physics
  Brookdale Community College, Lincroft, NJ, 1997

- Associate in Applied Science in Design Technology
  Brookdale Community College, Lincroft, NJ 1992

Major: Industrial Engineering

Presentations and Publications:

- Abdou, G., Tereshkovich, W. "An Optimal Operating Parameters Heuristic for a PMBDCLM as a CNC Feed Drive". International Journal of Production Research. Submitted, 1999.

- Abdou, G., Tereshkovich, W. "Experimental Comparison to Dynamic FEA Results of a Permanent Magnet Brushless DC Linear Motor". International Journal of Computer Integrated Manufacturing, Taylor and Francis, London, Philadelphia. To Appear 2000.

- Abdou, G., Tereshkovich, W. "Performance Evaluation of a Permanent Magnet Brushless DC Linear Drive for High Speed Machining using Finite Element

Analysis". International Journal of Applied Finite Elements and Computer Aided Engineering. To Appear 2000.

- Abdou, G., Tereshkovich, W. "Magneto-Thermal Analysis of a Linear Drive using Coupled Electromagnetic/Heat Transfer Finite Element Analysis". Second International Symposium on Linear Drives for Industry Applications. Tokyo, Japan. 1998. Pp. 408-411.

- Abdou, G., Tereshkovich, W. "Finite Element Analysis of a Linear Motor Drive" The Sixth Annual Industrial Engineering Research Conference. Proceedings of the Institute of Industrial Engineers, IERC. May 17-18, Miami Beach, Florida. 1997. Pp.592-597.

- Abdou, G., Tereshkovich, W. "Performance Evaluation of a Permanent Magnet DC Linear Motor and a DC Servo Motor using Electromagnetic Finite Element Analysis". Fourth International Conference on Ultraprecision in Manufacturing Engineering. 1996. Braunschweig, Germany. May 26-30, 1997. Pp. 394-398.

- McDermott, K., Tereshkovich, W. "Hardware/Software Design Interfacing between CAD Systems and Industrial Robots". Proceedings of the Japan/USA Symposium on Flexible Automation. Vol. 1. Boston, Massachusetts. July 7-10,1996. Pp. 521-524.

To my Mother, for her Loving Support and Encouragement During this Research

ACKNOWLEDGEMENT

The author wishes to express his sincerest gratitude to his dissertation advisor, Dr. George Abdou of the Industrial and Manufacturing Engineering Department at the New Jersey Institute of Technology for his timely and expert assistance, guidance and encouragement, friendship and support, during this research.

Special thanks is given to the following dissertation committee members: Dr. Sanchoy Das, Dr. One-Jang Jeng, Dr. Durgamadhab Misra, and Dr. Stephen Tricamo for serving as members of the dissertation committee.

Sincere thanks must be given to Dr. Saul K. Fenster, President of New Jersey Institute of Technology, for the prestigious NJIT presidential fellowship and Dr. Ronald Kane of the NJIT graduate studies department for his expert and timely assistance. For generous financial contribution during this research, the author would like to sincerely thank the following: James and Velma Emmi of the EMMI Foundation, the American Society of Manufacturing Engineers Chapter 14, and the American Institute of Plant Engineers Chapter 115.

The author also sincerely thanks Mr. Richard Whipple and Mr. David Hoffman of the Kingsbury Corporation for their expert assistance on linear motor technology applied to CNC machining and for providing facilities and equipment, Wayne Chaneski and Art Sutphen of the Center of Manufacturing Systems, and John (Jack) Gidney of the Department of Industrial and Manufacturing Engineering.

TABLE OF CONTENTS

TABLE OF CONTENTS
(Continued)

Chapter **Page**

TABLE OF CONTENTS
(Continued)

Chapter **Page**

LIST OF TABLES

LIST OF TABLES
(Continued)

LIST OF TABLES
(Continued)

LIST OF FIGURES

LIST OF FIGURES
(Continued)

Figure **Page**

LIST OF FIGURES
(Continued)

Figure **Page**

LIST OF FIGURES
(Continued)

Figure **Page**

CHAPTER 1

INTRODUCTION

The permanent magnet brushless DC linear motor (PMBDCLM) is a relatively recent development for computer numerical control (CNC) machine feed drive applications. Such feed drive motors and feedback devices enable CNC machines to achieve a high level of precision at increased machining rates.

The production of parts with greater accuracy and at higher feedrates always presents a challenge for the manufacturing industry. Recently, the application of the PMBDCLM as a CNC machine tool feed drive has gained wide attention in the machining center community due to certain advantageous performance characteristics inherent in its design. Foremost among these is that linear motors act directly on the moving component of the machine cutting system. This eliminates the need for mechanical linkages to the traditional drive motor in order to convert rotary motion into linear motion. Linear motors and their drivers also eliminate the need for brushes, thus increasing reliability. Further advances in magnetic technology allow smoother action and less ripple. The result is extremely smooth motion, which improves tolerance and surface finish for many machining applications. Whereas a rotary motor interfaces with the mechanical system through the shaft, or a leadscrew/ball-nut-type gear train to convert the rotary motion into linear motion, a linear motor interacts with a moving member, which is the mechanical system itself.

Conventional machining centers utilize a ballscrew, rack and pinion, or a belt drive to convert rotary motion into linear motion. Ballscrews, which make up more than 99 percent of the linear movement market, are produced by manufactures that have always worked to boost performance. Several features of the ballscrew design contribute to error such as the windup in the motor shaft and screws. Gear reducers only add more backlash and inertia.

As an alternative, four types of linear motors have been developed in industry. Types of linear motor designs include voice coil, step, induction, and synchronous (permanent magnet). The essential difference between linear motors and rotary motors is topology. In many cases, linear motors are special purpose devices, unlike their rotary counterparts, linear motors are tailored to specific needs.

The recent advances in linear motion technology have also improved motor reliability. One inherent advantage of the linear motor is the non-contact design. The design provides built-in reliability and requires minimal maintenance when compared to other drives. Although such a system is currently being utilized for high precision applications, there has been little research into the effect of PMBDCLM feed drive CNC milling of straight and contouring motion on tolerance and surface finish.

Problem Definition

Although the advantages of PMBDCLM CNC implementation are known and significant progress has been made in the design and study of linear motors in machining, there remains the need for a method to select the optimal operating parameters on such machines, specifically in the area of high speed milling. The current research fills this need by examining the effects of linear motor drive technology on tolerance and surface

finish based on a specific material and a specific machine configuration and by providing the selection of optimal operating parameters to achieve required design specifications.

1.1 Research Objectives

From the literature review, presented in chapter 2, it is shown that there is a need for research of PMBDCLM's as CNC feed drives in machining operations, namely high speed milling. Three main research objectives are:

- To determine PMBDCLM and DC servomotor/ballscrew drive performance based on design and experimentation. Results will be based on milling 7075-T6 aluminum with a vertical machine configuration.
- To determine optimal operating parameters for any PMBDCLM milling conditions by developing a heuristic.
- To determine the PMBDCLM replacement components for conventional CNC machines.

The following sections describe the procedures used to achieve the research objectives and outlines the dissertation organization.

1. In order to fulfill all objectives, a heuristic has been developed to derive optimal operating parameters (spindle speed, feedrate, and depth of cut) for any machine configuration, material and tool type, and coolant status.
2. In order to fulfill objective (1), from a design point of view, finite element analysis (FEA) is utilized to determine the performance characteristics (electromagnetic, dynamic, and magneto-thermal) of a PMBDCLM and a DC servomotor. The finite

element results have been derived from FEA models and the velocity has been utilized as the feedrate for design of experiments.

a) To determine FEA performance effects by varying PMBDCLM air-gap size. Performance characteristics have been analyzed such as force and electromagnetic output by varying the air-gap size between the current carrying elements and the permanent magnet elements.

b) To determine FEA performance effects by varying input voltage. Performance characteristics has been analyzed by varying specific field potential and current density in current carrying elements.

c) To determine FEA performance effects by varying applied cutting force. Performance characteristics have been analyzed by varying applied force in the opposite direction of the generated force.

3. In order to fulfill the remainder of objective (1), from an experiment point of view, design of experiments (DOE) has been conducted to determine the performance characteristics in terms of tolerance and surface finish, of a PMBDCLM and a DC servomotor.

4. In order to fulfill objective (2), a proposed heuristic based on DOE has been developed and applied to a case study to provide optimal spindle speed, feedrate, and depth of cut.

5. In order to fulfill objective (3), the retrofitting of an existing CNC machine with PMBDCLM components has been studied and used to evaluate the research recommendations.

The proposed research objectives relate to the problem definition by first, providing a method to derive operating parameters for milling on any machine configuration, tool and material type, and coolant specification. Second, the research objectives illustrate the effects of linear motor technology on tolerance and surface finish through application of the developed heuristic to a case study.

1.2 Dissertation Overview

The dissertation is organized into six chapters, which incorporate the overall methodology, analysis, and design. Figure 1-1 illustrates the organization of the conducted research.

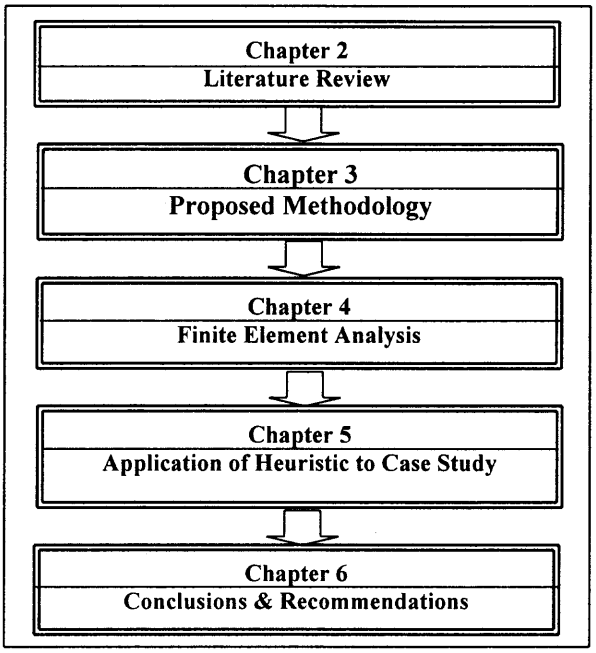

Figure 1-1. Dissertation Flow

Chapter 2 describes the current literature and research conducted by different authors researching PMBDCLM implementation as an alternative to conventional processes. A literature review is conducted and limitations are stated.

Chapter 3 provides the general form of the proposed heuristic. Explanation of the solution procedure includes experimental design and measurement methodology, application of statistical tools, knowledge base development, knowledge base rule development, and operating parameter alternative selection.

Chapter 4 describes finite element analysis and modeling techniques including preprocessor and postprocessor functions. Preprocessor sections include meshing, element identification, node identification, mechanical and material properties, internal boundary conditions, and external boundary conditions. Postprocessor sections include electric field analysis, magnetic field analysis, force and torque calculations, coupled magneto-thermal analysis, static analysis, and dynamic analysis. Application of FEA will provide feedrate data for design of experiments. The chapter provides FEA application to both a PMBDCLM and a DC servomotor and describes the motor's specifications and model assumptions.

Chapter 5 incorporates the application of the proposed heuristic to 7075-T6 aluminum contour and straight/taper components using a 0.75 inch solid carbide cutter on a PMBDCLM equipped vertical CNC milling machine. Retrofit components of a conventional CNC milling machine are introduced to illustrate the proposed research benefits. Chapter 6 provides conclusions and recommendations based on the analysis of results.

CHAPTER 2

LITERATURE REVIEW

There has been various research conducted in the design and application of a PMBDCLM as a CNC machine tool feed drive and recently, it has gained wide attention in the machining center community for improvement in overall machining performance. For the past few decades there has been much design optimization and analysis of PMBDCLM characteristics based on experimental, theoretical, and simulation methods.

2.1 Literature Review and Limitations

The literature review is divided into three areas. They include (1) direct application of linear motor technology for industrial process improvement, (2) design and optimization of linear motor systems, and (3) control system design and analysis of linear motor systems. A summary of the literature is provided in Table 2-1.

Table 2-1. Summary of Literature Review

Research Attributes	**Objective**						**Process Application**				**Motion**		**Design Analysis**						
															FEA				
	Surface Finish	**Tolerance**	**MRR**	**Operating Parameter**	**Design Analysis**	**Control System**	**Milling**	**Turning**	**Grinding**	**Material Handling**	**Straight**	**Contour**	**Theoretical**	**Experimental**	**Dynamic**	**Thermal**	**E-field**	**M-field**	**Static**
Alter and Tsao (1994)	X							X			X		X	X					
Sato et. al. (1992)					X					X	X		X	X					
Dapeng and Ziqiang (1997)	X								X		X			X					
Abdou and Sherif (1991)					X					X	X		X	X					
Basak et al. (1997),					X					X	X		X				X	X	

Table 2-1. (Continued)

Akmese and Eastham (1992)					X					X	X		X				X	X	
In-Soung Jung et al. (1997)					X					X	X		X					X	
Evers et al. (1998)					X					X	X		X				X	X	
Groning et al. (1998)					X					X	X		X					X	
Wang and Gieras (1998)					X					X	X		X					X	
Kwon et al. (1998)					X					X	X		X		X			X	
Moghani and Eastham (1996)					X					X	X		X	X					
Casadei et al. (1994)					X					X	X		X						
Basak (1996)					X					X	X		X		X		X	X	
Basak and Anayi (1995)					X					X	X		X	X				X	
Muraguchi et al. (1998)					X					X	X		X	X					
Lequesne (1996)					X					X	X		X						
Trumper et al. (1996)					X					X	X		X	X					
Hanaoka et al (1992)					X								X	X					
Laithwaite (1995)					X					X	X		X						
Hur et al. (1997)						X				X	X		X	X					
Basak and Demirci (1996)						X				X	X		X	X					
Proposed (2000)	X	X	X	X	X		X				X	X		X	X	X	X	X	X

First, direct application of linear motor technology for process improvement was performed by Alter and Tsao (1994). In an attempt to enhance machining performance, while increasing cutting speed, accuracy and reducing chatter marks on a workpiece surface, Alter and Tsao implemented a permanent magnet DC linear motor as a lathe feed drive and measured the tool vibration while investigating the dynamic interaction and active damping utilization for machining stability. In evaluating performance, a second order workpiece structure represented a first vibratory mode involving mass, velocity and

friction. The research presented a unifying control formulation that considered cutting process chatter, disturbance rejection, and servo tracking. Two major areas included (1) the stability factors introduced by the dynamic interactions between machining and a linear motor drive and (2) the design of optimal feed-forward controllers to improve tracking performance.

The application of linear drives for surface shape control of molten tin was illustrated by Sato et al. (1992), The authors presented experimental design and theoretical design analysis for a single-sided linear motor material handling configuration having the potential for improving the float process of flat glass production. They provided strong evidence, theoretically and experimentally, illustrating that location of a single-sided linear induction motor is a contributing factor in the formation of molten tin.

Dapeng and Ziqiang (1997) utilized linear motor technology for the application of precision grinding of high-speed bearings. Utilizing high precision linear motors, a precise non-circular inner race of a bearing was machined with an experimental setup to solve roller slippage and surface finish problems in the use of aircraft engines. To overcome roller slippage, the authors developed a linear motion control technique for linear drives to replace traditional grinding processes.

In another design analysis, Abdou and Sherif (1991) provided a theoretical and experimental study to asses the feasibility of employing linear induction motors for automated manufacturing systems as the drive for flexible material handling systems. A linear motor system was designed to move a weight of 50 lb. at a speed of up to 300 ft./min. and to reach a maximum speed in 2 seconds. Their design analysis included the

weight of the motor and starting friction with power requirements of a three-phase, 220-V, 60 Hz supply.

Second, design analysis and optimization of linear motor systems using finite element analysis has received some attention in the literature. Most studies in the way of electromagnetic analysis, such as Basak et al. (1997), focused on the importance of magnetic flux distribution of a PMBDCLM's secondary for material handling purposes. Three-dimensional FEA was used to compute the static force and flux distribution of a novel brushless DC linear motor containing Neodymium Iron Boron (NdFeB) magnets. Design analysis and force calculation of an NdFeB and Ferrite flat linear motor for standstill applications involving electromagnetic FEA was also performed by Akmese and Eastham (1992). They have analyzed linear motor electromagnetic forces at standstill operation with a 7 mm air-gap size using a 3,000 node, two dimensional FEA model. Thrust force-to-armature current analysis of a short secondary permanent magnet linear synchronous motor, for material handling purposes, using two-dimensional FEA was determined by In-Soung Jung et al. (1997). The authors developed an FEA magnetic field model to illustrate that detent force ripple can be reduced by changing the magnet width-slot pitch in a short secondary linear motor and that the detent force ripple is larger in a short primary type linear motor.

Recently, more researchers have focused on utilizing the finite element method to determine a linear motor's secondary thrust force by varying current and secondary position. Such design analysis was performed by Evers et al. (1998) for the purpose of material handling. Using 280,000 3D elements and 51,700 field nodes for electromagnetic FEA, the authors illustrated that a double-sided linear motor provides

low normal forces depending upon the normal displacement of the secondary and that the force is proportional to the current in the quadrature axis. Groning et al. (1998) provided design analysis for both a 2D and 3D magnetic field finite element model of a linear drive magnetic levitation material handling system to compute the propulsion force and air-gap size changes due to the number of Ampere turns in the coil. Magnetic field FEA was used to analyze both static and instantaneous forces of a hybrid linear motor material handling system with four-layered air-gap elements by Wang and Gieras (1998). Their analysis demonstrated that the accuracy of the force calculation depends on the discretization of the air-gap region and that the ripple force is due to the existence of permanent magnets and a tooth-structure design. In another design analysis involving dynamic and magnetic field FEA, Kwon et al. (1998) analyzed the thrust response and static characteristics for direct thrust control in a NdFeB linear synchronous motor material handling system by a time stepped method and moving mesh FEA.

In a design analysis by Moghani and Eastham (1996), dynamic response of electromagnetic force and simulation of modulated and un-modulated current waveforms were performed using the Matlab Analogue Simulation Toolbox 'SIMULINK'. The simulated results were later validated by experimentation using an NdFeB equipped linear machine for material handling. Performance of a slotless permanent magnet linear DC material handling actuator under speed control in the presence of variants such as winding resistance, moving mass, load, force, and friction was simulated and analyzed by Casadei et al. (1994). The authors used numerical simulation to describe when a force disturbance is applied, secondary speed, position, and current values differ to reference models. Numerical results related to the system were shown when $t < 3.5$ seconds since

the linear motor slider ran outside the limits for the working length as shown by the simulation.

Three dimensional electromagnetic and dynamic FEA was utilized by Basak (1996) to analyze the dynamic characteristics of a square-armature DC linear motor for material handling systems. The design analysis included velocity versus time by varying current, output force and power versus velocity, and efficiency versus velocity. In an earlier study through experimentation and analysis, Basak and Anayi (1995) measured and computed the linear motor's static thrust, axial flux, and flux density with change in the linear motor's slider position. Performance characteristics were further measured through experimentation and design analysis by Muraguchi et al. (1998), in which a high thrust density linear motor, linear synchronous motor, and linear induction motor were compared for dynamic thrust and efficiency for material handling purposes. Each of the experimental linear motors contained different parameters such as air-gap size, coil resistance, coil inductance, and secondary weight.

In an analytical approach, Lequesne (1996) analyzed two forces acting on a PMBDCLM moving armature. Unlike Basak who analyzed the direct force from the cross product of the flux density and current density, Lequesne analyzed force attributed to the leakage flux on the extremities of the armature. From this, it was shown that the specific linear motor design exhibited easier position controllability which may be used extensively in position and material handling applications requiring fast motion. It was also shown that armature lengthening can provide faster linear travel up to a point beyond which added mass cancels out higher forces, however, the linear motor analyzed was shown to be limited by heat-dissipation considerations. A design analysis framework by

Trumper et al. (1996) was developed for linear motors in the application of wafer stepper material handling systems for clean room operations. From their research, the authors illustrated the design effects of complex magnet arrays, such as the Halbach Array and winding patterns, and verified theoretical results by constructing an experimental magnetic levitator.

Design analysis of a linear motor's thrust force in the moving secondary has also been shown in the literature. Hanaoka et al (1992) analyzed the energy gradient from the magnetic flux distribution of a Samarium Cobalt magnetic array to determine thrust force. Assumption was made to equate the permanent magnet as a plate-shaped electromagnet with a single turn coil. The application of computer peripherals and office automation was provided to illustrate a two straight stator design. For moving large masses to high velocities, Laithwaite (1995) analyzed the features required in the design of a linear induction motor which will accelerate a mass of 200 kg to 1200 m/s over a distance of 1500 meters. Reference to large mass/force material handling and transportation was provided. Special attention was given to factors such as drag forces, current and flux loading, and specific force for unconventional machine topology such as a moving primary or moving secondary and a large track.

Third, commercial control system design and analysis of linear motor systems has also received some attention in the literature. Hur et al. (1997) presented a position control method of a DC linear motor using seek control to consider variation of switching lines according to load mass variation. Attention was given to high speed material handling applications for conveying electronic parts. The authors illustrated a control method utilizing an Artificial Neural Network (ANN) in which linear or nonlinear

mapping between inputs and outputs of a linear electric drive system, without the knowledge of any predetermined model, was feasible. Experimental results illustrated that the proposed method was very efficient in the position control of the linear DC motor in commercial applications.

A real-time model reference adaptive velocity controller for a permanent magnet DC linear motor was presented by Basak and Demirci (1996). The authors designed a prototype linear motor and implemented a model reference adaptive velocity controller to reduce the effects of parameter variations on motor performance for material handling applications. Experimental results illustrated that ripple effects in the actual velocity of the linear motor prototype using an adaptive controller is acceptable for commercial applications.

Limitations

By examining the research, it is suggested that there is a need for analysis to be performed for the application of machining and operating parameters. The proposed research application addresses this issue by considering the applied force and cutting conditions due to the machining process. Cutting force and thermal effects are present which effects the motor's generated force, displacement, and stresses in the moving secondary. Variants such as input voltage (variant 1), air-gap size (variant 2), and applied force (variant 3) are required to determine the optimum level of performance measures and operating parameters for machining applications.

The selection of air-gap and voltage should consider many factors related to the cost of operation and optimal performance of the linear motor for the cutting of metal.

Large external forces during operation alters overall machine performance. Although considerable progress has been made in the use of PMBDCLM's in manufacturing facilities, a solution to recognize the effect of motor performance rating due to the variants is needed. Development of an FEA model to represent this problem is required to aid in operating parameter selection.

Eight areas considered important have not been thoroughly investigated in the previous studies. The first area involves the thermal effects upon linear motor performance. The second area involves itself with the electromagnetic field effects of the NdFeB magnet array and the air-gap region. The third area involves itself with the force comparison of a PMBDCLM and a DC servomotor. The fourth area involves itself with dynamic characteristics such as velocity, displacement, and acceleration. The fifth area is the surface finish and tolerance performance effects from machined surfaces using high speed linear motor feed drives. The sixth area is the optimal operating parameters at which an ideal surface or tolerance may be obtained. The seventh area is the cost of PMBDCLM implementation in terms of power requirements and MRR. Finally, the literature does not separate the performance characteristic differences between DC servomotor and PMBDCLM implementation.

CHAPTER 3

PROPOSED HEURISTIC

The proposed optimal operating parameters heuristic is a general 'rule of thumb' process to determine a good solution to a set of tolerance and surface finish requirements or to a set of operating parameters. The proposed heuristic will provide an optimal solution of any combination of machine type, material type, tool type, and coolant specification.

There are many factors in machining that contribute to tolerance and surface finish. Four major factors considered to be the most important and that can be controlled by the user, which are addressed in the proposed heuristic, include the machine tool configuration, the material being machined, the tool being used, and the use of coolant.

The machine type may include the type of feed motion, such as a moving tool/column configuration or a moving table configuration. The material type may include aluminum, titanium, high speed steel or any other material grade. The tool type may include carbide, high speed steel, tungsten, or any other type of tool grade and number of cutters. The coolant specification indicates if coolant is to be used.

3.1 General Model

The general model consists of two phases. The first phase involves the extraction of knowledge for the machine parameter selection, such as machine, material, tool, and coolant type. The following is the first phase of the solution procedure.

1. *Simulation of feedrate and motor performance*. Determine the performance under simulated cutting conditions.
2. *Conduct design of experiments.* Set up the operating parameters and performance measures that will be used.
3. *Perform experimentation according to the design of experiments.*
4. *Performance measurement.* Measure the performance of the machine parameter specification by measuring the tolerance and surface finish.
5. *Statistical analysis.* Perform statistical analysis to provide empirical relationships between experimental operating parameters and performance measures, rating databases, significant factors databases, benefit/cost ratio databases, and knowledge base rules.

The following is the second phase of the solution procedure.

1. *User input (A).* Tolerance and surface finish specification(s) are input by the user for a particular surface.
2. *User input (B).* Spindle speed, feedrate, and depth of cut is specified by the user for a particular surface.
3. *Fix depth (D), call rating database.* Based on tolerance and surface user specification, the developed rating database is called to fix the depth of cut level. The depth of cut level is fixed by utilizing the tolerance and surface finish performance specifications by matching the specifications in the developed performance rating database. The highest frequency determines the fixed depth of cut level.
4. *Relationship decision or preference, call empirical relationship database and developed production rules.* Simple regression relationships are called from the

developed empirical relationship database where cutting force is the independent variable and surface finish and tolerance are the dependent variables. Multiple regression relationships are called for a direct link to the operating parameters. The empirical relationship decision is determined either by the relationship strength or by user preference.

5. *Solve empirical relationships simultaneously.* Operating parameters are determined by setting empirical relationships equal to user specified performance index values and determining feasible solutions that satisfy performance requirements.
6. *Significant level of input variable, call significant factors database.* The levels of spindle speed, feedrate, and depth of cut are checked for significance by calling the significant factors database.
7. *Significant factors decision.* If significant factor(s) are detected, the optimal significant level, listed in the significant factor database, is fixed. Else, if no significant factors are detected the levels are set to determine the benefit/cost ratio.
8. *Close to specification decision.* By changing spindle speed, feedrate, and/or depth of cut levels to the new optimal significant levels, tolerance and surface finish performance indices are checked by substituting the significant optimal level values into the empirical relationships. The result is accepted if the performance value is within the user specification and is rejected if it is outside the user specification.
9. *Original relationship.* A single alternative since other alternatives are not acceptable due to nonconformity with the user specifications.
10. *Significant alternatives.* The feasible, within user specification, alternative(s) for each change in significant optimal level(s).

11. *Benefit/cost rating database.* Benefit/cost ratio is determined for the feasible alternatives.
12. *Expert rules.* Expert rules provide tie resolution, conflict resolution, and endless loop resolution. An expert rule may be fired and considered a feasible alternative.
13. *Other surface decision.* A decision to check another surface using the same acquired performance data, knowledge bases, rules etc.
14. *Acceptable output decision.* A decision to accept or reject alternative operating parameters. If the operating parameters are unacceptable, performance specifications may be modified. If the operating parameters are acceptable, the alternatives are displayed.
15. *Other machine parameter specification.* A decision to start the solution procedure for another machine, material, tool, or coolant type.

The proposed optimal operating parameters heuristic, as provided by the solution procedure above, is illustrated in Figure 3-1.

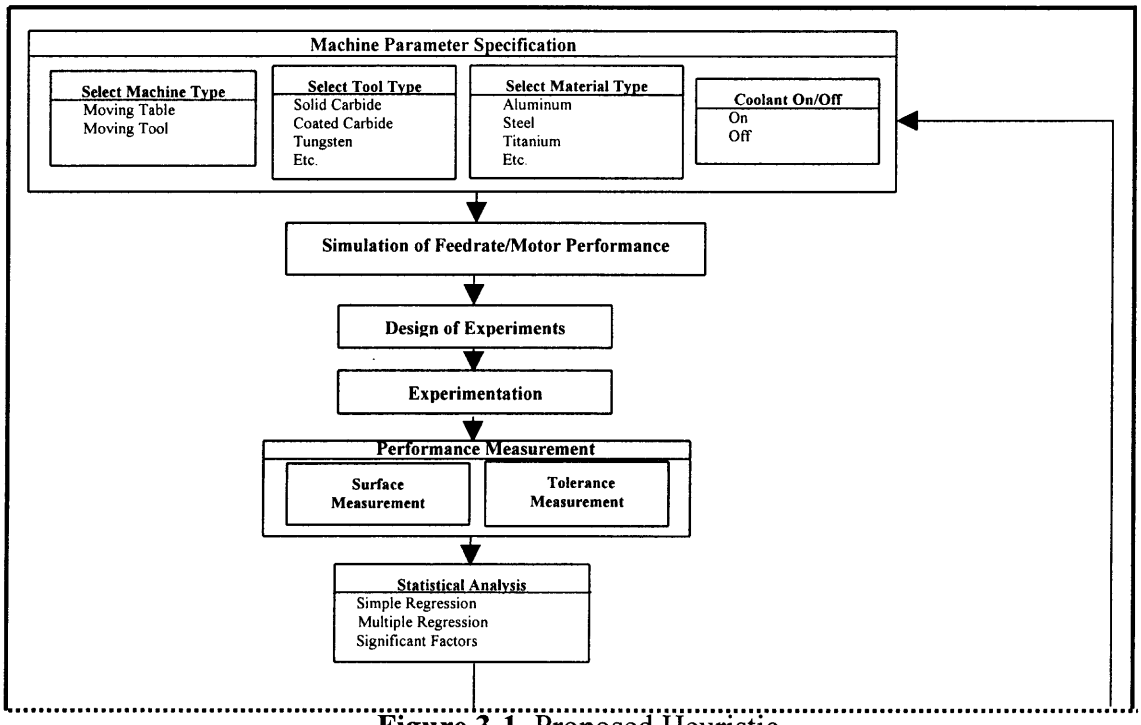

Figure 3-1. Proposed Heuristic

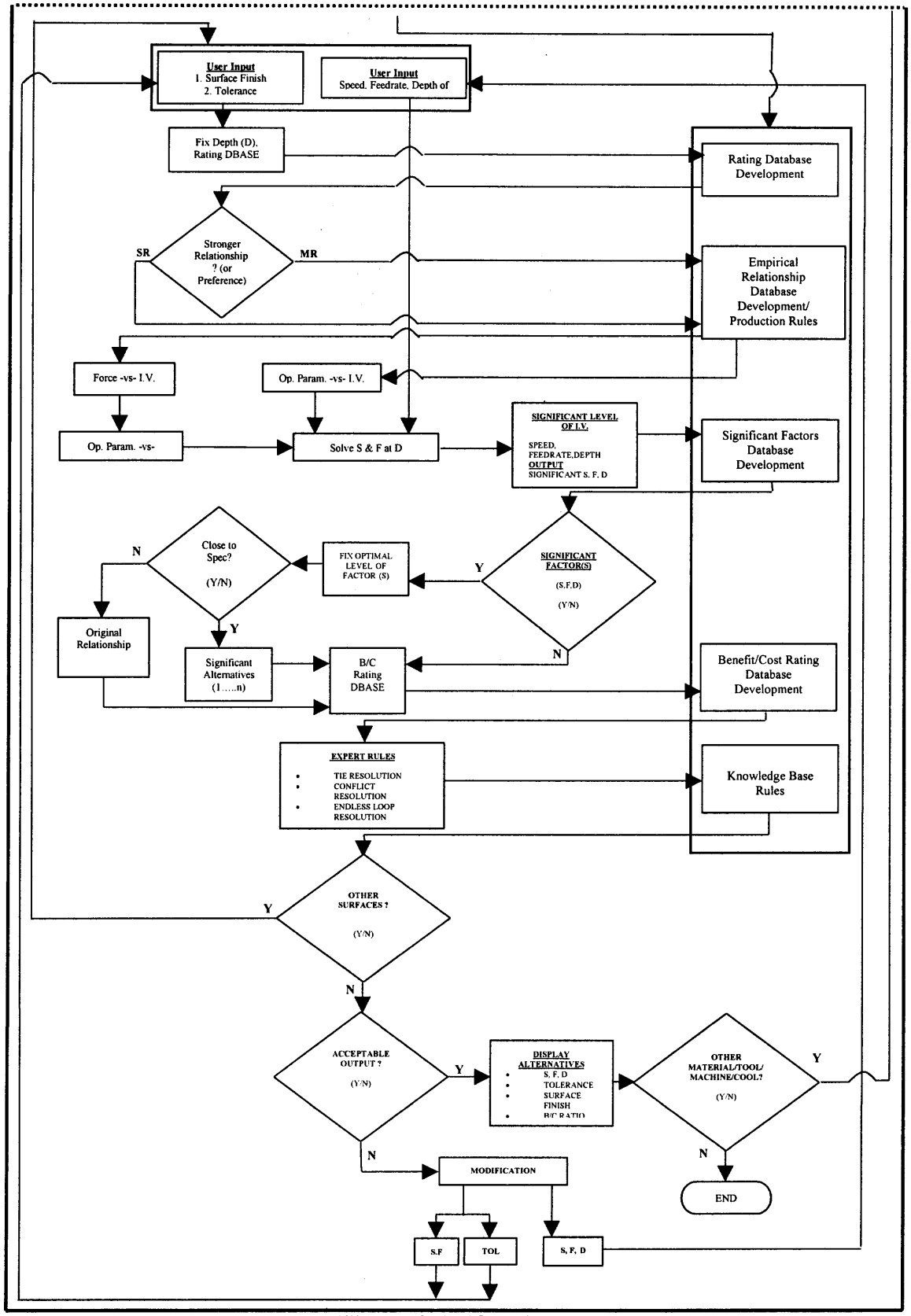

Figure 3-1. (Continued)

3.2 Design of Experiments

Design of experiments is performed to determine the system performance and optimum levels as set by the parameter design goals. By setting a quality characteristic for tolerance, cutting force, and surface characteristics, it is convenient to use the S/N ratio since this will combine both the average response and variation into a single measure. It is a method to evaluate the impact of the design parameters on the output quality characteristic and will incorporate both the desirable and undesirable aspects of the linear motor performance. The "signal" is the average value (mean) representing the desirable characteristic, which will be preferably close to a specified target value. "Noise" is the measure of variability and it represents the undesirable aspects of the linear motor's performance. From the replicate runs, the error variation is estimated, therefore the average of each level is taken.

To reduce the variability around a target value, the parameter design goals must be established. The design goal for linear motor quality design is the "Nominal-is-Best". This is where the characteristic has a nominal value and the objective is to reduce the variability around a specific target. The "Nominal-is Best" measure is expressed by:

$$SN_T = 10LOG_{10}\left(\frac{\bar{y}^2}{s^2}\right) = 20LOG_{10}\left(\frac{\bar{y}}{s}\right) \text{ (dB)} \qquad (3\text{-}1)$$

The performance measure parameter design goals are separated for contour and straight/taper experimental geometry. For contouring tolerances, they are:

- *Position, (Position Tolerance).* Defines a zone within which the axis or center plane of a feature is permitted to vary from the theoretically exact position.
- *Total Runout, (Geometric Tolerance).* The simultaneous composite control of all elements of a surface at all circular and profile measuring positions. Total runout is

used to control variations of circularity, straightness, coaxiality, angularity, taper, and the profile of a surface.

- *Runout, (Geometric Tolerance).* Composite deviation from the desired form of a part surface of revolution. Runout is used to control the cumulative variations of circularity and coaxiality.
- *Circularity, (Form Tolerance).* Condition on a surface of revolution where all points of the surface intersected by any plane, perpendicular to a common axis, or passing through a common center are equidistant from the center.
- *Cylindricity, (Form Tolerance).* Condition of a surface of revolution in which all points of the surface are equidistant from a common axis.

The performance measure parameter design goals for the straight/taper tolerances are:

- *Position, (Position Tolerance).* Defines a zone within which the axis or center plane of a feature is permitted to vary from the theoretically exact position.
- *Flatness, (Form Tolerance).* Condition of having all elements in one plane. Flatness tolerance specifies a zone defined by two parallel planes within which the surface feature must lie.
- *Straightness, (Form Tolerance).* Similar to flatness, it is a condition where an element of a surface or an axis is a straight line or centerline. Straightness tolerance specifies a zone within which the surface or centerline must lie and is applied in the view where the elements are to be controlled by a straight line.
- *Angularity, (Orientation Tolerance).* Condition of a surface, axis, or center plane, which is at a specified angle (other than zero or 90 degrees), from a datum plane or

axis. Angularity tolerance specifies a tolerance zone defined by two parallel planes at the specified basic angle from a datum plane.

- *Parallelism, (Orientation Tolerance).* Condition of a surface, line, or axis which is equidistant at all points from a datum plane or axis. Parallelism tolerance is defined by two planes or lines, parallel to a datum plane or axis, within which the line elements of the surface or center line must lie.

For both contour and straight/taper geometry, the surface quality characteristics are:

- *Rku (Kurtosis), (Amplitude Parameter: A measure of the vertical characteristics of the surface deviations).* The measure of the shape (sharpness) of the amplitude distribution curve. A 'spiky' surface will have a high kurtosis value and a 'bumpy' surface will have a low value. Kurtosis will detect if the profile peaks are evenly distributed and is an indication of non-normality.
- *Rsk (Skewness), (Amplitude Parameter: A measure of the vertical characteristics of the surface deviations).* The measure of symmetry of the amplitude curve about the mean. Skewness distinguishes between asymmetrical surfaces.
- *Sm (Mean Spacing), (Spacing Parameter: A measure of the horizontal characteristics of the surface deviation).* The spacing between profile peaks at the mean line, measured over the assessment length.
- *Lq (Spatial Wavelength), (Hybrid Parameter: a combination of the amplitude and spacing parameters).* The RMS measure of spatial wavelength content of the surface
- *Rtm (Mean of Maximum Peak-to-Valley Height), (Amplitude Parameter: A measure of the vertical characteristics of the surface deviations).* The maximum peak-to-valley height of the profile in one sampling length.

From the signal-to-noise, variance, and mean data for the linear motor performance measures, the factor main and interaction effects are estimated. The main effect is the measured variation of a specific treatment and the interaction effect is the measured variation as a result of the combined effect of two or more treatments.

Analysis of the significant factors to determine the optimal operating level, depending on the assigned quality characteristic, is conducted since a performance measure should have the property that when it is maximized, the expected loss will be minimized. By maximizing the S/N, it is equivalent to minimizing the variability. Significant factors are determined to reveal which operating level is causing the most variability in the data. Significant factors can then be adjusted to their optimal level or the level that reduces the variability. From the optimal levels, an estimate of the optimized quality characteristic is obtained by using the optimum treatment and level input variables.

3.3 Experimental Setup

An experimental setup can be adopted to provide the necessary data for the knowledge base. The following hardware and software components can be utilized.

3.3.1 Hardware

Hardware components include force measurement, tolerance measurement, and surface finish measurement. Online forces can be measured using a Kistler force transducer and amplifier. Offline tolerance measurements can be made using a Brown and Sharpe

coordinate measuring machine and offline surface finish measurements can be made using a Taylor-Hobson surface profilometer.

3.3.1.1 Force Measurement: Cutting force data can be obtained using a Kistler 3-component type 9067 force transducer, amplified using a Kistler model 5004 dual mode amplifier, and stored using a Pentium desktop computer.

The Kistler three component quartz force transducer, type 9067, provides measurement of three orthogonal components of a dynamic or quasi-static force acting in an arbitrary direction providing extended measuring ranges, high rigidity and minimal cross talk. The force transducer contains 3 pairs of quartz rings that are mounted between two steel plates in the transducer case. Two quartz pairs, sensitive to shear, measure the force components F_x and F_y, while one quartz pair sensitive to pressure measures the component F_z of force acting in an arbitrary direction onto the transducer. The electrical charges generated proportionally to the different components are lead via electrodes to the corresponding connector contacts. The electrical signal is transmitted through mini-plug coaxial cables to the amplifier. The transducer is mounted preloaded with a centered preloading bolt between two aluminum mounts. The blanks are secured on top of the mount and placed on the working table of the milling machine, as illustrated in Figure 3-2. The computer and amplifier setup is illustrated in Figure 3-3. The transducer specifications are listed in Table 3-1.

Table 3-1. Kistler 9067 Transducer Specifications

Data	Direction	Unit	Range
Range	Fx, Fy	kN	-20....20
	Fz	kN	-40....40
Overload	Fx, Fy	kN	-22/22
	Fz	kN	-44/44

Table 3-1. (Continued)

Threshold Sensitivity	Fx, Fy	pC/N	-8
	Fz	pC/N	-3,8
Linearity (each axis)		%FSO	<=+/- 0,5
Hysteresis (each axis)		%FSO	<=0,5
Cross Talk	Fx → Fx,y	%	<=+/- 1
	Fx ⇔ Fy	%	<=+/- 1
	Fx,y → Fz	%	<=+/- 1
Allowed Moments	Mx, My	Nm	-350/350
Operating Temperature		°C	-50....150

The force transducer is connected, via low-noise mini-plug coaxial cables, to a Kistler model 5004 dual mode amplifier placed in a 3-position/direction cabinet. The 5004 amplifier is a single channel charge amplifier and constant current supply. The unit converts the piezoelectric transducer signal into a proportional output voltage. The dual mode allows the 5004 to be used as either a charge (high impedance) or a voltage (low impedance) mode transducer. The amplifier sensitivity is set equal to the transducer sensitivity. The scale setting sets the gain of the charge amplifier. It is designed to allow the user to select the number of mechanical units per volt (MU/V). The mode selection allows the amplifier to be set to charge or voltage and the time constant selection (low, medium, or high) allows for the change in resistance that is in parallel with the range capacitor. Time constant selections are provided since a drift current flows via the insulation resistance of the transducer or its cable, which may cause the amplifier to drift into saturation. Filtering is also possible with the 5004 amplifier. Table 3-2 lists the 4005 amplifier specifications.

Table 3-2. Type 5004 Amplifier Specifications

Parameter	**Unit**	**Value/Type**
Measuring Range	pC	+/- 10 to 999000
Transducer Sensitivity	PC/MU or mV/MU	0.01 to 9990.0
Scale	MU/V	0.002 to 1000000
Accuracy	%	<= 0.5

Table 3-2. (Continued)

Time Constant (s)	Long, Medium, Short	Up to 100000/1-10000/0.01-100
Noise due to input capacitance	pCrms/pF	<2E-5
Filter Type		One Pole Passive
Cutoff Frequency	Hz	180K
Impedance	Ohm	100
Voltage Range	V	+/- 10.0
Current Limit	mA	+/- 5.0
Operating Temp. Range	°C	0 to 50

The UEI WIN-30 data acquisition board is required to provide the ability to import, analyze, and store the cutting force signals. The WIN-30 board can be inserted into any 16-bit slot of a PC/AT computer and can be controlled using the STATUS software. Table 3-3 lists the WIN-30 data acquisition board specifications.

Table 3-3. WIN-30 Data Acquisition Board Specifications

Number of input Channels	16 Single-Ended
Resolution	12-bit, 1 in 4096
Total System Accuracy	+/- 0.06% (+/- 2.5 LSB)
Effective Number of Bits	11.2 (min)
Signal/Noise plus Distortion Ratio	69 dB
Gain Error	+/- 5.0 LSB, Adjustable to 0.0
A/D Clock Divider	16 Bit
Block Scan Mode	256 Channels per block
Connector	2 x 50 way IDC, one Analog I/O, one Digital I/O
Operating Temperature	0 to 70 Degrees Celcius

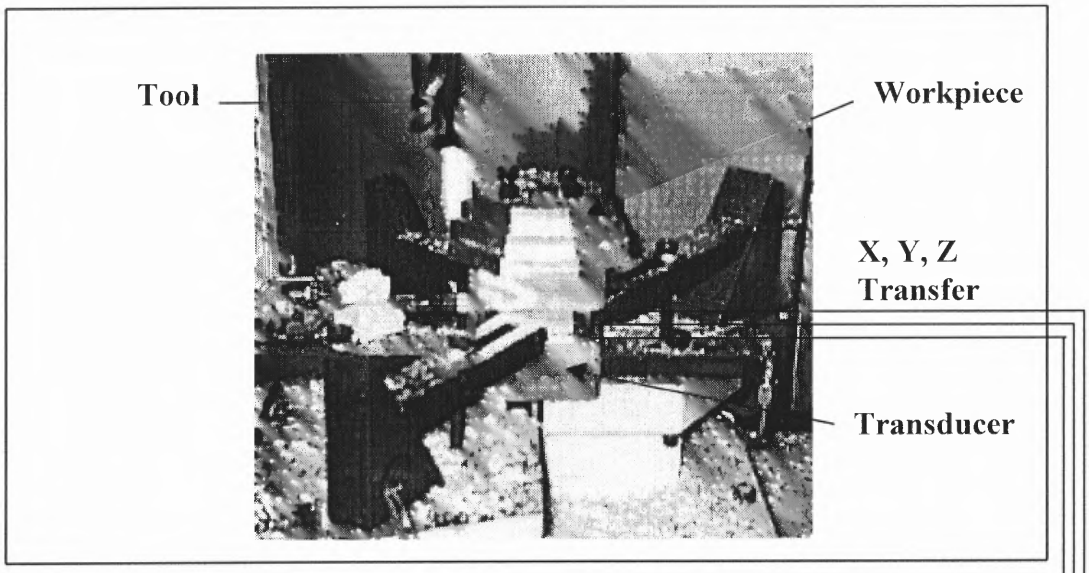

Figure 3-2. Workpiece/Transducer Setup

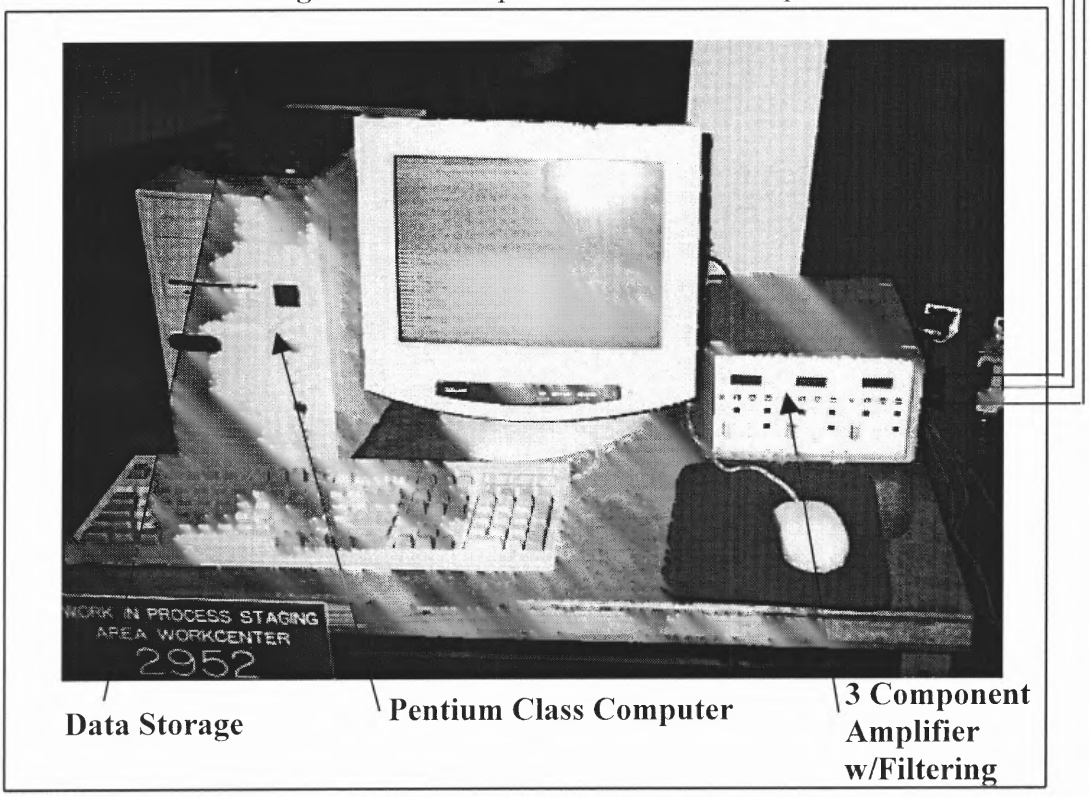

Figure 3-3. Amplifier/Computer Setup

3.3.1.2 Tolerance Measurement: Tolerance measurements can be made using a Brown and Sharpe XCEL 765 coordinate measuring machine. The XCEL 765 CMM consists of a contact probe and a manual/automated positioning system to provide three dimensional

probe movement relative to the surfaces and features of the workpiece. The probe location is accurately and precisely recorded to obtain dimensional data concerning the part geometry. The XCEL 765 is what is known as a standard bridge type CMM. Its 3 servomotor driven axes are all interfaced to a main controller via encoder circuits and the main controller is connected to a microcomputer. The Brown and Sharpe XCEL 765 CMM specifications are listed in Table 3-4. Figure 3-4 illustrates the CMM and the CMM probe in relation to the workpiece.

Table 3-4. XCEL 765 CMM Specifications

Parameter	**Range**	
Measuring Range	**Lower (inch)**	**Upper (inch)**
X-Axis	25.6	35.4
Y-Axis	39.4	59.1
Z-Axis	25.6	33.5
Work Capacity	**Lower (inch)**	**Upper (inch)**
X-Axis	31.5	41.1
Y-Axis	63.0	82.7
Z-Axis	27.2	35.0
Linear Displacement	**Lower (inch)**	**Upper (inch)**
X-Axis	0.00018	0.00020
Accuracy	**Lower (inch)**	**Upper (inch)**
Y-Axis	0.00021	0.00027
Z-Axis	0.00015	0.00019
	Lower (inch)	**Upper (inch)**
Volumetric Performance	0.00035	0.00040
Repeatability	0.00013	0.00010
	Lower (°C)	**Upper (°C)**
Standard Ambient Temperature	20	20
Daily Temperature Cycle	+/- 1.0	+/- 1.0
Maximum Variation in System Space	1.0	1.0

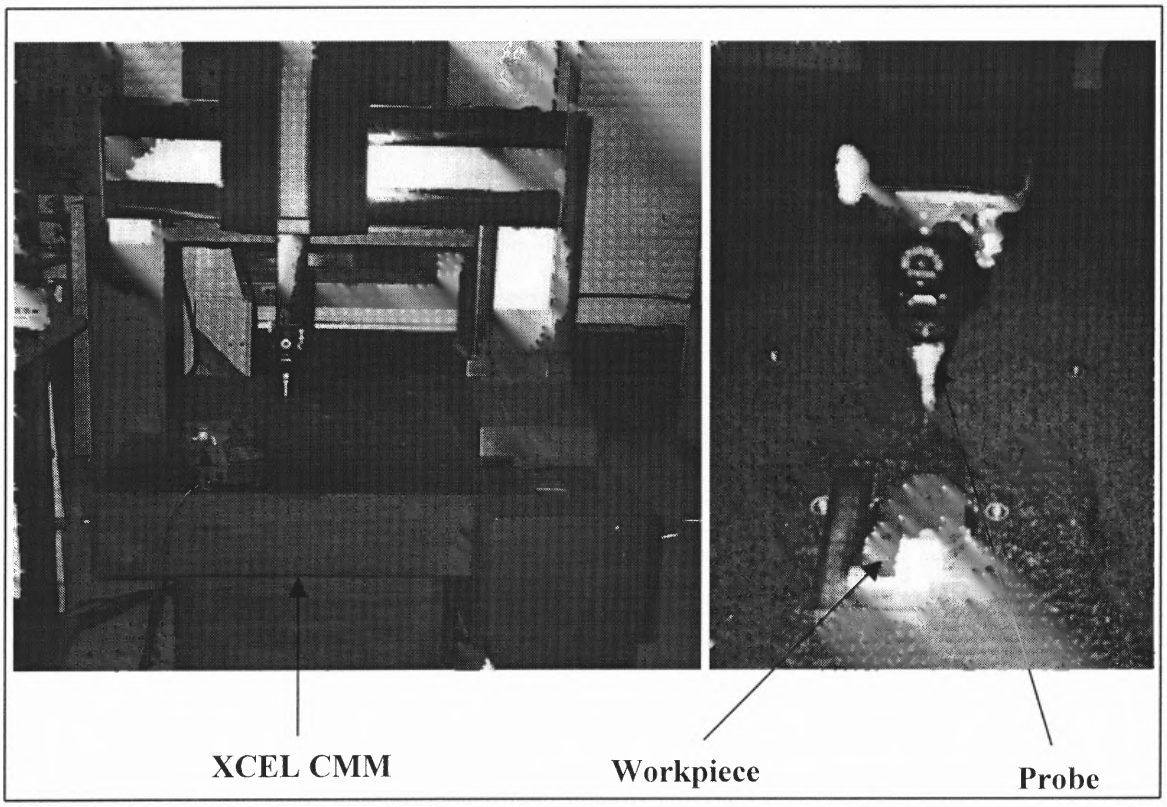

Figure 3-4. CMM Setup

3.3.1.3 Surface Finish Measurement: The surface measurements can be taken using a Taylor-Hobson Surtronic 3+ profilometer and the data is recorded on a Pentium class desktop computer. A sample length of 4 mm, 2 mm from the center of the test surface, provides 8,000 samples of the surface moving against the cutting tool motion. Table 3-5 lists the surface profilometer specifications and Figure 3-5 illustrates the profilometer skid direction in relation to the cutting direction.

Table 3-5. Taylor-Hobson Surtronic Surface Profilometer Specifications

Parameter	Unit
Traverse Unit	Traverse Speed: 1mm/sec.
Measurement Units	Metric/Inch Preset by DIP Switch
Cut-off Values	0.25mm, 0.80 mm, and 2.50 mm
Traverse Lengths	¼ Lambda + n*Lambda; n=1, 3, 5, 10, or 25.4 + 0.2mm at 0.8mm cut-off
Display	LCD Matrix. 2 lines X 16 Characters
Keyboard	Membrane Switch Panel tactile
Filter	Digital Gauss Filter or 2CR Filter (ISO)

Table 3-5. (Continued)

Parameters	Ra, Rq, Rz(DIN), Ry, and Sm
Calculation Time	< reversal time or 2 seconds
Accessory Socket	9 Pin D-Connector RS232

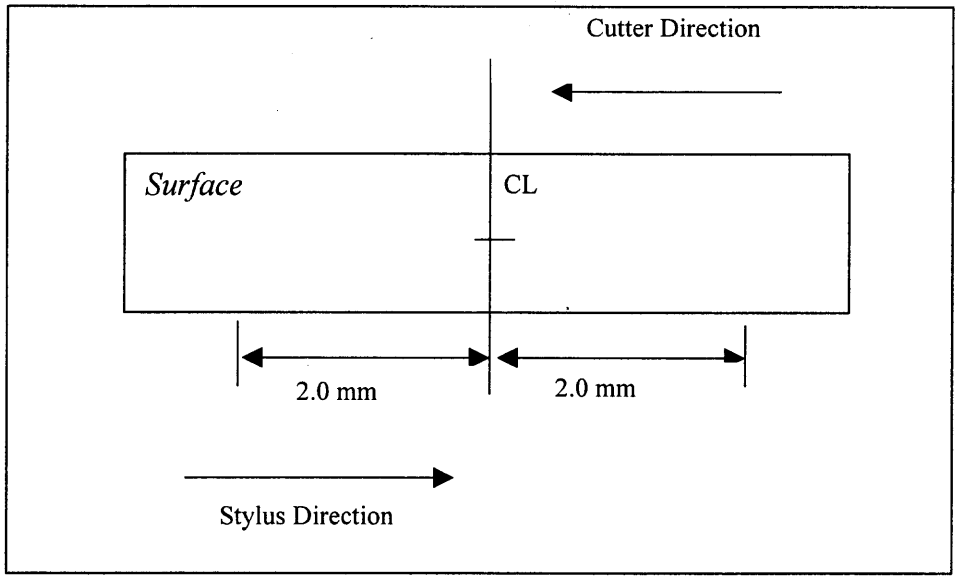

Figure 3-5. Surface Measurement Setup

As illustrated in Figure 3-5, each surface measurement is taken opposite of the cutter direction. The stylus is placed 2 mm from the centerline to provide a central traverse distance of 4 mm. The stylus is also placed centrally in the z-direction. By using the proposed surface measuring technique, error is eliminated since cutter acceleration and deceleration is not accounted for. Figure 3-6 illustrates the surface acquisition setup.

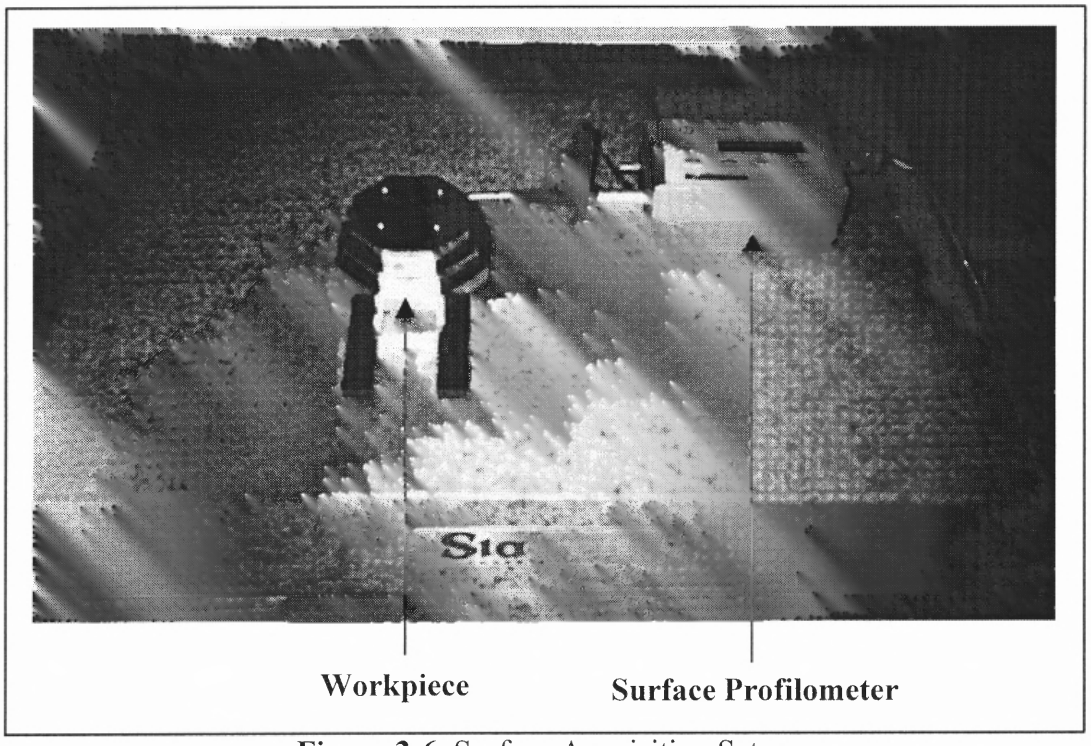

Figure 3-6. Surface Acquisition Setup

3.3.2 Software

The following sections provide a description of measurement software, analysis software, and part programming software utilization. Measurement software includes United Electronics Industries (UEI) STATUS force measurement control environment, Taylor–Hobson Surtronic 3-Plus control environment, and the Browne and Sharp XCEL AVAIL tolerance control environment. Software utilized to perform data analysis include MS EXCEL, Table-Curve 2D, Table-Curve 3D, MathCAD and Peak-Fit. Part programming methodology for the proposed experimental geometric design is also discussed.

3.3.2.1 Part Programming: Contour and straight/taper part programming can be performed offline using an ASCII text editor and checked by importing part programs into a graphical milling simulator called CNCEZ. CNCEZ allows for error detection of

spindle position in relation to the proposed workpieces and provides the total cutting time which is beneficial for providing sampling rate and frequency settings for the WIN-30 data acquisition board. Figures 3-7 and 3-8 illustrate the CNCEZ software environment for contour and straight/taper programming. The part programs written with a text editor is imported into CNCEZ for program testing. Tool type and size, blank size, and material type for the experiment is defined with CNCEZ.

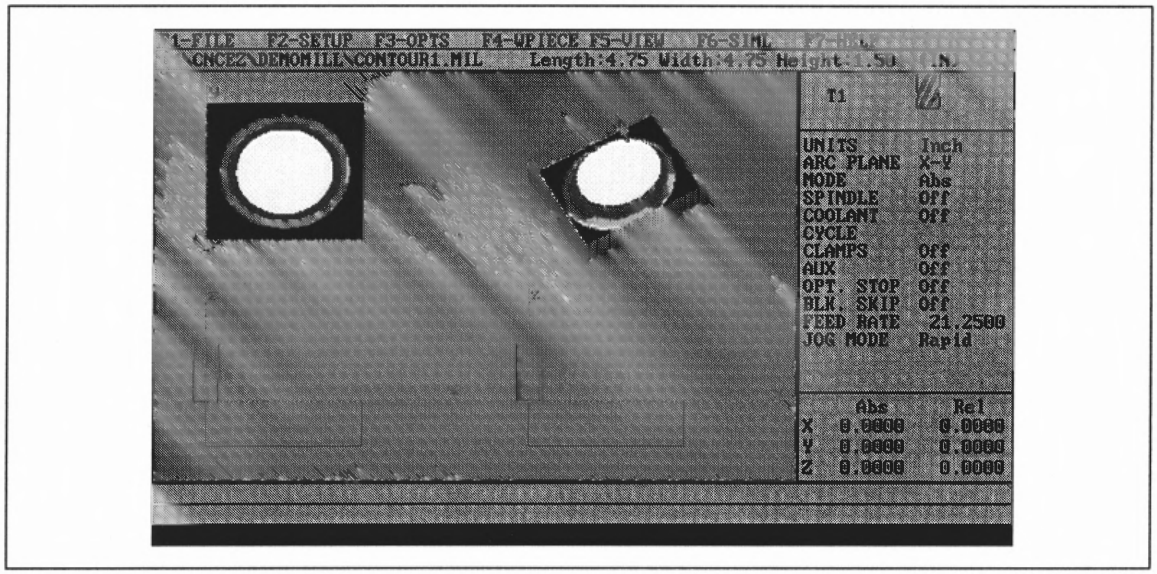

Figure 3-7. CNCEZ Contour Geometry

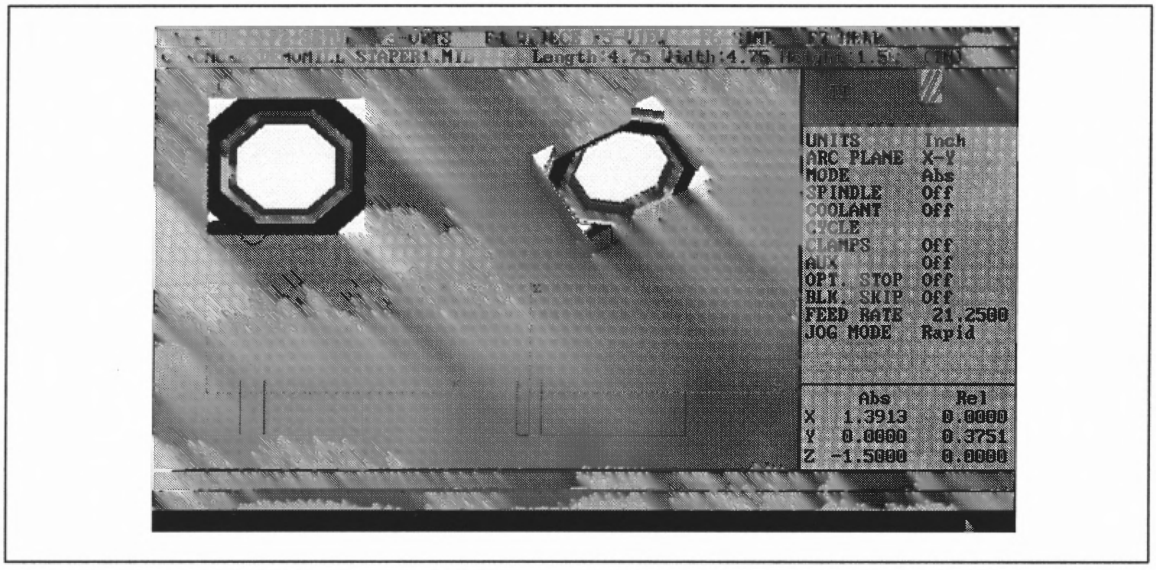

Figure 3-8. CNCEZ Straight/Taper Geometry

3.3.2.2 Measurement: Control and storage of online force measurement can be performed using United Electronics Incorporated (UEI) STATUS for windows. STATUS is data acquisition software for the WIN-30 data acquisition board. Utilization of UEI's STATUS is due to the following reasons: (1) cutting force data can be acquired from the UEI WIN-30 board for which multi-channel data acquisition (X, Y, and Z-direction cutting force) is fully supported, (2) the acquired cutting force data can be displayed in multiple units in either graphical or text form, a cross-hair system allows the measurement of voltage and time, (3) the acquired cutting force data can be processed by FFT or Chirp-Z methods to yield a frequency domain representation, and (4) the cutting force data can be stored for recall and can be written as an ASCII text file for use with spreadsheet or graphing programs. A sample of the STATUS output is provided in Figure 3-9.

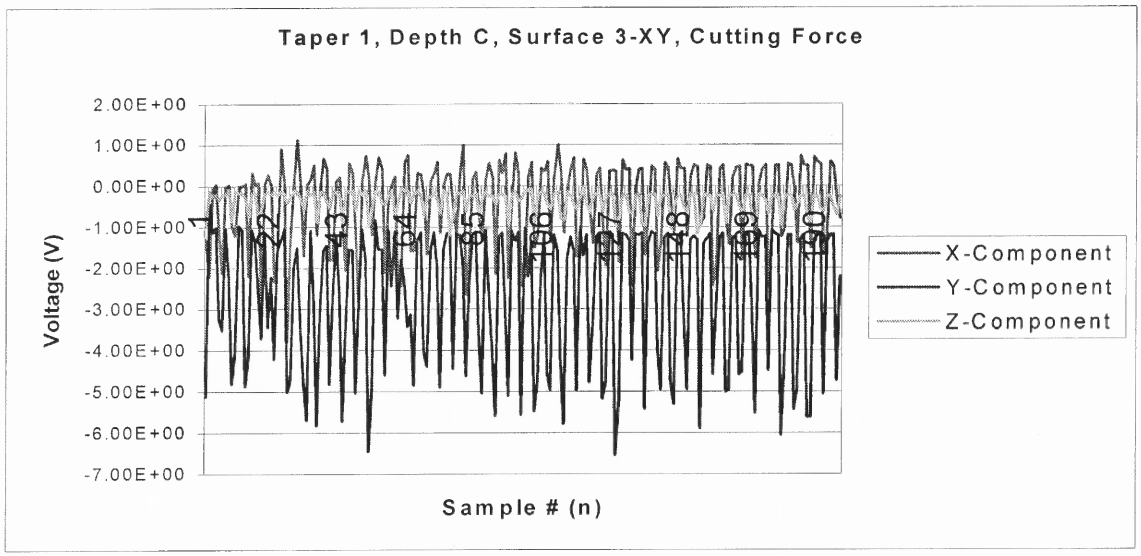

Figure 3-9. Sample STATUS Signal Output

Surface finish control and measurements taken by the Surtronic 3-Plus is uploaded into the computer via RS-232 connection. The raw data is processed by the software package using the following relationships.

A. Surface Skewness $$R_{sk} = \frac{1}{nR^3{}_q}\sum_{i=1}^{n}(Y_i)^3 \quad (3\text{-}2)$$

B. Surface Kurtosis $$R_{ku} = \frac{1}{nR_q^{\ 4}}\sum_{i=1}^{n}(Y_i)^4 \quad (3\text{-}3)$$

C. Mean Spacing $$S_m = \frac{1}{n}\sum_{i=1}^{i=n} S_i \quad (3\text{-}4)$$

D. Surface Wavelength $$\lambda_q = \frac{2\pi R_q}{\Delta_q} \quad (3\text{-}5)$$

E. Peak-to-Valley Height $$R_{tm} = \frac{1}{n}\sum_{i-1}^{i=n} R_{ti} \quad (3\text{-}6)$$

R_q is the RMS of the roughness average, Y_i is the profile area, S_i is the peak spacing, n is the number of peaks, Δ_q is the RMS slope of the profile, and R_{ti} is the maximum peak-to-valley height of the surface profile in one sampling length. A sample of the Surtronic 3 Plus software environment is given in Figure 3-10.

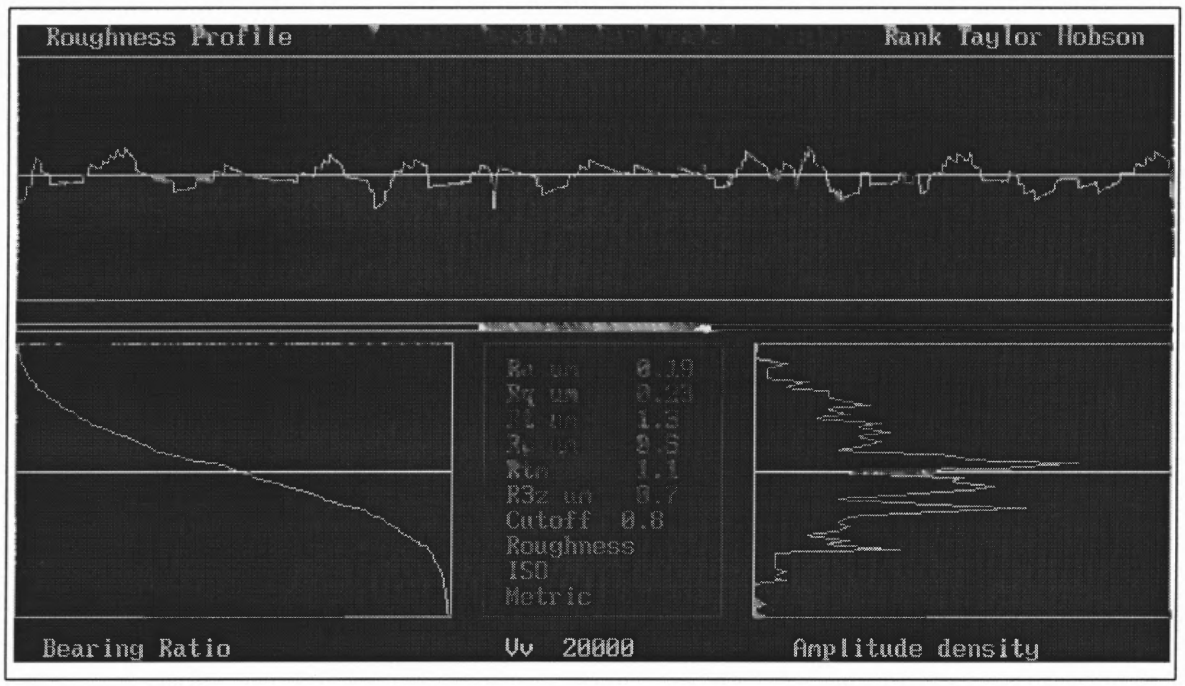

Figure 3-10. Sample Surface Profile Output

From the completed surface measurement, the data may be output graphically, in parameter-only form, and as a raw data ASCII file.

Offline tolerance measurement of the contour and straight/taper geometry can be performed using the AVAIL command language. It is implemented for the recording and storage of tolerance data performed on the Brown and Shape XCEL 765 coordinate measuring machine. The AVAIL software handles the measurement of only primitive geometries. For complex surfaces, the recorded measurements are analyzed by a contour analysis package. Prior to performing measurement of both the proposed straight/taper and contour geometries, an "OUTPUT/DEVICE" command is invoked to specify the storage location of the tolerance data. The "OUTPUT/DEVICE" command is commonly issued at the beginning of the measurement program allowing the file to remain open for data input. A "SETUP/PARAMETERS" command defines the action for and the range of the physical measurement envelope before the parts are measured. During contact measurement, the XYZ coordinate is specified by the value "PTx", where "x" is the point number. An example of the AVAIL CMM output is illustrated in Figure 3-11.

```
                UNITS/METRIC;
                PROBE/DIAMETER; 2
                UNITS/ENGLISH;
DATUMZ      = GEOMETRIC/PLANE;
                MANUAL/; 4
                DONE/;
DATUMX      = GEOMETRIC/2D_LINE; DATUMZ
                MANUAL/; 2
                DONE/;
DATUMY      = GEOMETRIC/2D_LINE; DATUMZ
                MANUAL/; 2
                DONE/;
CORNER      = INTERSECT/POINT; DATUMX,DATUMY
                ALIGNMENT/PART; DATUMZ,DATUMX,CORNER,XYZ
                PAUSE/;
                MOVE/TO; 0,0,0
              = GEOMETRIC/2D_LINE; DATUMZ
                MEASURE/; 1.20356,-0.03271,-1.36209
                MEASURE/; 1.26453,-0.03317,-1.36207
                MEASURE/; 1.35482,-0.03300,-1.36202
                MEASURE/; 1.45041,-0.03342,-1.36196
                MEASURE/; 1.48117,-0.03376,-1.36194
                MEASURE/; 1.51231,-0.03343,-1.36192
                MEASURE/; 1.58878,-0.03345,-1.36187
                MEASURE/; 1.66601,-0.03360,-1.36182
                MEASURE/; 1.69196,-0.03370,-1.36180
                MEASURE/; 1.72725,-0.03398,-1.36178
                MEASURE/; 1.76672,-0.03388,-1.36175
                MEASURE/; 1.78429,-0.03383,-1.36174
                MEASURE/; 1.86632,-0.03402,-1.36169
                MEASURE/; 1.89652,-0.03414,-1.36167
                MEASURE/; 1.94403,-0.03431,-1.36164
                MEASURE/; 2.05806,-0.03449,-1.36157
                MEASURE/; 2.08852,-0.03486,-1.36155
                MEASURE/; 2.13174,-0.03482,-1.36152
```

Figure 3-11. AVAIL CMM Sample Output

3.3.2.3 Analysis: Direct data analysis for PMBDCLM and DC servomotor force, tolerance, and surface finish performance indices, determination of mean, standard deviation, and signal-to-noise for probability plotting can be determined utilizing a spreadsheet such as MS EXCEL. Spreadsheet utilization is beneficial since experimental cutting force data, stored as an ASCII text file by UEI's STATUS, is easily imported into row/column format. Utilizing the spreadsheet's statistical features such as probability plotting, operating parameter levels can be tested for significance graphically.

Simple regression (SR) is used to determine the relationship between cutting force and each of the performance indices is performed using the equation discovery software Table-Curve 2D. Table-Curve 2D is a program that combines a curve fitter with the ability to find the ideal equation to describe 2D empirical data. Table-Curve 2D will automatically fit 3,665 built-in equations from all disciplines to find the one that provides the ideal fit. Once the fit is complete, Table-Curve 2D presents a statistically ranked list of the best-fit equations and provides graphic capabilities. A sample of the Table-Curve 2D output for contour, surface wavelength at a central depth of cut is shown in Figure 3-12.

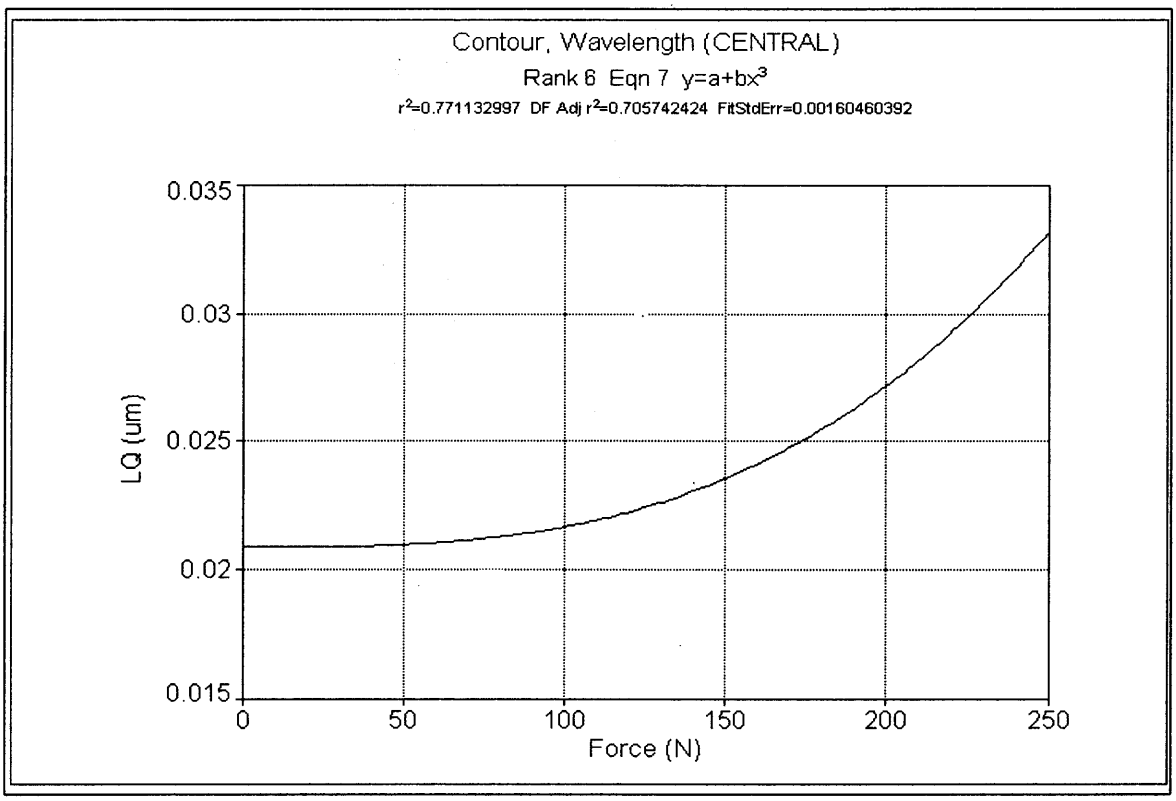

Figure 3-12. Simple Regression (Surface Wavelength, N=12) Sample

Multiple regression (MR) is utilized to determine the relationship between spindle speed and feedrate with (1) tolerance, (2) surface finish, and (3) force performance indices. It is performed using the equation discovery software Table-Curve 3D. Table-Curve 3D is a software that combines a surface fitter with the ability to find an ideal equation to describe three dimensional empirical data. Table-Curve 3D uses a selective subset procedure to fit 36,000 of its 453,697,387 built-in equations to find the one that provides the ideal fit. Table-Curve 3D presents a statistically ranked list of best-fit equations and provides graphic capabilities. A sample of the MR output is shown in Figure 3-13.

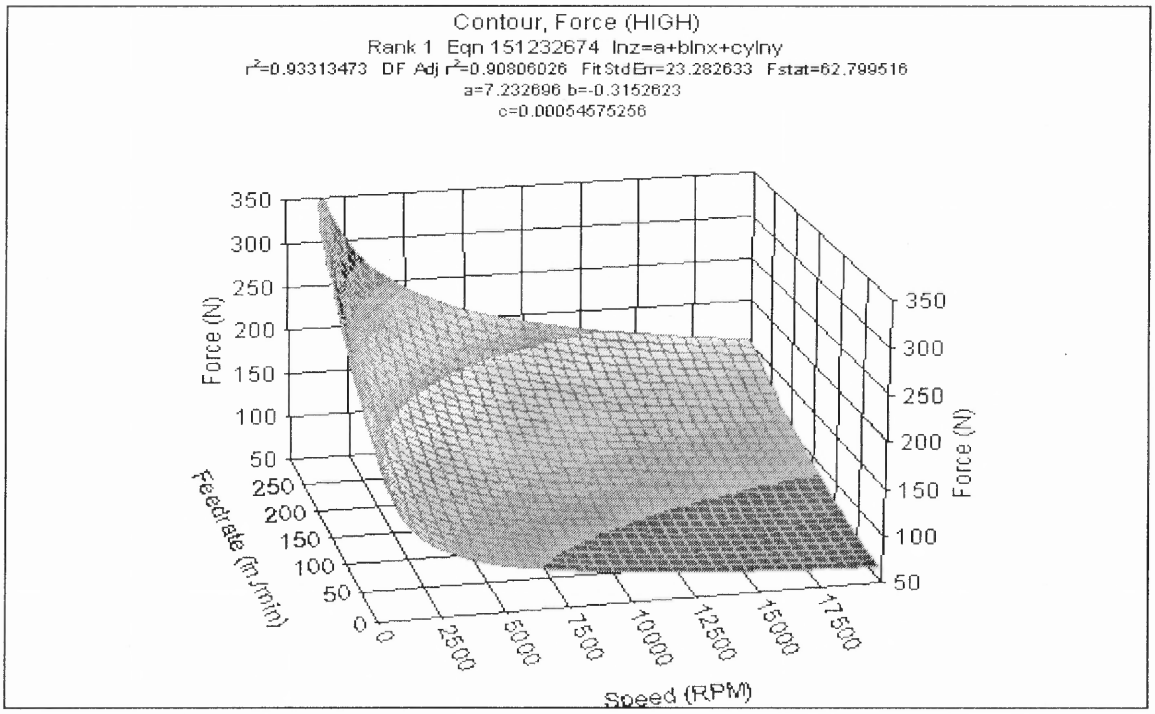

Figure 3-13. Multiple Regression (Force, N=12) Sample

From the force data obtained during the experimentation, the amplitude, center, and width of the force curve will change for each treatment level. Obtaining these characteristics can be made using a peak separation and analysis software called Peak-Fit. Cutting force data obtained from experimentation is imported, via an ASCII text file, into Peak-Fit where the force signal is best-fit and separated into peaks revealing amplitude, width, and height. For the proposed methodology, a statistical peak function family is selected within Peak-Fit and fitted. Using the best-fit beta (amplitude) function, represented by,

$$y = \frac{\left(\frac{x - a_1 + \frac{a_2(a_3 - 1)}{a_3 + a_4 - 2}}{a_2}\right)^{a_3 - 1} \left(1 - \frac{x - a_1 + \frac{a_2(a_3 - 1)}{a_3 + a_4 - 2}}{a_2}\right)^{a_4 - 1}}{\left(\frac{a_3 - 1}{a_3 + a_4 - 2}\right)^{a_3 - 1} \left(\frac{a_4 - 1}{a_3 + a_4 - 2}\right)^{a_4 - 1}} \qquad (3\text{-}7)$$

Each component force signal is separated in three criteria such as peak force amplitude *(a0)*, force center *(a1)*, and force width *(a2)*. The *(a3)* and *(a4)* components are shape distortion indices for the force center and width. The *(a3)* component is equal to *shape (1)* with the condition *(>1.01)* and the *(a4)* component is equal to the *shape (2)* with the condition *(>1.01)*. A sample of Peak-Fit output for contour cutting force at a high depth of cut is illustrated in Figure 3-14.

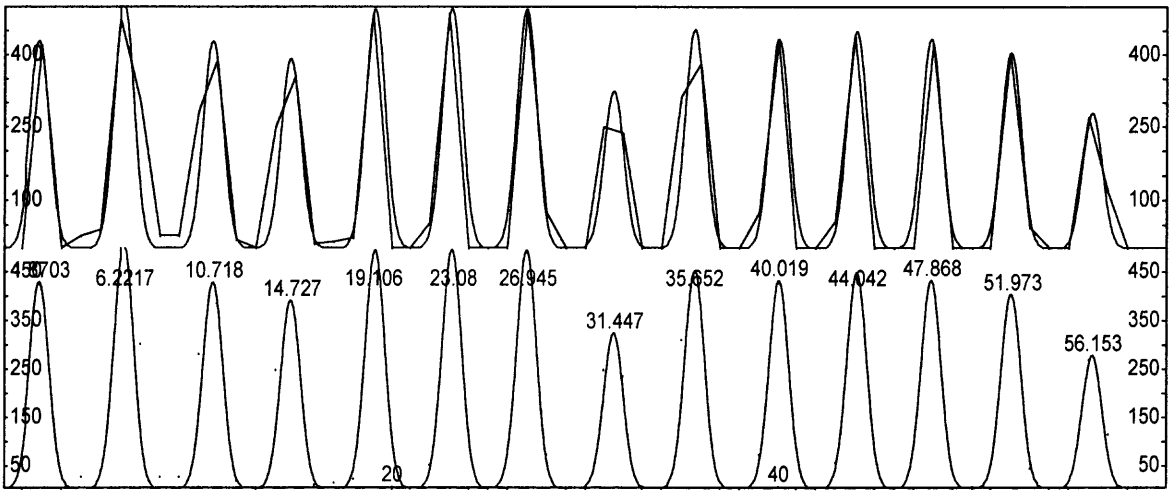

Figure 3-14. Peak Fit Output

3.4 Statistical Analysis and Database Development

Statistical analysis is applied to contour and straight/taper geometry PMBDCLM results. Statistical analysis such as probability plotting, significance of factors, peak force extraction, simple regression, and multiple regression provides data for knowledge base development. Database development based on experimentation and statistical analysis provides a concise summary of knowledge to be extracted during heuristic execution.

3.4.1 Performance Rating Database

The performance rating database consists of both contour and straight/taper geometry mean performance data obtained from the design of experiments. Tolerance ratings include position, runout, total runout, circularity, and cylindricity for the contour geometry and position, straightness, flatness, parallelism, and angularity for the straight/taper geometry. Surface ratings include kurtosis, skewness, spacing, wavelength, and peak-to-valley height. Cutting force, force amplitude, force center, and force width obtained from Peak-Fit are also rated. For each depth of cut, each performance measure is rated according to the proposed Taguchi quality characteristics. For example, a rating of 5 for position tolerance indicates the best performance and a rating of 1 indicates the worst performance. A rating of 1 indicates very low and a rating of 5 indicates very high for cutting force. Standard deviation for each performance measure at each depth of cut is also given a rating. A rating of 1 indicates a very small standard deviation and a rating of 5 indicates a very high standard deviation.

3.4.2 Generated Probability Plots

Since significant factors are important in effecting the output characteristic, a graphical technique can be used to check the normality of sample data and to identify the significant factor(s) that causes variability. A normal probability plot, executed using MS EXCEL, is used for determining whether the sample data conforms to a hypothesized normal distribution based on visual examination of the data. For the linear motor experimental data, the S/N, log(s), and mean are:

1. Ranked from smallest to largest

2. Plotted against the cumulative frequency V_i, where $V_i = (i-0.5)/n$

From the linear motor experimental data, the main and interaction effects that lie outside a straight line are considered to have a significant effect.

3.4.3 Significant Factors

For the contour and straight/taper geometry, three depths of cut for each surface is checked for significant factors using the method described. Single, dual interaction, and triple interaction effects are determined for the proposed tolerance and surface finish indices. The effects can include speed [S], feedrate [F], depth of cut [D], the dual interaction effects may include [S x F], [S x D], [F x D], and the triple interaction effect is [S x F x D].

The significance database is based on significant factors for both contour and straight/taper geometry. Single level, dual interaction, and triple interaction significant optimal levels are provided to reduce variability. Significance is provided for mean, variance, and signal-to-noise ratio for tolerance indices, surface finish indices, cutting force, force amplitude, force center, and force width. An optimal performance value is provided based on the quality characteristic.

3.4.4 Regression and Parameter Estimates

Simple regression, multiple regression, and peak force curve fitting is conducted to provide functional relationships with controllable factors such as spindle speed, feedrate and depth of cut with the proposed tolerance and surface finish indices. Simple regression is conducted to determine the relationship between cutting force with the proposed

tolerance and surface finish indices. Multiple regression is conducted to determine the relationship with operating parameters and the proposed tolerance and surface finish indices. Peak separation of the force data is also conducted to determine the peak force, force center, and force width.

3.4.4.1 Peak Extraction: For each surface force measurement taken, according to the design of experiments, the components of the force signal for the direction of cut is separated using the Peak-Fit software package. Each component force signal is separated in three criteria such as peak force amplitude *(a0)*, force center *(a1)*, and force width *(a2)*. The *(a3)* and *(a4)* components are shape distortion indices for the force center and width. The *(a3)* component is equal to *shape (1)* with the condition *(>1.01)* and the *(a4)* component is equal to the *shape (2)* with the condition *(>1.01)*. The strength of the fit is measured by the R-square value. A strong fit is indicated with a value close to 1.0. A weak fit is indicated by a value close to zero. For each surface, the number of peaks is also determined.

3.4.4.2 Simple Regression: Simple regression is performed utilizing the Table-Curve 2D software. By using the force data obtained from the proposed design of experiments, empirical relationships are determined. The "goodness" of fit is determined by the R-square value. A value of 1.0 indicates a perfect fit. A value close to zero indicates that there is no relationship between the independent and dependent variables. Simple regression provides relationships between the cutting force obtained from the design of experiments at each depth level of the tolerance and surface finish indices.

3.4.4.3 Multiple Regression: Multiple regression is conducted to determine the relationship between spindle speed and feedrate with the proposed tolerance and surface finish indices at a fixed depth of cut. The functional relationship between spindle speed and feedrate with cutting force is determined. Peak force, force center, and force width, is determined by the peak separation analysis. By using the tolerance and surface finish data at the proposed levels, obtained from the proposed design of experiments, functional relationships are determined. The "goodness" of fit is determined by the R-square value. A value of 1.0 indicates a perfect fit. A value close to zero indicates that there is no relationship between the independent and dependent variables. For multiple regression, the independent variables are spindle speed and feedrate and the dependent variables are tolerance, surface finish, and force.

3.5 Adequacy of Models and Validation

The correlation coefficient and the F-test are two measures for checking adequacy of the empirical relationships. The hypothesis H_0 is tested by the F-value. H_0 is rejected if the calculated F-value is greater than the tabulated value, which indicates that the independent variables are significant to the dependent variables at a specific confidence level.

Other methods to confirm model adequacy is where the residual is applied to determine whether there is any pattern in the residuals or if there is any relationship between any of the variables and the residuals. Therefore, the residuals analysis is a tool to confirm the assumption of normality. Thus, the residuals are calculated and the

assumption of normality is confirmed if 95% of the residuals fall into the interval. The partial correlation matrix is another measure of the empirical relationship adequacy.

For pure error and lack of fit, and when there are multiple Y observations at a specific X value, the variance in these Y values can be said to consist of pure or random error. When such repeats or replicates are present in a data set, it is possible to separate the portion of the variance attributable to pure error from that portion associated with the fitted model.

The r^2 attainable is the maximum r^2 that can be achieved with any model. The pure error sum of squares will reflect that portion of the sum of squared residuals attributable to pure error in these repeat observations. The lack of fit sum of squares is simply the difference between the overall sum of squared residuals and this pure error sum of squares. When this lack of fit F-statistic is significant (>>1), the model may be inadequate. In such cases, the residuals should be checked closely for systematic trends which would confirm the insufficiency of the model.

A precision summary can be used to determine how much precision is preserved in the current equation when the successively fewer digits of precision is used in the coefficients. The absolute error is measured at the eight points defining the boundary of the data and the point closest to the center of the data region. For linear equations, the impact of removing (zeroing) can also be determined.

For volume and function extrema, the volume below the fitted surface is computed using a Gaussian quadrature double integration from the lowest active X value in the data set to the highest active X value, and from the lowest active Y value in the data set to the highest active Y value.

The empirical models can also be validated for new operating conditions for one way, two way, and three way interactions between spindle speed, feedrate, and depth of cut.

3.6 Solving Simultaneous Empirical Relationships

From the empirical relationships obtained from simple and multiple regression, spindle speed and feedrate are unknowns for each performance index. To solve the unknowns in the functions to determine the spindle speed and feedrate, MathCAD can be utilized. MathCAD combines a live document interface of a spreadsheet with a WYSIWYG interface of a word processor. As with a spreadsheet, as soon as a change is made in either a global or local variable definition, changes in the results occur. For systems of equations, initial values of spindle speed and feedrate are determined in the following manner. (1) Provide an initial feasible guess value for spindle speed (x) and an initial feasible guess value for feedrate (y), (2) enter the keyword "GIVEN" to initiate MathCAD for solving systems of equations, (3) enter the equations with parameter estimates for each performance index, for example, a system containing a position tolerance, straightness tolerance, and peak-to-valley height function set equal to the user specified performance value, and (4) invoke the "Find(x,y)" function to display the system solution.

3.7 Knowledge Base Rules

For the proposed heuristic, two sets of rules are developed for decision making. The rules include set 1 (relationship/production) rules and set 2 (expert).

Set 1 Rules

For tolerance and surface finish indices, there are two models. The first model is obtained from simple regression and the second model is obtained from multiple regression. Relationship rules provide a decision on which relationship to use throughout the heuristic based on the relationship strength. Figure 3-15 illustrates the relationship network.

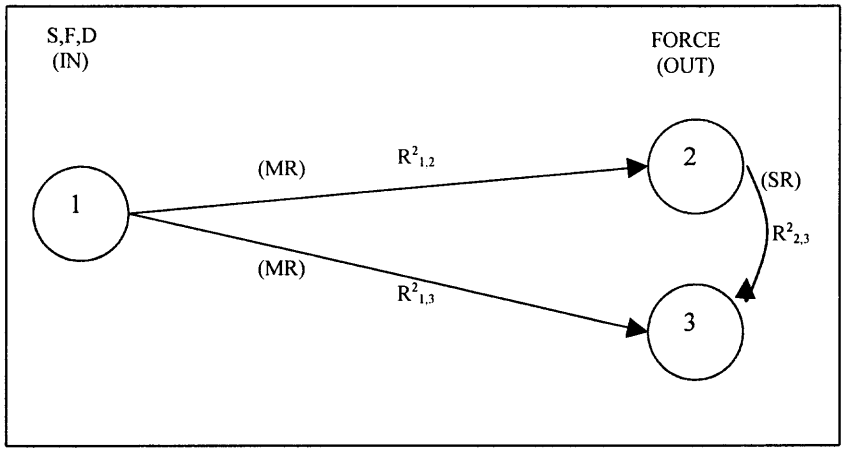

Figure 3-15. Relationship Network

Set 2 Rules

Expert rules are obtained from an expert or experts that can provide special insights into a problem because expertise is built over a long period of task performance. Such expert knowledge is represented by a set of arguments that will satisfy a particular condition. Based on knowledge from experts in PMBDCLM CNC design and operation, a set of expert rules is developed.

The expert rules dictate that if the position tolerance and surface finish peak-to-valley height specifications are both met, then such a spindle speed, feedrate, and depth of cut is expected. Such rules are necessary, and utilized in the proposed optimal operating parameters heuristic for the following reasons:

- Tie resolution between similar operating parameter, tolerance index, and surface finish index solutions.
- Conflict resolution between operating parameter, tolerance index, and surface finish solutions.
- Endless loop resolution when no solutions are found.

CHAPTER 4

FINITE ELEMENT ANALYSIS AND MODELING

Finite element analysis is a numerical method for obtaining approximate solutions for a wide variety of scientific problems. In it's gradual development, starting with the broad field of continuum mechanics, analysis flexibility allows static, dynamic, thermal, electromagnetic, and fluid analysis to represent actual problems.

4.1 Preprocessor

The first step in the process of analyzing a model is to represent the geometry of the object(s) involved. This consists of a mathematical description of the model's boundary and the interior regions. An option within a finite element package such as EMRC NISA (Numerically Integrated Elements for System Analysis) DISPLAY, provides commands to define locations in three dimensional space, which are called grids, straight or curved line segments, called lines, surfaces, called patches, and solids called hyperpatches. Such a description within NISA is referred to as geometric entities for preprocessing.

The PMBDCLM and DC servomotor FEA models were developed using the NISA preprocessor software. Within NISA there are different tools to help the user construct and process finite element models. 'DISPLAY' is an interactive, processing window for preprocessing modeling and post-result analysis. Such a module allows for easy transfer of data from one analysis to another.

EMAG, STATIC, and DYNAMIC post-processors directly interface with the preprocessing model of the 'DISPLAY' program. Some highlights of the preprocessing

capabilities include, CAD/CAM interfacing, three dimensional geometric modeling, including points, lines, arcs, curves, etc., and a variety of modeling tools.

Applying boundary conditions such as directional forces or distributed forces provide a method to simulate the effect of cutting forces on the PMBDCLM to help determine operating parameters for design of experiments and justification for replacement of existing DC servomotors on CNC machines. The performance of such a model consideration has been determined utilizing electromagnetic, magnetic, static, dynamic, and magneto-thermal finite element analysis. The PMBDCLM FEA model represents the orthogonal cutting forces using one axis of a working table holding a work-piece. Three-dimensional solid elements are applied for modeling the 3D state of the field distribution inside the linear motor. Simulation of the cutting force is defined within a force data group of the NISA finite element software. In addition, other boundary conditions, namely electric and magnetic field characteristics such as E-field, flux, effective power, and current density in the X, Y, and Z direction is applied.

The primary reasons to model the PMBDCLM and DC servomotor in the preprocessor are:

- To illustrate that higher feedrate may be possible and to use the theoretical velocity to bridge the gap between FEA and design of experiments.
- To illustrate linear motor performance is not compromised due to thermal considerations, static considerations (secondary stresses and displacement), electromagnetic considerations (E-Field, M-Field, Force), and dynamic considerations (displacement, acceleration, and velocity).

- To illustrate a force comparison for cutting conditions of a PMBDCLM and DC servomotor.

4.1.1 Meshing

Discretization of the geometric domain to define nodes and elements provides the mesh. Within NISA, element and node generation is applied to a PMBDCLM and DC servomotor.

A mesh can be generated either manually or automatically for each geometric entity that is active. Boundary conditions of the model, in terms of loads, constraints, etc., need to be applied to complete the analysis.

The geometry of the generated elements can be triangular (two-dimensional) or tetrahedral (three-dimensional). Basic elements (sometimes called simplexes) are more generally called quadrilaterals and polyhedrals. An element is characterized by its number of nodes and by the degree of the unknown approximation function. It can be rectangular or curvilinear and the order of approximation can vary from 1 to 6 for various applications.

The principle of finite element analysis consists of defining a partition over the domain (decomposition into sub-domains (finite elements) which cover the whole domain but which do not overlap). The original domain is usually characterized by a grid of points, which are the nodes common to adjacent elements. The unknown function is described by its value at each of the nodes of the grid. The unknown function will be interpolated over the domain from its nodal values (at the nodes) which come from one

solution. The continuity conditions will be defined by the nature of the elements in conjunction with the continuity conditions imposed by the nature of the problem.

Steps illustrating where meshing occurs in finite element modeling are listed below.

1. Definition of the Domain (Preprocessing).
2. Decomposition into finite elements (Preprocessing, Meshing).
3. Calculation of the coefficients of the algebraic system (Postprocessing).
4. Solution of the equations (Postprocessing).

Linear motor geometry has been developed within DISPLAY using 3D solid primitives, planes, and hyper-patches made from grid points. Once the required geometry was chosen, FEA patches were defined since patch size varies due to the requirements of different degrees of resolution. This is important when the frequency of changing conditions and the accuracy of results are extremely high. After the development of the patch geometry, hyperpatches, elements and nodes were created. Hyperpatches, which were generated from the FEA software, allowed nodes and elements to be generated. For each element, which is defined by two parameters NKTP (element type) and NORDR (element order), material and mechanical properties were assigned. The generated permanent magnet elements were defined with coercive field strength (H_{cx}, H_{cy}, H_{cz}) in the X, Y, and Z direction.

The selection of elements for an application should be based on its capabilities, its cost such as stiffness matrix generation, decomposition and stress calculation, and the desired accuracy in the results.

During meshing, DISPLAY allows a variety of operations for verifying and checking the model. The operations range from sophisticated checks for distortion, warping, skewness, etc. of elements producing graphic checks that visually highlight boundary conditions as well as potential discontinuity in the finite element model.

Elements should be of regular shapes as much as possible. This is achieved when the element aspect ratio is close to unity. The best shape of a quadrilateral is a square, and that of a hexahedron is a cube. The distortion index, calculated by DISPLAY, is the indicator of how well the element maps to the ideal or the best shape of an element. The ratio of the minimum Jacobian to the average Jacobian is defined as the distortion index. The most desirable distortion index is 1, which indicates the element maps perfectly to the ideal shape.

There are several methods to create nodes in DISPLAY. Nodes can be individually defined by their coordinates or by utilizing transformation operations such as translation, rotation, etc. Whenever elements are generated, nodes describing the connectivity of elements are generated.

Several commands may be utilized for node identification and manipulation. By merging nodes, models can be merged into one integral surface/solid. Inactive nodes can be automatically deleted and node ID's can be renumbered preserving all associatives.

4.1.2 Material Properties

Nodes and their associated coordinates define element configuration and connectivity. However, some element properties such as thickness for plate or shell elements, and

cross-sectional properties for beam elements have to be specified separately. Tables for particular property set identifications are to be specified by the model requirements.

General properties include mass density, modulus of elasticity, shear modulus, and the thermal expansion coefficient. Composite element properties include compressive failure stress and tensile failure stress. Thermal properties include thermal expansion coefficient and specific heat. Electromagnetic properties include permittivity, permeability, conductivity, and reluctivity.

Definition of material properties for the elements is required. Depending on the type of analysis, material properties such as modulus of elasticity, poison's ratio, coefficient of thermal expansion, density, etc., need to be provided. Material and property tables are required for each set identification which are assigned to an element during element generation.

4.1.3 Boundary Conditions

Internal boundary conditions are required attributes for finite element model solutions. These conditions may include mass density, material and mechanical properties, element types, and degrees of freedom per node.

Internal boundary conditions consist of element types for property definition such as shell, beam, 2D/3D mass, 2D/3D gap, friction, etc., with individual physical property specifications. For example, 3D beam elements require cross section area, moment of inertia, torsional constant, and the eccentricity. Torsional spring elements require a torsional spring constant and a component coordinate system.

For material property definition, a MAT-ADD command in DISPLAY is utilized to add a data set of material property values that are tagged with a unique integer called the material identification, or MAT-ID. When elements are created in DISPLAY, a part of their data is in the material identification. Thus the material identification serves as the link between the finite element entities and the actual material property values. Different element formulations require the specification of different material property values.

Mechanical property definition acts in the same way as material property definition. When elements are created in DISPLAY, a part of their data is also in the mechanical property identification. As with the material identifications, different formulations require the specification of different mechanical property values.

External boundary conditions usually consist of imposed excitations upon a model. Depending on the analysis type, these may consist of force, moment, displacement, specific field potential, current density, coercive field strength, etc.

For magnetic field analysis with an imposed directional force acting as a cutting force, the excitations and boundary conditions are governed by the simplifying assumptions. Based on these assumptions, utilization of boundary conditions such as initial field potential, specific field potential, electric flux, magnetic flux, permanent magnet, and force is possible. Force is specified in a particular direction for an object. Such a condition is useful when analyzing linear movement such as when net force calculation is required on a moving object. This boundary condition is particularly useful in the proposed research since force excitations can be used to simulate cutting forces generated in metal cutting operations. It can also be placed in a specified direction at a

specified node. Torque is also a boundary condition that is utilized when a net torque calculation is required on a rotating object.

Electric flux density and magnetic flux density is defined and specified on an element face. It can either be uniform or non-uniform. Permanent magnet boundary conditions are utilized in E-field and M-field analysis. This excitation is utilized on the elements previously defined as permanent magnet material. For this boundary condition, the coercive field strength, in the X, Y, and Z directions is specified.

4.2 Postprocessor

Analysis modules of DISPLAY provide a direct interface with the entire library of sub-analysis programs. The analysis capabilities include linear static analysis, non-linear static analysis, linear direct transient analysis, eigenvalue analysis, modal dynamic analysis including transient dynamic, random vibration, frequency response, and shock spectrum analysis, buckling analysis, and steady state/transient heat transfer analysis.

Graphical representation and manipulation of the results is performed directly using the DISPLAY post-processing module. The DISPLAY post-processor features include deformed geometry plots, separate or superimposed on un-deformed geometry, contour plots of displacement, stresses, strains, and temperatures. The post-processor also includes stress, torque including error estimates, contour plots of composite sections for three dimensional models, animation for transient analysis, and deformed/modal shapes on graphics devices. Displacement in the X, Y, and Z directions, resultant displacement in the X, Y, and Z directions, linear displacement in X, Y, and Z directions, maximum shear stress, stress, octahedral and principal stresses are included.

Graphical representation of results is obtained by utilizing the post-processing module of DISPLAY. Post-processing features include various geometric graphic options including hidden line removal, boundary and thermal plots and view manipulation including rotation, scaling, and clipping. Some unique DISPLAY post-processor functions include:

1. *Electrostatics*. Potential, electric field intensity, electric flux density, stored electric energy, total stored electric energy, and capacitance.
2. *Steady Current Flow*. Potential, electric field intensity, current density, dissipated power, total dissipated power, inductance.
3. *Magnetostatics*. Magnetic vector potential or scalar potential, magnetic flux density, stored magnetic energy, magnetic force, total stored magnetic energy, and inductance.
4. *Magnetodynamics*. Magnetic vector potential, magnetic flux density, eddy current density, total current density, electric field due to eddy currents, total electric field, power loss density, stored magnetic energy density, total stored energy, total power loss, inductance, and resistance.
5. *Transient Magnetic Field Analysis*. Magnetic vector potential, magnetic flux density, stored magnetic energy and coenergy, induced any current density, electric fields due to eddy currents, power loss density, and total stored energy.
6. *Coupled Magneto-Thermal Analysis*. Temperature distribution due to induced currents in the electromagnetic device including heat transfer analysis, steady state and transient analysis. Thermal post-processing is incorporated into EMAG to provide the analysis of temperature variations in electromagnetic devices due to the presence of

induced currents in these devices. The following steps are required when executing a coupled analysis such as magneto-thermal analysis:

- Create an EMAG input file containing the finite element model and the appropriate EMAG executive command, analysis data, boundary conditions, and loading.
- Activate the coupled magneto-thermal executive command in the EMAG input file, such as [CHEAT = ON, SAVE = 26, 20].
- Create a heat input file containing the same finite element model and the appropriate heat executive commands, analysis data, and boundary conditions.
- Insert the command, [*READ, FILENAME], where file name is the *file20* name of EMAG, into the analysis data block of the heat input file.

During the EMAG post-process run, both input files will be read, then the electromagnetic analysis will be performed followed by heat transfer analysis. The EMAG output quantities, for example, electric and magnetic fields, flux densities, and current density, are available in the EMAG output files, while the heat output quantities, such as temperature distribution, are available in the heat output files. Post-processor results may be shown graphically as:

- Contour plots such as electric scalar potential, voltage, magnetic vector potential, current and flux densities, and electric and magnetic fields, heat, force, displacement, stress, velocity etc. can be obtained depending on the analysis types.
- X and Y profiles for various output quantities.
- Vector plots for flux densities, current densities and electric and magnetic fields.

Post processing of the parameters must take place to obtain results. Post processing must be initiated with a .NIS file. The .NIS file can be written into a *26.dat file. The *26.dat file can then be used to observe the post-processor results within DISPLAY.

4.3 Motor Design and Analysis

Linear motor performance under large cutting forces at varying air-gap sizes and voltages is investigated. Under loading conditions, electromagnetic, thermal, dynamic, and static analysis of the secondary elements is determined using EMRC NISA FEA software. Electric and magnetic field distribution is determined for force generation by varying voltages and gap sizes. Due to the presence of conduction currents in electromechanical devices such as a PMBDCLM, power losses in the form of heat dissipation are produced which alters the temperature distribution in the device. Change in temperature effects the generated force, electric and magnetic fields, thus overall performance.

Single sided linear motor and DC servomotor geometry is presented. An overall rating based on performance and cost is determined. The post processing analyses is performed in conjunction with steady current flow analysis, magnetic field analysis, electric field analysis, electromagnetic sub-analysis, dynamic analysis, and static analysis.

4.3.1 Motor Specifications

The proposed single sided PMBDCLM model is discretized using 1,463 3-dimensional hexahedron elements and 1,920 nodes. The entire model is 640.08 mm in length, 190.50 mm in width, and ranges from 70.475 mm to 76.20 mm in height due to the change in air-

gap size. Air-gap sizes are 0.625 mm, 3.175 mm, and 6.350 mm. For the current-carrying elements, there is a resistance of 10.0 Ω and the number of coil-turns is 150.

The finite element model of the DC servomotor is discretized using 1,280 3-dimensional hexahedron elements and 1,632 nodes. The entire model is 247.65 mm in length and 203.20 mm in diameter. The air-gap size is 3.175 mm. For the current-carrying elements, there is a resistance of 10.0 Ω and the number of coil-turns is 150. Table 4-1 provides the general motor specifications for the analysis.

Table 4-1. FEA General Motor Specifications

	Physical Dimensions (mm)		**Magnet Type**	**Magnet Area (mm^2)**	**# Coil-Turns (N)**	**DC Coil Resistance (Ω)**
PMBDCLM	Length	640.08	NdFeB	108,386.88	150	10.0
	Width	190.50				
	Height	70.475 - 76.200				
	Air-Gap Sizes	0.625 - 6.350				
DC Servo Motor	Diameter	203.20	NdFeB	108,064.30	150	10.0
	Length	247.65				
	Air-Gap Size	3.175				

Element types include 3D solid, 3D gap, and 3D gap/friction defined by the element type number (NKTP) and the element order (NORDR).

4.3.2 Model Assumptions

The following assumptions are made to determine the field, thermal flux distribution, static and dynamic characteristics. The assumptions include:

- The fields outside the motor periphery is negligible, therefore, the outer periphery of the motor can be treated as a zero vector potential line.
- The magnetic material is isotropic and the magnetization curve is single valued.

- The vector potential and the current density are invariant in direction.
- The field distribution is quasi-stationary.
- Time harmonic effects are absent.
- Specific temperature outside the motor periphery is negligible, therefore the outer periphery of the motor is defined as having a zero specific temperature (0.0 °C).
- Specific field potential outside the motor periphery is negligible, therefore the outer periphery of the motor is defined as having a zero specific field potential (0.0V).
- The primary elements and nodes are fixed for displacement, moment, and rotation.

4.3.3 Application of FEA to a PMBDCLM and DC Servo Motor

Finite element analysis is performed to provide force, magneto-thermal, electric field, magnetic field, and stress solutions of a PMBDCLM and generated force of a DC servomotor. Meshing of both motors and internal boundary conditions are listed in Table 4-3. External boundary conditions are listed in Table 4-4. Material properties are listed in Table 4-5. Results of analysis are listed in Table 4-6. Three air-gap sizes (0.625 mm, 3.175 mm, and 6.350 mm) and voltages ranging from 50V to 265V in the current-carrying elements are implemented using the analysis/sub-analysis and main boundary conditions listed in Table 4-2.

Table 4-2. Finite Element Analysis and Boundary Conditions

FE Analysis/Sub-Analysis	**Pre-Processor Boundary Conditions (Input)**	**Post-Processor Results/Performance Characteristics (Output)**
Electromagnetic/Force-Torque	Specific Field Potential/Coercive Field Strength/Current Density	1.Generated Force 2. Generated Torque
Electric Field/Steady Current Flow (SCFL)	Specific Field Potential	Electric Field Strength

Table 4-2. (Continued)

Magnetic Field Analysis (MGSS)	Permanent Magnet Coercive Field Strength	Magnetic Field Strength
Coupled Magneto-Thermal (SCFL/TMAG)	Specific Temperature/Current Density	Temperature
Linear Static	Component Force	1. Stress 2. Displacement
Eigenvalue/ (Dynamic)/Subspace-Iteration	Force/Friction/Displacement/ Rotation/Moment/Initial Velocity/Event Time/Time Amplitude/Convergence Tolerance (RTOL)/Cutoff Frequency	Natural Frequency
Linear Transient (Dynamic)	Force/Friction/Displacement/ Rotation/Moment/Initial Velocity/Event Time/Time Amplitude	1. Velocity 2. Acceleration 3. Displacement

To analyze the forces generated in the PMBDCLM and the torque in the DC servomotor, a force/torque data group is applied when the net force/torque calculation is required on a moving object (linear motor moving coil secondary)/rotating object (armature).

The electric field analysis is required to determine the electric field intensity within the air-gap region where steady current flow sub-analysis provides the electric field calculations in the conducting media which is due to the steady flow of electric charges.

The magnetic field analysis is required to determine the magnetic flux density within the air-gap region where 3D magneto-static sub-analysis provides the magnetic field calculations in the magnetic material due to direct current excitation and/or permanent magnets. A permanent magnet data group boundary condition is utilized to define the permanent magnet element coercive field strength.

To analyze the effect of temperature on the magnet array and air-gap region, the finite difference equations for the three-dimensional steady state and transient condition

are used with the aid of the coupled electromagnetic and thermal analysis to provide temperature and heat flux distributions along the primary, magnet array, and the air-gap region.

Linear static analysis is utilized to determine the stresses and displacement in the PMBDCLM secondary when a component force boundary condition is applied to the secondary nodes.

Six input voltages (50V - 265V) for experimental data are applied along with three force levels (L-(73.2 N), C-(125 N), and H-(204 N) obtained from experimentation are implemented using the dynamic analysis/sub-analysis and main boundary conditions.

For the PMBDCLM force and DC servomotor torque solutions, a forces/torque data group is applied when the corresponding values are required to be calculated on the moving secondary/rotor using electromagnetic analysis.

Linear transient and eigenvalue analysis is required to determine the velocity, acceleration, displacement, and frequency. The post processing is conducted utilizing the NISA post-processing module. Graphical results, such as vector plots, contour plots, and X, Y, Z profiles, is illustrated using the DISPLAY post processor module. Electric field, magnetic field, and force analysis solutions are obtained from the EMAG software module. Stress analysis solutions are obtained from the LSTATIC software module. Thermal analysis solutions are obtained by coupling the EMAG module using steady current flow analysis to the SHEAT module.

Post processing is performed utilizing the NISA dynamic post-processing module. Graphical results such as vector plots, contour plots, and X, Y, Z profiles, may be shown using a DISPLAY module. Velocity, acceleration, position, and frequency solutions are

obtained from the DYNAMIC software module. Force calculations are obtained using the EMAG software module.

Sub-analysis of dynamic and electromagnetic processing is required. The electromagnetic analysis requires a steady current flow sub-analysis for force calculations. Dynamic analysis requires a linear-transient sub-analysis for position, velocity, and acceleration calculations and an eigenvalue sub-analysis for natural frequency. The assigned properties of the proposed FEA models are provided in Table 4-3.

Table 4-3. Element Identifications and Internal Boundary Conditions

PMBDCLM							
Mat. ID #	**Geometry**	**Element Type**	**Element**	**Nodes/ Element**	**D.O.F /Node**	**NKTP/ NORDR**	**Materials Definition**
1	Primary	3-D Solid (Hex.)	418	8	1	104/1	Aluminum
2	Secondary Guideway	3-D Gap/ Friction (Hex.)	70	8	1	50/1	Aluminum
3	Permanent Magnet	3-D Solid (Hex.)	136	8	1	104/1	NdFeB Magnet
4	Air-Gap	3-D Gap (Hex.)	212	8	1	43/1	Air
5	Current Carrying Coil	3-D Solid (Hex.)	136	8	1	104/1	Copper
6	Secondary	3-D Solid (Hex.)	491	8	1	104/1	High Carbon Steel
DC Servo Motor							
1	Housing	3-D Solid (Hex.)	416	8	1	104/10	Aluminum
2	Permanent Magnet	3-D Solid (Hex.)	192	8	1	104/10	NdFeB Magnet
3	Armature	3-D Solid (Hex.)	216	8	1	104/10	High Carbon Steel
3	Air-Gap	3-D Gap (Hex.)	240	8	1	43/10	Air
4	Coil	3-D Hex	216	8	1	104/10	Copper

Boundary conditions include a 50V to 265V specific field potential in the current carrying elements, 0.0-V specific field potential at the motor periphery, and 2.067 x 10^6 A/m-*Hci* (26,000 Oe-*Hci*) in the magnet array. For thermal analysis, the specific temperature at the outer boundary nodes is 0.0 °C. There is a 700 N x-component force boundary condition imposed on the representative secondary elements for the applied force FEA model and a 700 CCW torque boundary condition imposed on the rotor.

Magnetic properties of NdFeB are accounted for due to thermal demagnetization. The higher the permeance coefficient the magnet array operates at, the higher the temperature it will withstand. High *Hci* NdFeB materials operating at a high permeance coefficient can operate about 210 °C.

For force generation comparison, a 1,280 element DC servomotor is subjected to the same boundary conditions and material properties. To perform the proposed finite element analyses, Table 4-4 lists the associated material properties with the representative elements.

Table 4-4. Material Properties

Isotropic Material Property	Aluminum	Copper	Magnet	H.C Steel	Air
GENERAL MECHANICAL/PHYSICAL PROPERTIES					
Mass Density	2712.6 kg/m^3	8900 kg/m^3	7300 kg/m^3	7850 kg/m^3	1.29 kg/m^3
Modulus of Elasticity (EX,Y,Z)	7.0 x 10^{10} N/m^2 (70 GPa)	11.5 x 10^{10} N/m^2 (115 GPa)	5.5 x 10^{10} N/m^2 (55 GPa)	20 x 10^{10} N/m^2 (200 GPa)	*
Poisson's Ratio (NUX,Y,Z)	0.334	0.35	0.340	0.280	*
Shear Modulus in XY Plane; (GX,Y)	2.8 x 10^{10} N/m^2 (28 GPa)	4.4 x 10^{10} N/m^2 (44 GPa)	3.5 x 10^{10} N/m^2 (35 GPa)	7.75 x 10^{10} N/m^2 (77.5 GPa)	*
Thermal Expansion Coefficient (ALPX,Y,X)	3.9 x 10^{-3} α(°C)$^{-1}$	1.7 x 10^{-8} α(°C)$^{-1}$	4.2 x 10^{-6} α(°C)$^{-1}$	11 x 10^{-6} α(°C)$^{-1}$	3.67 x 10^{-4} α(°C)$^{-1}$
COMPOSITE ELEMENT PROPERTIES					
Compressive Failure Stress; (FX,Y,Z;C)	1.379 x 10^8 N/m^2 (137.9 GPa)	3.322 x 10^8 N/m^2 (332.2 GPa)	92.5 kg/mm^2	1.931 x 10 N/m^2 (193.1 GPa)	*
Tensile Failure Stress (FX,Y,Z;T)	3.20 x 10^8 N/m^2 (320 GPa)	7.20 x 10^8 N/m^2 (720 GPa)	7.5 kg/mm^2	1.2 x 10^8 N/m^2 (120 GPa)	*
THERMAL PROPERTIES					

Table 4-4. (Continued)

Thermal Conductivity (KX,Y,Z)	238 W/m °C @25	397 W/m °C @25	79.5 W/m °C @25	14 x 10^{-6} W/m °C @25	0.0234 W/m °C @20
Specific Heat; C	900 J/kg °C	385 J/kg °C	205 J/kg °C	502 J/kg °C	1005.0 J/kg °C
ELECTROMAGNETIC PROPERTIES					
Permittivity (EX,Y,Z)	*	*	*	*	8.85 x 10^{-12} C^2/Nm^2
Permeability (MUX,Y,Z)	8802.8 m/H	7957780.0 m/H	150000.0 m/H	7243.1 m/H	4π x 10^{-7} T m/A (795780.0 m/H)
Conductivity (SIX,Y,Z)	3.57 x 10^7 $(\Omega m)^{-1}$	5.88 x 10^7 $(\Omega m)^{-1}$	1.50 x 10^7 $(\Omega m)^{-1}$	1.0 x 10^7 $(\Omega m)^{-1}$	0.0
Reluctivity (NUX,Y,Z)	1.136 x 10^{-4} H/m	1.25 x 10^{-6} H/m	6.67 x 10^{-6} H/m	1.380 x 10^{-4} H/m	1.25 x 10^{-6} H/m

(*): Not Applicable

The applied external boundary conditions for the PMBDCLM and DC servomotor FEA models are listed in Table 4-5.

Table 4-5. External Boundary Conditions

External B.C	Value	Direction	Geometric Location
Specific Field Potential *(V)*	0.0 V	*	Periphery
	50V – 265 V	*	Current Region/Coil
Current Density *(J)*	10.47 x 10^5 A/m^2 – 55.50 x 10^5 A/m^2	X,Y,Z-Component	Current Region/Coil
Coercive Field Strength *(Hc)* (PMAGNET)	2.067 x 10^6 A/m-*Hci* (26,000 Oe-*Hci*)	X,Y,Z-Component	Permanent Magnet Array on Primary
Specific Temperature *(Tp)*	0.0 °C	*	Periphery
Applied Force *(F)*	700 N	X-Component	Secondary
Applied Torque *(T)*	700 N	CW	Armature
Moment *(M)*	0.0	CW-CCW	Primary
Rotation *(R)*	0.0	θ, ϕ, ω	Primary
Displacement *(X)*	0.0	X, Y, Z	Primary
Friction Coefficient *(μ_k)*	0.08	*	Secondary Guideway

(*): Not Applicable

4.3.3.1 FEA Results: From the proposed analysis, thermal, static, dynamic, and electromagnetic results are listed in Table 4-6. Figures 4-1 through 4-6 provide a graphical representation.

Table 4-6. Finite Element Analysis Results

Applied Voltage/ Gap Size	(50V)	(100 V)	(150 V)	(200 V)	(250 V)	(265V)
Magnet Array Temperature (°C) [No Force/Force(700N, -X Dir.)]						
0.625 mm	123.2/139.5	138.6/156.9	152.9/173.1	166.3/188.2	178.7/202.3	182.9/206.5
3.175 mm	115.0/130.7	129.3/147.0	142.7/162.2	155.1/176.3	166.8/189.5	171.0/193.7
6.350 mm	107.0/122.2	120.4/137.4	132.8/151.6	144.4/164.9	155.2/177.2	159.4/181.4
Air-gap Temperature (°C) [No Force/Force(700N, -X Dir.)]						
0.625 mm	181.2/200.8	203.9/225.9	224.9/249.2	244.5/271.0	262.9/291.3	267.1/295.5
3.175 mm	171.2/190.2	192.6/214.0	212.5/236.1	231.0/256.7	248.3/276.0	252.5/280.2
6.350 mm	144.0/180.0	161.9/202.4	178.6/223.3	194.2/242.8	208.8/261.1	213.0/265.3
Ampere's Force (N) [No Force/Force(700N, -X Dir.)]						
0.625 mm	124/376	1332/1586	2541/2800	3743/4011	4969/5225	5473/5722
3.175 mm	106/321	1174/1389	2240/2455	3292/3515	4358/4581	4769/4987
6.350 mm	29/244	949/1168	1880/2093	2800/3018	3719/3940	4011/4231
DC Servo Torque (N-m) [No Force/Force(700N, Counterclockwise)]						
	-31/218	-593/778	-1154/1337	-1714/1895	-2272/2453	-2564/2743
Linear Displacement, X-Direction. (mm) [No Force/Force(700N, -X Dir.)]						
0.625 mm	-299/434.4	-547.7/-241.3	-796.8/-515.1	-1102.9/-941.8	-1481.7/-1372.1	-1549.8/-1417.6
3.175 mm	-174/607.5	-462.3/342.6	-712.8/-7.138	-1021.2/-702.1	-1398.6/-1017.2	-1471.5/-1109.5
6.350 mm	-120/712.8	-371.5/433.1	-623.7/131.4	-929.8/-589.7	-1307.2/-705.4	-1391.9/-812.9
Resultant Flux Density Wb/m^2, T [No Force/Force(700N, -X Dir.)]						
0.625 mm	8.338/10.49	15.53/17.68	22.71/24.87	29.90/32.06	37.09/39.25	37.52/39.68
3.175 mm	9.063/9.377	14.43/16.59	21.64/23.80	28.85/31.02	36.07/38.23	37.51/39.67
6.350 mm	5.997/8.139	13.14/15.28	20.27/22.42	27.41/29.56	34.55/36.69	35.98/38.12
Resultant Electric Field V/m [No Force/Force(700N, -X Dir.)]						
0.625 mm	538E1/7285E1	952.1E1/114.2E2	136.6E2/155.6E2	178.0E2/197.0E2	218.6E2/238.4E2	231.8E2/250.8E2
3.175 mm	491.7E1/717.9E1	983.5E1/121.0E2	147.5E2/170.1E2	196.7E2/219.3E2	245.9E2/268.5E2	260.6E2/283.2E2
6.350 mm	132.3E1/233.8E1	352.9E1/454.4E1	573.5E1/675.0E1	794.1E1/895.5E1	101.5E2/111.6E2	108.1E2/118.2E2
X-Direction Stress (SXX) N/m^2 [No Force/Force(700N, -X Dir.)]						
0.625 mm	0/574.2E3	0/112.2E4	0/225.7E4	0/325.3E4	0/504.8E4	0/549.3E4
3.175 mm	0/244.5E3	0/260.6E3	0/425.2E3	0/991.6E3	0/215.6E4	0/289.5E4
6.350 mm	0/244.8E3	0/245.2E3	0/331.3E3	0/910.1E3	0/128.7E4	0/136.9E4
Y-Direction Stress (SYY) N/m^2 [No Force/Force(700N, -X Dir.)]						
0.625 mm	0/278.0E3	0/577.1E3	0/119.6E4	0/173.9E4	0/271.954	0/296.2E4
3.175 mm	0/304.1E2	0/368.3E2	0/610.4E2	0/144.3E3	0/315.5E3	0/424.1E3
6.350 mm	0/302.9E2	0/299.4E2	0/467.0E2	0/130.3E3	0/184.7E3	0/225.4E3
Z-Direction Stress (SZZ) N/m^2 [No Force/Force(700N, -X Dir.)]						
0.625 mm	0/149.1E3	0/373.2E3	0/837.0E3	0/124.4E4	0/197.8E4	0/216.0E4
3.175 mm	0/990.6E2	0/959.4E2	0/150.6E3	0/364.4E3	0/804.0E3	0/108.3E4
6.350 mm	0/984.8E2	0/961.3E2	0/113.4E3	0/329.4E3	0/469.9E3	0/575.2E3
Maximum Shear Stress N/m^2 [No Force/Force(700N, -X Dir.)]						
0.625 mm	0/359.7E4	0/694.5E4	0/138.7E5	0/199.5E5	0/309.2E5	0/336.4E5
3.175 mm	0/179.4E3	0/177.9E3	0/288.8E3	0/677.4E3	0/147.6E4	0/198.3E4
6.350 mm	0/159.0E3	0/157.5E3	0/196.2E3	0/538.8E3	0/761.7E3	0/928.7E3
Ochtahedral Stress N/m^2 [No Force/Force(700N, -X Dir.)]						
0.625 mm	0/293.7E4	0/567.1E4	0/113.3E5	0/162.9E5	0/252.5E5	0/274.7E5
3.175 mm	0/146.8E3	0/145.7E3	0/236.7E3	0/554.7E3	0/120.9E4	0/162.4E4
6.350 mm	0/135.9E3	0/135.9E3	0/171.6E3	0/471.3E3	0/666.3E3	0/812.3E3

Dynamic Analysis Results							
Characteristics		**Input Voltage (V)**					
App. Force (N)	**Dynamic Response**	**50V (5A)**	**100V (10A)**	**150V (15A)**	**200V (20A)**	**250V (25A)**	**265V (26.5A)**

Table 4-6. (Continued)

0.0	Velocity (m/s)	-0.914	-1.545	-2.176	-2.806	-3.437	-3.595
	Accel. (m/s^2)	-1.016	-1.716	-2.418	-3.118	-3.819	-3.994
	Position (m)	-0.415	-0.701	-0.987	-1.273	-1.559	-1.631
	Frequency (10^{-3} KHz)	0.732	2.691	3.655	6.742	8.102	8.735
	Force (N)	29.0	263.0	491.0	748.0	972.0	1024.0
L (73.2)	Velocity (m/s)	0.0946	-0.221	-0.536	-0.852	-1.167	-1.325
	Accel. (m/s^2)	0.1051	-0.245	-0.596	-0.946	-1.296	-1.472
	Position (m)	0.0429	-0.100	-0.243	-0.386	-0.529	-0.601
	Frequency (10^{-2} KHz)	1.819	3.781	4.741	7.850	9.218	9.862
	Force (N)	41.0	276.0	508.0	752.0	988.0	1043.0
C (125)	Velocity (m/s)	0.1261	-0.190	-0.505	-0.821	-1.136	-1.294
	Accel. (m/s^2)	0.1401	-0.211	-0.561	-0.912	-1.262	-1.437
	Position (m)	0.0572	-0.086	-0.229	-0.372	-0.514	-0.586
	Frequency (10^{-2} KHz)	1.857	3.819	4.752	7.888	9.256	9.900
	Force (N)	93.0	321.0	562.0	791.0	1013.0	1066.0
H (204)	Velocity (m/s)	0.1673	-0.148	-0.464	-0.779	-1.095	-1.253
	Accel. (m/s^2)	0.1860	-0.164	-0.515	-0.866	-1.217	-1.392
	Position (m)	0.0769	-0.066	-0.209	-0.352	-0.495	-0.567
	Frequency (10^{-2} KHz)	1.906	3.868	4.801	7.937	9.305	9.949
	Force (N)	172.0	401.0	638.0	871.0	1103.0	1159.0

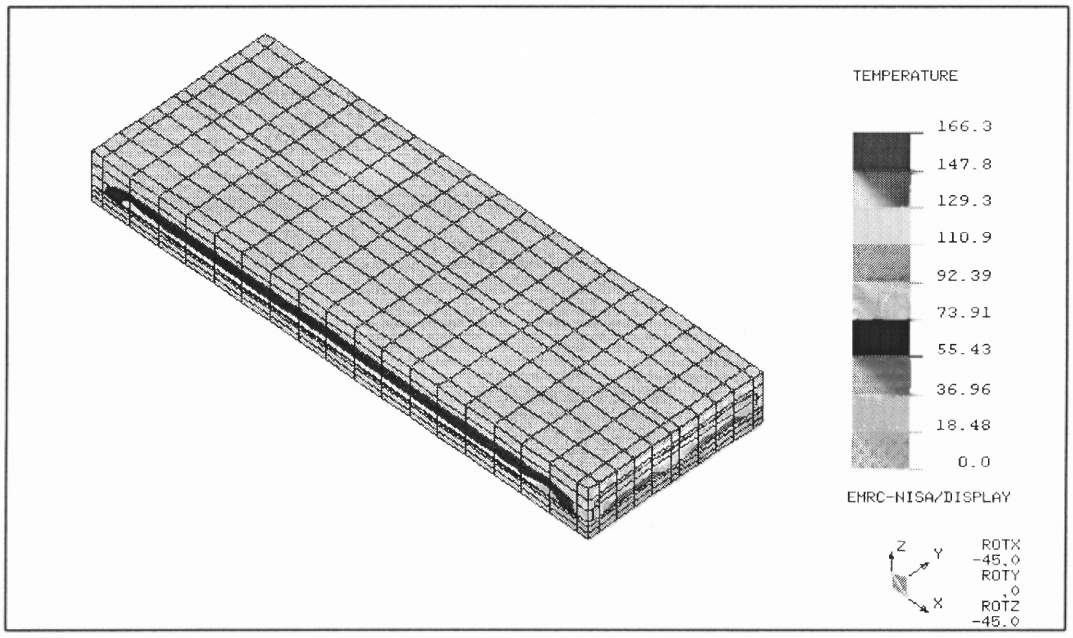

Figure 4-1. PMBDCLM Magneto-Thermal Analysis

Figure 4-1 illustrates the temperature distribution in the PMBDCLM at 200V with no applied force. A maximum temperature of 166.3 °C resides in the current carrying and air-gap elements.

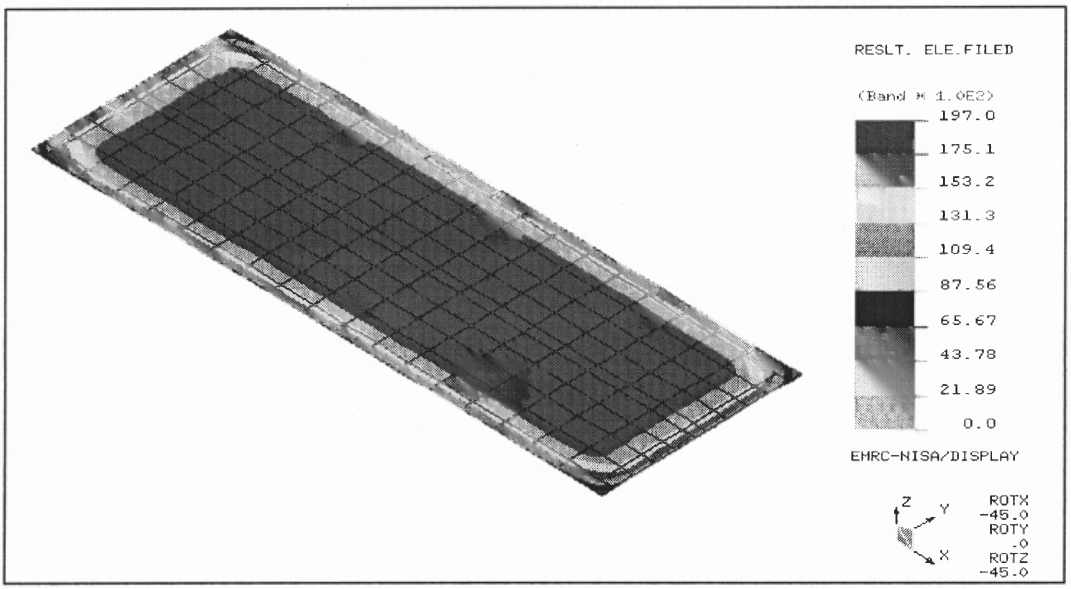

Figure 4-2. PMBDCLM (Air-Gap Region) Resultant Electric Field

Figure 4-2 illustrates the resultant electric field in the air-gap elements of the PMBDCLM at 200V with no applied force. A maximum field distribution of 197.0 x 10^2 V/m is evenly distributed at the center of the model.

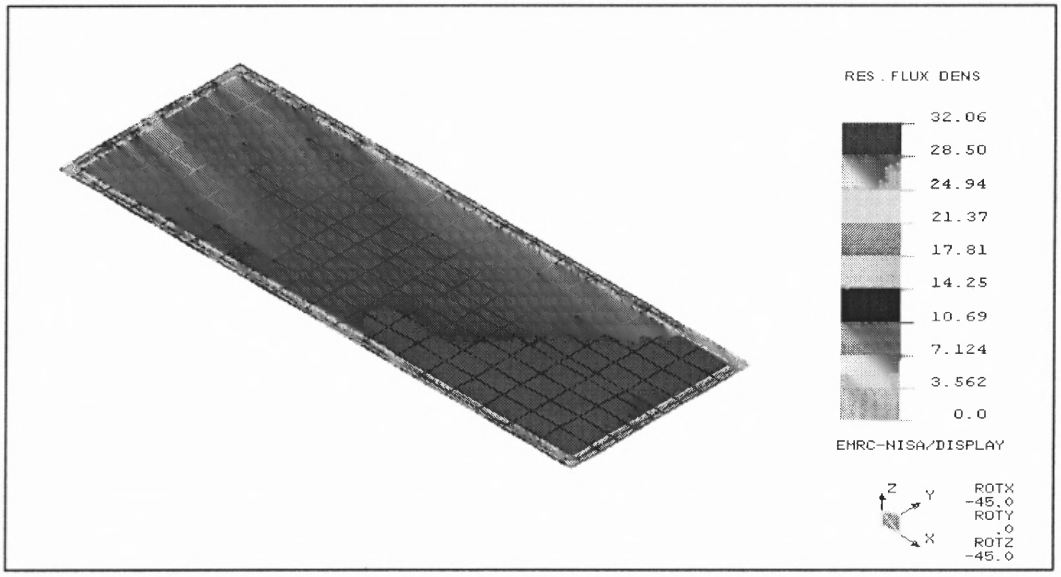

Figure 4-3. PMBDCLM (Air-Gap Region) Resultant Flux Density

Figure 4-3 illustrates the resultant flux density in the air-gap elements of the PMBDCLM at 200V with applied force. A maximum flux density distribution of 32.06 T is evenly distributed at the center of the model.

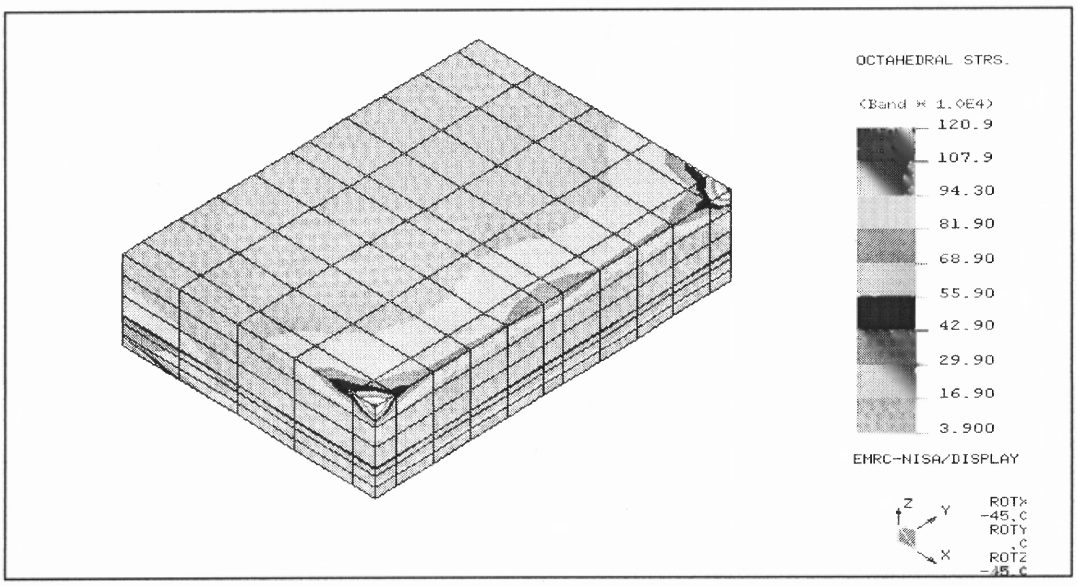

Figure 4-4. PMBDCLM (Quarter Region) Static Analysis

Figure 4-4 illustrates the octahedral stresses of the PMBDCLM quarter region at 250V with applied force. A maximum stress of 120.9 x 10^4 N/m^2 is located at the PMBDCLM slider edges and where stress is evenly distributed at the applied force region.

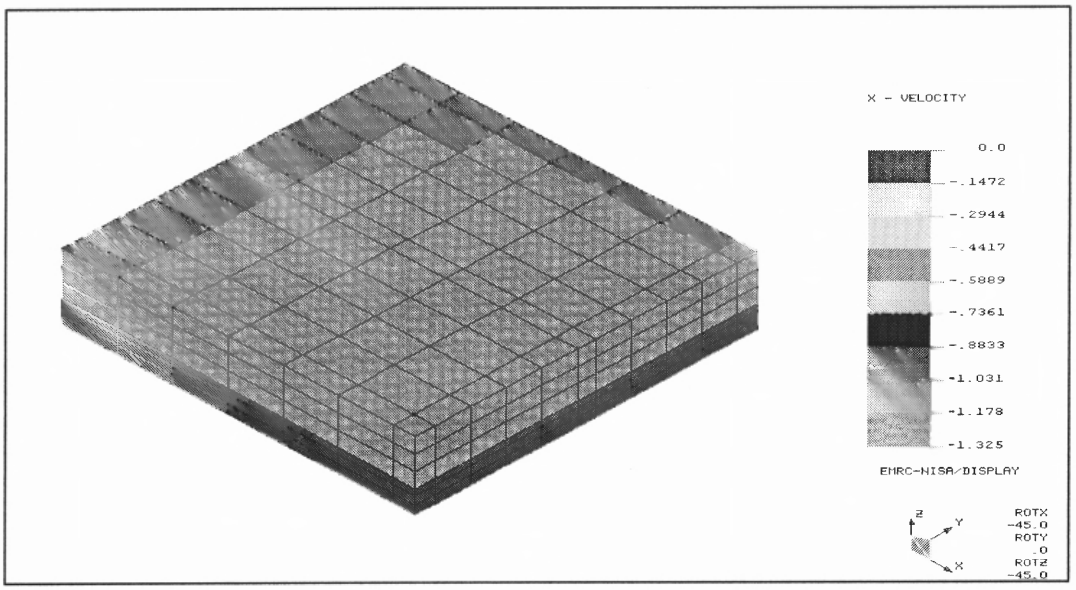

Figure 4-5. PMBDCLM Slider Velocity

Figure 4-5 illustrates the PMBDCLM slider velocity at 265V with applied force. The slider has a velocity of –1.325 m/s (the negative value indicates direction) while the permanent magnet primary remain fixed.

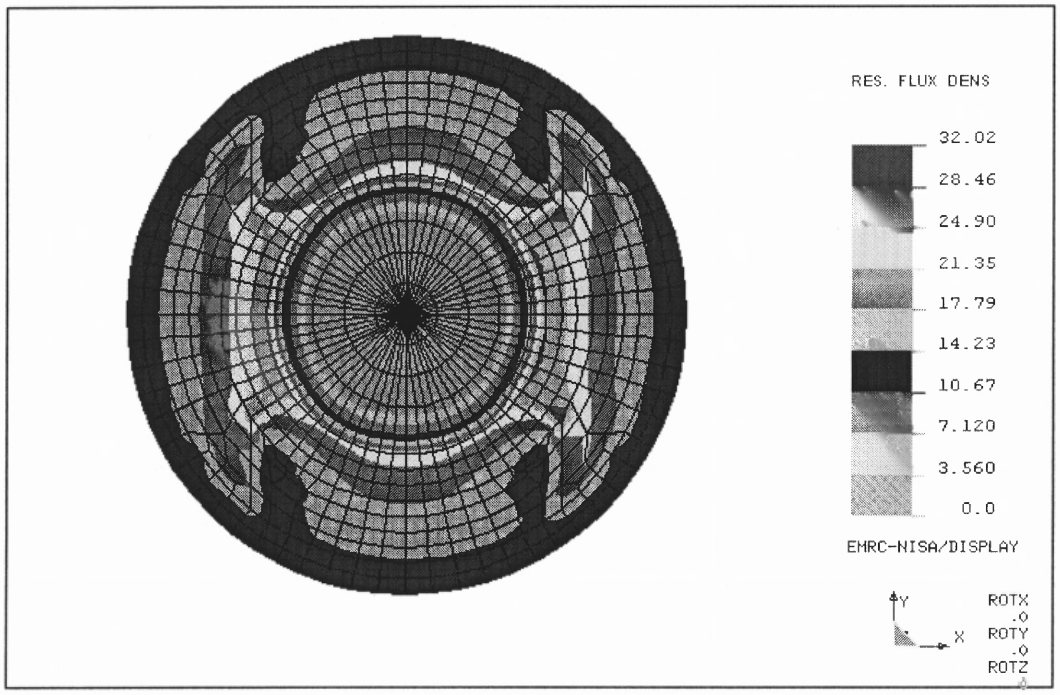

Figure 4-6. DC Servo Motor Magnetic Field Analysis

Figure 4-6 illustrates the DC servomotor resultant flux density at 250V with applied torque. A maximum flux density distribution of 32.02 T is evenly distributed between the permanent magnet and current carrying elements.

4.3.3.2 FEA Feedrate Justification: Utilization of fundamental relationships of velocity and power, and by using the generated force from the FEA, simulated feedrate values are generated from the following relationship:

$$\vec{V}_{\max} = \frac{\left(\frac{V}{R}\right)^2 R}{F_c} = \frac{\frac{V^2}{R}}{\left[\sum_{i=1}^{n}\left(\vec{B} \times \vec{J}\right)_i\right]} = \frac{\frac{V^2}{R}}{\vec{F}_{FEA}} \qquad (4\text{-}1)$$

where;

[V_{max}= Maximum Velocity, F_c= Force at Cutter, $\vec{F}_{FEA}$ = Generated Force, V = Input Voltage, R = Coil Resistance, $\vec{B}$ = Magnetic Flux Density, $\vec{J}$ = Current Density]

For the relationships described above, Table 4-7 lists the solution values of the PMBDCLM feed drive using the solutions obtained from the finite element analysis for each variant.

Table 4-7. Feedrate Results

PMBDCLM Secondary Velocity (Feedrate) m/s						
Air-Gap Size	**50V**	**100V**	**150V**	**200V**	**250V**	**265V**
0.625 mm	0.6648	0.6305	0.8036	0.9973	1.1961	1.227
3.175 mm	0.7788	0.7199	0.9199	1.1379	1.3643	1.4081
6.350 mm	1.0246	0.8562	1.0755	1.3263	1.5863	1.6597

An air gap size of 0.625 mm provides 0.6648 m/s feedrate at 50V and 1.227 m/s feedrate at 265V. An air gap size of 3.173 mm provides a feedrate of 0.7788 m/s at 50V and a feedrate of 1.4081 m/s at 265V. An air gap size of 6.350 mm provides a feedrate of 1.0246 m/s at 50V and a feedrate of 1.6597 m/s at 265V. These feedrate ranges are utilized for the design of experiments based on the proposed FEA models.

4.4 FEA Analysis of Results

Finite element analysis illustrates the effect of input voltage and applied force, as in machining applications, on a linear motor's performance characteristics such as generated force, temperature, stress, velocity, position, and acceleration. Including variants (voltage (variant 1), air-gap size (variant 2), and force (variant 3)) in the FEA simulation significantly changes the performance. Figures 4-7 through 4-18 illustrate the variant effects.

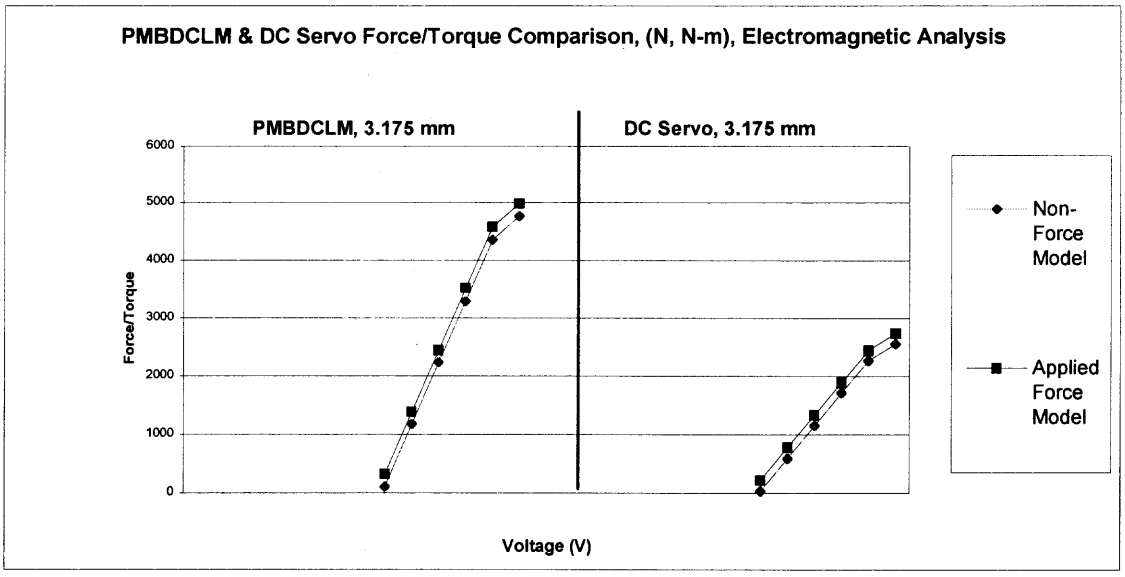

Figure 4-7. PMBDCLM/DC Servo Force/Torque Comparison

Figure 4-7 shows the comparison of force/torque between each PMBDCLM air-gap size and the DC servo motor at an air-gap size of 3.175 mm. From the analysis:

1. The DC servo motor generates a smaller torque/force relationship as compared to the PMBDCLM with the same boundary conditions.
2. As with the linear motor models, the torque increases with a torque/force boundary condition.
3. There is a linear relationship between voltage and generated force.

The localization of heat generation is approximated on the two surfaces shown in Figures 4-8 and 4-9. The two surfaces are:

i. The magnet array on the primary thermal distribution.

ii. The air-gap plane thermal distribution.

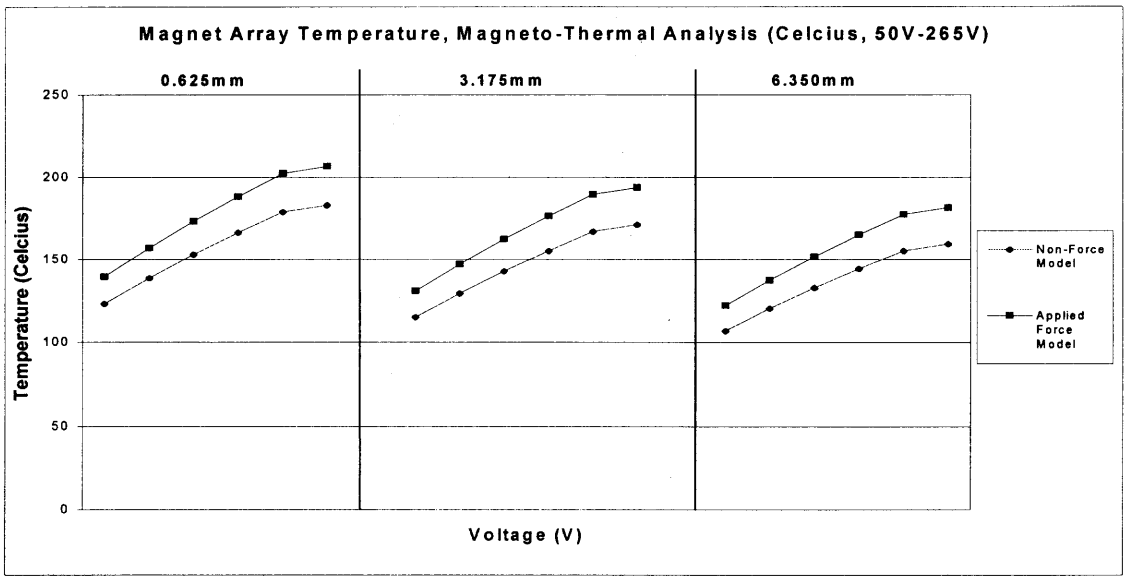

Figure 4-8. Magnet Array Temperature, Magneto-Thermal Analysis

Figure 4-8 illustrates the magnet array temperature of the PMBDCLM from 50V to 265V at each air-gap size using magneto-thermal finite element analysis. From the magneto-thermal analysis of the magnet-array temperature:

1. The finite element model with the applied force boundary condition results in a higher temperature than the model without applied force.
2. It is shown that as the PMBDCLM air-gap size increases, the magnet array temperature decreases. This indicates that a small air-gap size has the potential of reducing generated force due to thermal demagnetization of the NdFeB magnets.
3. The magnet array temperature is below the range where demagnetization occurs.

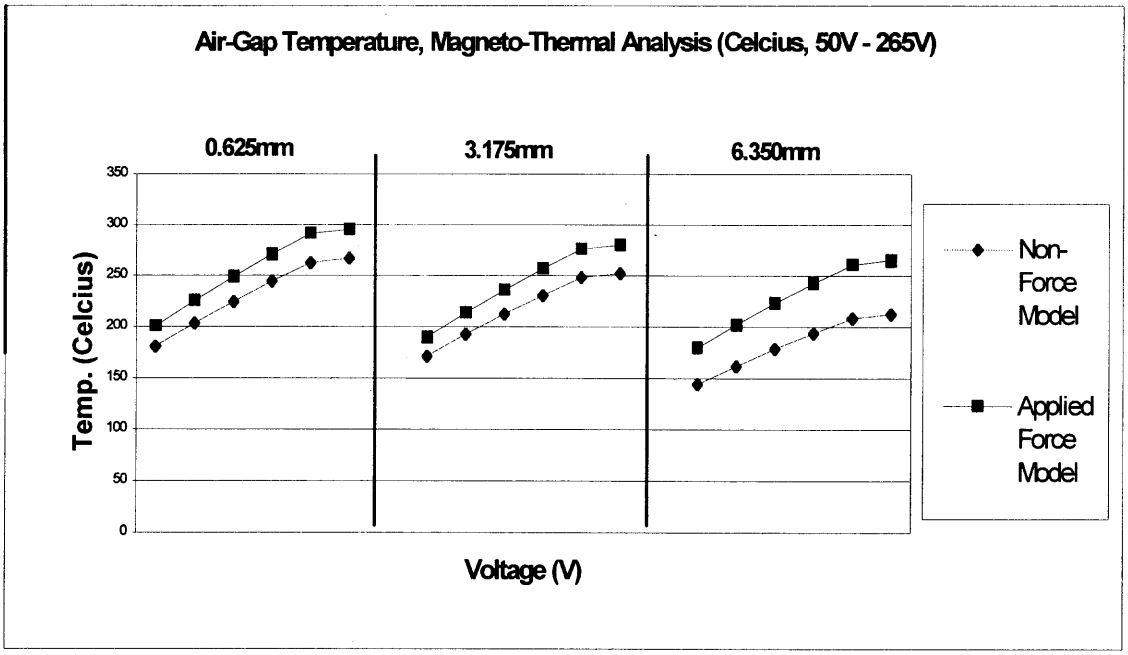

Figure 4-9. Air-Gap Temperature, Magneto-Thermal Analysis

Figure 4-9 illustrates the PMBDCLM air-gap temperature from 50V to 265V at the three air-gap sizes. Both the applied force and non-applied force models are shown. From the magneto-thermal analysis of the air-gap temperature:

1. The temperature distribution is higher in the air-gap region than in the magnet array region.
2. The applied force boundary condition model results in a higher temperature than the model without applied force.
3. The 6.350 mm air-gap size has a lower temperature with a larger difference between the applied force and non-applied force models.

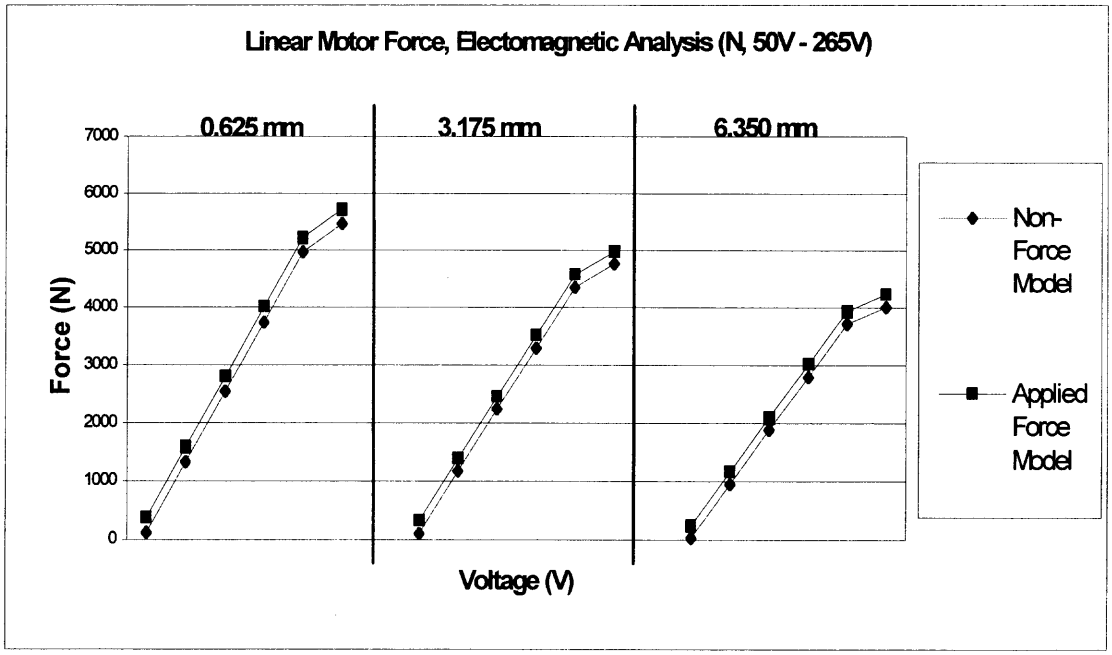

Figure 4-10. Linear Motor Force, Electromagnetic Analysis

Figure 4-10 illustrates the PMBDCLM generated force on the secondary form 50V to 265V at all three air-gap sizes. From the electromagnetic analysis for generated force on the motors' secondary:

1. A linear relationship exists between generated force and input voltage boundary conditions.
2. The applied force models result in a higher secondary thrust force.
3. A smaller air-gap size results in a higher secondary thrust force.

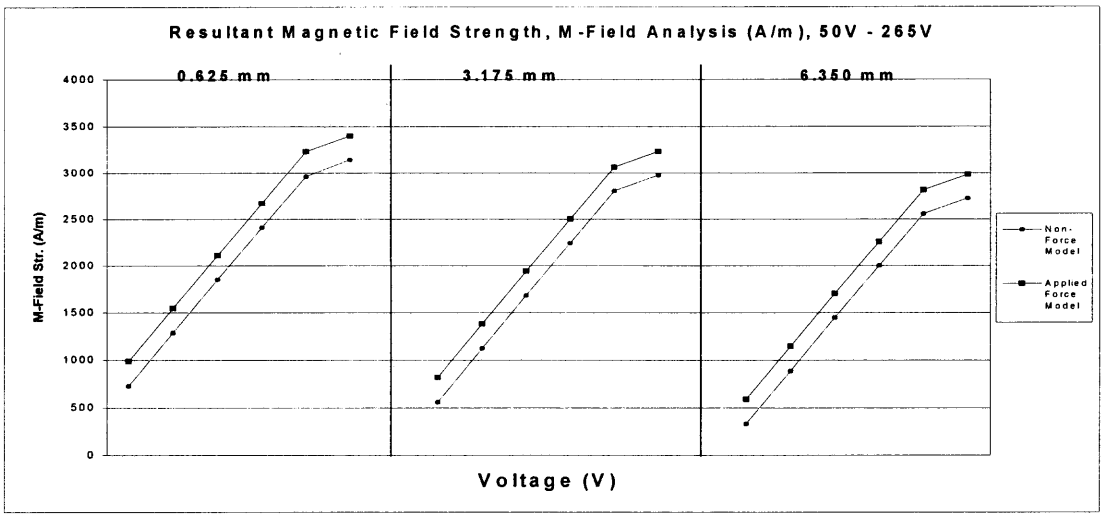

Figure 4-11. Resultant Magnetic Field Strength, Magnetic Field Analysis

Figure 4-11 illustrates the resultant magnetic field strength in the air-gap region at 50V to 265 V in all three air-gap sizes. From the magnetic field analysis:

1. The resultant magnetic field strength increases with the decease in the air-gap size.
2. The applied force models result in a higher resultant magnetic field strength.
3. A linear relationship exists between magnetic field strength and input voltage boundary conditions.

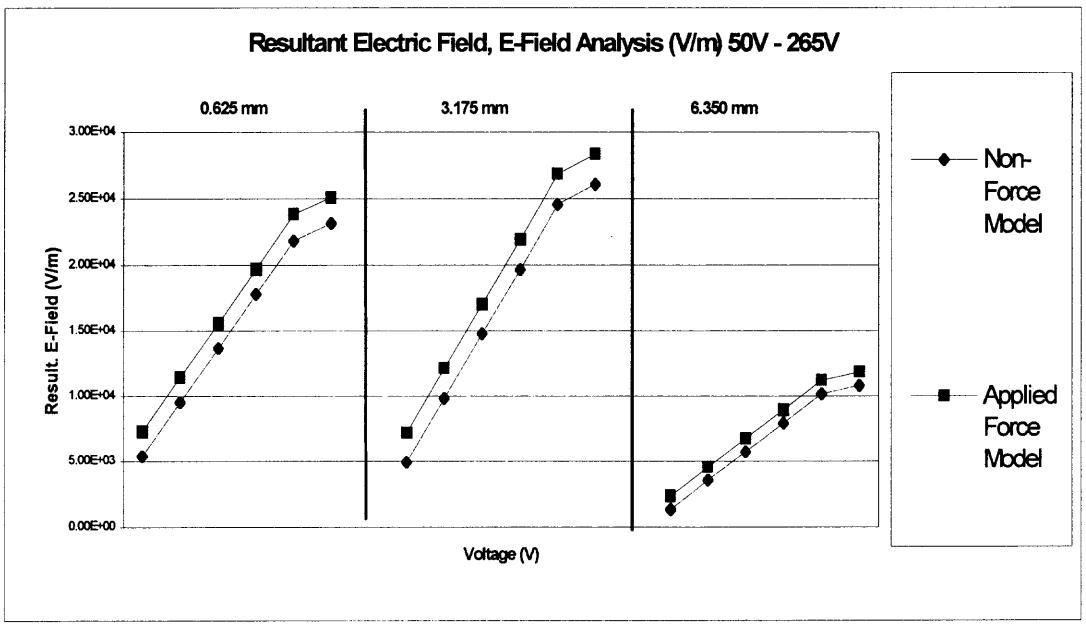

Figure 4-12. Resultant Electric Field Strength, E-Field Analysis

Figure 4-12 illustrates the resultant electric field strength in the air-gap region at 50V to 265V in all three air-gap sizes. From the electric field analysis:

1. A 3.175 mm air-gap size results in higher resultant electric field strength.
2. A linear relationship exists between electric field strength and input voltage boundary conditions.

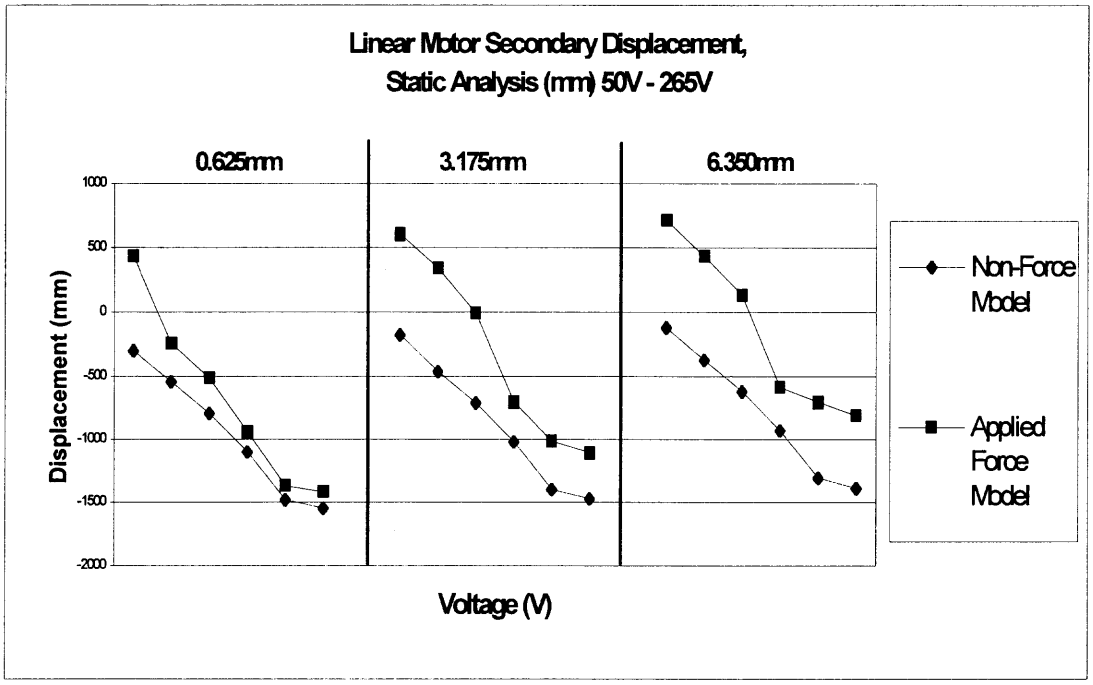

Figure 4-13. Linear Motor Secondary Displacement, Linear Static Analysis

Figure 4-13 illustrates the displacement of the PMBDCLM secondary at 50V to 265V in all three air-gap sizes. From the static analysis:

1. The applied force boundary condition model increases in displacement in the negative x-direction.
2. The larger air-gap size models generate less displacement due to the decrease in generated force.
3. The applied force models generate a displacement in the positive x-direction. This is due to the applied force being larger than the generated force of the motor.

4. Displacement decreases as air-gap size increases.

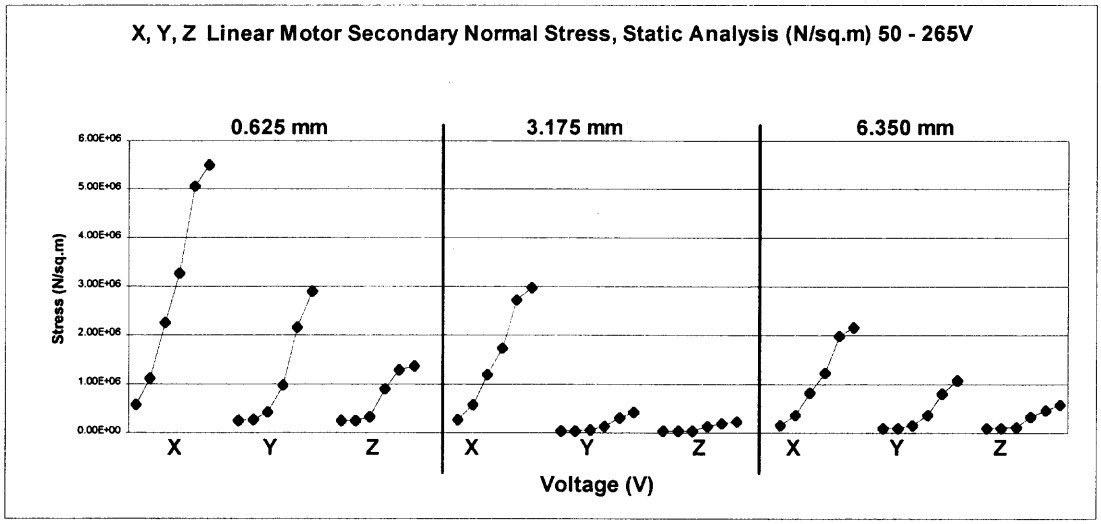

Figure 4-14. X, Y, Z-Component Normal Stress, Linear Static Analysis

Figure 4-14 illustrates the normal stress results at 50V to 265V of all three air-gap sizes. From the static analysis:

1. X-component normal stresses are the highest due to the applied force boundary condition on the motors' secondary.
2. Due to an increased generated force in the 0.625 mm air-gap model, normal stress is highest for each component.

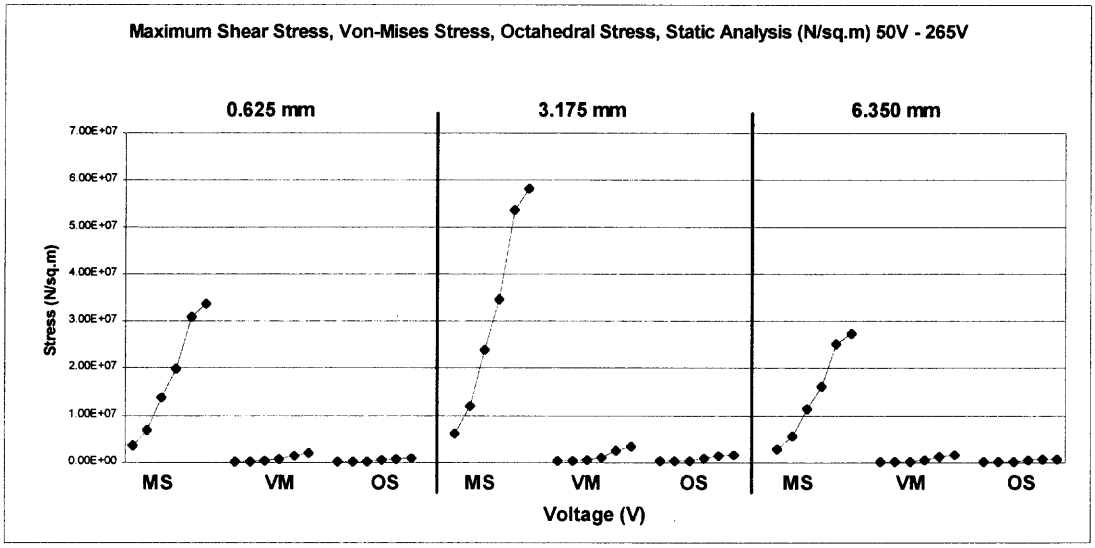

Figure 4-15. Maximum Shear Stress, Linear Static Analysis

Figure 4-15 illustrates the maximum shear stress, Von-Mises stress, and octahedral stress at 50V to 265V in all three air-gap size models. From the static analysis:

1. The maximum shear stress is the highest for all three air-gap sizes.
2. Von-Mises and octahedral stresses are not significant.

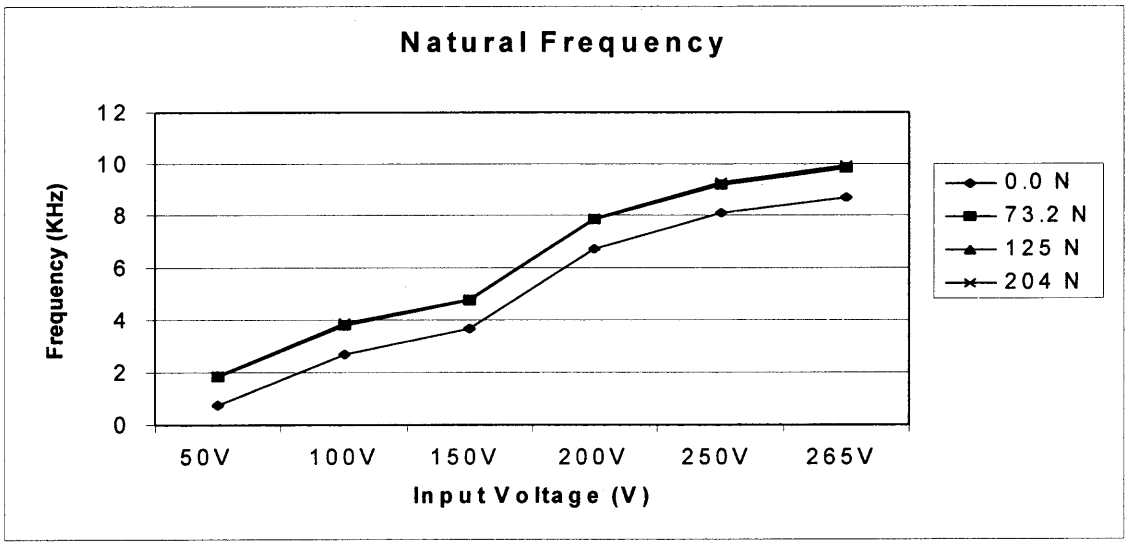

Figure 4-16. Natural Frequency

Figure 4-16 illustrates the FEA dynamic analysis natural frequency results of the PMBDCLM at each applied force boundary condition and at each input voltage.

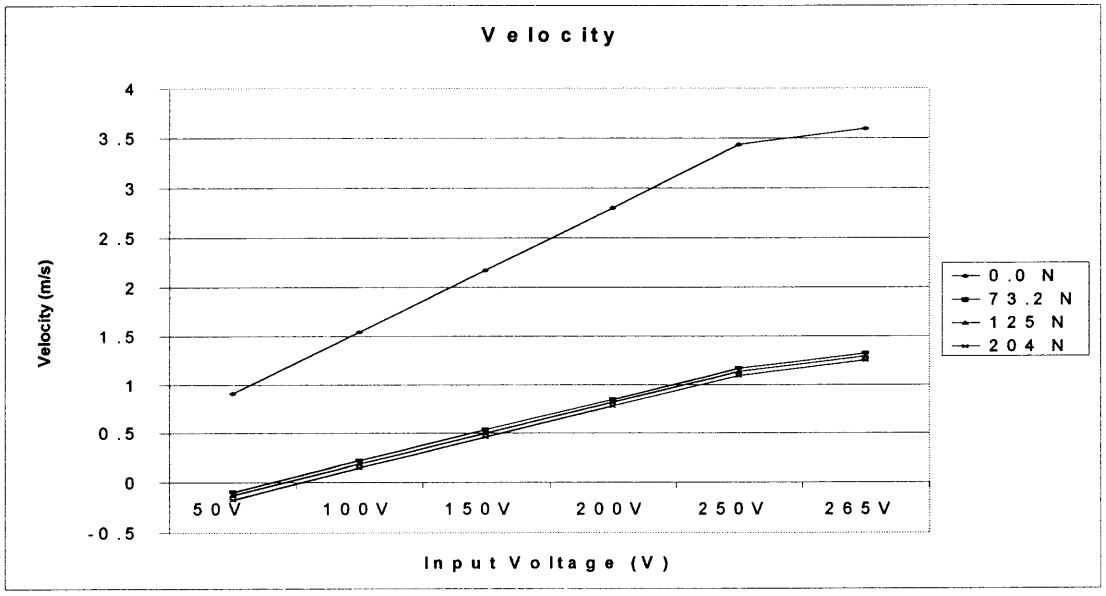

Figure 4-17. Velocity

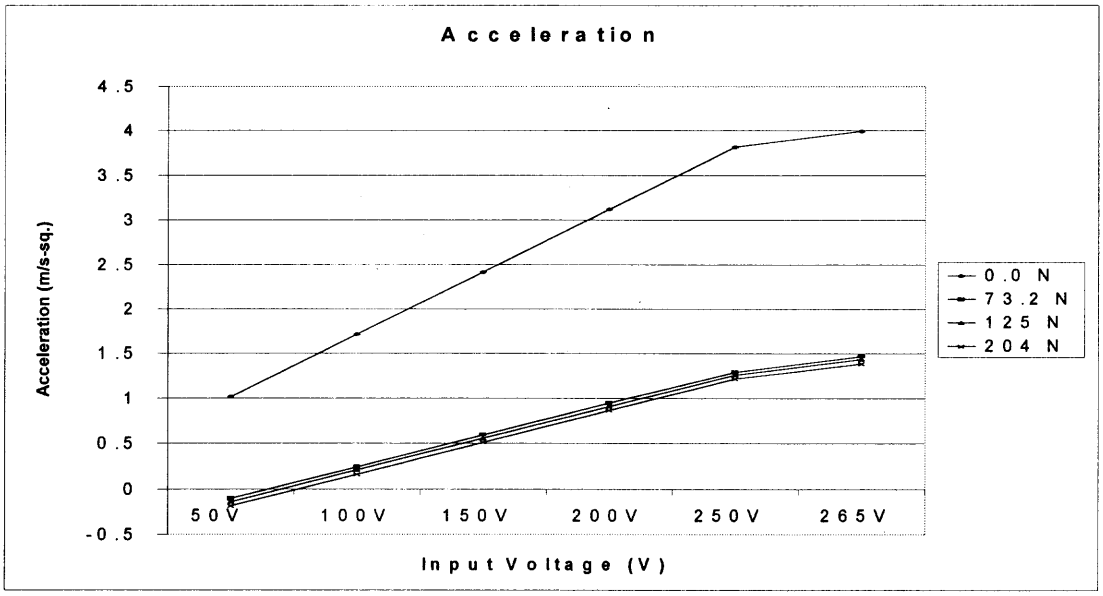

Figure 4-18. Acceleration

Figures 4-16, 4-17, and 4-18 illustrate generated force, velocity, and acceleration of the PMBDCLM using dynamic post processing. Each graph shows a linear relationship between input voltage and the performance measure.

The analysis results are useful in the selection of appropriate feedrate parameter levels using a PMBDCLM as a CNC feed drive. It is shown that the results from the FEA simulation can possibly enhance and allow feedback for the feedrate and required power selection criteria by providing insight into the effects of force and input voltage on linear motor position, velocity, and acceleration.

From the FEA results, the following observations are provided.

- Higher feedrate(s) may be possible due to the higher theoretical values shown from FEA. These values justify that recommended feedrate(s) for milling with linear drives can be increased without sacrificing surface quality amplitude parameters.
- Linear motor performance is not compromised due to thermal considerations, static considerations (secondary stresses and displacement), electromagnetic considerations

(E-field, M-field, Force), and dynamic considerations (displacement, acceleration, and velocity).

- Force comparison for cutting conditions of PMBDCLM's and DC servo motors reveal that the linear drive outperforms the DC servo motor under similar boundary conditions.
- Due to the temperature stability of the NdFeB permanent magnet array, magneto-thermal analysis indicates the thermal energy product below the maximum operating temperature. Field strength, thus dynamic performance is not subject to power losses due to demagnetization.
- Air-gap thickness determines the rate of heat convection into the representative primary magnet array. A larger gap size FEA model reveals a smaller temperature both in the air-gap and permanent magnet elements. Air-gap size impacts on system performance, thus machining performance.
- E-field and M-field FEA results show an increased magnitude for applied cutting force models.
- Applied cutting force FEA models for electromagnetic analysis models show an increased secondary thrust force.
- Static analysis shows that the maximum allowable stresses are near the elements and nodes about the points of cutting force and their respective linear guideways.

Results of Analysis

From the analysis of variant finite element models, the optimal overall rating of the PMBDCLM, in terms of operation cost and performance, is determined. The performance rating ranging from best to worst provides a benchmark for the desired output

performance. The cost rating ranging from least to most provides a benchmark for power consumption. Both the performance and cost ratings incorporate the input parameters, such as air-gap size and input voltage, and the output parameters such as generated force, temperature, and displacement which results in the overall performance rating.

The summary of results for each analysis providing the trends and ratings are listed in Table 4-8.

Table 4-8. Summary of FEA Results

Factors	Force /Non-Force F/N-F	Air-Gap Size (mm)	E-Field (V/m)	M-Field (T)	Force (N)	Temp. (°C)		Displ. (mm)	Perform Rating (**)	Cost Rating (***)	Overall Rating (****)
						Gap	Array				
Voltage Variation Trend (50-265) (*, ***)	Force	0.625	LI	LI(M)	LI(M)	MI(M)	MI(M)	LI(M)	B	M	O
		3.175	LI(M)	LI	LI	MI	MI	MI	C		
		6.350	MI(L)	LI(L)	LI(L)	MI	MI	MI(L)	W	L	
	Non-Force	0.625	LI	LI(M)	LI(M)	MI(M)	MI(M)	MI(M)	B	M	O
		3.175	LI(M)	LI	LI	MI	MI	MI	C		
		6.350	MI(L)	LI(L)	LI(L)	MI	MI	MI(L)	W	L	
	Stress (N/m^2)										
			Normal (Direction)			Shear	Von Mises	Octahedral			
			X	Y	Z						
	Force	0.625	LI (M)	LI (M)	MI (M)	LI(M)	SI(L)	SI(L)	W	M	
		3.175	LI	SI	SI	LI(M)	SI(L)	SI(L)	C		
		6.350	MI (L)	MI (L)	SI (L)	LI(M)	SI(L)	SI(L)	B	L	O

(*) SI: small increase (**) W: worst (***) L: least (****) O: optimum level
MI: moderate increase C: central M: most
LI: large increase B: best

4.4.1 Voltage

Due to the change in input voltages, the PMBDCLM FEA dynamic response is altered in the following ways.

1. Input of 265 V provides the highest velocity, and acceleration, and position.
2. There is a 22.45% increase in velocity, acceleration, and position between input voltages when the linear motor is unloaded, a 37.10% increase in velocity and position between input voltages when a low force is applied, a 38.49% increase in velocity, acceleration and position between input voltages when moderate force is

applied, and a 40.44% increase in velocity between input voltages when high force is applied.

3. There is a 40.0% increase in acceleration between input voltages when low force is applied, and a 27.13% increase in acceleration between input voltages when high force is applied.
4. There is a 28.8% increase in position between input voltages when high force is applied.
5. There is a 50.72% difference in frequency between the 50-V and 100-V models and a 39.51% difference in frequency between the 150-V and 200-V models.

4.4.2 Air-Gap

Due to the change in air-gap size, the PMBDCLM FEA response is altered in the following ways.

1. The 0.625 mm air-gap size models provides the best performance in terms of generated force and displacement although the cost rating is the largest.
2. As a tradeoff, the 0.625 mm air-gap size models generates the largest amount of heat due to the high input voltage and small air-gap size for both the applied and non-applied force models and only has a moderate increase in temperature due to the input voltage.
3. The 0.625 and 3.175 mm air-gap size models result in a large output increase for the increase in input voltage.
4. Due to the large generated force, the 0.625 mm air-gap size model generates the largest amount of displacement in the motors' moving secondary.

5. Stresses in the 0.625 mm air-gap size models are largest due to the high forces.

4.4.3 Force

The proposed FEA illustrates the effect of applied force, as in machining applications, on PMBDCLM performance characteristics such as generated force, displacement, and temperature. Including force in the finite element analysis significantly changes the design of the motor parameters such as input voltage and air-gap size. From the proposed analysis, the following changes occur in the output performance.

1. There is a 75.37% decrease in velocity, acceleration, and position when a low level force is applied, a 76.79% decrease in velocity, acceleration, and position when moderate force is applied.
2. There is a 13.5% increase in velocity, acceleration, and position between low and moderate levels of force.
3. There is a 22.11% increase in velocity, acceleration, and position between the moderate and high force models.

CHAPTER 5

HEURISTIC CASE STUDY AND ANALYSIS

To illustrate the proposed heuristic, a case study and analysis is presented. Knowledge is based on experimentation using 7075-T6 aluminum, a two-flute solid carbide tool, no coolant, on a moving column PMBDCLM equipped vertical milling machine.

5.1 Design of Experiments

A [3x4x3] design is adopted for rough, finish, and semi-finish milling. Three levels (low, central, and high) of spindle speed are defined, four levels of feedrate (low, semi-low, semi-high, and high) are defined and three levels (low, central, and high) of depth of cut is defined. Spindle speed ranges from 1,181 RPM to 18,000 RPM, feedrate ranges from 21.25 in./min to 354 in./min and depth of cut ranges from 0.029 inches to 0.090 inches. A total of 36 runs are defined. 12 runs are conducted at each depth of cut for both contour and straight/taper geometry. Each run contains three replicates for each surface and is repeated on two blanks of aluminum for contour and straight/taper geometry. The mean, variance, and signal-to-noise ratio will measure the factorial design responses.

Based on the proposed experimental design, the levels, variables, and responses are listed in Table 5-1.

Table 5-1. Experimental Factors and Levels/Proposed Factorial Design

Controllable Factors		**Levels**			
	Roughing				
A	**Cutting Speed (RPM)**	**L** (1,181)	**C** (9,590)		**H** (18,000)
B	**Feedrate (in./min)**	**L** (42.5)	**SL** (163)	**SH** (193)	**H** (260)
C	**Depth of Cut (in.)**	**C** (0.06252)			**H** (0.090315)

Table 5-1. (Continued)

Finishing									
A	**Cutting Speed (RPM)**			**L** (1,990)		**C** (10,205)		**H** (18,000)	
B	**Feedrate (in./min)**			**L** (21.25)		**SL** (120)	**SH** (243)		**H** (354)
C	**Depth of Cut (in.)**			**L** (0.02992)					
Proposed Factorial Design									
	VARIABLE			**RESPONSES**					
RUN	**A**	**B**	**C**				***Y***	***Log(S)***	***S/N***
High									
1	L	L	H	$Y_{1,1}$	$Y_{1,2}$	$Y_{1,3}$	Y_1	L_1	S/N_1
2	C	SL	H	$Y_{2,1}$	$Y_{2,2}$	$Y_{2,3}$	Y_2	L_2	S/N_2
3	H	SH	H	$Y_{3,1}$	$Y_{3,2}$	$Y_{3,3}$	Y_3	L_3	S/N_3
4	C	H	H	$Y_{4,1}$	$Y_{4,2}$	$Y_{4,3}$	Y_4	L_4	S/N_4
5	L	H	H	$Y_{5,1}$	$Y_{5,2}$	$Y_{5,3}$	Y_5	L_5	S/N_5
6	H	H	H	$Y_{6,1}$	$Y_{6,2}$	$Y_{6,3}$	Y_6	L_6	S/N_6
7	H	SL	H	$Y_{7,1}$	$Y_{7,2}$	$Y_{7,3}$	Y_7	L_7	S/N_7
8	C	L	H	$Y_{8,1}$	$Y_{8,2}$	$Y_{8,3}$	Y_8	L_8	S/N_8
9	L	SH	H	$Y_{9,1}$	$Y_{9,2}$	$Y_{9,3}$	Y_9	L_9	S/N_9
10	C	SH	H	$Y_{10,1}$	$Y_{10,2}$	$Y_{10,3}$	Y_{10}	L_{10}	S/N_{10}
11	H	L	H	$Y_{11,1}$	$Y_{11,2}$	$Y_{11,3}$	Y_{11}	L_{11}	S/N_{11}
12	L	SL	H	$Y_{12,1}$	$Y_{12,2}$	$Y_{12,3}$	Y_{12}	L_{12}	S/N_{12}
Central									
13	L	SH	C	$Y_{13,1}$	$Y_{13,2}$	$Y_{13,3}$	Y_{13}	L_{13}	S/N_{13}
14	H	H	C	$Y_{14,1}$	$Y_{14,2}$	$Y_{14,3}$	Y_{14}	L_{14}	S/N_{14}
15	C	L	C	$Y_{15,1}$	$Y_{15,2}$	$Y_{15,3}$	Y_{15}	L_{15}	S/N_{15}
16	H	SL	C	$Y_{16,1}$	$Y_{16,2}$	$Y_{16,3}$	Y_{16}	L_{16}	S/N_{16}
17	L	SL	C	$Y_{17,1}$	$Y_{17,2}$	$Y_{17,3}$	Y_{17}	L_{17}	S/N_{17}
18	C	SH	C	$Y_{18,1}$	$Y_{18,2}$	$Y_{18,3}$	Y_{18}	L_{18}	S/N_{18}
19	L	H	C	$Y_{19,1}$	$Y_{19,2}$	$Y_{19,3}$	Y_{19}	L_{19}	S/N_{19}
20	C	SH	C	$Y_{20,1}$	$Y_{20,2}$	$Y_{20,3}$	Y_{20}	L_{20}	S/N_{20}
21	H	L	C	$Y_{21,1}$	$Y_{21,2}$	$Y_{21,3}$	Y_{21}	L_{21}	S/N_{21}
22	C	SL	C	$Y_{22,1}$	$Y_{22,2}$	$Y_{22,3}$	Y_{22}	L_{22}	S/N_{22}
23	L	L	C	$Y_{23,1}$	$Y_{23,2}$	$Y_{23,3}$	Y_{23}	L_{23}	S/N_{23}
24	H	SH	C	$Y_{24,1}$	$Y_{24,2}$	$Y_{24,3}$	Y_{24}	L_{24}	S/N_{24}
Low									
25	C	L	L	$Y_{25,1}$	$Y_{25,2}$	$Y_{25,3}$	Y_{25}	L_{25}	S/N_{25}
26	L	SL	L	$Y_{26,1}$	$Y_{26,2}$	$Y_{26,3}$	Y_{26}	L_{26}	S/N_{26}
27	H	SH	L	$Y_{27,1}$	$Y_{27,2}$	$Y_{27,3}$	Y_{27}	L_{27}	S/N_{27}
28	L	H	L	$Y_{28,1}$	$Y_{28,2}$	$Y_{28,3}$	Y_{28}	L_{28}	S/N_{28}
29	C	H	L	$Y_{29,1}$	$Y_{29,2}$	$Y_{29,3}$	Y_{29}	L_{29}	S/N_{29}
30	H	H	L	$Y_{30,1}$	$Y_{30,2}$	$Y_{30,3}$	Y_{30}	L_{30}	S/N_{30}
31	H	SL	L	$Y_{31,1}$	$Y_{31,2}$	$Y_{31,3}$	Y_{31}	L_{31}	S/N_{31}
32	L	L	L	$Y_{32,1}$	$Y_{32,2}$	$Y_{32,3}$	Y_{32}	L_{32}	S/N_{32}
33	C	SH	L	$Y_{33,1}$	$Y_{33,2}$	$Y_{33,3}$	Y_{33}	L_{33}	S/N_{33}
34	L	SH	L	$Y_{34,1}$	$Y_{34,2}$	$Y_{34,3}$	Y_{34}	L_{34}	S/N_{34}
35	H	L	L	$Y_{35,1}$	$Y_{35,2}$	$Y_{35,3}$	Y_{35}	L_{35}	S/N_{35}
36	C	SL	L	$Y_{36,1}$	$Y_{36,2}$	$Y_{36,3}$	Y_{36}	L_{36}	S/N_{36}

Experimentation is conducted on both a PMBDCLM equipped vertical milling machine and DC servomotor ballscrew equipped vertical milling machine operating at a

18,000 RPM maximum spindle speed and 354 inch per minute maximum feedrate. For each of the four aluminum blanks cut per machine (2 contour and 2 straight/taper), a new 0.75-inch diameter, two-flute (20° helix) HSK-30A taper, solid carbide tool is used. Both a contour and straight/taper part geometry is machined using the defined levels of spindle speed, feedrate, and depth of cut.

The contour design is illustrated in Figure 5-1. A 3-step contour design provides 12 surfaces at three different depths of cut. There are 36 surfaces and 36 point locations. Depth C provides a 4-inch diameter geometry with 12 equally spaced surfaces measuring 1.047 inches. Depth B provides a 3.50 inch diameter geometry with 12 equally spaced surfaces measuring 0.916 inches. Depth A provides a 3.0 inch diameter geometry with 12 equally spaced surfaces measuring 0.785 inches. Three z-direction levels or steps provide a 0.5 inch surface with 3 replicate surfaces of 0.167 inches. Four equally spaced mounting holes insures direct contact with the force transducer mount while allowing a 0.20 inch clearance between the tool and the mounting Allen-Cap bolts.

The contour geometry tool path, illustrated in Figure 5-2, shows the tool motion in relation to each surface. Moving counterclockwise, the tool cuts along each of the 36 surfaces at each of the operating parameter settings as described in the proposed factorial design. By design, the part program will not be halted during execution, therefore when each cut is completed the tool moves 0.25 inches off the surface to allow the force signal to "flat-line". This is beneficial since cutting force is easily distinguished from surface to surface all will help provide accurate force signal separation.

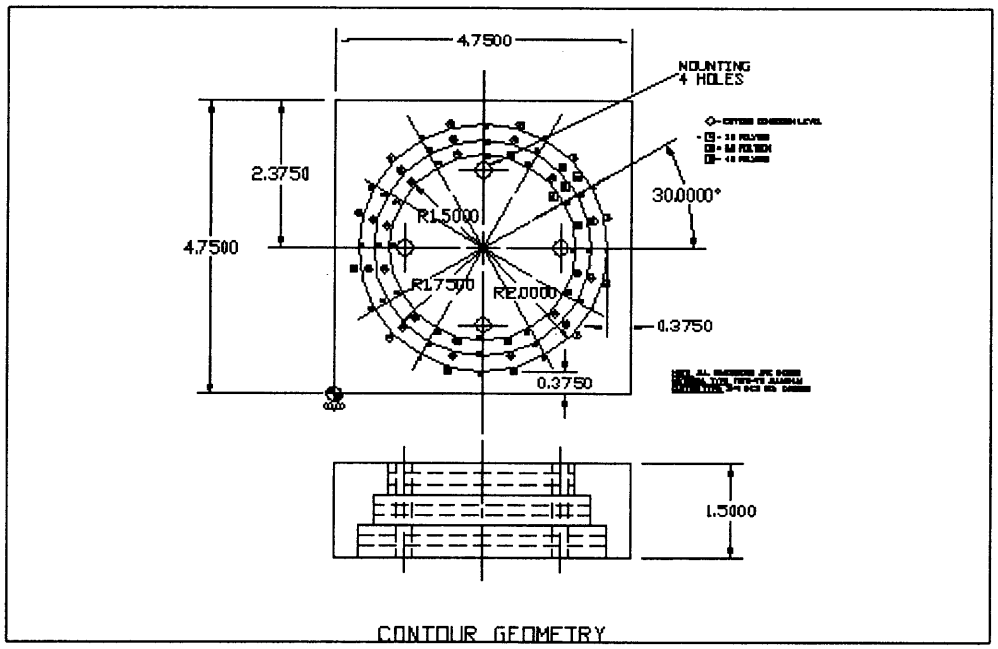

Figure 5-1. Contour Geometry

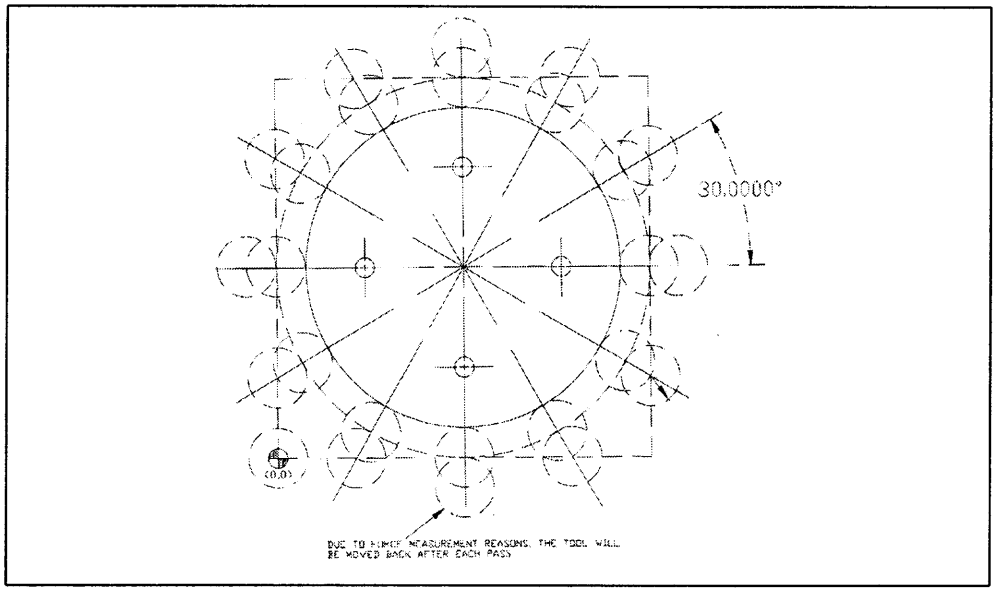

Figure 5-2. Contour Geometry Tool Path

The straight/taper design is illustrated in Figure 5-3. A 3-step polygon design provides 12 surfaces at three different depths of cut. There are 36 surfaces and 24 vertices. A blank size of 4.75 x 4.75 x 1.50 inches allows for 0.875 inch straight cuts along the X and Y axes and a 1.591 inch cut for each taper at depth C (roughing). Depth of cut B (3.50 inch polygon) provides a 0.75 inch length surface along the X and Y axes

and a 1.414 inch surface along each taper. Depth of cut A (finishing, 3-inch polygon) provides a 0.625 inch length surface along the X and Y-axes and a 1.237 inch surface along each taper. Three z-direction levels or steps provide a 0.5 inch surface with 3 replicate surfaces of 0.167 inches. Four equally spaced mounting holes insures direct contact with the force transducer mount while allowing a 0.20 inch clearance between the tool and the mounting Allen-Cap bolts.

The straight/taper geometry tool path, illustrated in Figure 5-4, shows to tool motion in relation to each surface. Moving counterclockwise, the tool cuts along each of the 36 surfaces at each of the operating settings as described in the proposed factorial design. By design, the part program will not be halted during execution, therefore when each cut is completed the tool moves 0.25 inches off the surface to allow the force signal to "flat-line". This is beneficial since cutting force is easily distinguished from surface to surface all will help provide accurate force signal separation.

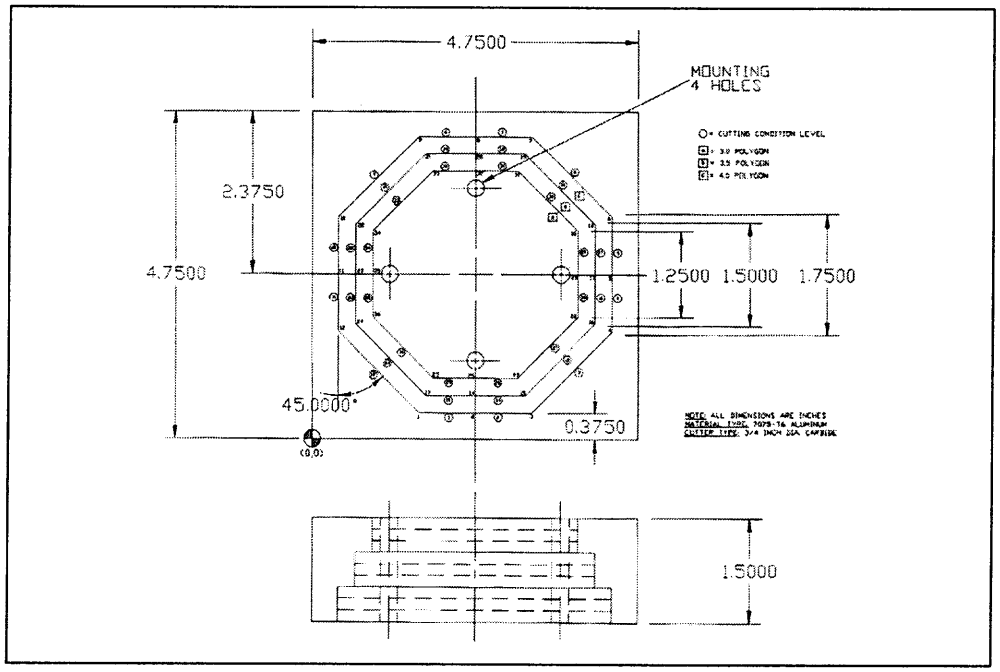

Figure 5-3. Straight/Taper Geometry

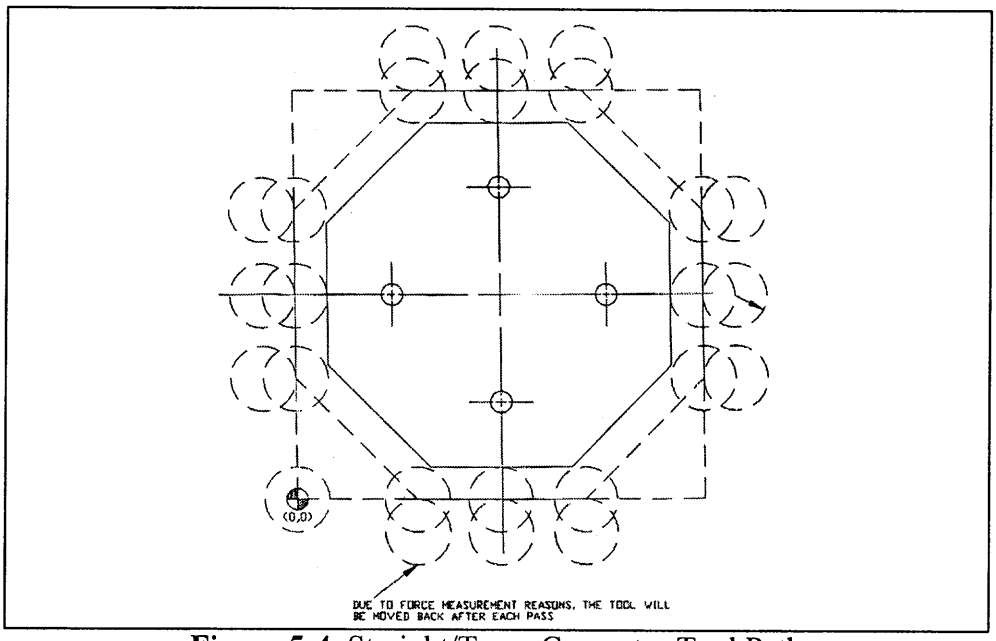

Figure 5-4. Straight/Taper Geometry Tool Path

Cutting is conducted on a PMBDCLM equipped vertical CNC milling machine and a DC servomotor/ballscrew equipped CNC vertical milling machine. Online cutting force data is measured and stored using a transducer, amplifier, and data acquisition board. Offline tolerance measurement is made using a Brown and Sharpe XCEL 765 coordinate measuring machine (BS765-CMM). Offline surface measurement is made with a Taylor and Hobson Surtronic 3+ surface profilometer.

Listed in Table 5-2 are the machine specifications for the PMBDCLM experimentation. Table 5-3 lists the DC servomotor/ballscrew specifications.

Table 5-2. PMBDCLM CNC Specifications

Overall Dimensions	1524 mm wide
	5435 mm long including utility packages
	3852 mm high
Machine Gross Weight	12,202 kg.
Anchoring	Above Floor design with 3 point leveling
Work Envelope	500 mm wide
	400 mm deep
	300 mm high
Work Table Size	500 mm
Work Height	1041 mm

Table 5-2. (Continued)

Machine Axis					
Label	**Axis Type**	**Motor Type**	**Stroke**	**Max .Travel Rate**	**Accel. Rate**
X	Horizontal	Linear Motor	500 mm	90 m/min	1.30 g
Y	Horizontal	Linear Motor	400 mm	90 m/min	0.75 g
Z	Vertical	Linear Motor	500 mm	90 m/min	1.60 g
C	Tool Drum	Servomotor	360 + °	300 deg/sec	5 deg/s/s
U	Gantry	Servomotor	882 mm	137 m/min	0.80 g

CNC Controller	Allen Bradley 9/290 CNC
Spindle	GMN High Frequency Spindle
	HCS 150 – 18000/9
	Automatic Tool Change
	Hydraulic Toolbar
	Coolant Through Spindle
	Grease Lubrication
Spindle Speed	0 to 18,000 RPM
Spindle Taper Size	HSK-50A Taper
Motor	12 HP @ 7,500 RPM to 18,000 RPM
Tool Changer	8 Tool Pocket Horizontal Rotating Disk
	Replaceable Breakaway Tool Holders
Maximum Tool Diameter	127 mm
Maximum Tool Length	296 mm
Operating Pressure	60 PSI

Table 5-3. DC Servo Motor CNC Specifications

Overall Dimensions	3175 mm wide
	1955.8 mm long
	2286 mm high
Machine Gross Weight	8,105 kg.
Work Envelope	889 mm wide
	500 mm deep
	375 mm high
Work Table Size	889 mm

Machine Axis				
Label	**Axis Type**	**Motor Type**	**Max. Travel Rate**	**Accel. Rate**
X	Horizontal	Servomotor	25.4 m/min	0.70 g
Y	Horizontal	Servomotor	25.4 m/min	0.70 g
Z	Vertical	Servomotor	25.4 m/min	0.70 g
C	Tool Drum	Air	160 deg/sec	2 deg/s/s

Ballscrew Size	31.75 mm
CNC Controller	Ultimax CNC Control
	115,000 Baud Transmission
	8 MB Memory, 650 MB HD

Table 5-3. (Continued)

Spindle	Automatic Tool Change
	Hydraulic Toolbar
	Grease Lubrication
Spindle Speed	Variable 40 to 18,000 RPM
Spindle Taper Size	NO. 50
Motor	15 HP @ 8,000 RPM to 18,000 RPM
Tool Changer	24 Position Horizontal Rotating Disk
Maximum Tool Diameter	76.2 mm
Maximum Tool Length	381 mm
Operating Pressure	80 PSI

Cutting force measurement is made using a Kistler force transducer and amplifier. During cutting, data is transferred to the UEI data acquisition board controlled by the STATUS software. Experimental settings are listed in Table 5-4.

Table 5-4. Force Acquisition Experimental Settings

Amplifier Settings for Experimentation		
Parameter	**Unit**	**Value**
Filtering (Low Pass)	Hz	10.0 KHz
Mode	V	Voltage
Transducer Sensitivity	mV/MU	10.0
Scale	MU/V	50.0
Voltage Range	V	-10.0 V to +10.0 V
Time Constant	Short (s)	0.10
Operating Temperature	°C	Room Temperature
Time Before Operation	Hour	1.0
STATUS Software Settings for Experiment		
Invoked Channels	0, 1, 2 (X, Y, Z)	
Range (Volts)	-10 to +10	
Gain	1.0	
Sampling Rate	500 Hz	
Samples/Channel	65536	
Total number of Samples	393,216	
Sampling Clock	Internal	
Data Transfer	Smart Cache	
Interrupt Level	11	
Analog Input	Single Ended	
Base Address	700	

5.2 Experimental Results

Figures 5-5 through 5-18 illustrate the mean results of the contour geometry and the straight/taper geometry for PMBDCLM and DC servomotor feed drives, respectively. Contour geometry performance index results include [tolerance] (position, circularity, cylindricity, runout, and total runout) and [surface finish] (kurtosis, skewness, spacing, wavelength, and peak-to-valley height). Straight/taper performance index results include [tolerance] (position, straightness, flatness, angularity, and parallelism) and [surface finish] (kurtosis, skewness, spacing, wavelength, and peak-to-valley height). Surface 1 through 12 represents the highest depth of cut, surface 13 through 24 represents a central depth of cut, and surface 25 through 36 represents a low depth of cut.

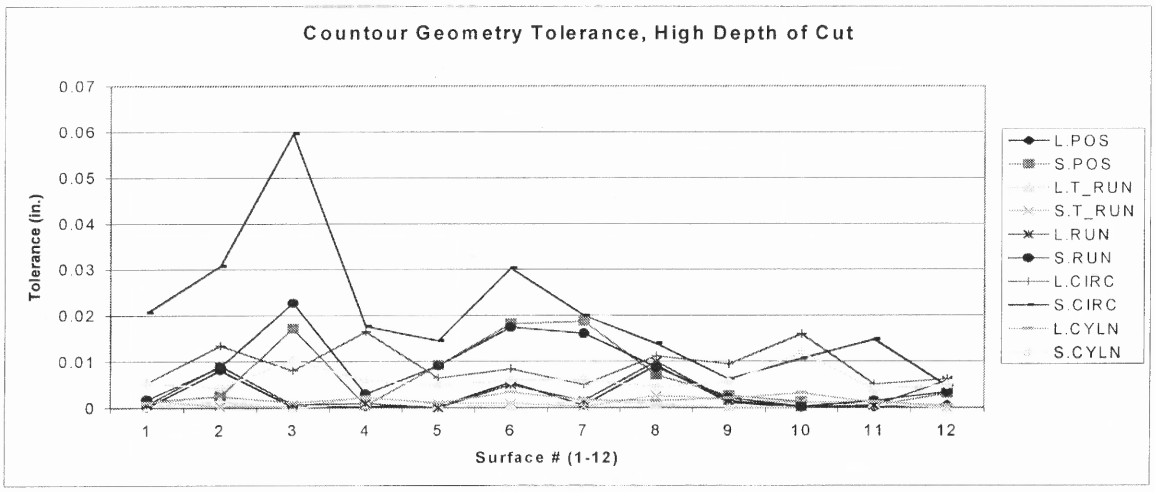

Figure 5-5. Contour Geometry Tolerance, High Depth of Cut

Figure 5-5 illustrates the PMBDCLM (L) and DC servomotor (S) contour geometry tolerance at a high depth of cut. From the figure, tolerance values are large at surface 3 and small at surface 12. DC servomotor tolerance values are generally larger than PMBDCLM tolerance values.

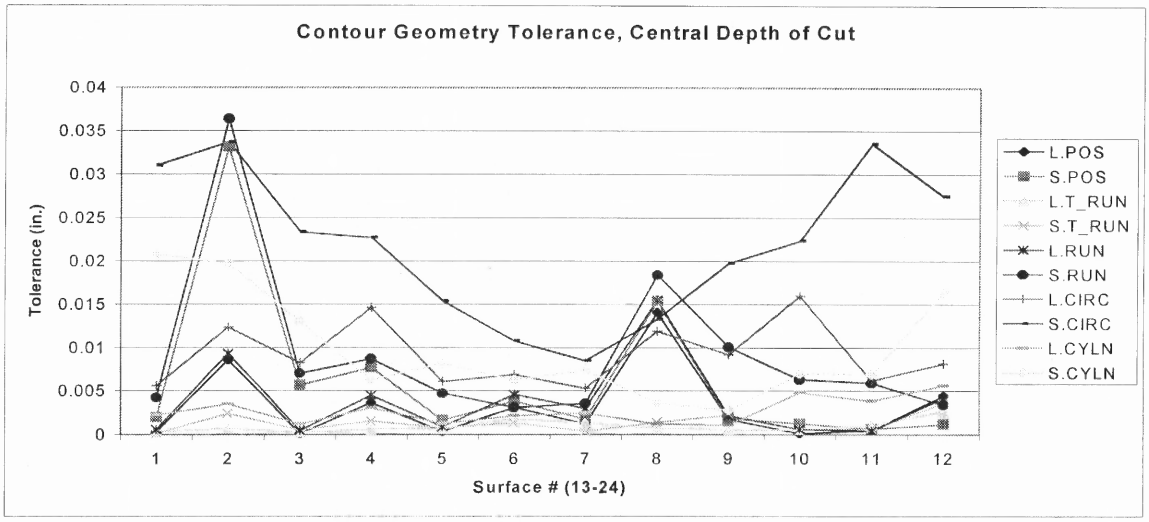

Figure 5-6. Contour Geometry Tolerance, Central Depth of Cut

Figure 5-6 illustrates the PMBDCLM (L) and DC servomotor (S) contour geometry tolerance at a central depth of cut. The figure shows that position, runout, and circularity tolerance at surface 14 (shown as 2) is the largest for the DC servomotor. Circularity tolerance also has similar values between surfaces 17-20, 16-21, 14-23, and 13-24.

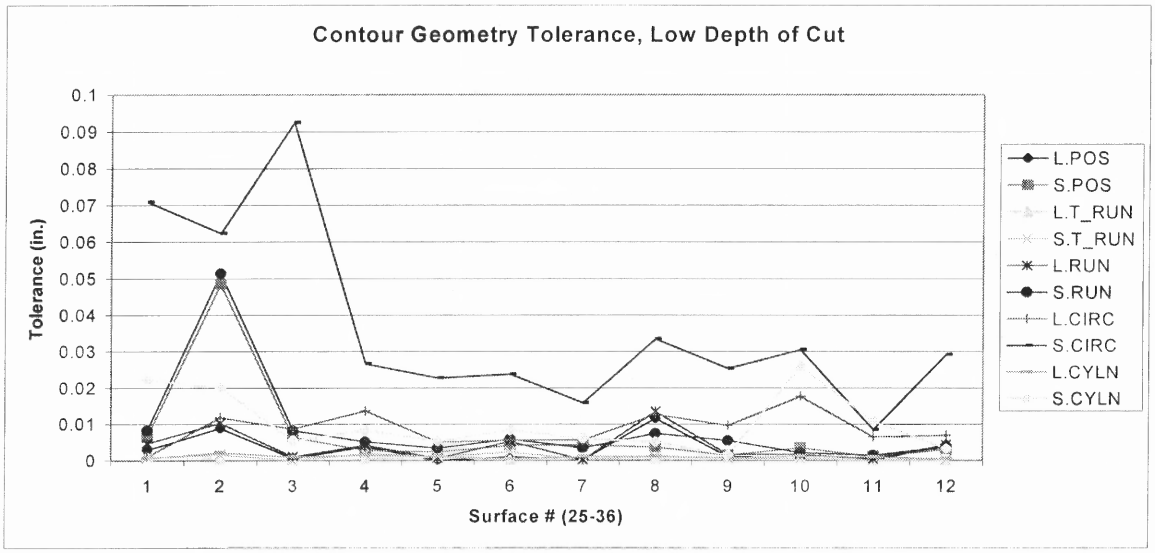

Figure 5-7. Contour Geometry Tolerance, Low Depth of Cut

Figure 5-7 illustrates the PMBDCLM (L) and DC servomotor (S) contour geometry tolerance at a low depth of cut. DC servomotor position, runout, and circularity values

show a downward trend from surface 26 to 36. DC servomotor tolerance values are generally larger than PMBDCLM values.

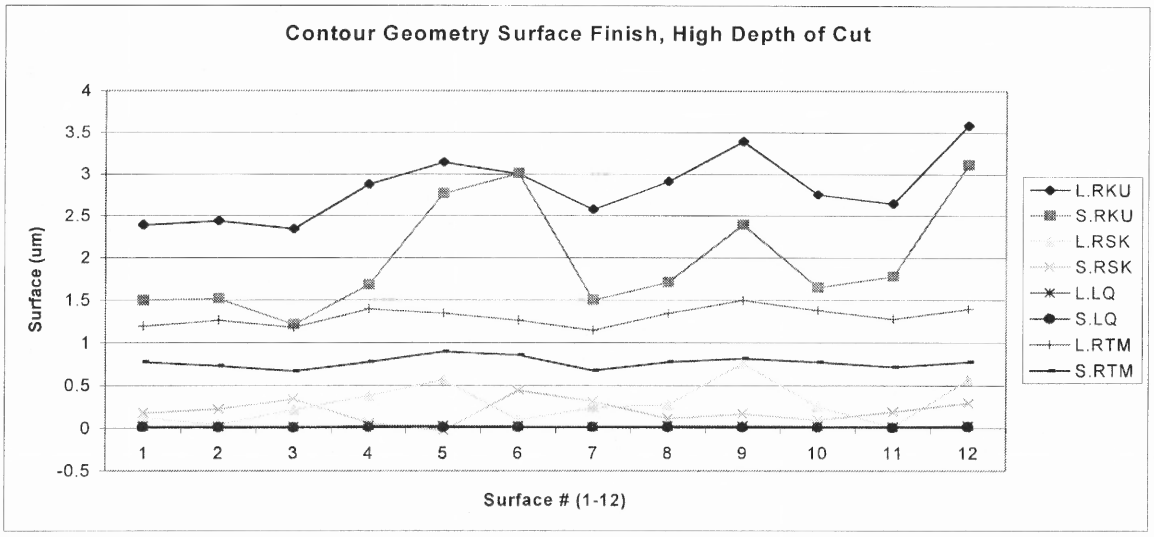

Figure 5-8. Contour Geometry Surface Finish, High Depth of Cut

Figure 5-8 illustrates the PMBDCLM (L) and DC servomotor (S) contour geometry surface finish at a high depth of cut. Surface finish values for both drives show a steady trend for skewness, wavelength, and peak-to-valley height. Kurtosis values for both drives show a slight upward trend from surface 1 to surface 12.

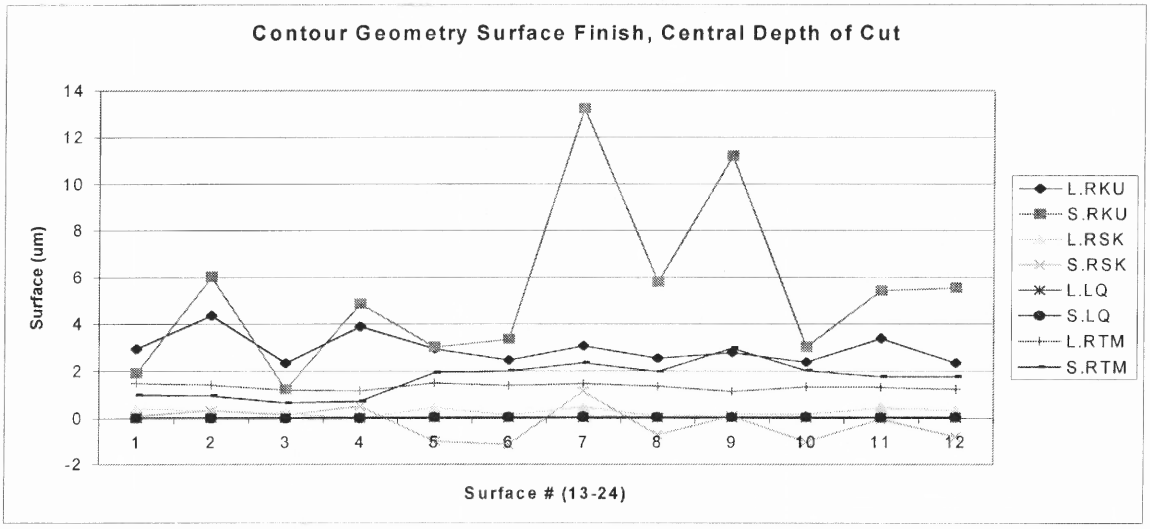

Figure 5-9. Contour Geometry Surface Finish, Central Depth of Cut

Figure 5-9 illustrates the PMBDCLM (L) and DC servomotor (S) contour geometry surface finish at a central depth of cut. There is a steady trend among each index except for DC servomotor kurtosis where surfaces 19 and 21 show a large increase.

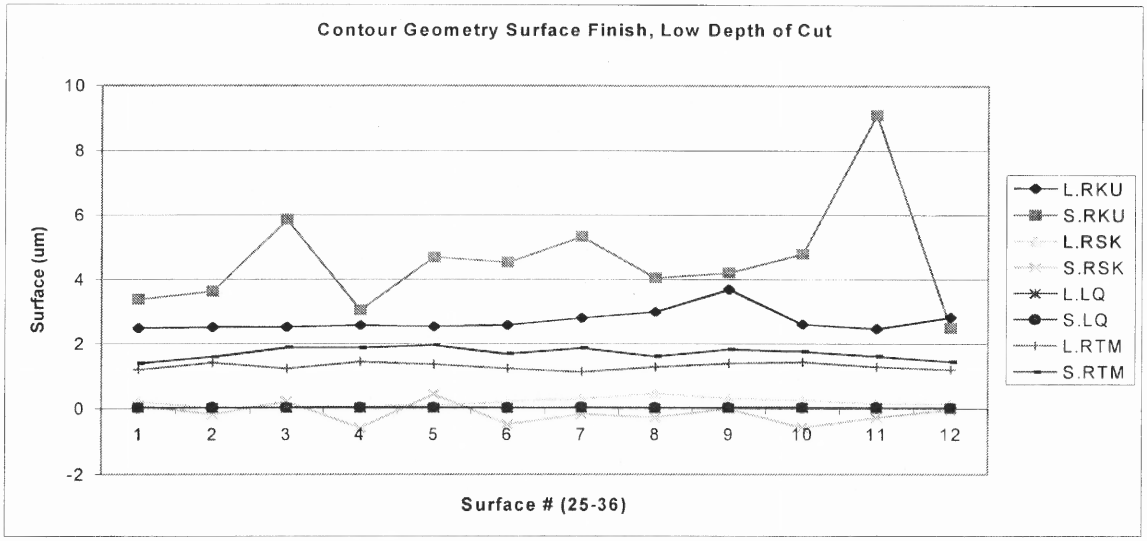

Figure 5-10. Contour Geometry Surface Finish, Low Depth of Cut

Figure 5-10 illustrates the PMBDCLM (L) and DC servomotor (S) contour geometry surface finish at a low depth of cut. The figure shows a steady trend between surface values except for DC servomotor kurtosis due to an increase at surface 35. In general, the DC servomotor surface finish values are larger than the PMBDCLM values.

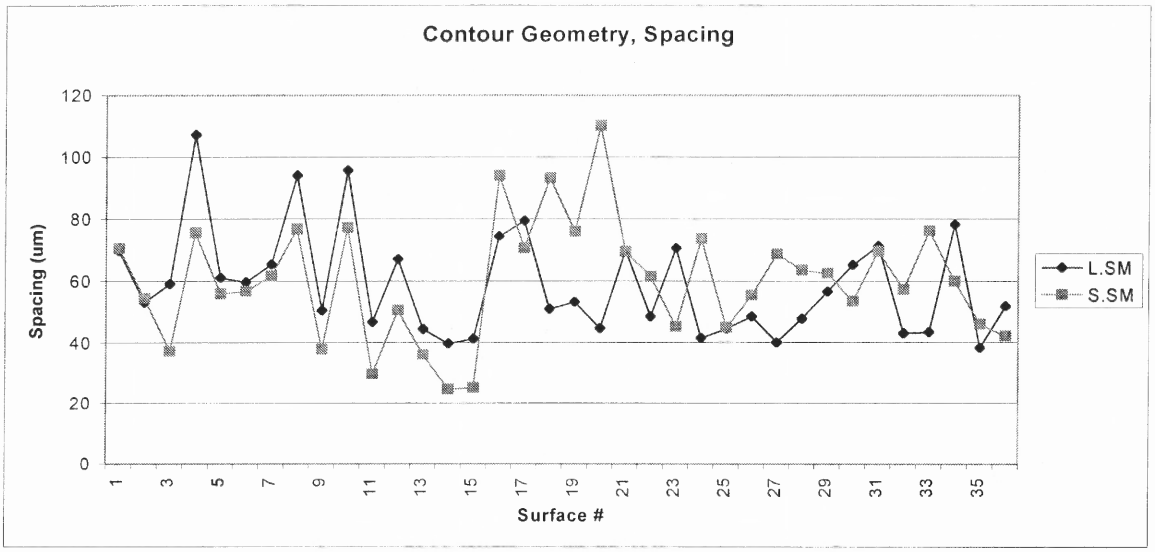

Figure 5-11. Contour Geometry Mean Spacing

Figure 5-11 illustates the PMBDCLM (L) and DC servomotor (S) contour geometry mean spacing. At a high depth of cut (surafces 1-12) both drives share a similar pattern where the PMBDCLM values are slightly higher. At a central (surfaces 13-24) and low (surfaces 25-36) depth of cut the PMBDCLM provides smaller spacing values.

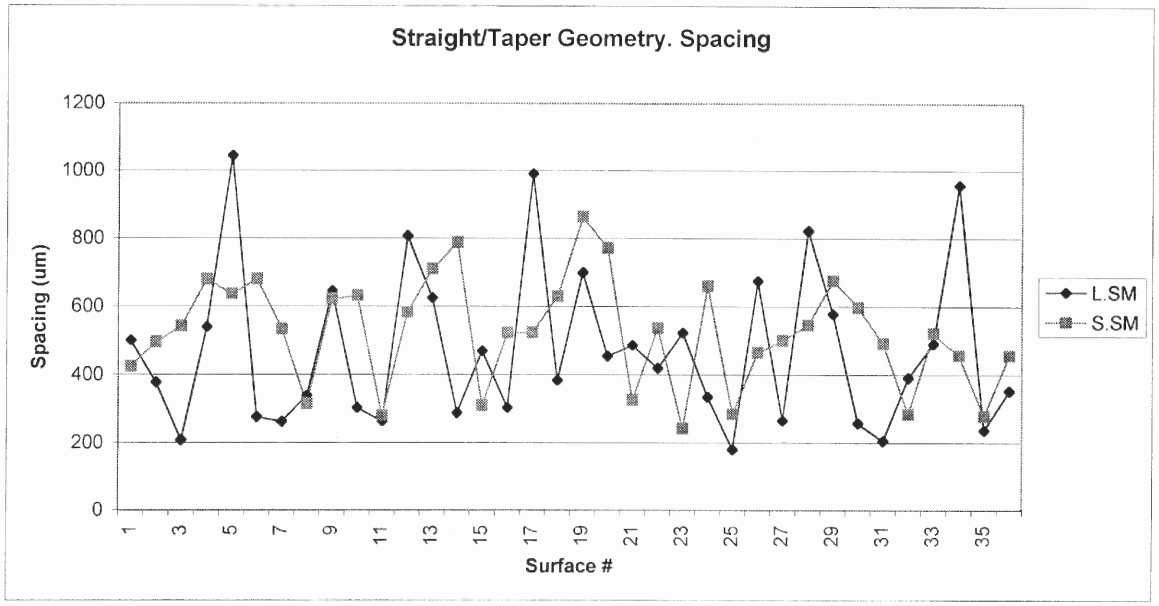

Figure 5-12. Straight/Taper Geometry Mean Spacing

Figure 5-12 illustrates the PMBDCLM (L) and DC servomotor (S) straight/taper geometry mean spacing. In general, the PMBDCLM spacing values are smaller than the DC servomotor spacing values, however the PMBDCLM spacing values peak at surface 5, 12, 17, 28, and 34. The DC servomotor spacing values peak at surfaces 14, 19, and 30.

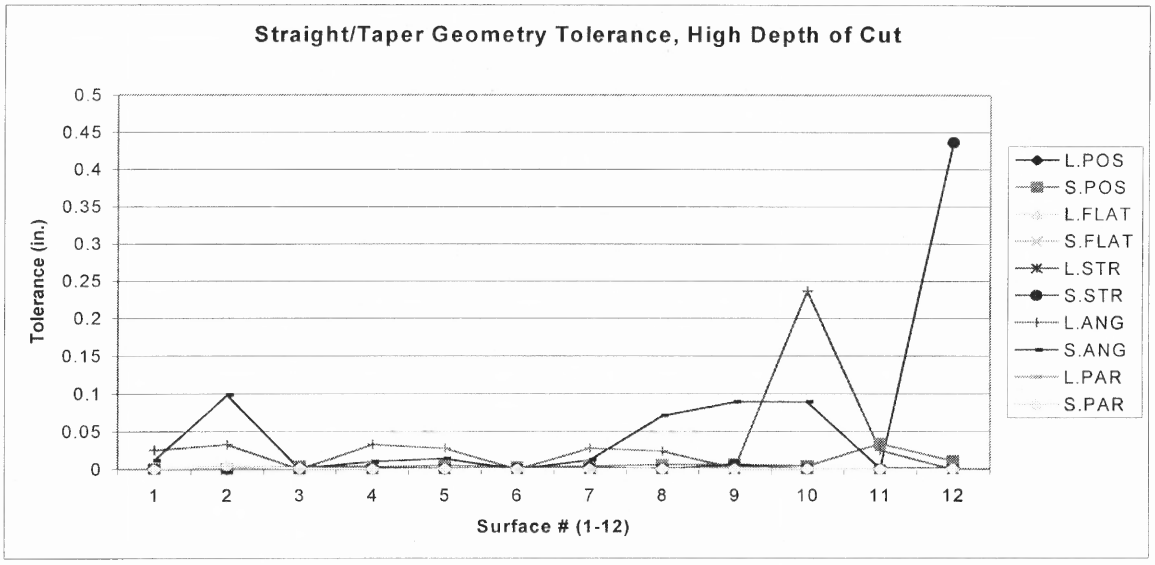

Figure 5-13. Straight/Taper Geometry Tolerance, High Depth of Cut

Figure 5-13 illustrates the PMBDCLM (L) and DC servomotor (S) tolerance values at a high depth of cut. DC servomotor angularity tolerance values are generally higher than PMBDCLM values. PMBDCLM angularity tolerance peaks at surface 10 and DC servomotor straightness tolerance peaks at surface 12.

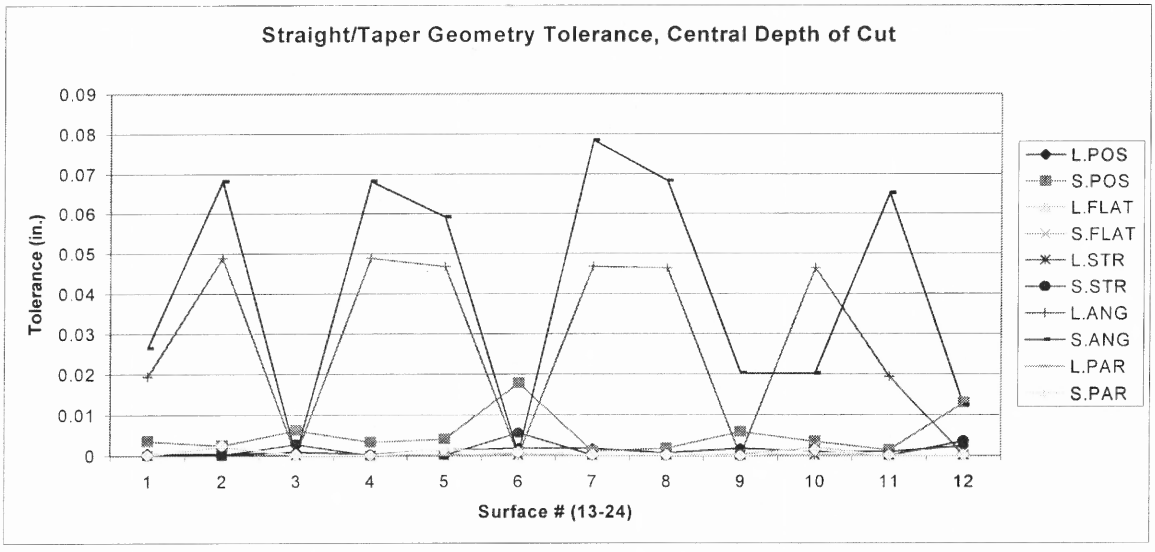

Figure 5-14. Straight/Taper Geometry Tolerance, Central Depth of Cut

Figure 5-14 illustrates the PMBDCLM (L) and DC servomotor (S) straight/taper geometry tolerance values at a central depth of cut. Position, flatness, straightness, and

parallelism tolerance values show a steady trend for each surface, however angularity tolerance shows a periodic trend where PMBDCLM values are smaller than DC servomotor values.

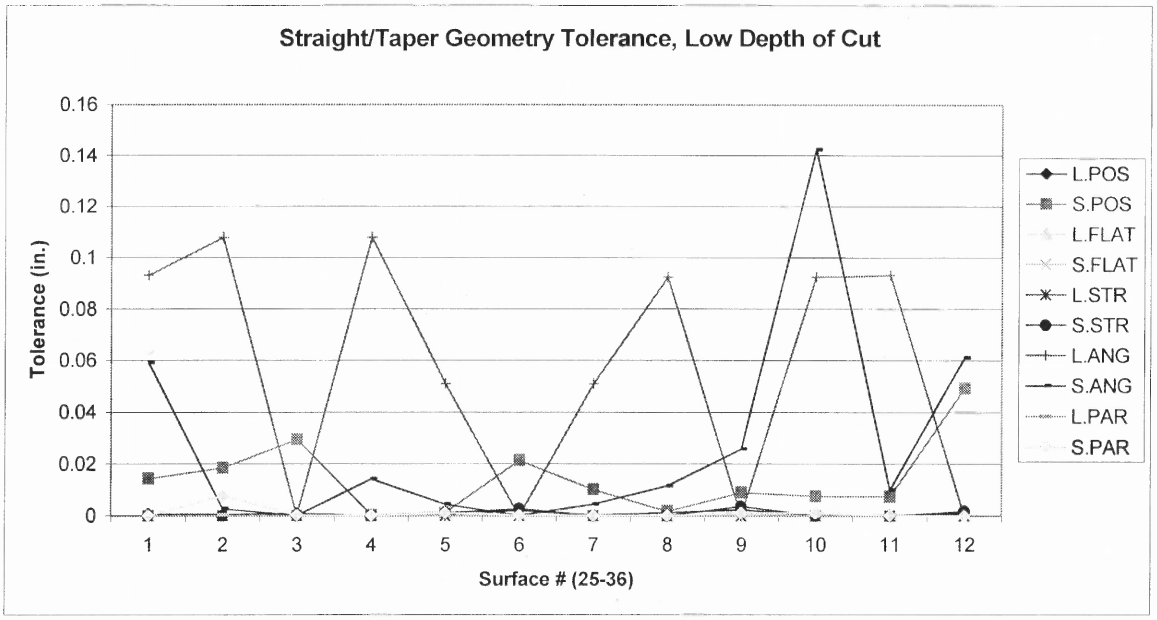

Figure 5-15. Straight/Taper Geometry Tolerance, Low Depth of Cut

Figure 5-15 illustrates the PMBDCLM (L) and DC servomotor (S) straight/taper geometry tolerance at a low depth of cut. PMBDCLM angularity tolerance shows a periodic trend from surface to surface and the DC servomotor angularity tolerance peaks at surface 34 (shown as 10). The figure also illustrates the larger position tolerance values of the DC servomotor.

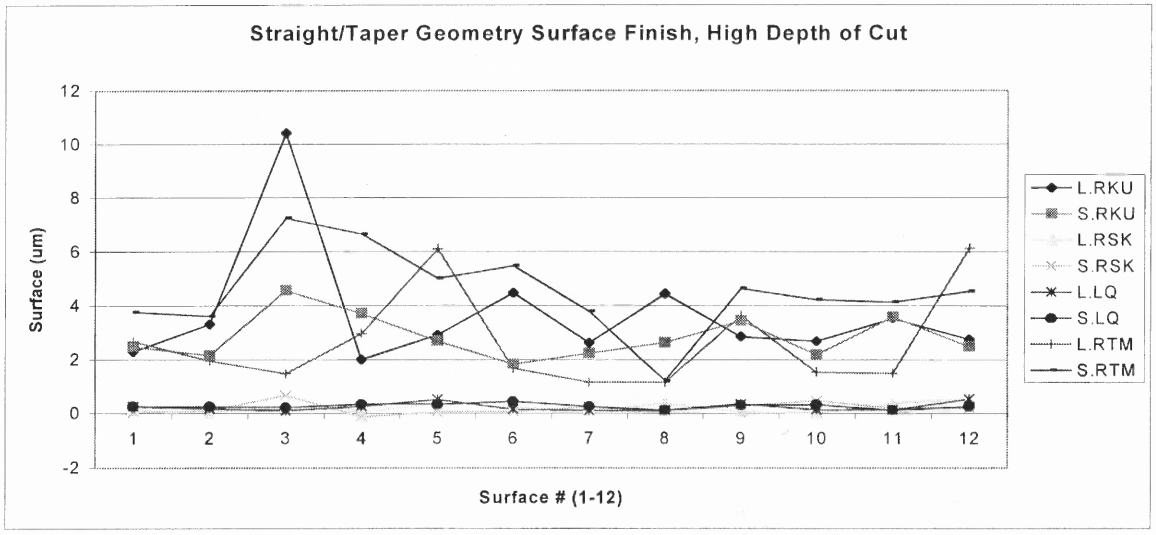

Figure 5-16. Straight/Taper Geometry Surface Finish, High Depth of Cut

Figure 5-16 illustrates the PMBDCLM (L) and DC servomotor (S) straight/taper geometry surface finish at a high depth of cut. Both kurtosis and peak-to-valley height show a downward trend starting from surface 1 to surface 12. In general, the PMBDCLM provides lower kurtosis and peak-to-valley height values. The figure also shows the small difference in skewness and wavelength.

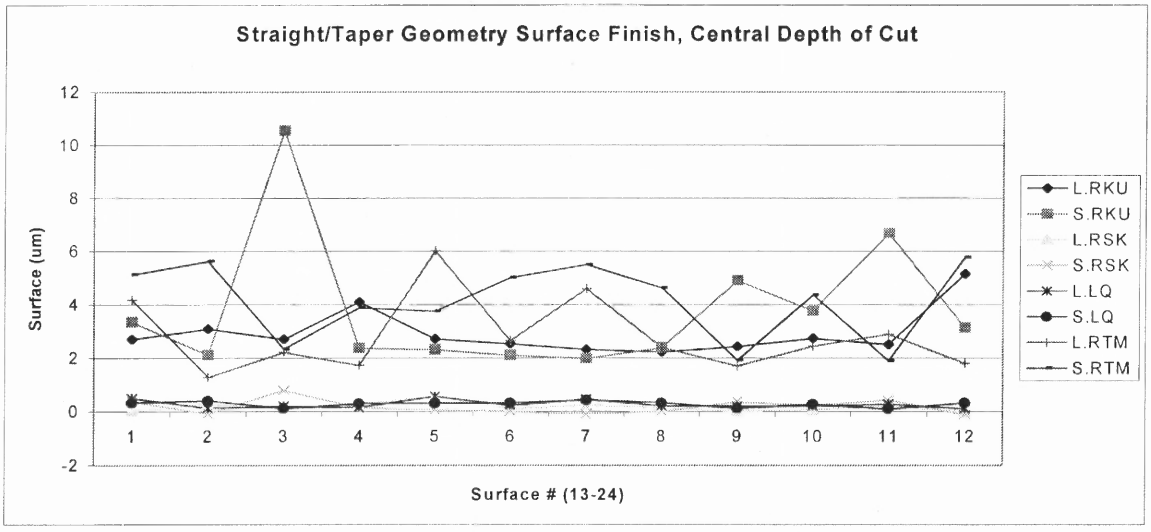

Figure 5-17. Straight/Taper Geometry Surface Finish, Central Depth of Cut

Figure 5-17 illustrates the PMBDCLM (L) and DC servomotor (S) straight/taper geometry surface finish at a central depth of cut. DC servomotor kurtosis peaks at surface

15 (shown as 3) although there is a steady trend in the remaining values. Overall, PMBDCLM surface finish values are smaller than DC servomotor values.

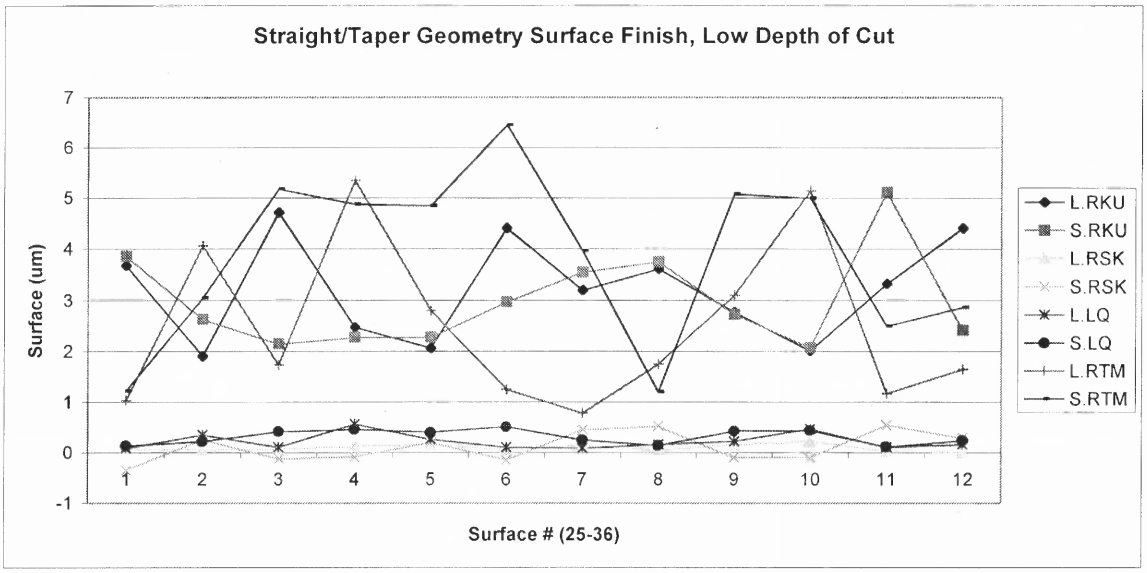

Figure 5-18. Straight/Taper Geometry Surface Finish, Low Depth of Cut

Figure 5-18 illustrates the PMBDCLM (L) and DC servomotor (S) straight/taper geometry surface finish at a low depth of cut. Both skewness and wavelength values show a steady trend but kurtosis and peak-to-valley height values show large performance difference from surface to surface.

Performance characteristics such as tolerance, force, and surface quality are determined for both a PMBDCLM and DC servomotor equipped CNC vertical milling machine. A total of 36 experiments are conducted (12 experiments at 3 depths of cut). For each depth of cut, the performance frequency, for mean and standard deviation, between the PMBDCLM and DC servomotor is provided. A percent benefit, for mean and standard deviation, is also provided. The average percent benefit is determined by dividing the PMBDCLM result with the DC servomotor result. For this, the smaller value favors the PMBDCLM and the larger value favors the DC servomotor. A value near 1.0

indicates there is not much difference in performance. The performance characteristics which a smaller percent benefit (< 1.0) is beneficial are:

- Standard deviation, position tolerance, runout tolerance, total runout tolerance, circularity tolerance, cylindricity tolerance, flatness tolerance, angularity tolerance, straightness tolerance, parallelism tolerance, force, surface finish spacing, surface finish wavelength, and surface finish peak-to-valley height

The performance characteristics which a larger percent benefit (> 1.0) is beneficial are:

- Surface finish kurtosis and surface finish skewness

A summary of contour and straight/taper geometry results is provided in Tables 5-5 and 5-6.

Table 5-5. Summary of Contour Geometry Results

Linear Motor/DC Servo Motor			**Depth C**	**Depth B**	**Depth A**	**Total**	**Best Overall Perform.**
Tolerance	**Position**	**Mean**	11/1	11/1	9/3	31/5	LM
		Std. Dev.	11/1	12/0	12/0	35/1	LM
	Runout	**Mean**	9/3	10/2	10/2	29/7	LM
		Std. Dev.	11/1	12/0	12/0	35/1	LM
	Total Runout	**Mean**	10/2	8/4	7/5	25/11	LM
		Std. Dev.	11/1	11/1	11/1	33/3	LM
	Circularity	**Mean**	8/4	12/0	12/0	32/4	LM
		Std. Dev.	12/0	12/0	12/0	36/0	LM
	Cylindricity	**Mean**	12/0	12/0	12/0	36/0	LM
		Std. Dev.	9/3	12/0	12/0	33/3	LM
Force	**Force**	**Mean**	12/0	10/2	9/3	31/5	LM
		Std. Dev.	0/12	0/12	1/11	1/35	SERVO
Peak-Fit (Force)	**A0**	**Mean**	0/12	0/12	0/12	0/36	SERVO
		Std. Dev.	1/11	2/10	0/12	3/33	SERVO
	A1	**Mean**	8/4	7/5	3/9	18/18	-
		Std. Dev.	7/5	3/9	3/9	13/23	SERVO
	A2	**Mean**	11/1	11/1	5/7	27/9	LM
		Std. Dev.	4/8	6/6	3/9	13/23	SERVO
	A3	**Mean**	12/0	12/0	12/0	36/0	LM
		Std. Dev.	12/0	12/0	12/0	36/0	LM
	A4	**Mean**	10/2	12/0	8/4	30/6	LM
		Std. Dev.	12/0	12/0	12/0	36/0	LM
Surface	**Rku (Kurtosis)**	**Mean**	11/1	10/2	7/5	28/8	LM
		Std. Dev.	12/0	12/0	12/0	36/0	LM
	Rsk (Skewness)	**Mean**	9/3	11/1	10/2	30/6	LM
		Std. Dev.	12/0	12/0	11/1	35/1	LM

Table 5-5. (Continued)

Surface	Sm (Mean Spacing)	Mean	3/9	6/6	8/4	17/19	SERVO
		Std. Dev.	11/1	8/4	6/6	25/11	LM
	Lq (Wavelength)	Mean	12/0	5/7	1/11	18/18	-
		Std. Dev.	12/0	11/1	11/1	34/2	LM
	Rtm	Mean	0/12	8/4	12/0	20/16	LM
		Std. Dev.	12/0	12/0	12/0	36/0	LM

Table 5-6. Summary of Straight/Taper Geometry Results

Linear Motor/DC-Servo Motor			Depth C	Depth B	Depth A	Total	Best Perform.
Tolerance	Position	Mean	11/1	11/1	12/0	34/2	LM
		Std. Dev.	10/2	9/3	8/4	27/9	LM
	Flatness	Mean	9/3	11/1	8/4	28/8	LM
		Std. Dev.	10/2	12/0	8/4	30/6	LM
	Straightness	Mean	10/2	11/1	8/4	29/7	LM
		Std. Dev.	7/5	11/1	9/3	27/9	LM
	Angularity	Mean	10/2	12/0	9/3	31/5	LM
		Std. Dev.	7/5	10/2	9/3	26/10	LM
	Parallelism	Mean	9/3	12/0	11/1	32/4	LM
		Std. Dev.	7/5	11/1	8/4	26/10	LM
Force	Force	Mean	10/2	8/4	12/0	30/6	LM
		Std. Dev.	5/7	2/10	6/6	13/23	SERVO
Peak-Fit (Force)	A0	Mean	7/5	1/11	9/3	17/19	SERVO
		Std. Dev.	5/7	0/12	5/7	10/26	SERVO
	A1	Mean	8/4	5/7	4/8	17/19	SERVO
		Std. Dev.	2/10	5/7	5/7	12/24	SERVO
	A2	Mean	7/5	5/7	8/4	20/16	LM
		Std. Dev.	9/3	0/12	6/6	15/21	SERVO
	A3	Mean	3/9	12/0	7/5	22/14	LM
		Std. Dev.	6/6	12/0	10/2	28/8	LM
	A4	Mean	3/9	9/3	9/3	21/15	LM
		Std. Dev.	6/6	12/0	11/1	29/7	LM
Surface	Rku (Kurtosis)	Mean	10/2	10/2	11/1	31/5	LM
		Std. Dev.	8/4	10/2	10/2	28/8	LM
	Rsk (Skewness)	Mean	11/1	10/2	12/0	33/3	LM
		Std. Dev.	9/3	10/2	10/2	29/7	LM
	Sm (Mean Spacing)	Mean	8/4	9/3	9/3	26/10	LM
		Std. Dev.	7/5	7/5	10/2	24/12	LM
	Lq (Wavelength)	Mean	6/6	9/3	9/3	24/12	LM
		Std. Dev.	10/2	11/1	9/3	30/6	LM
	Rtm	Mean	10/2	10/2	8/4	28/8	LM
		Std. Dev.	10/2	12/0	11/1	33/3	LM

Contour Geometry

The following are the contour geometry experimental results.

1. The PMBDCLM outperforms the DC servomotor 31 times for position tolerance mean with a 0.567 benefit and 35 times for position tolerance standard deviation with a

0.411 benefit. Depth of cut B and C provides the best mean position tolerance frequency and depth of cut A and B provides the best position tolerance standard deviation frequency.

2. The PMBDCLM outperforms the DC servomotor 29 times for runout tolerance mean with a 0.541 benefit and 35 times for runout tolerance standard deviation with a 0.381 benefit. Depth of cut A and B provides the best mean runout tolerance frequency and depth of cut A and B provides the best runout tolerance standard deviation frequency.
3. The PMBDCLM outperforms the DC servomotor 25 times for total runout tolerance mean with a 0.838 benefit and 33 times for runout tolerance standard deviation with a 0.369 benefit. Depth of cut C provides the best mean total runout tolerance frequency and all depths provide the best total runout tolerance standard deviation frequency.
4. The PMBDCLM outperforms the DC servomotor 32 times for circularity tolerance mean with a 0.500 benefit and 36 times for circularity tolerance standard deviation with a 0.263 benefit. Depth of cut A and B provides the best mean circularity tolerance frequency and all depths of cut and provides the best circularity tolerance standard deviation frequency.
5. The PMBDCLM outperforms the DC servomotor 36 times for cylindricity tolerance mean with a 0.270 benefit and 33 times for cylindricity tolerance standard deviation with a 0.333 benefit. All depths of cut provide the best mean cylindricity tolerance frequency and depth of cut A and B provides the best cylindricity tolerance standard deviation frequency. Both the PMBDCLM and DC servomotor provide the same resultant cutting forces. However, the PMBDCLM shows a smaller mean resultant force (5 N or less) than the DC servomotor. The PMBDCLM provides a smaller mean

resultant force 31 times with a benefit of 0.963. The DC servomotor provides a smaller standard deviation for each depth of cut.

6. The DC servomotor provides higher force amplitude than the PMBDCLM 36 times for mean force with a 17.23 benefit and 33 times for mean force standard deviation with a 5.620 benefit. Depth of cut A, B, and C provides the largest mean force amplitude and depth of cut A provides the best mean force standard deviation.
7. The PMBDCLM and DC servomotor provides an equal mean center frequency of 18 with a benefit of 1.089. The DC servomotor provides a smaller mean center standard deviation with a frequency of 23 and a benefit of 1.174. The PMBDCLM provides a smaller mean frequency for depth of cut B and C and a smaller standard deviation for depth of cut C.
8. The PMBDCLM provides a smaller mean force width than the DC servomotor 27 times at a benefit of 0.906. The DC servomotor provides a smaller force width standard deviation 23 times at a benefit of 1.184. The PMBDCLM performs best at depth of cut B and C for mean force width and depth of cut B for force width standard deviation.
9. The PMBDCLM provides a smaller force shape-1 than the DC servomotor 36 times at a benefit of 0.818 and a smaller shape-1 standard deviation 36 times at a benefit of 0.0. The PMBDCLM values are smaller for each depth of cut at the mean and standard deviation.
10. The PMBDCLM provides a smaller force shape-2 than the DC servomotor 30 times at a benefit of 0.802 and a smaller shape-2 standard deviation 36 times at a benefit of

0.0. For mean force shape-2, The PMBDCLM shows the best performance at depth of cut B and depth of cut A, B, and C for standard deviation.

11. The PMBDCLM provides better surface kurtosis than the DC servomotor 28 times at a benefit of 1.428 and a smaller standard deviation 36 times at a benefit of 0.361. The PMBDCLM provides the best mean surface kurtosis at depth of cut B and C and the best surface kurtosis standard deviation at depth of cut A, B, and C.
12. The PMBDCLM provides better surface skewness than the DC servomotor 30 times at a benefit 7.786 and a smaller standard deviation 35 times at a benefit of 0.474. The PMBDCLM provides the best mean surface skewness at depth of cut A and B and the best surface skewness standard deviation at depth of cut A, B, and C.
13. The DC servomotor provides a slightly better surface mean spacing than the PMBDCLM 19 times at a benefit of 1.033, indicating that mean spacing performance is nearly equal. The PMBDCLM provides a smaller spacing standard deviation 25 times at a benefit of 1.121 with the best performance at depth of cut B and C.
14. The PMBDCLM and DC servomotor provides the same mean wavelength at a frequency of 18 and a benefit of 1.033, however the PMBDCLM outperforms the DC servomotor by providing a smaller wavelength standard deviation at a benefit of 0.262. The PMBDCLM provides the best mean wavelength performance at depth of cut C and the best standard deviation at depth of cut A, B, C.
15. The PMBDCLM provides a smaller peak-to-valley height than the DC servomotor 20 times at a benefit 1.082 and provides a smaller standard deviation at a frequency of 36 and benefit of 0.232. The PMBDCLM provides the best mean peak-to-valley height at

depth of cut A and the best peak-to-valley height standard deviation at depth of cut A, B, and C.

16. The PMBDCLM outperformed the DC servomotor in 22 performance characteristics. The DC servomotor outperformed the PMBDCLM in 4 performance characteristics, mainly in peak forces. Equal performance is shown in 5 indices.

Straight-Taper Geometry

The following are the straight/taper geometry experimental results.

1. The PMBDCLM outperformed the DC servomotor 34 times for position tolerance mean with a 0.297 benefit and 27 times for position tolerance standard deviation with a 0.824 benefit. Depth of cut A, B and C provides the best mean position tolerance frequency and depth of cut A provides the best position tolerance standard deviation frequency.
2. The PMBDCLM outperformed the DC servomotor 28 times for flatness tolerance mean with a 0.954 benefit and 30 times for flatness tolerance standard deviation with a 0.596 benefit. Depth of cut B provides the best mean flatness tolerance frequency and depth of cut B and C provides the best flatness tolerance standard deviation frequency.
3. The PMBDCLM outperformed the DC servomotor 29 times for straightness tolerance mean with a 0.901 benefit and 27 times for straightness standard deviation with a 0.771 benefit. Depth of cut B and C provides the best mean straightness tolerance frequency and depth of cut B provides the best straightness tolerance standard deviation frequency.

4. The PMBDCLM outperformed the DC servomotor 31 times for angularity tolerance mean with a 0.816 benefit and 26 times for angularity tolerance standard deviation with a 1.30 benefit. Depth of cut B and C provides the best mean angularity tolerance frequency and depth of cut B provides the best angularity tolerance standard deviation frequency.
5. The PMBDCLM outperformed the DC servomotor 32 times for parallelism tolerance mean with a 0.571 benefit and 26 times for parallelism tolerance standard deviation with a 0.713 benefit. Depth of cut A and B provides the best mean parallelism tolerance frequency and depth of cut B provides the best parallelism tolerance standard deviation frequency.
6. Both the PMBDCLM and DC servomotor provide the same resultant cutting forces. However, the PMBDCLM shows a smaller mean resultant force (5 N or less) than the DC servomotor. The PMBDCLM provides a smaller mean resultant force 30 times with a benefit of 0.958. The DC servomotor provides a smaller standard deviation for each depth of cut.
7. The DC servomotor provides higher force amplitude than the PMBDCLM 19 times for mean force with a 2.506 benefit and 26 times for mean force standard deviation with a 3.230 benefit. For the PMBDCLM, depth of cut A and C provides the largest mean force amplitude and depth of cut A provides the best mean force standard deviation.
8. The PMBDCLM and DC servomotor provide an equal mean center frequency of 17/19 with a benefit of 0.978. The DC servomotor provides a smaller mean center standard deviation with a frequency of 24 and a benefit of 1.330. The PMBDCLM provides a smaller mean frequency for depth of cut C.

9. The PMBDCLM provides a smaller mean force width than the DC servomotor 20 times at a benefit of 0.978. The DC servomotor provides a smaller force width standard deviation 21 times at a benefit of 1.119. The PMBDCLM performs best at depth of cut A and C for mean force width and depth of cut C for force width standard deviation.
10. The PMBDCLM provides a smaller force shape-1 than the DC servomotor 22 times at a benefit of 0.986 and a smaller shape-1 standard deviation 28 times at a benefit of 0.265. The PMBDCLM performs best at depth of cut B for mean force shape-1 and depth of cut A and B for force shape-1 standard deviation.
11. The PMBDCLM provides a smaller force shape-2 than the DC servomotor 21 times at a benefit of 0.954 and a smaller shape-2 standard deviation 29 times at a benefit of 0.278. For mean force shape-2, The PMBDCLM shows the best performance at depth of cut A and B and depth of cut A and B for standard deviation.
12. The PMBDCLM provides better surface kurtosis than the DC servomotor 31 times at a benefit of 1.354 and a smaller standard deviation 28 times at a benefit of 0.908. The PMBDCLM provides the best mean surface kurtosis at depth of cut A, B and C and the best surface kurtosis standard deviation at depth of cut A and B.
13. The PMBDCLM provides better surface skewness than the DC servomotor 33 times at a benefit 2.797 and a smaller standard deviation 28 times at a benefit of 0.960. The PMBDCLM provides the best mean surface skewness at depth of cut A and C and the best surface skewness standard deviation at depth of cut A and B.

14. The PMBDCLM provides a better surface mean spacing than the DC servomotor 26 times at a benefit of 0.896. The PMBDCLM provides a smaller spacing standard deviation 24 times at a benefit of 0.960 with the best performance at depth of cut A.
15. The PMBDCLM provides a smaller mean wavelength at a frequency of 24 and a benefit of 0.803 and a smaller wavelength standard deviation 30 times at a benefit of 0.571. The PMBDCLM provides the best mean wavelength performance at depth of cut A and B and the best standard deviation at depth of cut C and B.
16. The PMBDCLM provides a smaller peak-to-valley height than the DC servomotor 28 times at a benefit of 0.707 and provides a smaller standard deviation at a frequency of 33 and benefit of 0.613. The PMBDCLM provides the best mean peak-to-valley height at depth of cut B and C and the best peak-to-valley standard deviation at depth of cut A and B.
17. The PMBDCLM outperformed the DC servomotor in 23 performance indices. The DC servomotor outperformed the PMBDCLM in 5 performance indices. Equal performance is shown in 4 indices.

Contour versus Straight-Taper Geometry Performance Characteristics

Comparison between contouring and straight cutting shows that:

- The PMBDCLM outperforms the DC servomotor in both mean tolerance and standard deviation for both contour and straight cutting.
- The PMBDCLM provides smaller percent benefit values for contour tolerance.
- The PMBDCLM outperforms the DC servomotor for all surface characteristics in straight cutting and all standard deviations in contour cutting.

- Cutting force for both contour and straight cutting indicates that mean forces in both PMBDCLM and DC servomotor tests are the same but the DC servomotor provides a smaller standard deviation.

Comparison of contour and straight/taper cutting percent benefits, where positive values indicate a smaller contour value and negative values indicate a larger straight/taper value, shows that:

- There is a 0.27 benefit difference in mean position and a –0.413 benefit difference in position standard deviation.
- There is a 0.005 benefit difference in mean cutting forces and a 2.629 benefit difference in force standard deviation.
- There is a 14.724 benefit difference in mean force amplitude and a 2.39 benefit difference in force amplitude standard deviation.
- There is a 0.111 benefit difference in mean force width and a –0.156 benefit difference in force width standard deviation.
- There is a –0.072 benefit difference in mean force center and a 0.065 benefit difference in force center standard deviation.
- There is a 0.074 benefit difference in mean surface kurtosis and a –0.547 benefit difference in surface kurtosis standard deviation.
- There is a 4.989 benefit difference in mean surface skewness and a –0.486 benefit difference in surface skewness standard deviation.
- There is a 0.137 benefit difference in mean surface spacing and a 0.161 benefit difference in surface spacing standard deviation.

- There is a 0.283 benefit difference in mean surface wavelength and a –0.309 benefit difference in surface wavelength standard deviation.
- There is a 0.375 benefit difference in mean surface peak-to-valley height and a –0.381 benefit difference in surface peak-to-valley height standard deviation.

Peak Extraction Results

Figures 5-19, 5-20, and 5-21 illustrate the contour geometry peak force values for each depth of cut from PMBDCLM and DC servomotor experimentation. Figures 5-22, 5-23, and 5-24 illustrate the straight/taper geometry peak force values for each depth of cut from PMBDCLM and DC servomotor experimentation.

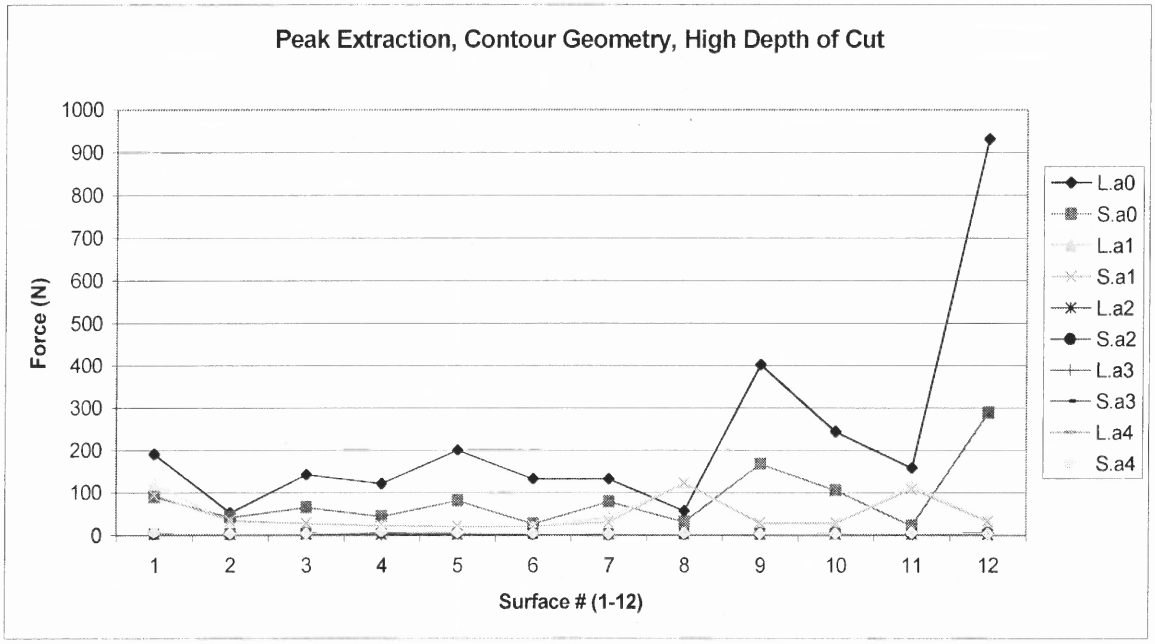

Figure 5-19. Contour Geometry Peak Extraction, High Depth of Cut

Figure 5-19 illustrates the PMBDCLM (L) and DC servomotor (S) peak force extraction of the contour geometry at a high depth of cut. Force characteristics show a steady trend for each surface although PMBDCLM peak force is largest at surface 9 and 12.

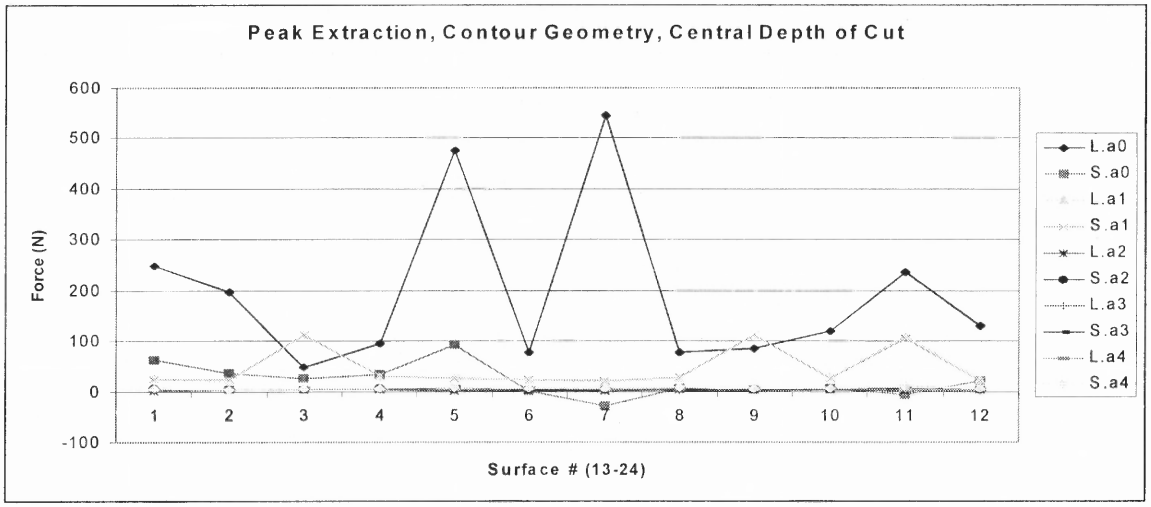

Figure 5-20. Contour Geometry Peak Extraction, Central Depth of Cut

Figure 5-20 illustrates the PMBDCLM (L) and DC servomotor (S) contour geometry peak force extraction at a central depth of cut. Force characteristics show a steady trend in force width and center. PMBDCLM peak force is the largest at surface 17 (shown as 5) and surface 19 (shown as 7).

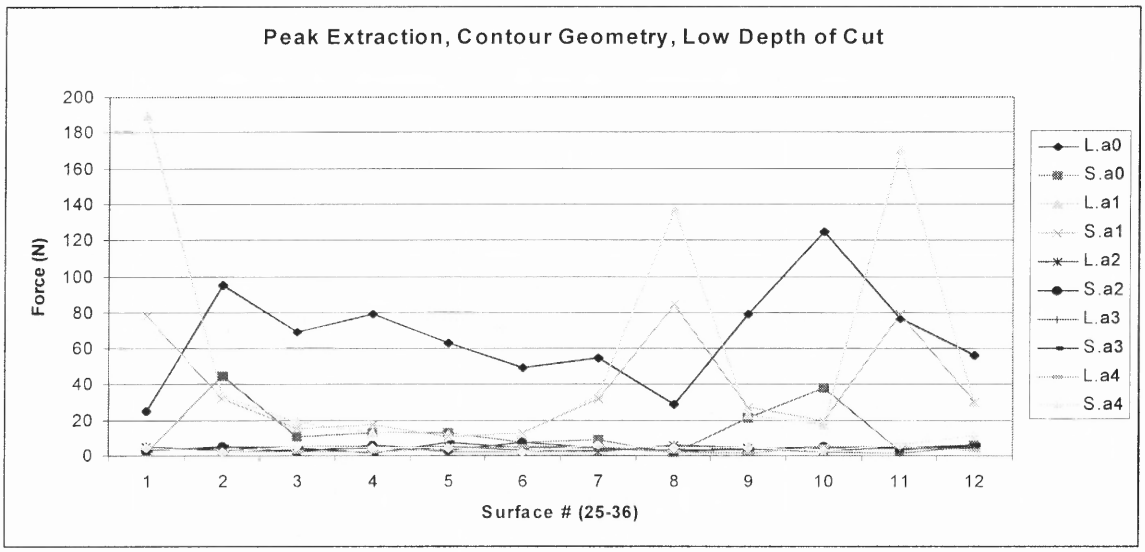

Figure 5-21. Contour Geometry Peak Extraction, Low Depth of Cut

Figure 5-21 illustrates the PMBDCLM (L) and DC servomotor (S) contour geometry peak force extraction at a low depth of cut. PMBDCLM force width peaks at surface 25 (shown as 1), surface 32 (shown as 8) and surface 35 (shown as 11). PMBDCLM peak force is highest at surface 26 (shown as 2) and surface 34 (shown as 10).

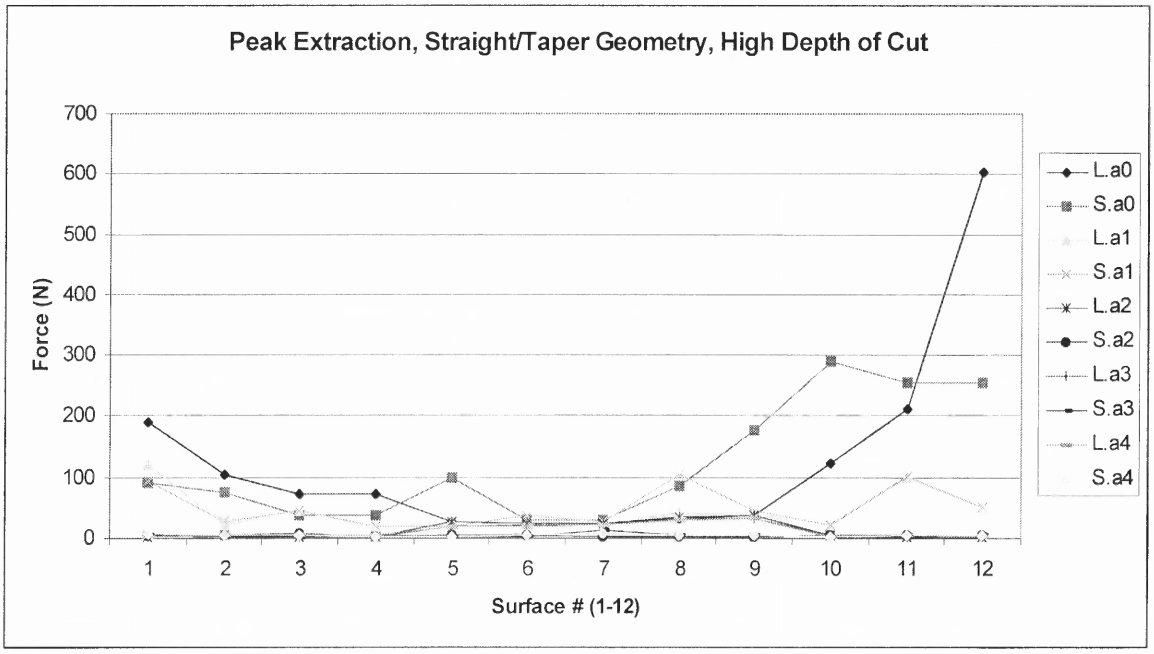

Figure 5-22. Straight/Taper Geometry Peak Extraction, High Depth of Cut

Figure 5-22 illustrates the PMBDCLM (L) and DC servomotor (S) straight/taper geometry peak force extraction at a high depth of cut. The force characteristics show an upward trend from surface 1 to surface 12. PMBDCLM and DC servomotor peak force is the highest at surface 12.

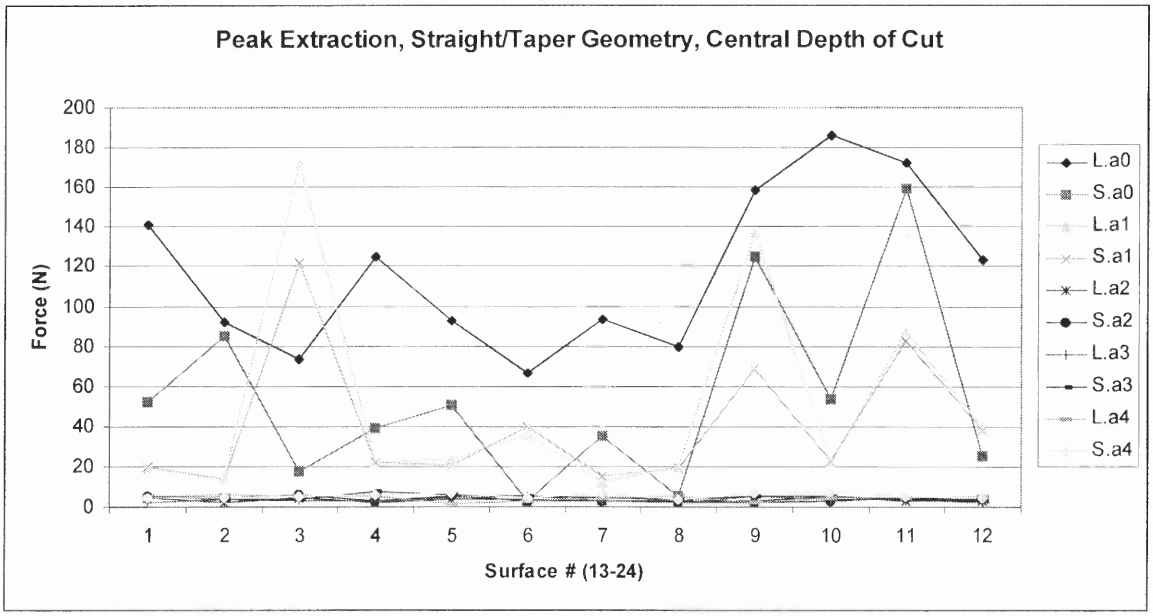

Figure 5-23. Straight/Taper Geometry Peak Extraction, Central Depth of Cut

Figure 5-23 illustrates the PMBDCLM (L) and DC servomotor (S) straight/taper geometry peak force extraction at a central depth of cut. Both the PMBDCLM and DC servomotor force width exhibit the same pattern from surface to surface. PMBDCLM peak force is the highest at surface 22 (shown as 10) and DC servomotor peak force is the highest at surface 23 (shown as 11).

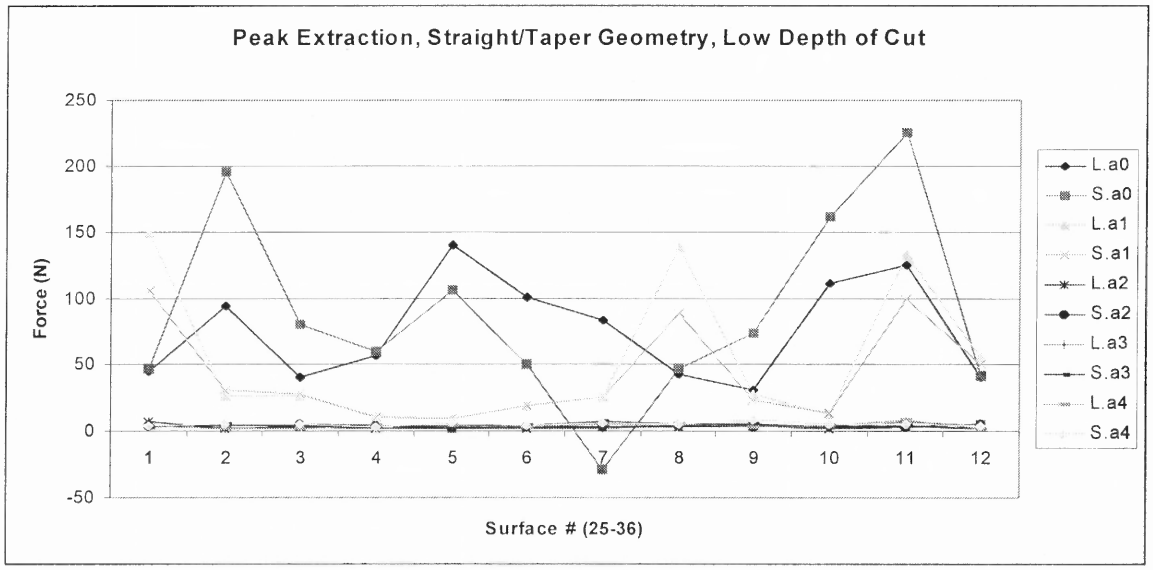

Figure 5-24. Straight/Taper Geometry Peak Extraction, Low Depth of Cut

Figure 5-24 illustrates the PMBDCLM (L) and DC servomotor (S) straight/taper geometry peak force extraction at a low depth of cut. PMBDCLM and DC servomotor force width exhibit the same trend from surface to surface. PMBDCLM peak force is the highest at surface 35 (shown as 11) and DC servomotor peak force is the highest at surface 29 (shown as 5).

From the simulated force, measured average force, and measured peak force, Table 5-7 lists the forces at each depth of cut and each set of operating parameters.

Table 5-7. Force Rating Comparison

Roughing (High Depth of Cut)												
Surface		**1**	**2**	**3**	**4**	**5**	**6**	**7**	**8**	**9**	**10**	**11**	**12**
S		***L***	***C***	***H***	***C***	***L***	***H***	***H***	***C***	***L***	***C***	***H***	***L***
F		***L***	***SL***	***SH***	***H***	***H***	***H***	***SL***	***L***	***SH***	***SH***	***L***	***SL***
D		***H***	***H***	***H***	***H***	***H***	***H***	***H***	***H***	***H***	***H***	***H***	***H***
C	**T**	4	2	3	3	5	3	2	1	5	4	2	5
	P	5	1	4	3	5	3	3	1	5	5	4	5
	M	2	2	2	4	5	3	2	2	4	3	1	3
S	**T**	2	2	2	2	2	1	2	1	4	5	5	5
	P	5	3	2	2	1	1	1	2	1	3	5	5
	M	2	2	2	4	5	3	2	2	4	3	1	3
Moderate Cutting (Moderate Depth of Cut)													
Surface		**13**	**14**	**15**	**16**	**17**	**18**	**19**	**20**	**21**	**22**	**23**	**24**
S		***L***	***H***	***C***	***H***	***L***	***C***	***L***	***C***	***H***	***C***	***L***	***H***
F		***SH***	***H***	***L***	***SL***	***SL***	***SH***	***H***	***SH***	***L***	***SL***	***L***	***SH***
D		***C***	***C***	***C***	***C***	***C***	***C***	***C***	***C***	***C***	***C***	***C***	***C***
C	**T**	5	4	1	2	5	1	5	2	2	2	3	3
	P	5	5	1	2	5	2	5	2	2	3	5	3
	M	3	3	1	1	2	2	4	2	1	2	2	2
S	**T**	3	2	2	2	2	1	2	1	3	4	5	3
	P	4	2	2	3	2	2	2	2	4	5	4	3
	M	3	3	1	1	2	2	4	2	1	2	2	2
Finishing (Low Depth of Cut)													
Surface		**25**	**26**	**27**	**28**	**29**	**30**	**31**	**32**	**33**	**34**	**35**	**36**
S		***C***	***L***	***H***	***L***	***C***	***H***	***H***	***L***	***C***	***L***	***H***	***C***
F		***L***	***SL***	***SH***	***H***	***H***	***H***	***SL***	***L***	***SH***	***SH***	***L***	***SL***
D		***L***	***L***	***L***	***L***	***L***	***L***	***L***	***L***	***L***	***L***	***L***	***L***

Table 5-7. (Continued)

C	**T**	1	3	2	1	1	1	1	1	2	3	3	1
	P	1	2	2	2	2	1	1	1	2	3	3	1
	M	1	2	1	3	2	2	1	1	2	2	1	1
S	**T**	1	2	2	1	3	2	1	1	2	4	4	2
	P	1	2	1	1	4	3	2	1	1	3	3	1
	M	1	2	1	3	2	2	1	1	2	2	1	1

S = (Spindle Speed) F = (Feedrate) D = (Depth of Cut)
C = Contour S = Straight/Taper
T = Theoretical Force P = Peak Force M = Measured Force

Overall Force Results

From Table 5-7, the following results are listed.

- Cutting conditions 25 and 32 provide the same force rating for theoretical, peak, and measured for both contour and straight-taper cutting.
- Uniform force ratings are shown in cutting conditions 5, 6, 15, 20, 25, 31, 32, 33, and 34 for contour cutting.
- Uniform force ratings are shown in cutting conditions 3, 17, 25, 26, and 32 for straight-taper cutting.
- Contour cutting provides more uniform ratings than straight/taper cutting.
- Ratings do not widely vary from each other except for contour cutting conditions 2, 11, 17, and 23 and cutting conditions 1, 5, 9, 22, and 23 for straight-taper cutting.
- Force ratings at the lowest depth of cut provide the most uniform force rating.

Theoretical versus Measured Force Rating

- Theoretical forces are greater than all measured forces except for cutting conditions 4, 18, 28, 29, 30 for contouring and conditions 4, 5, 6, 8, 14, 18, 19, and 28 for straight/taper cutting.

- The theoretical force rating and measured force either matches or varies by 1 rating point for each cutting condition.
- The theoretical and measured force varies the most at the highest depth of cut.
- In the straight/taper cutting conditions, both the theoretical and measured forces vary the most.

Measured versus Peak Force Rating

- Peak forces are greater than all measured forces except for cutting conditions 2, 4, 8, 30 for contouring and conditions 5, 6, 7, 9, 14, 28, and 33 for straight/taper cutting.
- The measured force rating and peak force rating either matches or varies by 1 rating point for each cutting condition.
- The measured and peak force ratings vary the most at the highest depth of cut.
- In the straight/taper cutting conditions, both the peak and measured forces vary the most.

Theoretical versus Peak Force Rating

- Theoretical and peak forces vary the least.
- The theoretical force rating and peak force rating either matches or varies by 1 rating point for each cutting condition.
- The theoretical and peak force ratings vary the most at the highest depth of cut.

Force Effect on Dynamic Performance

- There is a 2.05% increase in frequency between the low and moderate force models and a 2.57% increase in frequency between the moderate and high force models.

- There is a 75.37% decrease in velocity, acceleration, and position when low force is applied, a 76.79% decrease in velocity, acceleration, and position when moderate force is applied.
- There is a 13.5% increase in velocity, acceleration, and position between the low and moderate force.
- There is a 22.11% increase in velocity, acceleration, and position between the moderate and high force models.
- There is a 33.03% increase in velocity, acceleration, and position between the low and high force.

Simple Regression Results

Tables 5-8, 5-9, 5-10, and 5-11 list the simple regression empirical relationships with the associated p-values and r-square values for the contour and straight/taper geometry at each depth of cut.

By examining the relationship between cutting force and the contour geometry tolerance indices, it is shown that the increase in cutting force decreases tolerance and generally provides a higher tolerance value. It is evident that depth of cut, which changes the force, affects contour geometry tolerance. By examining the relationship between cutting force and contour geometry surface finish indices, it is also shown that the increase in cutting force increases the contour geometry surface finish values which may be detrimental based on the proposed quality characteristics.

Table 5-8. Contour (SR) Functions

Level	Function	P-Value	R-Square
POSITION TOLERANCE (P_TOL) (in.)			
LOW	$y = a + bx + ce^{x} + \frac{d}{\ln(x)} + e\frac{\ln(x)}{x}$	0.00041	0.936
CENTRAL	$y = a + b\exp\left(-\exp\left(-\left(\frac{x-c}{d}\right)\right)\right) - \left(\left(\frac{x-c}{d}\right)+1\right)$	0.00439	0.860
HIGH	$y = a + bx + c(\ln(x))^{2} + \frac{d}{\ln(x)} + e\frac{\ln(x)}{x}$	0.00395	0.815
TOTAL RUNOUT TOLERANCE (T_RUN_TOL) (in.)			
LOW	$y = a + b\left(\frac{4\left(\exp\left(-\frac{x-c}{d}\right)\right)}{\left(1+\exp\left(-\frac{x-c}{d}\right)^{2}\right)}\right)$	0.00038	0.891
CENTRAL		0.0002	0.834
HIGH		0.0048	0.847
RUNOUT TOLERANCE (RUN_TOL) (in.)			
LOW	$y = a + bx + c\exp^{x} + \frac{d}{\ln(x)} + e\frac{\ln(x)}{x}$	0.0037	0.833
CENTRAL	$y = a + b\exp\left(-\exp\left(-\left(\frac{x-c}{d}\right)\right)\right) - \left(\left(\frac{x-c}{d}\right)+1\right)$	0.00032	0.928
HIGH	$y = a + bx + cx^{2}\ln(x) + dx^{0.5}\ln(x) + e\frac{x}{\ln(x)}$	0.00012	0.867
CIRCULARITY TOLERANCE (CIRC_TOL) (in.)			
LOW	$y = a + bx + c\frac{x}{\ln(x)} + \frac{d}{x^{0.5}} + e\frac{x}{\ln(x)}$	0.00069	0.916
CENTRAL	$y = \frac{a + cx + ex^{2} + gx^{3}}{1 + bx + dx^{2} + fx^{3} + hx^{4}}$	0.0004	0.823
HIGH	$y = a + b\left(\frac{4\left(\exp\left(-\frac{x-c}{d}\right)\right)}{\left(1+\exp\left(-\frac{x-c}{d}\right)^{2}\right)}\right)$	0.00028	0.845
CYLINDRICITY TOLERANCE (CYLN_TOL) (in.)			
LOW	$y = a + bx + c\exp^{x} + \frac{d}{\ln(x)} + e\frac{\ln(x)}{x}$	0.0011	0.853
CENTRAL	$y = a + b\exp\left(-\exp\left(-\left(\frac{x-c}{d}\right)\right)\right) - \left(\left(\frac{x-c}{d}\right)+1\right)$	0.0048	0.766

Table 5-8. (Continued)

HIGH	$y = a + \frac{b}{\left(1 + \left(\frac{x-c}{d}\right)^2\right)}$	0.0193	0.622
KURTOSIS (RKU) (um)			
LOW	$y = a + b\exp\left(-0.5\left(\frac{x-c}{d}\right)^2\right)$	0.00104	0.937
CENTRAL		0.0003	0.875
HIGH	$y = \frac{a + c\ln(x) + e(\ln(x))^2 + g(\ln(x))^3 + i(\ln(x))^4 + k(\ln(x))^5}{1 + b\ln(x) + d(\ln(x))^2 + f(\ln(x))^3 + h(\ln(x))^4 + j(\ln(x))^5}$	0.0013	0.782
SKEWNESS (RSK) (um)			
LOW	$y = a + bx + c\frac{x}{\ln(x)} + \frac{d}{x^{0.5}} + e\frac{x}{\ln(x)}$	0.0011	0.948
CENTRAL	$y = a + b\sin^2\left(\frac{2\pi x}{d+c}\right)$	0.0211	0.720
HIGH		0.0258	0.681
WAVELENGTH (LQ) (um)			
LOW	$y = a + bx + c\exp^x + \frac{d}{x^2} + e\exp^{-x}$	0.0	0.941
CENTRAL	$y = a + b\sin\left(\frac{2\pi x}{d+c}\right)$	0.00043	0.909
HIGH		0.00031	0.902
SPACING (SM) (um)			
LOW	$y = \frac{a + c\ln(x) + e(\ln(x))^2 + g(\ln(x))^3 + i(\ln(x))^4}{1 + b\ln(x) + d(\ln(x))^2 + f(\ln(x))^3 + h(\ln(x))^4}$	0.00354	0.922
CENTRAL	$y = a + bx + cx^{0.5}\ln(x) + \frac{d}{\ln(x)} + \frac{e}{x^{0.5}}$	0.00225	0.910
HIGH	$y = a + bx + cx^{2.5}\ln(x) + \frac{d}{\ln(x)} + \frac{e}{x^{0.5}}$	0.02310	0.724
PEAK-TO-VALLEY HEIGHT (RTM) (um)			
LOW	$y = a + bx + cx^3 + dx^{0.5}\ln(x) + e\frac{x}{\ln(x)}$	0.0013	0.884
CENTRAL	$y = a + bx + cx^{2.5} + dx^{0.5}\ln(x) + e\frac{x}{\ln(x)}$	0.0032	0.943
HIGH	$y = a + bx + cx^2 + dx^{0.5}\ln(x) + e\frac{x}{x^{0.5}}$	0.0021	0.810

Table 5-9. Contour (SR) Parameter Estimates

Position Tolerance Parameter Estimates (P_TOL) (in.)				
Param.	**P-Value (L/C/H)**	**LOW**	**CENTRAL**	**HIGH**
a	0.001/0.021/0.014	23.59594967	-0.00046138	49.99352669
b	0.031/0.045/0.005	**-0.01355529***	0.049346097	0.002502379
c	0.042/0.003/0.001	1.06139e-47	**58.64826781***	**-0.41282681***
d	0.0/0.004/0.0623	-131.284457	1.068598150	-235.598147
e	0.0032/0.0283	**136.0064751***		209.9864471
Total Runout Tolerance Parameter Estimates (T_RUN_TOL) (in.)				
a	0.003/0.0/0.009	**0.000329345***	0.000648122	9.81559e-05
b	0.037/0.002/0.031	0.001614682	**0.002452390***	0.001187878
c	0.023/0.004/0.008	47.29518888	114.0892940	86.73527900
d	0.068/0.032/0.045	0.738386217	3.345718541	**21.83792822***
Runout Tolerance Estimates (RUN_TOL) (in.)				
a	0.012/0.0/0.024	-11.6428557	0.001543644	94.49518349
b	0.0/0.056/0.072	0.007363929	**2.312642946***	5.205931270
c	0.021/0.032/0.002	-1.8641e-48	55.24321201	**-1.4629e-05***
d	0.069/0.0/0.045	**64.14459223***	0.925728771	12.58933760
e	0.061/0.046	**-65.4285082***		-54.9937387
Circularity Tolerance Parameter Estimates (CIRC_TOL) (in.)				
a	0.042/0.0/0.034	293.0180386	1.11813e-05	0.006556679
b	0.008/0.093/0.041	2.022835635	**-4.9568e-06***	0.037698783
c	0.046/0.002/0.0	**-14.4925573***	0.000322827	124.1091288
d	0.037/0.012/0.351	-3437.77457	-0.00013423	**0.865980041***
e	0.098/0.0	**3543.598965***	-5.5456e-06	
f	0.074		**-7.5371e-07***	
g	0.08224		**2.2047e-08***	
h	0.10036		**8.61023e-09***	
Cylindricity Tolerance Parameter Estimates (CYLN_TOL) (in.)				
a	0.0/0.034/0.001	-2.85599734	0.001961275	0.001537068
b	0.037/0.041/0.078	0.001712145	0.005506903	**0.003965919***
c	0.065/0.002/0.016	**-2.3618e-49***	96.32551061	118.6610787
d	0.001/0.0/0.037	15.82867409	14.79602325	1.551553888
e	0.003	-16.2936092		
Kurtosis Parameter Estimates (RKU) (um)				
a	0.035/0.007/0.011	2.563265198	2.546009331	0.034859364
b	0.028/0.056/0.003	52.18210032	**1.884647227***	-0.20460034
c	0.218/0.0/0.011	**66.52764866***	148.7381380	0.062033190
d	0.091/0.036/0.002	**0.034656595***	0.129756445	-0.21744156
e	0.2433			**0.056719949***
f	0.0031			0.096522238
g	0.046			-0.05735172
h	0.068			**-0.01404263***
i	0.322			**0.013636952***
j	0.089			**0.000695039***

Table 5-9. (Continued)

k	0.038			-0.00099621
Skewness Parameter Estimates (RSK) (um)				
a	0.0/0.023/0.047	-24955.4932	-0.35662455	-0.87839496
b	0.001/0.038/0.0	-171.511787	0.640960161	0.860351148
c	0.011/0.032/0.041	1230.084945	2.325183310	0.401315664
d	0.0991/0.0/0.135	**293138.9654***	59.36641789	**615.9261623***
e	0.261	**-302229.091***		
Wavelength Parameter Estimates (LQ) (um)				
a	0.0/0.041/0.0	-0.00382348	34.68809083	-42.4233958
b	0.031/0.102/0.034	0.000195509	**0.019289826***	0.007549807
c	0.079/0.051/0.055	**1.75749e-48***	**-0.12596047***	**-1.8475e-07***
d	0.0/0.007/0.012	43.62606414	-178.071512	328.2985180
e	0.001/0.0/0.039	-4.5372e+12	170.9245445	-295.804927
Spacing Parameter Estimates (SM) (um)				
a	0.0/0.045/0.016	0.069857918	24.45825405	72.11674510
b	0.033/0.0/0.0	-0.98562409	45.95098198	19.38584260
c	0.0/0.046/0.026	0.108926811	1.647124489	5.343189105
d	0.014/0.008/0.189	0.367579416	134.5166002	**121.0912433***
e	0.0589	**0.094512937***		
f	0.0021	-0.06133468		
g	0.0421	-0.06493394		
h	0.05 76	**0.003854177***		
I	0.213	**0.008349991***		
Peak-to-Valley Height Parameter Estimates (RTM) (um)				
a	0.0/0.022/0.014	29316.62427	-3040.72700	-771.508558
b	0.003/0.043/0.025	1611.576421	-167.426598	0.152356788
c	0.032/0.056/0.077	-2.7434e-05	**0.000107867***	**-1.5936e-05***
d	0.0/0.002/0.151	3960.060739	-408.349904	**5959.301221***
e	0.088/0.0/0.006	**-17168.6773***	1776.631646	-5358.03455

*** Parameters are Eliminated.**

Listed in Table 5-10 is the straight/taper geometry relationships between the cutting force obtained from the proposed design of experiments at each depth level of the proposed tolerance and surface finish indices. Table 5-11 lists the parameter estimates for each relationship. The R-square value is also listed to indicate the strength of the relationship.

By examining the relationship between cutting force and the straight/taper geometry tolerance indices, it is shown that the increase in cutting force decreases straight/taper geometry tolerance and generally provides a higher tolerance value. It is

evident that depth of cut, which changes the force, effects straight/taper geometry tolerance.

By examining the relationship between cutting force and straight/taper geometry surface finish indices, it is also shown that the increase in cutting force increases the straight/taper geometry surface finish values which may be detrimental based on the proposed quality characteristics.

Table 5-10. Straight/Taper Geometry (SR) Functions

POSITION TOLERANCE (P_TOL) (in.)			
Level	**Function**	**P-Value**	**R-Square**
LOW	$y = a + bx + \frac{c}{x} + \frac{d}{x^{1.5}} + e\frac{\ln(x)}{x^2}$	0.00052	0.946
HIGH	$y = a + b\sin^2\left(\frac{2\pi x}{d+c}\right)$	0.00183	0.874
CENTRAL	$y = a + berf\left[\left(\frac{(x-c)^2}{d}\right)\right]$	0.02191	0.818
FLATNESS TOLERANCE (FLAT_TOL) (in.)			
LOW	$y = a + bx + cx^{1.5} + dx^{2.5} + ex^3$	0.00067	0.966
CENTRAL	$y = a + bx + cx^2\ln(x) + dx^{2.5} + ex^3$	0.0193	0.720
HIGH	$y = a + bx + cx^{1.5} + dx^{2.5} + ex^3$	0.00682	0.862
STRAIGHTNESS TOLERANCE (STR_TOL) (in.)			
LOW	$y = a + bx + cx^{0.5}\ln(x) + d\frac{\ln(x)}{x^2} + \frac{e}{x^2}$	0.00042	0.966
CENTRAL	$y = a + bx + cx^{1.5} + dx^3 + \frac{e}{x^2}$	0.00438	0.748
HIGH	$y = a + bx + cx^{2.5} + dx^{0.5}\ln(x) + e\frac{x}{\ln(x)}$	0.00194	0.870
ANGULARITY TOLERANCE (ANG_TOL) (in.)			
LOW	$y = a + b\exp\left(-\exp\left(-\left(\frac{x-c}{d}\right)\right)\right) - \left(\left(\frac{x-c}{d}\right)+1\right)$	0.00108	0.985
CENTRAL	$y = a + bx + cx\ln(x) + \frac{d}{\ln(x)} + e\frac{\ln(x)}{x}$	0.0002	0.735
HIGH	$y^{-1} = a + bx^3 + \frac{c}{x^2}$	0.00054	0.934
PARALLELISM TOLERANCE (PARA_TOL) (in.)			

Table 5-10. (Continued)

LOW	$y = a + b\exp\left(-\exp\left(-\left(\frac{x-c}{d}\right)\right)\right) - \left(\left(\frac{x-c}{d}\right)+1\right)$	0.00036	0.965
CENTRAL		0.00068	0.994
HIGH		0.00044	0.989
KURTOSIS (RKU) (um)			
LOW	$y = a + bx + cx^{1.5} + \frac{d}{\ln(x)} + e\frac{\ln(x)}{x}$	0.0193	0.781
CENTRAL	$y = a + b\exp\left(-\exp\left(-\left(\frac{x-c}{d}\right)\right)\right) - \left(\left(\frac{x-c}{d}\right)+1\right)$	0.00243	0.895
HIGH	$y = a + berf\left(\frac{x-c}{d^2}\right)$	0.0035	0.885
SKEWNESS (RSK) (um)			
LOW	$y = a + bx + c\ln(x) + \frac{d}{x^{0.5}} + e\frac{x}{\ln(x)}$	0.0115	0.764
CENTRAL	$y = \frac{a + c\ln(x) + e(\ln(x))^2 + g(\ln(x))^3}{1 + b\ln(x) + d(\ln(x))^2 + f(\ln(x))^3 + h(\ln(x))^4}$	0.00033	0.998
HIGH	$y = a + bx + cx^{2.5} + dx^{0.5}\ln(x) + e\frac{x}{\ln(x)}$	0.00384	0.851
WAVELENGTH (LQ) (um)			
LOW	$y = a + bx + cx^{2.5} + \frac{d}{\ln(x)} + e\frac{\ln(x)}{x}$	0.0193	0.824
CENTRAL	$y = a + b\exp\left(-0.5\left(\frac{x-c}{d}\right)\right)$	0.0211	0.816
HIGH	$y = a + b\sin^2\left(\frac{2\pi x}{d+c}\right)$	0.0236	0.754
SPACING (SM) (um)			
LOW	$y = a + bx + cx^{1.5} + \frac{d}{\ln(x)} + e\frac{\ln(x)}{x}$	0.0143	0.847
CENTRAL	$y = a + b\exp\left(-\exp\left(-\left(\frac{x-c}{d}\right)\right)\right) - \left(\left(\frac{x-c}{d}\right)+1\right)$	0.0175	0.752
HIGH	$y = a + bx + cx^2\ln(x) + dx^{2.5} + ex^3$	0.00315	0.702
PEAK-TO-VALLEY HEIGHT (RTM) (um)			
LOW	$y = a + bx + cx^2 + \frac{d}{x^2} + ee^{-x}$	0.00573	0.840
CENTRAL	$y = a + \frac{b}{\left(1 + \left(\frac{x-c}{d^2}\right)\right)}$	0.0193	0.708

Table 5-10. (Continued)

HIGH	$y = a + bx + cx^2 \ln(x) + dx^{0.5} \ln(x) + e\frac{x}{\ln(x)}$	0.00769	0.706

Table 5-11. Straight/Taper Geometry (SR) Parameter Estimates

Position Tolerance Parameter Estimates (P_TOL) (in.)				
Param.	**P-Value (L/C/H)**	**LOW**	**CENTRAL**	**HIGH**
a	0.007/0.0/0.025	-0.14982376	-4.8847e-05	-0.00565135
b	0.013/0.002/0.04	0.000257545	0.002022233	0.000201930
c	0.0/0.022/0.071	58.57784196	1.244256678	**-1.6004e-05***
d	0.052/0.112/0.03	**-934.028184***	**73.04768328***	1.3281e-09
e	0.0512	**1027.140453***		2.491844109
Flatness Tolerance Parameter Estimates (FLAT_TOL) (in.)				
a	0.0/0.0/0.003	-0.00102367	-0.00122717	4.73068e-05
b	0.014/0.219/0.03	9.25916e-05	**6.07145e-05***	-1.5867e-06
c	0.011/0.0/0.0912	-1.2758e-05	-1.0249e-06	**2.5257e-07***
d	0.109/0.042/0.06	**7.54851e-08***	5.6628e-07	**-2.1219e-09***
e	0.062/0.102/0.0	**-3.0246e-09***	**-1.427e-08***	9.51124e-11
Straightness Tolerance Estimates (STR_TOL) (in.)				
a	0.007/0.0/0.021	-0.00517966	-0.00565135	-0.66502912
b	0.038/0.042/0.04	-5.7754e-05	0.000201930	-0.03659317
c	0.0/0.0571/0.011	0.000217710	**-1.6004e-05***	2.32531e-08
d	0.0721/0.032/0.1	**6.027599349***	1.3281e-09	**-0.08924072***
e	0.025/0.005/0.07	-18.3405932	2.491844109	**0.388294575***
Angularity Tolerance Parameter Estimates (ANG_TOL) (in.)				
a	0.0/0.0/0.0	0.047032195	-1484.28538	97.56273417
b	0.562/0.031/0.0	**8.306355881***	3.722683103	-1.0136e-05
c	0.0/0.001/0.0233	122.8701866	-0.50212335	-308679.435
d	0.031/0.0	8.494965686	7819.762642	
e	0.0612		**-7703.30449***	
Parallelism Tolerance Parameter Estimates (PARA_TOL) (in.)				
a	0.002/0.0/0.0	6.20275e-05	0.000125170	8.28466e-05
b	0.0/0.023/0.0671	0.000204851	0.005242588	**0.019312378***
c	0.0/0.0435/0.003	64.45058111	76.70361728	170.4228699
d	0.0498/0.0/0.031	**3.529522173***	1.728339551	-1.50761518
Kurtosis Parameter Estimates (RKU) (um)				
a	0.008/0.024/0.03	12376.11259	2.529443404	3.088939394
b	0.012/0.004/0.0	-13.3167320	12.53848161	7.594004048
c	0.103/0.032/0.01	**0.408028081***	82.27816547	77.84547502
d	0.0/0.006/0.071	-67058.9766	4.179956646	**1.569012405***
e	0.07934	**67615.76162***		
Skewness Parameter Estimates (RSK) (um)				
a	0.006/0.032/0.0	1790.223031	0.177483056	-9068.79983
b	0.058/0.104/0.02	**0.151315122**	**-0.17476692**	-499.203133

Table 5-11. (Continued)

c	0.001/0.023/0.09	-232.540714	-0.11165900	**0.000309636***
d	0.0/0.0/0.0132	-12626.5576	-0.16856408	-1218.68271
e	0.0/0.213/0.0312	11472.75355	**0.023287938***	5299.632666
f	0.0		0.056469946	
g	0.0782		**-0.00160988***	
h	0.0944		**-0.00474742***	
Wavelength Parameter Estimates (LQ) (um)				
a	0.046/0.0/0.0213	-1450.15017	0.190739916	0.852394238
b	0.013/0.046/0.02	1.080275714	32.77503663	-0.03291797
c	0.113/0.0/0.0796	**-9.393e-05***	139.1007148	**0.000426353***
d	0.041/0.069/0.05	7931.239630	**4.709817555***	**-0.00021638***
e	0.002	-8046.13533		4.73987e-06
Spacing Parameter Estimates (SM) (um)				
a	0.0/0.0/0.0213	6.71135e+06	422.2020750	1546.594778
b	0.042/0.022/0.04	-7784.31037	588.6010675	-56.3639387
c	0.0/0.031/0.047	252.7403465	109.1740476	0.701474823
d	0.1/0.172/0.0891	**-3.6166e+07***	**-1.21596547***	**-0.35384126***
e	0.1317	**3.62242e+07***		**0.007689664***
Peak-to-Valley Parameter Estimates (RTM) (um)				
a	0.013/0.047/0.0	36.18217219	2.444432106	34056.45524
b	0.056/0.037/0.02	**-0.53808786***	4.215345718	1877.552761
c	0.051/0.0/0.153	**0.002087521***	108.8403930	**-0.00498976***
d	0.0/0.130/0.0	-28512.8865	**0.014458223***	4553.017925
e	0.0/0.10323	1.83213e+17		**-19859.7800**

*** Parameters are Eliminated.**

By examining the straight/taper geometry force relationships, the cutting force at a low and central depth of cut provides an increasing linear relationship between cutting force and feedrate. Cutting force is minimized when feedrate is low and maximized when feedrate is high. The cutting force relationship with spindle speed is non-linear where cutting force increases with the decrease in spindle speed. The feedrate-speed interaction minimizes force when feedrate is low and spindle speed is high and maximizes force when feedrate is high and spindle speed is low.

The cutting force at a high depth of cut provides an increasing linear relationship between cutting force and feedrate. Cutting force is minimized when feedrate is low and maximized when feedrate is high. The cutting force relationship with spindle speed is

non-linear where cutting force increases with the decrease in spindle speed. The feedrate-speed interaction minimizes force when feedrate is low and spindle speed is high and maximizes force when feedrate is high and spindle speed is low.

By examining the straight/taper geometry surface finish relationships, peak-to-valley height at a low depth of cut increases linearly when spindle speed decreases and increases non-linearly when feedrate increases. The feedrate-speed interaction minimizes peak-to-valley height when feedrate is low and spindle speed is high and maximizes peak-to-valley height when feedrate is high and spindle speed is low. The peak-to-valley height at a central depth of cut increases non-linearly when spindle speed decreases and feedrate increases, however, peak-to-valley height decreases when spindle speed is between 15,000 RPM and 18,000 RPM and feedrate is between 150 in./min and 250 in./min.

The peak-to-valley height at high depth of cut increases non-linearly when spindle speed decreases and feedrate increases, however, peak-to-valley height decreases when spindle speed is between 12,500 RPM and 17,000 RPM and feedrate is between 150 in./min and 250 in./min.

By examining the straight/taper geometry tolerance relationships, it is shown that the parallelism tolerance at a low depth of cut decreases non-linearly when spindle speed increases and increases non-linearly when feedrate increases. Parallelism tolerance is minimized when spindle speed is high and feedrate is low.

The parallelism tolerance at a central depth of cut increases when spindle speed decreases and feedrate increases. The feedrate-speed interaction provides a higher parallelism tolerance when feedrate is between 60 in./min and 170 in./min and when spindle speed decreases from 7,500 RPM and 1,000 RPM.

Parallelism tolerance at a high depth of cut is constant with spindle speed but rapidly increases with feedrate. The parallelism tolerance increases at a moderate feedrate starting a 100 in./min and peaking at 200 in./min. At the peak tolerance feedrate, parallelism tolerance decreases with an increase in spindle speed.

The position tolerance at a low depth of cut increases non-linearly as spindle speed and feedrate increases. Position tolerance is maximized when feedrate is between 150 in./min and 250 in./min and spindle speed is between 15,000 RPM and 18,000 RPM. Position tolerance is minimized when spindle speed and feedrate is low.

The position tolerance at a central depth of cut increases when spindle speed increases and decreases. This parabolic behavior minimizes position tolerance when spindle speed is between 7,500 RPM and 12,500 RPM. Feedrate also is parabolic where position tolerance is maximized at 50 in./min and 200 in./min to 265 in./min. A low feedrate and low spindle speed interaction provides the highest position tolerance.

Position tolerance at a high depth of cut increases non-linearly when spindle speed decreases at a central feedrate and increases when both feedrate and spindle speed are high. Position tolerance is minimized when spindle speed is high and feedrate is between 45 in./min and 200 in./min.

The straightness tolerance at a low depth of cut is parabolic for both the spindle speed and feedrate. Straightness tolerance is minimized when spindle speed is high and feedrate is between 200 in./min and 300 in./min. It is maximized when spindle speed is low and feedrate is high.

Straightness tolerance at a central depth of cut is parabolic for both the spindle speed and feedrate interaction. Straightness tolerance is minimized when spindle speed is

moderate and feedrate is moderate and is maximized when feedrate is high and spindle speed is low. No solutions exist when spindle speed is above 15,000 RPM and below 100 in./min.

Straightness tolerance at a high depth of cut is parabolic for both spindle speed and feedrate. Straightness tolerance is minimized when spindle speed is between 7,500 RPM and 12,500 RPM and feedrate is between 50 in./min and 150 in./min.

Multiple Regression Results

Table 5-12. (MR) Straight/Taper Geometry Performance Functions

Level	Function	P-Value	R-Square
KURTOSIS (RKU) (um)			
LOW	$z = a+bx+cy+dx^2+ey^2+fxy+gx^3+hy^3+ixy^2+jyx^2$	0.00247	0.816
HIGH		0.00143	0.860
CENTRAL	$z=a+b\exp\left[-0.5\left(\frac{x-c}{d}\right)^2\right]+e\exp\left[-0.5\left(\frac{y-f}{g}\right)^2\right]+h\exp\left[-0.5\left(\left(\frac{x-c}{d}\right)^2+\left(\frac{y-f}{g}\right)^2\right)\right]$	0.00041	0.933
SKEWNESS (RSK) (um)			
LOW	$z = a+bx+cy+dx^2+ey^2+fxy+gx^3+hy^3+ixy^2+jyx^2$	0.00024	0.926
CENTRAL		0.00038	0.986
HIGH		0.00219	0.994
WAVELENGTH (LQ) (um)			
LOW	$z^{-1} = a+bx+\frac{c}{\ln(y)}$	0.00086	0.985
CENTRAL	$z = a+\frac{b}{\left[1+\left(\frac{x-c}{d}\right)^2\right]\left[1+\left(\frac{y-e}{f}\right)^2\right]}$	0.00089	0.952
HIGH	$\ln(z) = a+b(\ln(x))^2+\frac{c}{\ln(y)}$	0.0298	0.876
SPACING (SM) (um)			
LOW	$\ln(z) = a+bx\ln(x)+c\ln(y)$	0.00328	0.932
CENTRAL	$z = a+by+cy^2+\frac{d}{1+\left(\frac{x-e}{f}\right)^2}$	0.00078	0.995

Table 5-12. (Continued)

HIGH	$z^{-1} = a + bx\ln(x) + cy\ln(y)$	0.00219	0.923
ANGULARITY TOLERANCE (ANG_TOL) (in.)			
LOW	$z = a + b\exp\left\{-0.5\left[\left(\frac{\ln\frac{x}{c}}{d}\right)^2 + \left(\frac{y-e}{f}\right)^2\right]\right\}$	0.0	0.953
CENTRAL	$z = 16a\left[\frac{\exp\left[-\left(\frac{x-b}{c}\right)\right]}{\left\{1+\exp\left[-\left(\frac{x-b}{c}\right)\right]\right\}^2}\right]\left[\frac{\exp\left[-\left(\frac{y-d}{e}\right)\right]}{\left\{1+\exp\left[-\left(\frac{y-d}{e}\right)\right]\right\}^2}\right]$	0.0	0.989
HIGH	$z = a\exp\left[-0.5\left(\left(\frac{x-b}{c}\right)^2 + \left(\frac{y-d}{e}\right)^2\right)\right]$	0.0	0.932
STRAIGHTNESS TOLERANCE (STR_TOL) (in.)			
LOW	$\ln(z) = a + bx^3 + cy^{1.5}$	0.0	0.962
CENTRAL	$\ln(z) = a + bx^{2.5} + cy^{1.5}$	0.0231	0.962
HIGH	$\ln(z) = a + bx^{2.5} + cy^{0.5}\ln(y)$	0.0119	0.855
POSITION TOLERANCE (P_TOL) (in.)			
LOW	$z = a+bx+cy+dx^2+ey^2+fxy+gx^3+hy^3+ixy^2+jyx^2$	0.00328	0.890
CENTRAL	$z = a+bx+cy+dx^2+ey^2+fxy+gx^3+hy^3+ixy^2+jyx^2$	0.0214	0.844
HIGH	$z = a+16b\left[\frac{\exp\left[-\left(\frac{x-c}{d}\right)\right]}{\left\{1+\exp\left[-\left(\frac{x-c}{d}\right)\right]\right\}^2}\right]\left[\frac{\exp\left[-\left(\frac{y-e}{f}\right)\right]}{\left\{1+\exp\left[-\left(\frac{y-e}{f}\right)\right]\right\}^2}\right]$	0.0148	0.811
PARALLELISM TOLERANCE (PARA_TOL) (in.)			
LOW	$z = a+b\ln(x)+\frac{c}{y}+d(\ln(x))^2+\frac{e}{y^2}+f\frac{\ln(x)}{y}+g(\ln(x))^2+\frac{h}{y^3}+i\frac{\ln(x)}{y^2}+j\frac{(\ln(x))^2}{y}$	0.0958	0.763
CENTRAL	$\ln(z) = a + bx^{2.5} + cy^{2.5}$	0.0294	0.840
HIGH	$z = a+b\exp\left[-0.5\left(\frac{x-c}{d}\right)^2\right]+e\exp\left[-0.5\left(\frac{y-f}{g}\right)^2\right]+h\exp\left[-0.5\left(\left(\frac{x-c}{d}\right)^2+\left(\frac{y-f}{g}\right)^2\right)\right]$	0.0193	0.700

Table 5-12. (Continued)

PEAK-TO-VALLEY HEIGHT (RTM) (um)			
LOW	$\ln(z) = a + bx + c\ln(y)$	0.0	0.944
CENTRAL	$z = a + b\ln(x) + cy + d(\ln(x))^2 + ey^2 + fy\ln(x) + g(\ln(x))^3 + hy^3 + iy^2\ln(x) + jy(\ln(x))$	0.0078	0.931
HIGH	$\ln(z) = a + b(\ln(x))^2 + c\ln(y)$	0.0593	0.833
CUTTING FORCE (N)			
LOW	$z = a + by + \dfrac{4c\exp\left[-\left(\dfrac{x-d}{e}\right)\right]}{\left\{1+\exp\left[-\left(\dfrac{x-d}{e}\right)\right]\right\}^2}$	0.00033	0.986
CENTRAL		0.00058	0.983
HIGH	$z = a + by + c\exp\left[-\exp\left(-\dfrac{x-d}{e}\right) - \dfrac{x-d}{e} + 1\right]$	0.00095	0.992
FLATNESS TOLERANCE (FLAT_TOL) (in.)			
LOW	$z = a + bx + cy + dx^2 + ey^2 + fxy + gx^3 + hy^3 + ixy^2 + jyx^2$	0.0486	0.831
CENTRAL		0.0211	0.801
HIGH	$z = \dfrac{a}{\left[1+\left(\dfrac{x-b}{c}\right)^2\right]\left[1+\left(\dfrac{y-d}{e}\right)^2\right]}$	0.0058	0.920

Table 5-13. (MR) Straight/Taper Geometry Parameter Estimates

Kurtosis Parameter Estimates (RKU) (um)				
Param.	**P-Value (L/C/H)**	**LOW**	**CENTRAL**	**HIGH**
a	0.0/0.031/0.047	2.496999069	2.514969904	3.756746678
b	0.047/0.058/0.0	0.000775553	**-0.16757091***	0.00106011
c	0.0/0.0/0.0	-0.01950289	20586.65158	-0.08044323
d	0.147/0.001/0.02	**-7.5137e-08***	2538.089722	-4.1638e-08
e	0.041/0.083/0.03	7.66661e-05	**0.178538572***	0.000686325
f	0.067/0.019/0.08	**-4.3991e-07***	192.2609102	**-7.1893e-06***
g	0.025/0.21/0.036	1.83562e-12	**42.72764909***	-4.1784e-13
h	0.078/0.089/0.07	**-7.047e-08***	**3.645623509***	**-1.4686e-06***
I	0.064/0.247	**-3.2834e-09***		**4.72426e-09***
j	0.0899/0.0531	**1.06104e-10***		**3.0791e-10***
Skewness Parameter Estimates (RSK) (um)				
a	0.0/0.0/0.0351	-0.0160682	-0.103439	0.471057569
b	0.0738/0.0/0.031	**3.00967e-05***	-0.00011042	1.88145e-05
c	0.042/0.018/0.03	0.000512324	0.015585363	-0.0118141
d	0.0/0.024/0.110	-3.1233e-09	5.25376e-09	**8.31057e-09***
e	0.0846/0.007/0.0	**-6.4612e-06***	-0.00015001	0.000115846
f	0.078/0.135/0.03	**1.3588e-07***	**7.46732e-07***	-1.3014e-06

Table 5-13. (Continued)

g	0.034/0.017/0.0	8.11531e-14	5.0102e-13	-4.2613e-13
h	0.058/0.0/0.0143	**1.56541e-08***	3.53967e-07	**-2.4921e-07***
I	0.079/0.216/0.08	**-2.7807e-10***	**2.93515e-09***	**1.01379e-09***
j	0.104/0.068/0.06	**-2.0575e-12***	**-1.1211e-10***	**4.50989e-11***
Wavelength Parameter Estimates (LQ) (um)				
a	0.0/0.0/0.0	-3.09562819	0.150865572	1.845321931
b	0.003/0.24/0.002	2.16167e-08	**0.40937799***	-0.02556971
c	0.0/0.0/0.0	28.0537094	1960.966883	-6.75699357
d	0.0041		3241.190095	
e	0.0795		**199.9912331***	
f	0.1572		**122.8952296***	
Spacing Parameter Estimates (SM) (um)				
a	0.027/0.036/0.0	5.357513131	325.6953786	0.001850704
b	0.0/0.087/0.001	-6.777e-06	**0.201615371***	1.38811e-08
c	0.047/0.136/0.03	0.269260111	**-0.00176849***	-7.0018e-07
d	0.00058		548.5614485	
e	0.02119		2006.445633	
f	0.07941		**3752.14484***	
Angularity Parameter Estimates (ANG_TOL) (in.)				
a	0.0/0.019/0.034	0.014507916	1.081372482	1.081883593
b	0.026/0.045/0.02	0.951160594	218.9758235	17002.68708
c	0.034/0.041/0.0	17846.35488	2113.497491	4295.651078
d	0.097/0.112/0.13	**0.254453401***	**176.2993146***	**29.65723419***
e	0.096/0.084/0.0	**1.004064709***	**24.16635831***	32.73289421
f	0.0	49.92005896		
Flatness Parameter Estimates (FLAT_TOL) (in.)				
a	0.004/0.019/0.0	-5.7909e-06	-0.00022576	0.000145215
b	0.037/0.023/0.0	1.07727e-08	-1.3069e-08	1181
c	0.0/0.139/0.024	5.11866e-07	**7.59813e-06***	3433.123176
d	0.081/0.0/0.0	**-1.1479e-12***	9.78773e-13	163
e	0.0/0.002/0.083	-2.9694e-09	-5.9539e-08	**43.11815163***
f	0.0045/0.01335	-1.883e-11	2.92771e-10	
g	0.0011/0.09578	3.19875e-17	**-1.6529e-17***	
h	0.1523/0.07993	**5.77892e-12***	**1.56817e-10***	
I	0.0698/0.03927	**-7.6166e-14***	-8.0636e-13	
j	0.0951/0.0835	**2.26184e-15***	**-9.696e-15***	
Straightness Tolerance Parameter Estimates (STR_TOL) (in.)				
a	0.0/0.003/0.018	-9.22621131	60665.26505	-10.9084187
b	0.0/0.0/0.0	-2.0501e-13	2.58631e-05	-2.3052e-11
c	0.021/0.047/0.01	0.000396016	-11097.1759	0.051266044
Position Tolerance Parameter Estimates (P_TOL) (in.)				
a	0.023/0.0471/0.0	0.006233275	-0.00085079	3.48889e-05
b	0.0/0.027/0.006	-4.7222e-07	-1.4944e-07	0.004847331
c	0.007/0.183/0.0	-9.2288e-05	**7.02634e-05***	1181

Table 5-13. (Continued)

d	0.006/0.03/0.046	-6.3501e-12	8.76985e-12	3585.82285
e	0.098/0.024/0.0	**3.99502e-07***	-6.1379e-07	260
f	0.078/0.231/0.04	**7.39953e-09***	**2.28801e-09***	41.13615488
g	0.003/0.0194	7.75677e-16	-3.5653e-16	
h	0.0859/0.0078	**-5.5762e-10***	1.53432e-09	
I	0.07947/0.01427	**-1.0888e-11***	**-6.2991e-12***	
j	0.9483/0.05795	**-1.6841e-13***	**-4.2145e-14***	
Parallelism Tolerance Parameter Estimates (PARA_TOL) (in.)				
a	0.0/0.002/0.0056	0.000369625	-10.0227762	0.000442486
b	0.097/0.031/0.08	**1.23207e-05***	2.36847e-11	**-0.00043869***
c	0.0/0.005/0.0216	0.235591711	2.70584e-06	4429.200376
d	0.1846/0.0057	**-3.094e-05***		5866.981887
e	0.00036/0.06991	-8.17850301		**-0.0053941***
f	0.00631/0.00057	-0.01810755		540.5169473
g	0.00026/0.05993	2.68621e-06		**121.6612837***
h	0.00372/0.09217	64.22490625		**0.060055983***
I	0.0958	**0.466952558***		
j	0.16834	**-0.0003129***		
Peak-to-Valley Height Parameter Estimates (RTM) (um)				
a	0.028/0.011/0.0	-0.0443295	-51.3936096	1.099740041
b	0.001/0.0/0.046	-7.1853e-05	16.73449794	-0.0258224
c	0.03/0.004/0.013	0.323689884	0.235504543	0.359776805
d	0.009476		-1.8433783	
e	0.078254		**-0.00108726***	
f	0.281675		**-0.01366154***	
g	0.004627		0.067070701	
h	0.068853		**1.495e-06***	
I	0.057441		**3.63589e-05***	
j	0.104563		**-2.2369e-05***	
Cutting Force Parameter Estimates (N)				
a	0.037/0.004/0.01	47.56557637	23.75148849	49.04506607
b	0.068/0.059/0.0	**0.055041779***	**0.125210867***	0.149431263
c	0.0/0.125/0.002	112.201731	**125.4784456***	238.5441716
d	0.002/0.035/0.13	476.4616121	245.1043323	**-959.570996***
e	0.14/0.0/0.00468	**3313.767707***	3491.408113	2985.480245

*** Parameters are Eliminated.**

MR empirical relationships for the contour geometry are listed in Table 5-14 and the contour geometry parameter estimates are listed in Table 5-15. By examining the contour geometry force relationships, the cutting force at a low and central depth of cut provides an increasing linear relationship between cutting force and feedrate. Cutting

force is minimized when feedrate is low and maximized when feedrate is high. The cutting force relationship with spindle speed is non-linear where cutting force increases with the decrease in spindle speed. The feedrate-speed interaction minimizes force when feedrate is low and spindle speed is high and maximizes force when feedrate is high and spindle speed is low.

The cutting force at a high depth of cut provides an increasing linear relationship between cutting force and feedrate. Cutting force is minimized when feedrate is low and maximized when feedrate is high. The cutting force relationship with spindle speed is non-linear where cutting force increases with the decrease in spindle speed. The feedrate-speed interaction minimizes force when feedrate is low and spindle speed is high and maximizes force when feedrate is high and spindle speed is low.

By examining the contour geometry surface finish relationships, peak-to-valley height at a low depth of cut increases linearly when spindle speed decreases and increases non-linearly when feedrate increases. The feedrate-speed interaction minimizes peak-to-valley height when feedrate is low and spindle speed is high and maximizes peak-to-valley height when feedrate is high and spindle speed is low. The peak-to-valley height at central depth of cut increases non-linearly when spindle speed decreases and feedrate increases. The peak-to-valley height at high depth of cut increases non-linearly when spindle speed decreases and feedrate increases.

By examining the contour geometry tolerance relationships, it is shown that the total runout tolerance at a low depth of cut decreases non-linearly when spindle speed increases and increases non-linearly when feedrate increases. Total runout tolerance is minimized when spindle speed is high and feedrate is low.

Total runout tolerance at a central depth of cut increases when spindle speed decreases and feedrate increases and at a high depth of cut, the total runout tolerance increases rapidly as spindle speed decreases and feedrate increases.

The position tolerance at a low depth of cut increases non-linearly as spindle speed and feedrate increases. Position tolerance is maximized when feedrate is at central speed and spindle speed is high Position tolerance is minimized when spindle speed and feedrate are low.

The position tolerance at a central depth of cut increases when spindle speed decreases. A low feedrate and low spindle speed interaction provides the highest position tolerance.

Position tolerance at a high depth of cut increases non-linearly when spindle speed decreases at a central feedrate and increases when both feedrate and spindle speed are high.

The circularity tolerance at a low, central, and high depth of cut provides an increasing linear relationship between circularity tolerance and feedrate. Circularity tolerance is minimized when feedrate is low and maximized when feedrate is high. The circularity tolerance relationship with spindle speed is non-linear where tolerance improves with an increase in spindle speed. The feedrate-speed interaction minimizes circularity when feedrate is low and spindle speed is high and maximizes circularity when feedrate is high and spindle speed is low.

Table 5-14. Contour Geometry (MR) Functions

POSITION TOLERANCE (P_TOL) (in.)			
Level	**Function**	**P-Value**	**R-Square**
LOW	$z = a + bx + cy + d(\ln(x))^2 + ey^2 + fy\ln(x)$	0.0021	0.860
CENTRAL	$z = a + bx + cy + dy^2 + ey^3$	0.00145	0.900

Table 5-14. (Continued)

HIGH	$z = a + bx + cy + d(\ln(x))^2 + ey^2 + fy\ln(x)$	0.0319	0.846
TOTAL RUNOUT TOLERANCE (T_RUN_TOL) (in.)			
LOW	$z = a + b\sqrt{x} + c\ln(x)$	0.0036	0.900
CENTRAL	$z = a + bx + cy + d(\ln(x))^2 + ey^2 + fy\ln(x)$	0.00104	0.988
HIGH	$\ln(z) = a + bx^{1.5} + cy^2\ln(y) + dy^3$	0.0052	0.810
RUNOUT TOLERANCE (RUN_TOL) (in.)			
LOW	$z = a + bx + cy + dx^2 + ey^2 + fxy + gx^3 + hy^3 + ixy^2 + jyx^2$	0.00091	0.968
CENTRAL	$z = \dfrac{a}{\left[1 + \left(\dfrac{x-b}{c}\right)^2\right]\left[1 + \left(\dfrac{y-d}{e}\right)^2\right]}$	0.0068	0.913
HIGH	$\ln(z) = a + bx\ln(x) + \dfrac{c}{x^{1.5}} + dy^2\ln(y) + ey^{2.5} + fy^3$	0.00045	0.980
CIRCULARITY TOLERANCE (CIRC_TOL) (in.)			
LOW	$z = a + b\ln(x) + cy + d(\ln(x))^2 + ey^2 + fy\ln(x) + g(\ln(x))^3 + hy^3 + iy^2\ln(x) + jy(\ln(x))^2$	0.0214	0.938
CENTRAL	$z = a + bx + cy + dx^2 + ey^2 + fxy + gx^3 + hy^3 + ixy^2 + jyx^2$	0.0488	0.794
HIGH	$z = a + bx + cy + dx^2 + ey^2 + fxy$	0.0068	0.831
CYLINDRICITY TOLERANCE (CYLN_TOL) (in.)			
LOW	$z = a + b\ln(x) + cy + d(\ln(x))^2 + ey^2 + fy\ln(x) + g(\ln(x))^3 + hy^3 + iy^2\ln(x) + jy(\ln(x))^2$	0.0113	0.783
CENTRAL		0.0322	0.887
HIGH	$z = a + bx + cy + dx^2 + ey^2 + fxy$	0.0054	0.843
CUTTING FORCE (N)			
LOW	$z = a\exp\left[-\exp\left(-\dfrac{x-b}{c}\right)\right]\exp\left[-\exp\left(-\dfrac{y-d}{c}\right)\right]$	0.00064	0.994
CENTRAL	$z = a + b\exp\left[-\exp\left(-\dfrac{x-c}{d}\right)\right] + e\exp\left[-\exp\left(-\dfrac{y-f}{g}\right)\right]$	0.00057	0.997
HIGH	$\ln(z) = a + b\ln(x) + cy\ln(y)$	0.00095	0.933
A0 PEAK FORCE (N)			
LOW	$z = a + bx + cy + dx^2 + ey^2 + fxy + gx^3 + hy^3 + ixy^2 + jyx^2$	0.00075	0.989

Table 5-14. (Continued)

CENTRAL	$z = a + by + cy^2 + \dfrac{4d\exp\left[-\left(\dfrac{x-e}{f}\right)\right]}{\left\{1+\exp\left[-\left(\dfrac{x-e}{f}\right)\right]\right\}^2}$	0.00069	0.996
HIGH	$\ln(z) = a + \dfrac{b}{\ln(x)} + cy^{2.5} + dy^3$	0.00376	0.847
A1 FORCE (N)			
LOW	$z = a + \frac{b}{2}\left\{1-erf\left[\frac{d}{\sqrt{2}} - \frac{\ln\left(\frac{x}{c}\right)}{d\sqrt{2}}\right]\right\} + \frac{e}{2}\left\{1-erf\left[\frac{g}{\sqrt{2}} - \frac{\ln\left(\frac{y}{f}\right)}{g\sqrt{2}}\right]\right\} + \frac{h}{2}\left\{1-erf\left[\frac{d}{\sqrt{2}} - \frac{\ln\left(\frac{x}{c}\right)}{d\sqrt{2}}\right]\right\}\left\{1-erf\left[\frac{g}{\sqrt{2}} - \frac{\ln\left(\frac{y}{f}\right)}{g\sqrt{2}}\right]\right\}$	0.00042	0.993
CENTRAL	$z = a + \dfrac{b}{x} + c\ln(y) + \dfrac{d}{x^2} + e(\ln(y))^2 + f\dfrac{\ln(x)}{x}$	0.00065	0.999
HIGH	$z = a + by^2\ln(y) + c(\ln(y))^2$	0.00096	0.994
A2 FORCE (N)			
LOW	$z = a + bx + cy + dx^2 + ey^2 + fxy + gx^3 + hy^3 + ixy^2 + jyx^2$	0.0194	0.910
CENTRAL	$\ln(z) = a + \dfrac{b}{x} + cy^{0.5}\ln(y)$	0.0114	0.726
HIGH	$z = a + b\ln(x) + cy + d(\ln(x))^2 + ey^2 + fy\ln(x)$	0.0446	0.892
KURTOSIS (RKU) (um)			
LOW	$z = a + bx + cy + dx^2 + ey^2 + fxy + gx^3 + hy^3 + ixy^2 + jyx^2$	0.00097	0.987
CENTRAL	$z = \dfrac{a + b\ln(x) + c(\ln(x))^2 + d(\ln(x))^3 + ey + fy^2}{1 + g\ln(x) + hy + iy^2 + jy^3}$	0.00143	0.937
HIGH	$z = a + b\ln(x) + cy + d(\ln(x))^2 + ey^2 + fy\ln(x) + g(\ln(x))^3 + hy^3 + iy^2\ln(x) + jy(\ln(x))^2$	0.0396	0.930
SKEWNESS (RSK) (um)			
LOW	$z = a + b\ln(x) + cy + d(\ln(x))^2 + ey^2 + fy\ln(x)$	0.0145	0.908
CENTRAL	$z = a + be^{-x} + cy^3$	0.0496	0.741
HIGH	$z = a + b\ln(x) + \dfrac{c}{y} + d(\ln(x))^2 + \dfrac{e}{y^2} + f\dfrac{\ln(x)}{y}$	0.0396	0.825
WAVELENGTH (LQ) (um)			
LOW	$z = a + by + c\exp\left(-\dfrac{x}{d}\right)$	0.0344	0.930

Table 5-14. (Continued)

CENTRAL	$z=a+\frac{b}{2}\left\{1-erf\left[\frac{d}{\sqrt{2}}-\frac{\ln\left(\frac{x}{c}\right)}{d\sqrt{2}}\right]\right\}+\frac{e}{2}\left\{1-erf\left[\frac{g}{\sqrt{2}}-\frac{\ln\left(\frac{y}{f}\right)}{g\sqrt{2}}\right]\right\}$	0.0056	0.945
HIGH	$z=a+by+\frac{c}{2}\left\{1-erf\left[\frac{e}{\sqrt{2}}-\frac{\ln\left(\frac{x}{d}\right)}{e\sqrt{2}}\right]\right\}$	0.0643	0.700
SPACING (SM) (um)			
LOW	$z=a+b\ln(x)+cy+d(\ln(x))^2+ey^2+fy\ln(x)+g(\ln(x))^3+hy^3+iy^2\ln(x)+jy(\ln(x))^2$	0.0351	0.926
CENTRAL	$z=a+bx+cy+dx^2+ey^2+fxy+gx^3+hy^3+ixy^2+jyx^2$	0.00461	0.944
HIGH		0.0164	0.830
PEAK-TO-VALLEY HEIGHT (RTM) (um)			
LOW	$z=a+bx+cy+dx^2+ey^2+fxy+gx^3+hy^3+ixy^2+jyx^2$	0.00242	0.919
CENTRAL	$z=a+bx+cy\ln(y)$	0.0295	0.865
HIGH	$z=a+bx\sqrt{x}+cy\ln(y)$	0.00538	0.854

Table 5-15. Contour Geometry (MR) Parameter Estimates

Position Tolerance Parameter Estimates (P_TOL) (in.)				
Param.	**P-Value(L/C/H)**	**LOW**	**CENTRAL**	**HIGH**
a	0.002/0.021/0.03	-0.0646865	-0.00099035	-0.00121121
b	0.0/0.079/0.001	0.014710081	**-1.1604e-08***	6.33494e-05
c	0.007/0.026/0.01	6.41842e-05	4.61042e-05	2.65144e-05
d	0.0/0.0/0.09947	-0.0008272	-3.664e-07	**1.3255e-05***
e	0.211/0.079/0.12	**-1.7968e-08***	**8.4898e-10***	**3.29616e-08***
f	0.07891/0.10352	**-6.0966e-06***		**-3.5765e-06***
Total Runout Tolerance Parameter Estimates (T_RUN_TOL) (in.)				
a	0.0/0.0/0.0	-0.01791176	0.000536628	-6.61712537
b	0.036/0.041/0.02	-7.2077e-05	-0.00033268	-5.1204e-07
c	0.001/0.958/0.02	0.002839663	**1.77358e-05***	-4.1969e-05
d	0.0019/0.08947		3.41079e-05	**9.20362e-07***
e	0.088372		**4.80012e-09***	
f	0.102651		**-1.8788e-06***	
Runout Tolerance Estimates (RUN_TOL) (in.)				
a	0.003/0.01/0.004	-0.00254173	0.004158251	-11.3051638
b	0.0271/0.0/0.007	1.71881e-06	9590	1.88099e-05
c	0.131/0.003/0.02	**4.37119e-05***	3760.842734	129621.5232

Table 5-15. (Continued)

d	0.0021/0.0/0.044	-9.3228e-11	193	0.000976801
e	0.0/0.103/0.0	-2.3058e-07	**35.71218863***	-0.00058126
f	0.06987/0.9968	**-7.6328e-09***		**1.53079e-05***
g	0.000574	-3.892e-16		
h	0.003726	5.09764e-10		
I	0.069978	**-2.476e-12***		
j	0.100362	**4.73092e-13***		
Circularity Tolerance Parameter Estimates (CIRC_TOL) (in.)				
a	0.002/0.0/0.0266	0.083624625	9.87348e-05	0.002368492
b	0.006/0.010/0.02	0.021911481	2.88016e-06	1.94555e-06
c	0.001/0.024/0.08	-0.00090232	-7.5177e-05	**1.77809e-05***
d	0.0/0.0/0.00362	-0.00781041	-1.261e-10	-1.0604e-10
e	0.019/0.008/0.01	6.00932e-07	1.12414e-06	-1.8963e-08
f	0.127/0.103/0.07	**0.000200356***	**-2.5065e-08***	**4.58454e-10***
g	0.004631/0.0995	0.000486646	**-2.9041e-16***	
h	0.07961/0.13262	**-1.0887e-09***	**-2.8463e-09***	
I	0.07899/0.00361	**-1.1778e-08***	3.76568e-11	
j	0.08593/0.0321	**-1.1464e-05***	7.58668e-13	
Cylindricity Tolerance Parameter Estimates (CYLN_TOL) (in.)				
a	0.003/0.0/0.0271	0.063247772	-0.09022451	0.001680258
b	0.011/0.037/0.0	-0.01436561	0.037977525	1.27861e-07
c	0.019/0.078/0.05	-0.00023344	**-0.00051232***	**-1.3717e-05***
d	0.0/0.007/0.0311	0.000787425	-0.00511965	-1.2683e-11
e	0.102/0.079/0.09	**-2.5531e-07***	**-9.894e-07***	**3.55547e-08***
f	0.013/0.01/0.081	6.43059e-05	0.0001484	**8.96316e-10***
g	0.00287/0.00057	3.30709e-06	0.000213258	
h	0.13354/0.09681	**-5.3939e-12***	**4.78971e-09***	
I	0.06855/0.00048	**2.7088e-08***	-1.3523e-07	
j	0.08991/0.17261	**-4.1773e-06***	**-6.4189e-06***	
Cutting Force (N)				
a	0.0/0.0/0.003726	122.012268	82.34840257	7.23269598
b	0.079/0.103/0.01	**-7.1602e+08***	**19.55000958***	-0.3152623
c	0.009/0.012/0.0	322.9971464	10178.03726	0.000545753
d	0.00237/0.00387	12.35000514	811.928413	
e	0.089912		**86.33424129***	
f	0.003176		117.7473568	
g	0.010947		38.67104544	
A0 Peak Force (N)				
a	0.010/0.0/0.0071	37.84589641	83.30660081	2.405380181
b	0.003/0.035/0.02	-0.01413614	-0.2219763	21.30620725
c	0.011/0.006/0.03	0.779917126	0.00107607	3.53997e-06
d	0.0462/0.07/0.07	1.60636e-06	**450.75511***	**-1.7633e-07***
e	0.00372/0.06251	-0.00015084	**657.460303***	
f	0.07985/0.00046	**-4.7174e-05***	3281.87567	

Table 5-15. (Continued)

g	0.0002716	-3.7713e-11		
h	0.0894721	**-4.4489e-06***		
I	0.1083477	**1.52388e-07***		
j	0.1221043	**-1.1772e-09***		
A1 Force (N)				
a	0.003/0.013/0.01	13.04133349	763.5244653	236.8742334
b	0.0/0.0/0.00362	58.65615955	-1289.56237	0.000110945
c	0.100/0.003/0.04	**1e-12***	-256.831813	-8.33121953
d	0.00463/0.00215	58.66155867	-9.0229e+06	
e	0.02738/0.09658	122.534866	**22.08596896***	
f	0.00372/0.03661	136.8502905	1969.895491	
g	0.79894	**-0.29523334***		
h	0.10035	**-5.14963504***		
A2 Force (N)				
a	0.002/0.0413/0.0	6.773743481	1.447459551	-1.95679953
b	0.0/0.002/0.0173	0.000180547	-512.383848	3.34700206
c	0.025/0.011/0.03	-0.04915351	-0.00230859	-0.08549427
d	0.0034/0.07899	-1.6881e-08		**-0.28074245***
e	0.03625.0.1324	0.000157348		**8.11233e-05***
f	0.09687/0.00265	**1.69051e-06***		0.00693227
g	0.069851	**1.99524e-15***		
h	0.231561	**-1.167e-07***		
I	0.068873	**-3.1988e-09***		
j	0.087362	**-1.7843e-11***		
Kurtosis Parameter Estimates (RKU) (um)				
a	0.031/0.008/0.02	1.369773378	3.72322092	0.623219847
b	0.023/0.0/0.0051	4.41413e-05	-0.1613909	-2.45418915
c	0.002/0.034/0.01	0.012363013	-0.06225283	0.225177497
d	0.0985/0.003/0.0	**1.12231e-08***	0.004991794	0.57902884
e	0.002/0.036/0.01	-1.8051e-05	-0.00671541	-0.00044668
f	0.103/0.0895/0.0	**-7.9821e-07***	**1.95329e-05***	-0.03702759
g	0.068/0.021/0.01	**-5.5362e-13***	-0.05846554	-0.03146145
h	0.109/0.003/0.08	**-5.3364e-08***	-0.0058185	**2.72296e-07***
I	0.0699/0.132/0.1	**2.81516e-09***	**3.02003e-05***	**3.66748e-05***
j	0.078/0.079/0.01	**-8.7682e-12***	**-4.8654e-08***	0.001496542
Skewness Parameter Estimates (RSK) (um)				
a	0.028/0.004/0.01	1.023171665	-0.18080483	5.648245882
b	0.045/0.006/0.02	-0.41969906	15191.54068	-1.0392531
c	0.001/0.089/0.02	0.008893682	**-0.02214246***	-73.1569694
d	0.025/0.002/0.09	0.037280741	-2.6931e+07	**0.049571307***
e	0.133/0.0/0.0051	**6.34968e-06***	0.000240527	-95.0823423
f	0.006/0.01/0.042	-0.00117586	-89.3591258	6.781734645
g	0.004732		1.20424e+10	
h	0.089941		**-5.8842e-07***	

Table 5-15. (Continued)

I	0.000473		0.044751252	
j	0.003726		84588.85017	
Wavelength Parameter Estimates (LQ) (um)				
a	0.015/0.003/0.0	0.056288848	0.022670331	0.024944469
b	0.027/0.031/0.03	0.004557406	-1.78e-06	-3.4713e-06
c	0.0/0.0/0.00362	-0.00043126	0.000303998	0.000137669
d	0.002/0.113/0.03	-0.0026693	**5.42582e-11***	5.96987e-10
e	0.0976/0.0/0.002	**-8.1072e-07***	-1.9043e-06	-6.3922e-07
f	0.0217/0.04/0.08	0.000151022	-4.9467e-09	**-1.4843e-08***
g	0.002/0.091/0.07	0.000188618	**1.48637e-15***	**-2.2885e-14***
h	0.10/0.089/0.05	**5.1944e-11***	**3.02952e-09***	**1.05551e-09***
I	0.132/0.089/0.23	**9.02683e-08***	**3.09153e-11***	**3.24295e-11***
j	0.101/0.071/0.07	**-1.1268e-05***	**-1.3847e-13***	**2.83745e-13***
Spacing Parameter Estimates (SM) (um)				
a	0.006/0.042/0.02	1.95811e+07	41.84411895	54.6053863
b	0.078/0.023/0.11	**0.0312165***	17.39148906	**0.023545722***
c	0.032/0.011/0.12	-1.9581e+07	8236.114864	**2.788005152***
d	0.01/0.568/0.003	-5.2279e+24	**-0.24912506***	116098.0271
e	0.00372/0.00362		28374.36336	-32.7478953
f	0.09758		**1e-12***	
g	0.11625		**988.3325217***	
Peak-to-Valley Height Parameter Estimates (RTM) (um)				
a	0.0/0.003/0.012	1.422490339	1.315776225	1.391062194
b	0.011/0.007/0.0	-7.3804e-05	-1.2139e-05	-7.4904e-08
c	0.032/0.016/0.0	-0.00030999	0.000177129	-2.6048e-05
d	0.003621	7.243e-09		
e	0.08793	**9.91721e-06***		
f	0.21362	**-2.5044e-08***		
g	0.16152	**-1.9154e-13***		
h	0.09574	**-2.4057e-08***		
i	0.68941	**3.42819e-10***		
j	0.13352	**-6.6912e-12***		

*** Parameters are Eliminated.**

5.3 Databases

Table 5-16 lists the PMBDCLM performance rating database for the contour geometry and Table 5-17 lists the PMBDCLM performance rating database for the straight/taper geometry. Table 5-18 lists the PMBDCLM performance rating database key for the proposed contour geometry. The rating key provides the performance ranges for the

assigned rating value based on the proposed Taguchi quality characteristics. Table 5-19 lists the PMBDCLM performance rating database key for the proposed straight/taper geometry.

Position tolerance for the proposed contour and straight/taper geometry ranges from best [X < 0.0001 in.] to worst [X > 0.005 in.]. Circularity tolerance ranges from best [X < 0.006 in.] to worst [X > 0.015 in.]. Total runout tolerance ranges from best [X < 0.0001 in.] to worst [X > 0.005 in.]. Cylindricity tolerance ranges from best [X < 0.0020 in.] to worst [X > 0.0035 in.]. Parallelism tolerance ranges from best [X < 0.00005 in.] to worst [X > 0.0010 in.]. Flatness tolerance ranges from best [X < 0.000028 in.] to worst [X > 0.000049 in.] and straightness tolerance ranges from best [X < 0.00004 in.] to worst [X > 0.0001in.].

Surface finish peak-to-valley height ranges from best [X < 1.25 um] to worst [X > 1.40 um] for the proposed contour geometry and ranges from best [X < 1.20 um] to worst [X > 3.90 um] for the proposed straight/taper geometry. Surface finish kurtosis ranges from best [X < 2.50 um] to worst [X > 3.25 um] for the proposed contour geometry and ranges from best [X < 2.50 um] to worst [X > 3.25 um] for the proposed straight/taper geometry.

Table 5-16. PMBDCLM Contour Geometry Performance Rating Database

Input				Output																															
				Tolerance Analysis (inch)										Surface Analysis (um)										Cutting Force Analysis (N)								Performance Analysis			
				Position (Dim.)		Runout (Geom.)		T.Runout (Geom.)		Circularit (Form)		Cylindrici (Form)		Rku (Amp.)		Rsk (Amp.)		Sm (Spacing)		Lq (Hybrid)		Rtm (Amp.)		Cutting Force		a0 (Amp.)		a1 (Center)		a2 (Width)		Criteria			
Operating Parameters				Mean (*)	S.D. (P#)	Mean (*)	S.D. (P#)	Mean (*)	S.D. (#)	Mean (CR*)	S.D. (C#)	Mean (CY*)	S.D. (C#)	Mean (K&)	S.D. (K*)	Mean (S&)	S.D. (S*)	Mean (P&)	S.D. (P*)	Mean (L&)	S.D. (L*)	Mean (T&)	S.D. (T*)	Mean (@)	S.D. (^)	Mean (@)	S.D. (^)	Mean (!)	S.D. (^C)	Mean (W!)	S.D. (^W)	Cost ($F)	Cost ($M)	Power (P)	MRR (+)
High Depth of Cut																																			
	S	**F**	**D**																																
1	L	L	H	4	3	3	3	4	3	4	2	5	2	5	1	5	1	3	5	4	5	5	2	4	4	5	3	5	5	5	3	4	4	4	2
2	C	SL	H	1	5	1	5	2	3	2	3	3	4	5	1	5	3	4	4	5	2	4	3	2	3	1	2	5	3	2	2	2	2	2	4
3	H	SH	H	4	4	3	4	5	4	4	2	5	3	5	1	4	3	4	2	5	1	5	1	3	3	4	3	4	2	4	3	3	1	3	5
4	C	H	H	4	5	3	5	2	3	1	3	4	5	3	1	3	2	1	5	2	1	2	2	3	3	3	5	1	1	4	4	3	1	3	5
5	L	H	H	4	3	5	3	4	2	4	2	5	3	2	5	2	3	3	5	2	1	2	5	5	5	5	5	1	1	1	2	5	1	5	5
6	H	H	H	1	2	1	2	3	4	4	4	2	5	2	5	5	3	4	5	3	5	4	5	3	4	3	3	1	1	5	4	3	1	3	5
7	H	SL	H	3	2	2	3	2	4	5	2	5	1	4	1	4	4	3	5	5	5	5	2	2	3	3	3	5	1	3	5	2	2	2	4
8	C	L	H	1	5	1	5	3	5	3	2	5	3	3	2	4	2	2	5	2	5	2	2	1	2	1	2	5	5	5	2	1	4	1	2
9	L	SH	H	2	4	2	4	4	1	3	3	4	5	1	4	1	4	4	3	2	1	1	2	5	5	5	5	3	2	5	2	5	1	5	5
10	C	SH	H	5	5	4	5	4	2	1	4	2	5	3	2	4	2	2	5	3	5	2	2	4	5	5	5	4	2	3	2	4	1	4	5
11	H	L	H	4	2	4	3	3	2	5	2	5	4	4	2	5	2	4	1	5	1	4	1	2	4	4	3	5	5	3	3	2	4	2	2
12	L	SL	H	3	1	1	1	5	2	4	1	5	1	1	5	2	4	3	4	2	5	2	2	5	5	5	5	5	3	1	2	5	2	5	4
Central Depth of Cut																																			
13	L	SH	C	4	3	3	3	4	1	5	4	4	5	3	3	3	2	4	2	2	1	1	5	5	5	5	5	3	2	1	2	5	2	5	4
14	H	H	C	1	5	1	5	3	4	2	4	1	4	1	5	3	5	5	1	5	5	2	5	4	4	5	3	1	2	4	2	4	2	4	4
15	C	L	C	4	4	4	4	4	3	4	2	5	2	1	1	5	1	4	1	5	1	5	1	1	2	1	2	5	5	5	3	1	4	1	2
16	H	SL	C	2	5	2	5	3	3	2	4	2	4	1	5	5	5	3	5	5	5	5	4	2	3	2	3	4	3	5	5	4	3	4	3
17	L	SL	C	4	3	3	3	3	2	4	2	5	1	3	3	2	3	3	5	1	2	1	3	5	5	5	4	4	3	1	2	3	3	3	3
18	C	SH	C	2	1	2	2	2	5	4	3	4	4	5	1	5	2	4	2	5	5	2	5	1	2	2	2	2	2	2	3	5	2	5	4

Table 5-16. (Continued)

19	L	H	C	2	3	2	3	2	5	5	3	4	5	2	5	2	2	4	5	4	5	1	1	5	5	5	4	1	1	1	2	1	2	1	4
20	C	SH	C	1	5	1	5	3	5	3	2	5	2	4	2	5	2	4	1	5	1	2	2	2	2	2	2	3	2	4	5	2	2	2	4
21	H	L	C	1	4	2	4	3	2	3	2	5	2	3	2	4	4	3	5	5	5	5	4	2	2	2	2	5	5	5	3	4	4	4	2
22	C	SL	C	4	5	3	5	3	1	1	5	1	5	5	1	4	1	4	2	5	1	2	3	2	3	3	4	4	3	5	2	3	3	3	3
23	L	L	C	3	3	4	3	2	5	4	5	1	5	1	4	3	2	3	2	2	5	3	5	3	5	5	2	5	5	1	1	5	4	5	2
24	H	SH	C	2	1	2	2	2	5	4	5	1	5	5	1	3	1	4	1	5	1	5	1	3	4	3	4	2	2	2	2	1	2	1	4
Low Depth of Cut																																			
25	C	L	L	3	2	2	2	3	3	5	1	5	3	5	1	4	2	3	1	5	1	5	1	1	1	1	1	5	5	5	4	1	5	1	1
26	L	SL	L	1	5	1	5	4	3	3	3	4	2	4	1	5	1	4	2	5	5	1	3	3	3	2	2	5	3	3	2	3	4	3	2
27	H	SH	L	3	4	2	4	4	3	1	1	5	2	4	2	5	2	4	2	5	5	5	1	2	3	2	2	1	1	5	2	2	3	2	3
28	L	H	L	2	5	2	5	4	2	2	2	5	1	4	2	5	2	4	2	2	5	1	4	1	2	2	2	1	1	5	4	1	2	1	4
29	C	H	L	5	2	3	3	3	3	5	2	5	3	4	1	5	2	4	1	3	5	2	3	1	2	2	2	1	1	1	3	1	2	1	4
30	H	H	L	2	1	1	1	4	1	5	1	5	1	4	1	4	3	3	5	5	5	5	5	1	2	1	2	1	1	5	5	1	2	1	4
31	H	SL	L	4	3	4	4	4	2	5	2	5	3	3	1	3	2	3	3	5	5	5	2	1	2	1	2	5	3	5	2	1	4	1	2
32	L	L	L	1	5	1	5	3	2	2	2	5	2	3	3	2	2	4	1	5	5	4	1	1	1	1	1	5	5	5	1	1	5	1	1
33	C	SH	L	2	4	2	4	3	3	3	1	5	2	1	5	3	4	4	1	5	1	2	5	2	3	2	2	2	1	5	5	2	3	2	3
34	L	SH	L	3	5	2	5	3	2	1	2	5	4	4	1	4	1	3	5	1	5	1	1	3	3	3	3	5	1	5	4	3	3	3	3
35	H	L	L	4	3	4	3	4	2	4	2	5	1	5	1	5	1	5	5	5	5	4	1	3	3	3	3	5	3	5	5	3	5	3	1
36	C	SL	L	2	1	2	1	5	2	4	1	5	1	3	3	4	2	4	2	5	1	5	1	1	2	1	2	4	3	5	3	1	4	1	2

Table 5-17. PMBDCLM Straight/Taper Geometry Performance Rating Database

Input	**Output**														
Operating Parameters	**Tolerance Analysis (in.)**					**Surface Analysis (um)**					**Cutting Force Analysis (N)**				**Performance Analysis**
	Position (Dim.)	**Flatness (Form)**	**Straight. (Form)**	**Angularit (Orient)**	**Parallel (Orienr)**	**Rku (Amp.)**	**Rsk (Amp.)**	**Sm (Spacing)**	**Lq (Hybrid)**	**Rtm (Amp.)**	**Cutting Force**	**a0 (Amp.)**	**a1 (Center)**	**a2 (Width)**	**Criteria**

Table 5-17. (Continued)

				Mean (*)	S.D. (PS#)	Mean (F-)	S.D. (#)	Mean (-)	S.D. (S#)	Mean (A*)	S.D. (A#)	Mean (Pl*)	S.D. (P#)	Mean (K&)	S.D. (K*)	Mean (S&)	S.D. (S*)	Mean (P&)	S.D. (P*)	Mean (L&)	S.D. (L*)	Mean (T&)	S.D. (T*)	Mean (@)	S.D. (^)	Mean (@)	S.D. (A^)	Mean (!)	S.D. (^C)	Mean (W!)	S.D. (^W)	Cost ($F)	Cost ($M)	Power (P)	MRR (+)
High Depth of Cut																																	
	S	**F**	**D**																														
1	L	L	H	4	1	5	3	4	1	5	5	4	1	5	1	3	2	3	2	3	2	3	4	2	4	5	2	5	5	5	3	2	4	2	2
2	C	SL	H	5	1	2	2	3	2	4	1	3	2	1	5	5	4	4	3	5	5	4	4	2	3	3	3	2	1	5	3	2	2	2	4
3	H	SH	H	1	2	1	1	2	3	4	1	1	5	1	5	2	5	5	1	5	2	4	3	2	2	2	2	5	2	3	3	2	1	2	5
4	C	H	H	1	1	4	2	5	2	4	1	5	1	5	1	5	1	2	3	3	3	4	5	2	3	2	2	1	1	1	2	2	1	2	5
5	L	H	H	2	5	5	2	5	4	4	2	4	4	3	5	1	2	1	5	1	5	1	5	2	3	1	2	3	4	5	5	2	1	2	5
6	H	H	H	1	4	5	1	4	4	4	2	3	5	1	5	2	3	5	2	5	4	4	2	1	2	1	2	3	3	5	5	1	1	1	5
7	H	SL	H	5	1	5	2	5	2	4	2	3	2	4	1	3	3	5	2	5	1	5	1	2	3	1	2	2	4	5	5	2	2	2	4
8	C	L	H	2	1	2	2	1	2	1	5	4	1	1	5	1	5	4	4	5	5	5	1	1	2	2	2	5	4	5	5	1	4	1	2
9	L	SH	H	1	5	1	5	1	5	1	5	1	5	3	3	5	3	1	5	2	5	2	3	4	5	1	5	5	5	5	5	4	1	4	5
10	C	SH	H	4	1	5	2	5	1	1	5	4	4	4	2	5	2	4	1	5	1	4	2	5	5	3	5	1	1	5	3	5	1	5	5
11	H	L	H	3	1	5	2	5	1	5	5	5	1	1	2	1	2	5	5	5	2	5	4	5	5	5	4	5	5	3	2	5	4	5	2
12	L	SL	H	1	3	1	2	5	4	5	5	3	5	3	3	1	2	1	5	1	5	1	5	5	5	5	5	5	2	1	1	5	2	5	4
Central Depth of Cut																																	
13	L	SH	C	3	3	5	1	4	2	5	1	3	2	4	1	5	2	1	5	1	5	1	4	3	3	4	2	1	1	5	3	3	2	3	4
14	H	H	C	4	2	3	3	1	3	3	3	1	5	2	3	2	2	5	1	5	1	4	2	2	2	2	3	1	1	1	2	2	2	2	4
15	C	L	C	2	2	5	2	3	1	3	3	4	1	4	2	4	3	3	2	4	4	3	2	2	1	2	1	5	5	1	2	2	4	2	2
16	H	SL	C	4	1	5	3	5	1	3	3	4	2	1	5	2	4	4	1	5	3	4	3	2	3	3	4	2	1	1	1	2	3	2	3
17	L	SL	C	1	4	1	3	5	3	3	2	3	5	4	2	1	2	1	5	1	5	1	5	2	2	2	3	2	1	5	4	2	3	2	3
18	C	SH	C	1	4	4	3	5	5	3	2	3	5	4	2	4	2	4	1	4	1	3	2	1	1	2	2	5	2	5	3	1	2	1	4
19	L	H	C	1	4	1	4	1	2	3	2	1	5	5	1	2	1	1	5	1	5	1	5	2	2	2	3	1	1	4	2	2	2	2	4
20	C	SH	C	3	1	5	2	5	1	4	2	3	2	5	1	3	1	3	1	4	1	3	3	1	2	2	3	1	1	3	3	1	2	1	4
21	H	L	C	1	2	1	2	5	2	4	2	4	1	5	1	5	2	3	2	5	1	4	3	3	3	4	1	5	5	3	3	3	4	3	2
22	C	SL	C	1	5	1	4	1	5	4	2	3	5	4	3	5	3	3	1	4	1	3	5	4	4	5	5	2	1	5	4	4	3	4	3
23	L	L	C	1	1	5	5	4	1	5	1	4	2	4	3	2	3	2	1	2	3	3	3	5	3	4	2	5	4	3	1	5	4	5	2
24	H	SH	C	1	4	1	5	1	3	5	1	3	5	1	5	5	2	4	4	5	2	4	3	3	3	3	1	5	2	3	4	3	2	3	4
Low Depth of Cut																																	
25	C	L	L	2	1	4	2	4	2	1	5	4	2	1	5	5	3	5	1	5	1	5	2	1	2	1	1	5	5	5	4	1	5	1	1

Table 5-17. (Continued)

26	L	SL	L	3	2	2	2	2	2	1	5	3	5	5	1	5	1	5	4	2	4	1	4	2	2	2	1	3	1	2	2	2	4	2	2
27	H	SH	L	1	4	2	2	2	5	1	5	3	5	1	5	5	3	5	1	5	2	4	2	2	1	1	1	3	1	4	3	2	3	2	3
28	L	H	L	5	1	1	2	4	2	1	5	4	3	5	4	3	2	1	5	1	5	1	5	1	1	1	1	1	1	1	1	1	2	1	4
29	C	H	L	4	1	5	1	5	1	3	5	4	1	5	1	3	1	2	1	3	2	4	2	3	3	4	3	5	1	1	1	3	2	3	4
30	H	H	L	1	2	3	2	4	3	3	5	2	2	1	5	5	4	5	1	5	2	4	2	2	2	3	3	1	1	1	1	2	2	2	4
31	H	SL	L	4	1	1	2	5	3	3	5	3	5	2	3	3	3	5	1	5	1	5	1	1	2	2	2	3	1	3	3	1	4	1	2
32	L	L	L	1	2	5	2	5	2	1	5	4	2	1	5	5	5	4	1	5	1	4	1	1	1	1	1	5	5	3	3	1	5	1	1
33	C	SH	L	1	4	4	2	4	4	1	5	3	5	3	5	3	1	3	4	4	5	2	5	2	1	1	1	4	1	5	3	2	3	2	3
34	L	SH	L	4	1	5	2	5	1	1	5	4	1	5	1	2	2	5	5	1	5	1	3	4	3	3	3	1	1	2	2	4	3	4	3
35	H	L	L	4	1	5	2	4	1	1	5	4	3	1	4	5	3	5	1	5	1	5	1	4	3	3	2	5	5	4	2	4	5	4	1
36	C	SL	L	2	3	4	2	4	2	1	5	2	2	1	5	5	5	4	2	5	5	4	3	2	1	1	1	5	2	5	4	2	4	2	2

Table 5-18. PMBDCLM Contour Geometry Performance Rating Database Key

Measure	**Output Rating**				
	Mean				
	(1) Very low	**(2) Low**	**(3) Moderate**	**(4) High**	**(5) Very High**
$F	Very low cost based on force/power	Low cost based on force/power	Moderate cost based on force/power	High cost based on force/power	Very high cost based on force/power
$M	Very low cost based on MRR	Low cost based on MRR	Moderate cost based on MRR	High cost based on MRR	Very high cost based on MRR
P	Very low power based on force	Low power based on force	Moderate power based on force	High power based on force	Very high power based on force
	(1) Worst	**(2) Worse**	**(3) Expected**	**(4) Better**	**(5) Best**
*	[X > 0.005]	[0.005 >= X > 0.001]	[0.001 >= X > 0.0005]	[0.0005 >= X >= 0.0001]	[X < 0.0001]
CR*	[X > 0.015]	[0.015 >= X > 0.012]	[0.012 >= X > 0.009]	[0.009 >= X >= 0.006]	[X < 0.006]
CY*	[X > 0.0035]	[0.0035 >= X > 0.0030]	[0.0030 >= X > 0.0025]	[0.0025 >= X >= 0.0020]	[X < 0.0020]
K&	[X > 3.25]	[3.25 >= X > 3.0]	[3.0 >= X > 2.75]	[2.75 >= X >= 2.50]	[X < 2.50]
S&	[X > 0.60]	[0.60 >= X > 0.45]	[0.45 >= X > 0.30]	[0.30 >= X >= 0.15]	[X < 0.15]
P&	[X > 100.0]	[100.0 >= X > 80.0]	[80.0 >= X > 60.0]	[60.0 >= X >= 40.0]	[X < 40.0]
L&	[X > 0.031]	[0.031 >= X > 0.028]	[0.028 >= X > 0.026]	[0.026 >= X >= 0.024]	[X < 0.024]
T&	[X > 1.40]	[1.40 >= X > 1.35]	[1.35 >= X > 1.30]	[1.30 >= X >= 1.25]	[X < 1.25]
	(1) Very Low	**(2) Low**	**(3) Moderate**	**(4) High**	**(5) Very High**
@	[X < 60.0]	[100.0 >= X >= 60.0]	[140.0 >= X > 100.0]	[180.0 >= X > 140.0]	[X > 180.0]
!	[X < 22.0]	[25.0 >= X >= 22.0]	[28.0 >= X > 25.0]	[31.0 >= X > 28.0]	[X >31.0]

Table 5-18. (Continued)

W!	[X < 2.60]	[2.90 >= X >= 2.60]	[3.30 >= X > 2.90]	[3.60 >= X > 3.30]	[X > 3.60]
			Standard Deviation		
	(1) Very Small	**(2) Small**	**(3) Moderate**	**(4) Large**	**(5) Very Large**
P#	[X < 0.0015]	[0.0035 >= X >= 0.0015]	[0.0055 >= X > 0.0035]	[0.0075 >= X > 0.0055]	[X >0.0075]
#	[X < 0.0002]	[0.0005 >= X >= 0.0002]	[0.0008 >= X > 0.0005]	[0.0011 >= X > 0.0008]	[X > 0.0011]
C#	[X < 0.0005]	[0.0010 >= X >= 0.0005]	[0.0015 >= X > 0.0010]	[0.0020 >= X > 0.0015]	[X > 0.0017]
K*	[X < 0.30]	[0.45 >= X >= 0.30]	[0.60 >= X > 0.45]	[0.75 >= X > 0.60]	[X > 0.75]
S*	[X < 0.20]	[0.35 >= X >= 0.20]	[0.50 >= X > 0.35]	[0.65 >= X > 0.50]	[X > 0.65]
P*	[X < 8.0]	[14.0 >= X >= 8.0]	[18.0 >= X > 12.0]	[22.0 >= X >18.0]	[X > 22.0]
L*	[X < 0.0001]	[0.0010 >= X >= 0.0001]	[0.0020 >= X > 0.0010]	[0.003 >= X > 0.002]	[X > 0.003]
T*	[X < 0.085]	[0.110 >= X >= 0.085]	[0.135 >= X >0.110]	[0.160 >= X > 0.135]	[X > 0.160]
^	[X < 20.0]	[40.0 >= X >= 20.0]	[60.0 >= X > 40.0]	[80.0 >= X > 60.0]	[X > 80.0]
^C	[X < 13.0]	[17.0 >= X > 13.0]	[21.0 >= X > 17.0]	[25.0 >= X > 21.0]	[X > 25.0]
^W	[X < 0.70]	[1.10 >= X > 0.70]	[1.50 >= X > 1.10]	[1.90 >= X > 1.50]	[X > 1.90]

Table 5-19. PMBDCLM Straight/Taper Geometry Performance Rating Database Key

Measure	Output Rating				
	Mean				
	(1) Very low	**(2) Low**	**(3) Moderate**	**(4) High**	**(5) Very High**
$F	Very low cost based on force/power	Low cost based on force/power	Moderate cost based on force/power	High cost based on force/power	Very high cost based on force/power
$M	Very low cost based on MRR	Low cost based on MRR	Moderate cost based on MRR	High cost based on MRR	Very high cost based on MRR
P	Very low power based on force	Low power based on force	Moderate power based on force	High power based on force	Very high power based on force
	(1) Worst	**(2) Worse**	**(3) Expected**	**(4) Better**	**(5) Best**
*	[X > 0.001]	[0.001 >= X > 0.0007]	[0.0007 >= X > 0.0004]	[0.0004 >= X >= 0.0001]	[X < 0.0001]

Table 5-19. (Continued)

Pl*	[X > 0.0010]	[0.0010 >= X > 0.00050]	[0.00050 >= X > 0.00010]	[0.00010 >= X >= 0.00005]	[X < 0.00005]
F-	[X > 0.000049]	[0.000049 >= X > 0.000042]	[0.000042>=X > 0.000035]	[0.000035 >= X > 0.000028]	[X < 0.000028]
-	[X > 0.0001]	[0.0001 >= X > 0.00008]	[0.00008>=X > 0.00006]	[0.00006 >= X > 0.00004]	[X < 0.00004]
A*	[X > 0.087]	[0.087 >= X > 0.067]	[0.067 >= X > 0.047]	[0.047 >= X >= 0.027]	[X < 0.027]
K&	[X > 3.25]	[3.25 >= X > 3.0]	[3.0 >= X > 2.75]	[2.75 >= X >= 2.50]	[X < 2.50]
S&	[X > 0.30]	[0.30 >= X > 0.20]	[0.20 >= X > 0.10]	[0.10 >= X >= 0.09]	[X < 0.009]
P&	[X > 600.0]	[600.0 >= X > 500.0]	[500.0 >= X > 400.0]	[400.0 >= X >= 300.0]	[X < 300.0]
L&	[X > 0.41]	[0.41 >= X > 0.27]	[0.27 >= X > 0.23]	[0.23 >= X >= 0.19]	[X < 0.19]
T&	[X > 3.90]	[3.90 >= X > 3.00]	[3.00 >= X > 2.10]	[2.10 >= X >= 1.20]	[X < 1.20]
	(1) Very Low	**(2) Low**	**(3) Moderate**	**(4) High**	**(5) Very High**
@	[X < 60.0]	[100.0 >= X >= 60.0]	[140.0 >= X > 100.0]	[180.0 >= X > 140.0]	[X > 180.0]
!	[X < 22]	[25 >= X >= 22]	[28 >= X > 25]	[31 >= X > 28]	[X >31]
W!	[X < 2.6]	[2.9 >= X >=2.6]	[3.3 >= X > 2.9]	[3.6 >= X > 3.3]	[X > 3.6]
			Standard Deviation		
	(1) Very Small	**(2) Small**	**(3) Moderate**	**(4) Large**	**(5) Very Large**
PS#	[X < 0.0004]	[0.00055 >= X > 0.0004]	[0.0007 >= X > 0.00055]	[0.00085 >= X > 0.0007]	[X > 0.00085]
#	[X < 0.0001]	[0.0005 >= X > 0.0001]	[0.0009 >= X > 0.0005]	[0.0013 >= X > 0.0009]	[X > 0.0013]
S#	[X < 0.00003]	[0.00005 >= X > 0.00003]	[0.00007 >= X > 0.00005]	[0.0009 >= X > 0.00007]	[X > 0.0009]
A#	[X < 0.017]	[0.025 >= X > 0.017]	[0.033 >= X > 0.025]	[0.041 >= X > 0.033]	[X > 0.041]
P#	[X < 0.0000320]	[0.0000420 >= X > 0.0000320]	[0.0000520 >= X > 0.0000420]	[0.0000620 >= X > 0.0000520]	[X > 0.0000620]
K*	[X < 0.30]	[0.50 >= X >= 0.30]	[0.70 >= X > 0.50]	[0.90 >= X > 0.70]	[X > 0.90]
S*	[X < 0.15]	[0.30 >= X >= 0.15]	[0.45 >= X > 0.30]	[0.60 >= X > 0.45]	[X > 0.60]
P*	[X < 80.0]	[110.0 >= X >= 80.0]	[140.0 >= X > 110.0]	[170.0 >= X >140.0]	[X >170.0]
L*	[X < 0.025]	[0.035 >= X >= 0.025]	[0.045 >= X > 0.035]	[0.055 >= X > 0.045]	[X < 0.055]
T*	[X < 0.150]	[0.270 >= X >= 0.150]	[0.390 >= X >0.270]	[0.510 >= X > 0.390]	[X > 0.510]
^	[X < 33.0]	[53.0 >= X >= 33.0]	[73.0 >= X > 53.0]	[93.0 >= X > 73.0]	[X > 93.0]
A^	[X < 33.0]	[43.0 >= X >= 33.0]	[53.0 >= X > 43.0]	[63.0 >= X > 53.0]	[X > 63.0]
^C	[X < 20.0]	[30.0 >= X >= 20.0]	[40.0 >= X > 30.0]	[50.0 >= X > 40.0]	[X > 50.0]
^W	[X < 0.70]	[1.20 >= X >= 0.70]	[1.70 >= X > 1.20]	[2.20 >= X > 1.70]	[X > 2.20]

Benefit/cost ratio operating parameter rating is listed in Table 5-20. A rating value of 2 is assigned to low level spindle speed, feedrate, and depth of cut. A rating value of 4 is assigned for central level spindle speed and depth cut, and a level of semi-low for feedrate. A rating value of 8 is assigned to a high level of spindle speed and depth of cut, and a level of semi-high for feedrate. A rating value of 16 is assigned for the high level of feedrate.

The benefit/cost ratio rating is determined by dividing the benefit rating value by the cost rating value. A higher benefit-to-cost ratio is desired and a low benefit-to-cost ratio is avoided.

Table 5-20. Benefit/Cost Ratio Operating Parameter Ratio

Rating	**Proposed Levels**		
	Spindle Speed	**Feedrate**	**Depth of Cut**
2	Low	Low	Low
4	Central	Semi-Low	Central
8	High	Semi-High	High
16		High	
Benefit = MRR = Feedrate Rating + Depth Rating			
Cost = Power = Spindle Speed Rating			

The performance measure, statistic(s), significant factor(s), optimal value(s), and optimal level(s) are provided. At a high depth of cut for the contour geometry, the surface skewness, runout tolerance, cutting force, and force amplitude are effected either on the mean, variance, and/or signal-to-noise. At a central depth of cut for the contour geometry, total runout tolerance, force center, surface wavelength, and surface peak-to-valley height are effected either for the mean, variance, and/or signal-to-noise. At a low depth of cut for the contour geometry, position tolerance, total runout tolerance, runout tolerance, circularity tolerance, cutting force, force amplitude, center, and width, surface skewness, surface wavelength, and surface peak-to-valley height are effected on either mean,

variance and/or signal-to-noise. The straight/taper geometry shows that angularity tolerance, parallelism tolerance, force amplitude and center are effected either on the mean, variance, and/or signal-to-noise at a high depth of cut. At a central and low depth of cut, parallelism tolerance, force width, surface spacing, and surface peak-to-valley height are effected on the mean, variance, and/or signal-to-noise.

Table 5-21. Significance Factors/Database

Perf. Measure (Y)	STAT.	SIG. FACTOR	Optimal Value	Optimal Level														
				L	SL	C	SH	H	HxC	LxHxL	LxSL	HxSHxL	HxSL	LxL	SHxH	HxHxH	CxSLxL
CONTOUR (HIGH)																		
Rsk	MEAN	(S)	2.1131	X														
RUN_TOL	S/N	(F)*, (FxD)**	-6.66091, 0.68182		X*				X**									
FORCE	LOG(S)	(F)	1.6694	X														
	S/N	(S)*, (F)**	-39.0535, -39.5628	X**		X*												
A0	LOG(S)	(F)*, (D)**	1.7513, 1.6670					X*, X**										
CONTOUR (CENTRAL)																		
T_RUN_TOL	MEAN	(S)*, (SxD)**	0.000859, 0.001116					X*	X**									
	S/N	(S)	-2.1176			X												
A1	MEAN	(F)	115.69	X														
	LOG(S)	(F)	1.0641					X										
	S/N	(F)	-27.5709					X										
Lq	MEAN	(S)	0.02625	X														
	LOG(S)	(D)*, (SxD)**, (SxFxD)***	1.7967, -1.7663, 0.02	X*					X**	X**								
	S/N	(D)*, (SxF)**, (SxFxD)***	8.3340, 15.0060, 0			X*					X**	X**						
Rtm	MEAN	(F)	1.3833					X										
	S/N	(F)	-1.9929	X														
CONTOUR (LOW)																		
P_TOL	LOG(S)	(F)	-2.5155		X													
T_RUN_TOL	LOG(S)	(S)	-3.5840					X										
	S/N	(S)	0.7381					X										
RUN_TOL	LOG(S)	(F)	-6.6609		X													

Table 5-21. (Continued)

CIRC_TOL	**MEAN**	(S)	0.0139	X													
FORCE	**LOG(S)**	(S)	1.4732			X											
A0	**MEAN**	(F)	90.9269				X										
	LOG(S)	(F)	1.1321	X													
	S/N	(F)	-32.1706	X													
A1	**MEAN**	(F)	115.69	X													
	LOG(S)	(F)	0.8220					X									
	S/N	(F)	-22.7558					X									
A2	**MEAN**	(SxF)	-8.1011										X				
	LOG(S)	(SxF)	-0.5565											X			
	S/N	(SxF)	6.3813											X			
Rsk	**MEAN**	(SxF)	0.4650											X			
Lq	**MEAN**	(S)	0.0262	X													
	LOG(S)	(S)	-2.3636	X													
	S/N	(S)	15.5546	X													
Rtm	**MEAN**	(S)	1.3960	X													
	S/N	(S)	-2.9070					X									
S_TAPER (HIGH)																	
P_TOL	**LOG(S)**	(F)	-2.3247	X													
ANG_TOL	**MEAN**	$(S)^{*}$ $(FxD)^{**}$ $(SxFxD)^{***}$	101.227, 44.9940, 135.2367	X^{*}					X^{**}			X^{**}_{*}					
	S/N	$(S)^{*}$ $(FxD)^{**}$ $(SxFxD)^{***}$	43.9490, 72.2870, 81.7203	X^{*}					X^{**}							X^{**}_{*}	
PARA_TOL	**LOG(S)**	$(S)^{*}$, $(F)^{**}$	-4.1805, -4.5158	X^{**}		X^{*}											
A0	**S/N**	(F)	-39.823					X									
A1	**MEAN**	(F)	19.4764					X									
	LOG(S)	(F)	1.1777					X									
	S/N	(F)	-26.2557					X									
S_TAPER (CENTRAL)																	
STR_TOL	**MEAN**	$(S)^{*}$ $(FxD)^{**}$ $(SxFxD)^{***}$	18.7441, 29.9101, 45.0277					X^{*}							X^{**}	X^{**}_{*}	
PARA_TOL	**MEAN**	$(S)^{*}$, $(F)^{**}$	0.00026, 0.000503				X^{**}	X^{*}									
A0	**MEAN**	(S)	169.6528	X													
A2	**S/N**	(F)	10.1915					X									

Table 5-21. (Continued)

	MEAN	(D)*, (FxD)**	14.12963, 2.86897					X*	X**								
Rku	**LOG(S)**	(SxFxD)	2.005														X
	S/N	(SxFxD)	28.4234							X							
Sm	**S/N**	(S)	14.3718			X											
Rtm	**S/N**	(S)	-3.8017					X									
S_TAPER_(LOW)																	
FLAT_TOL	**MEAN**	(F)	4.49E-05		X												
ANG_TOL	**LOG(S)**	(S)	-1.3287					X									
	S/N	(S)	67.7766	X													
PARA_TOL	**LOG(S)**	(S)	-4.4237	X													
	S/N	(S)	7.5390	X													
FORCE	**MEAN**	(S)	92.5245					X									
A1	**MEAN**	(F)	139.6631	X													
	LOG(S)	(F)	0.7809					X									
	S/N	(F)	-23.0960					X									
A2	**S/N**	(F)	-7.7504					X									
Rtm	**LOG(S)**	(SxF)	-0.7266								X						
Rsk	**MEAN**	(F)	-0.0406				X										
	LOG(S)	(SxF)	-1.0442								X						
	S/N	(F)	0.0594		X												
Sm	**S/N**	(S)	14.6563					X									
Lq	**MEAN**	(F)	0.3128					X									
Rtm	**MEAN**	(S)	4.0792	X													
	LOG(S)	(S)	-0.8562					X									

Table 5-22. Significant Effect Database

PROPOSED CONTOUR GEOMETRY									
S MAIN EFFECT (HIGH)		**L**	**C**	**H**	**MIN**	**MAX**	**EFFECT**	**OVERALL MEAN**	**PREDICTED VALUE**
Force	Mean	-47.6	-39.054	-41.06535	-47.59982	-39.05354	8.546279	-42.573	-38.29986
Rsk	S/N	2.11308	-3.044154	-11.461	-11.46118	2.113084	13.57426	-4.1307	-10.91783

Table 5-22. (Continued)

S MAIN EFFECT (CENTRAL)		L	C	H	MIN	MAX	EFFECT	OVERALL MEAN	PREDICTED VALUE
T.Runout	S/N	-2.8517	-1.1177	-2.1176	-2.851713	-1.117732	1.733981	-2.029	-1.162009
	Mean	0.00053	0.000859	0.00091	0.000526	0.000906	0.00038	0.00076	0.00095
Lq	Mean	0.02938	0.02375	0.02208	0.022083	0.029375	0.007292	0.02507	0.021424
S MAIN EFFECT (LOW)		**L**	**C**	**H**	**MIN**	**MAX**	**EFFECT**	**OVERALL MEAN**	**PREDICTED VALUE**
T. Runout	S/N	-4.4723	-3.227068	0.73806	-4.472319	0.738062	5.210381	-2.3204	0.28479
	LOG(S)	-3.0635	-3.292872	-3.584	-3.584042	-3.063468	0.520575	-3.3135	-3.573787
Circular	Mean	0.01399	0.00665	0.00664	0.006643	0.013991	0.007348	0.00909	0.005416
Force	LOG(S)	1.49662	1.47323	1.55063	1.473235	1.550629	0.077394	1.42173	1.460427
Lq	S/N	15.5546	3.56492	10.51026	3.564922	15.55456	11.98964	9.87658	3.881762
	LOG(S)	-2.3636	-0.5718	-1.791807	-2.363561	-0.571754	1.791807	-1.5757	-0.679797
	Mean	0.02625	0.021667	0.02042	0.020417	0.02625	0.005833	0.02278	0.019863
Rtm	S/N	-2.9069	-2.216555	-1.7571	-2.906942	-1.757079	1.149863	-2.2935	-1.718568
	Mean	1.39583	1.291667	1.22083	1.220833	1.395833	0.175	1.30278	1.21528

F MAIN EFFECT (HIGH)		L	SL	SH	H	MIN	MAX	EFFECT	OVERALL MEAN	PREDICTED VALUE
Runout	S/N	-13.912	-6.6609	-11.39241	-8.287954	-13.91174	-6.660914	7.250822	-10.063	-6.437589
Force	S/N	-39.563	-43.5069	-42.65724	-44.565	-44.56459	-39.56281	5.001781	-42.573	-45.07389
	LOG(S)	1.6694	1.94572	1.942096	1.916221	1.6694	1.945716	0.276316	1.86836	2.006518
a0 Peak	LOG(S)	1.52311	1.781278	1.87175	1.751357	1.523106	1.87175	0.348644	1.73187	1.906192
F MAIN EFFECT (CENTRAL)		**L**	**SL**	**SH**	**H**	**MIN**	**MAX**	**EFFECT**	**OVERALL MEAN**	**PREDICTED VALUE**
a1 Peak	S/N	-42.502	-30.82794	-29.38421	-27.571	-42.50156	-27.57092	14.93064	-32.571	-25.10568
	LOG(S)	1.826	1.213712	1.161911	1.06414	1.064144	1.826001	0.761857	1.31644	0.935512
	Mean	115.69	32.40478	25.92812	21.2484	21.2484	115.69	94.44161	48.8178	1.596993
Rtm	S/N	-1.9929	-2.346402	-2.71802	-2.8647	-2.864721	-1.992884	0.871837	-2.481	-2.916919

Table 5-22. (Continued)

	Mean	1.25278	1.311111	1.366667	1.38333	1.252778	1.383333	0.130556	1.3285	1.393778
F MAIN EFFECT (LOW)		**L**	**SL**	**SH**	**H**	**MIN**	**MAX**	**EFFECT**	**OVERALL MEAN**	**PREDICTED VALUE**
Position	LOG(S)	-2.32470	-2.5155	-2.0945	-2.472025	-2.515515	-2.094474	0.421041	-2.3517	-2.14118
Runout	LOG(S)	-2.30041	-2.4869	-2.0717	-2.437544	-2.48694	-2.071739	0.415201	-2.3248	-2.117199
a0 Peak	S/N	-32.171	-37.4466	-39.641	-36.6987	-39.64135	-32.17062	7.470736	-36.489	-40.22437
	LOG(S)	1.13214	1.515181	1.60698	1.432601	1.132144	1.606981	0.474837	1.42173	1.659149
	Mean	43.6259	68.65641	90.9269	64.09152	43.62589	90.92689	47.301	66.8252	90.4757
a1 Peak	S/N	-45.543	-31.45591	-26.64434	-22.756	-45.54259	-22.75576	22.78683	-31.6	-20.20659
	LOG(S)	1.97759	1.274529	0.964436	0.82197	0.82197	1.977586	1.155616	1.25963	0.681822
	Mean	165.494	32.59559	19.67841	12.3091	12.30908	165.4944	153.1853	57.5194	-19.07327

D MAIN EFFECT (HIGH)		**C**	**H**	**MIN**	**MAX**	**EFFECT**	**OVERALL MEAN**	**PREDICTED VALUE**
a0 Peak	LOG(S)	1.796739	1.667006	1.667006	1.796739	0.129733	1.73187	1.6670035
D MAIN EFFECT (CENTRAL)		**C**	**H**	**MIN**	**MAX**	**EFFECT**	**OVERALL MEAN**	**PREDICTED VALUE**
Lq	S/N	8.333992	7.727066	7.727066	8.333992	0.606926	8.03053	7.7270672
	Mean	0.025972	0.024167	0.024167	0.025972	0.001806	0.02507	0.0241672

SxF INT. (CENTRAL)		**LxL**	**LxSL**	**LxSH**	**LxH**	**CxL**	**CxSL**	**CxSH**	**CxH**	**HxL**	**HxSL**	**HxSH**	**HxH**	**MIN**	**MAX**	**EFFT.**	**OVRAL MEAN**	**PRED. VALUE**
Lq	S/N	13.354	15.006	0	6.5937	8.4137	7.2486	13.679	0	7.2486	11.141	0	13.679	0	15.00602	15.00602	8.03053	0.527518
SxF INT. (LOW)		**LxL**	**LxSL**	**LxSH**	**LxH**	**CxL**	**CxSL**	**CxSH**	**CxH**	**HxL**	**HxSL**	**HxSH**	**HxH**	**MIN**	**MAX**	**EFFT.**	**OVRAL MEAN**	**PRED. VALUE**
a2 Peak	S/N	-16.106	-10.63	-10.5	-13.92	-15.46	-10.63	-13.19	-14.40	-13.73	-8.1011	-9.796	-11.530	-16.10636	-8.101121	8.00524	-10.801	-6.79838
	LOG(S)	-0.5565	-0.032	0.194	0.2187	0.2677	-0.032	0.1617	0.1136	0.3076	0.0086	0.0092	0.2943	-0.556493	0.307671	0.864163	0.06193	0.494012
	Mean	6.3813	3.2776	3.039	4.7343	5.6427	3.2776	4.3641	5.1157	4.4214	2.3369	2.9330	3.3014	2.336909	6.381333	4.044424	3.33243	1.310218
Rsk	Mean	0.465	-0.023	-0.26	-0.083	0.2116	-0.023	0.32	-0.106	-0.145	0.3116	-0.07	0.21	-0.26	0.465	0.725	-0.1674	-0.5299

Table 5-22. (Continued)

SxD INT. (CENTRAL)		LxC	LxH	CxC	CxH	HxC	HxH	MIN	MAX	EFFECT	OVERALL MEAN	PREDICTED VALUE
T.Run out	Mean	0.000879	0.00017	0.000858	0.00086	0.00112	0.000697	0.000174	0.001116	0.000942	0.00076	0.001231
Lq	LOG(S)	-1.63711	-1.16262	-0.5718	-1.7663	-1.740777	-1.10258	-1.766292	-0.571754	1.194538	-1.3302	-1.927469

FxD INT. (HIGH)		LxC	LxH	SLxC	SLxH	SHxC	SHxH	HxC	HxH	MIN	MAX	EFFECT	OVERALL MEAN	PREDICTED VALUE
Runout	S/N	-17.48	-10.33	-14.9170	-3.4040	-1.10404	-21.681	0.68182	-17.25773	-21.680	0.68182	22.3626	-10.063	1.1183

SxFxD INT. (CENTRAL)		MIN		MAX		EFFECT	OVERALL MEAN	PREDICTED VALUE
Lq	S/N	-2.38907	CxSLxH	0	HxSHxL	2.389076	8.03053	9.225068
	LOG(S)	0.02	LxHxL	0.033333	CxSLxL	0.013333	-1.3302	-1.323533

PROPOSED STRAIGHT/TAPER GEOMETRY

S MAIN EFFECT (HIGH)		L	C	H	MIN	MAX	EFFECT	OVERALL MEAN	PREDICTED VALUE
Angular	S/N	43.949	29.02259	2.11025	2.11025	43.94895	41.8387	25.0273	4.107948
Parallel	LOG(S)	-4.00948	-4.1805	-3.8385	-4.180495	-3.838525	0.34197	-4.0095	-3.838515
Angular	Mean	101.227	101.329	67.5057	67.50568	101.329	33.82333	90.0206	73.10894

S MAIN EFFECT (CENTRAL)		L	C	H	MIN	MAX	EFFECT	OVERALL MEAN	PREDICTED VALUE
Straight	Mean	11.22355	7.49594	18.7441	7.495937	18.74407	11.24814	12.4879	18.11197
Parallel	Mean	0.000259	0.00022	0.00053	0.00022	0.00053	0.00031	0.00034	0.000495
a0 Peak	Mean	169.653	92.3438	103.806	92.34382	169.6528	77.30902	121.934	83.27949
Rtm	S/N	-12.826	-6.493981	-3.8017	-12.82637	-3.801652	9.024719	-7.7073	-3.194941
Sm	S/N	10.5888	14.6411	11.86173	10.58884	14.64106	4.052222	12.3639	14.39001

S MAIN EFFECT (LOW)	L	C	H	MIN	MAX	EFFECT	OVERALL MEAN	PREDICTED VALUE

Table 5-22. (Continued)

Angul	S/N	67.7766	4.03992	5.623268	4.039917	67.7766	63.73668	25.8133	-6.055042
Parall	S/N	7.53903	4.18094	4.272198	4.180937	7.539031	3.358094	5.33072	3.651673
Angular	LOG(S)	-1.2582	-1.284951	-1.3287	-1.328663	-1.258174	0.070489	-1.2906	-1.325844
Parallel	LOG(S)	-4.4236	-4.422271	-4.2932	-4.423646	-4.293239	0.130407	-4.3797	-4.314496
Force	Mean	82.28806	76.7526	92.5245	76.75259	92.52452	15.77193	83.8551	91.74107
a1 Peak	Mean	76.29508	64.2323	87.5364	64.23225	87.5364	23.30415	53.0152	64.66728
Sm	S/N	11.3098	14.3718	14.65634	11.30983	14.65634	3.346508	13.446	15.11925
Rtm	LOG(S)	-0.5218	-0.548304	-0.8562	-0.856171	-0.52176	0.33441	-0.6421	-0.809305
	Mean	4.07917	2.145833	1.23333	1.233333	4.079167	2.845833	2.48611	1.063193

F MAIN EFFECT (HIGH)		L	SL	SH	H	MIN	MAX	EFFECT	OVERALL MEAN	PREDICTED VALUE
Position	LOG(S)	-3.465	-3.29717	-3.1023	-3.259289	-3.464988	-3.102264	0.362723	-3.2809	-3.099538
Parallel	LOG(S)	-4.5158	-3.893385	-3.6596	-3.969246	-4.515763	-3.659616	0.856147	-4.0095	-3.581426
a0 Peak	S/N	-43.03625	-44.561	-42.38147	-39.823	-44.56117	-39.82297	4.738202	-42.45	-44.8191
a1 Peak	S/N	-42.518	-29.77188	-31.37604	-26.256	-42.51804	-26.25573	16.26231	-32.48	-24.34885
	LOG(S)	1.81251	1.271753	1.339761	1.1777	1.177699	1.81251	0.634811	1.40043	1.083024
	Mean	109.194	27.72649	33.22536	19.4764	19.47643	109.1938	89.71737	47.4055	2.546815

F MAIN EFFECT (CENTRAL)		L	SL	SH	H	MIN	MAX	EFFECT	OVERALL MEAN	PREDICTED VALUE
Parallel	Mean	6.6E-05	0.000294	0.0005	0.000482	6.64E-05	0.000503	0.000437	0.00034	0.000558
a2 Peak	S/N	8.999934	6.9406	9.236611	10.1915	6.940597	10.19154	3.250943	8.84217	10.46764

F MAIN EFFECT (LOW)		L	SL	SH	H	MIN	MAX	EFFECT	OVERALL MEAN	PREDICTED VALUE
Flatness	Mean	2.3E-05	4.5E-05	3.07E-05	2.85E-05	2.3E-05	4.49E-05	2.18E-05	3.20E-05	4.29E-05
a1 Peak	S/N	-44.102	-31.74735	-27.76447	-23.096	-44.10195	-23.09603	21.00592	-31.677	-21.17404
	LOG(S)	1.9007	1.277059	1.095613	0.78086	0.780857	1.900699	1.119842	1.26356	0.703639
	Mean	139.663	36.17732	22.53911	13.6815	13.68146	139.6631	125.9816	53.0152	-9.975597
a2 Peak	S/N	-13.456	-11.74507	-10.98661	-7.7504	-13.45564	-7.75036	5.705282	-10.984	-8.131359
Rsk	S/N	-18.29653	-21.264	-5.4206	-7.109272	-21.2643	-5.420642	15.84366	-13.023	-5.101172
	Mean	0.053333	0.05944	-0.0406	-0.009444	-0.040556	0.059444	0.1	0.01569	-0.03431

Table 5-22. (Continued)

Lq	Mean	0.11667	0.201111	0.267222	0.31278	0.116667	0.312778	0.196111	0.22444	0.322496
D MAIN EFFECT (CENTRAL)		**C**	**H**	**MIN**	**MAX**		**EFFECT**		**OVERALL MEAN**	**PREDICTED VALUE**
a2 Peak	**Mean**	14.12963	3.554712	3.554712	14.12963		10.57492		8.84217	3.5547113

SxF INT. (LOW)		**LxL**	**LxSL**	**LxSH**	**LxH**	**CxL**	**CxSL**	**CxSH**	**CxH**	**HxL**	**HxSL**	**HxSH**	**HxH**	**MIN**	**MAX**	**EFFECT**	**OVERALL MEAN**	**PRED VAL.**
Rku	**LOG(S)**	0.421	-0.726	-0.9	-0.12	0.062	-0.72	0.123	-0.70	-0.12	-0.18	0.488	0.265	-0.923	0.488	1.412467	-0.2658	0.440
Rsk	**LOG(S)**	-0.219	-1.044	-0.63	-0.540	-0.453	-1.044	-0.859	-0.947	-0.493	-0.36	-0.328	-0.312	-1.044	-0.219	0.824268	-0.5584	-0.97

FxD INT. (HIGH)		**LxC**	**LxH**	**SLxC**	**SLxH**	**SHxC**	**SHxH**	**HxC**	**HxH**	**MIN**	**MAX**	**EFFECT**	**OVERALL MEAN**	**PREDICT VALUE**
Angular	**S/N**	-12.43	64.2895	75.286	27.7484	-53.15	-13.340	75.2869	33.55288	-53.15013	75.28695	128.4371	-1.2318	62.98674
	Mean	44.993	135.062	135.01	89.9824	44.9935	45.0793	135.0162	90.00175	44.99349	135.0623	90.06881	90.0206	135.055
FxD INT. (CENTRAL)		**LxC**	**LxH**	**SLxC**	**SLxH**	**SHxC**	**SHxH**	**HxC**	**HxH**	**MIN**	**MAX**	**EFFECT**	**OVERALL MEAN**	**PREDICT VALUE**
Straight	**Mean**	29.968	2.6E-05	-6E-05	15.0083	10.0068	29.9101	6.81E-05	15.00925	-6.05E-05	29.96824	29.9683	12.4879	27.47205
a2 Peak	**Mean**	3.7320	14.2678	3.8184	9.88638	3.79946	14.6737	2.86897	17.5141	2.868967	17.51411	14.64514	3.61501	10.93758

SxFxD INT. (HIGH)		**MIN**		**MAX**		**EFFECT**	**OVERALL MEAN**	**PREDICTED VALUE**
Angular	**Mean**	-6.38E-05	**CxLxC**	135.2367	**LxSHxH**	135.2368	90.0206	157.639
	S/N	-129.403	**HxSLxC**	81.72034	**HxHxH**	211.1233	25.0273	130.589
SxFxD INT. (CENTRAL)		**MIN**		**MAX**		**EFFECT**	**OVERALL MEAN**	**PREDICTED VALUE**
Straight	**Mean**	-0.000156	**CxSLxC**	45.02773	**HxHxH**	45.02788	12.4879	35.00184
Rku	**S/N**	-1.074167	**HxHxC**	28.42343	**LxHxL**	29.4976	15.0781	29.8269
	LOG(S)	2.005	**CxSLxL**	0.917068	**LxLxH**	-1.087932	-0.2658	-0.809766

From Tables 5-21 and 5-22, the following observations are made for contour and straight/taper geometry significance.

Contour, High Depth of Cut

- Spindle speed has an effect on mean skewness. The significant optimal level for spindle speed is low.
- Feedrate and the dual interaction of feedrate and depth of cut have an effect on runout tolerance signal-to-noise. The significant optimal level for feedrate is semi-low and the significant optimal level for the dual interaction is [H x C].
- Spindle speed is significant for force signal-to-noise and feedrate is significant for both force variance and signal-to-noise. The significant optimal level for feedrate is low and the significant optimal level for spindle speed is central.
- Feedrate and depth of cut has an effect of peak force variance. The significant optimal level for both feedrate and depth of cut is high.

Contour, Central Depth of Cut

- Spindle speed is significant for mean total runout and total runout signal-to-noise and the dual interaction of spindle speed and depth of cut has an effect. The significant optimal level for spindle speed is central to minimize signal-to-noise variability and is high to minimize mean variability. The significant optimal level for the [S x D] dual interaction is [H x C].

- Feedrate has a significant effect on center force mean, variance, and signal-to-noise. The significant optimal level to reduce the variability in variance and signal-to-noise is high and the significant optimal level for mean is low.
- Depth of cut, the dual interaction of spindle speed and depth of cut [S x D], the dual interaction of spindle speed and feedrate [S x F], and the [S x F x D] triple interaction for wavelength is significant. The significant optimal level for spindle speed is low, depth of cut is low for variance and is central for signal-to-noise. The significant optimal levels for the dual interactions are [H x C] for variance and [L x SL] for signal-to-noise. The significant optimum level for the [S x F x D] triple interaction is [L x H x L] for variance and [H x SH x L] for signal-to-noise.
- Feedrate has a significant effect on mean peak-to-valley height and signal-to-noise. The significant optimal level for mean is high and the significant optimal level for signal-to-noise is low.

Contour, Low Depth of Cut

- Feedrate has a significant effect on position tolerance variance. The significant optimal level is semi-low.
- Spindle speed is significant for total runout variance and signal-to-noise. A high level of spindle speed is optimal for both variance and signal-to-noise.
- Feedrate is significant for runout tolerance variance. The significant optimal level is semi-low to reduce runout tolerance variability.
- Spindle speed is significant for mean circularity tolerance, force variance, wavelength mean, signal-to-noise, and variance, and peak-to-valley mean and signal-to-noise.

- Feedrate has a significant effect on force center mean, variance, and signal-to-noise. The significant optimum level for each is low.
- The dual interaction of spindle speed and feedrate has a significant effect on force width mean, variance, and signal-to-noise and mean surface skewness. The significant optimal levels [L x L] and [H x SL] for mean force width.

Straight/Taper, High Depth of Cut

- Feedrate has a significant effect on position tolerance variance. The significant optimal level is low.
- Spindle speed, the dual interaction of [F x D] and the [S x F x D] triple interaction effect are significant for angularity tolerance mean and signal-to-noise. The significant optimum levels are low, [H x C], and [H x SH x L], respectively.
- Spindle speed and feedrate are significant for parallelism tolerance variance. The significant optimum levels are semi-high and low, respectively.
- Feedrate is significant for peak force signal-to-noise. The significant optimum level is high.
- Feedrate has a significant effect on force center mean, variance, and signal-to-noise. The optimum levels for each effect is high.

Straight/Taper, Central Depth of Cut

- Spindle speed, the dual interaction of feedrate and depth of cut, and the [S x F x D] triple interaction are significant for mean straightness tolerance. The optimum level

for spindle speed is high, the optimum level for the dual interaction is [SH x H], and the optimum level for the triple interaction is [H x H x H].

- Spindle speed and feedrate has a significant effect on mean parallelism tolerance. The significant optimum level for spindle speed is high and the significant optimum level for feedrate is semi-high.
- Spindle speed is significant for mean peak force. The optimum level is low.
- Feedrate, depth of cut, and the dual interaction of feedrate and depth of cut is significant for force width mean and signal-to-noise. The significant optimum level for feedrate is high, the optimum level for depth of cut is high, and the optimum dual interaction is [H x C].
- The triple interaction of [S x F x D] is significant for surface kurtosis variance and signal-to-noise. The optimum levels for kurtosis variance is [L x H x L] and the optimum levels for kurtosis signal-to-noise is [C x SL x L].
- Spindle speed has a significant effect on spacing and peak-to-valley height signal to noise. The significant optimum level for surface spacing is central and the optimum level for peak-to-valley height is high.

Straight/Taper, Low Depth of Cut

- Feedrate is significant for flatness tolerance mean and surface skewness signal-to-noise. The significant optimum level is semi-low.
- Spindle speed is significant for mean peak-to-valley height, angularity tolerance signal-to-noise ratio, parallelism tolerance variance and signal-to-noise ratio. The significant optimum level is low.

- Spindle speed has a significant effect on angularity tolerance variance, mean force, surface spacing signal-to-noise, and peak-to-valley variance. The significant optimum level is high.
- Feedrate has a significant effect on force center variance and signal-to-noise ratio, mean surface wavelength, and force width signal-to-noise ratio. The significant optimum level is high.
- The dual interaction of spindle speed and feedrate has a significant effect on peak-to-valley height variance and surface skewness variance. The optimum levels for the dual interaction are [L x SL].

To summarize, spindle speed and feedrate have the most effect on performance. For contour geometry, feedrate is significant for 15 performance indices, spindle speed is significant for 14 performance indices, and depth of cut is significant for 3 performance indices. For straight/taper geometry, spindle speed and feedrate are significant for 14 performance indices, and depth of cut is significant for force center. Both the proposed contour and straight/taper geometry illustrated that a low depth of cut is not significant for each tolerance and surface finish index.

5.4 Knowledge Base Rules

The developed case study knowledge base rules are divided into two sets. Set 1 rules provide SR/MR empirical relationship resolution. Set 2 rules incorporate expert knowledge to provide tie resolution, conflict resolution, or endless loop resolution.

Set 1 Rules

Rule 1: IF R_SQ[1,2] IS LOW
and R_SQ[1,3] IS LOW
and R_SQ[2,3] IS LOW
THEN NO FEASIBLE VALUES (CONFLICT)

Rule 2: IF R_SQ[1,2]*R_SQ[2,3] IS HIGH
and R_SQ[1,3] IS HIGH
and R_SQ[1,2]*R_SQ[2,3]>R_SQ[1,3]
THEN R_SQ[2,3] IS FEASIBLE

Rule 3: IF R_SQ[1,2]*R_SQ[2,3] IS HIGH
and R_SQ[1,3] IS HIGH
and R_SQ[1,2]*R_SQ[2,3]<R_SQ[1,3]
THEN R_SQ[1,3] IS FEASIBLE

Rule 4: IF R_SQ[1,2] IS HIGH
and R_SQ[2,3] IS LOW
and R_SQ[1,3] IS HIGH
THEN R_SQ[1,3] IS FEASIBLE

Rule 5: IF R_SQ[1,2] IS LOW
and R_SQ[2,3] IS HIGH
and R_SQ[1,3] IS HIGH
THEN R_SQ[1,3] IS FEASIBLE

Rule 6: IF R_SQ[1,2]*R_SQ[2,3] IS LOW
and R_SQ[1,3] IS HIGH
THEN R_SQ[1,3] IS FEASIBLE

Rule 7: IF R_SQ[1,2] IS LOW
and R_SQ[1,3] IS LOW
and R_SQ[2,3] IS HIGH
and R_SQ[1,2]*R_SQ[2,3] > R_SQ[1,3]
THEN R_SQ[2,3] IS FEASIBLE

Rule 8: IF R_SQ[1,2] IS HIGH
and R_SQ[2,3] IS LOW
and R_SQ[1,3] IS LOW
and R_SQ[1,2]*R_SQ[2,3] < R_SQ[1,3]
THEN R_SQ[1,3] IS FEASIBLE

Set 2 Rules

The expert rules are:

Rule 9:
IF [P_TOL] IS EQUAL TO [X>0.001 (inch)]
and [RTM] IS EQUIVALENT TO [2.10>=X>1.20 (um)]
THEN [S_SPEED] IS EQUIVALENT TO [5,940<=X<=14,080 (RPM)]
and [FEEDRATE] IS EQUIVALENT TO [70.86<=X<=148.06 (IN/MIN)]
and [DEPTH_CUT] IS [HIGH]

Rule 10:
IF [P_TOL] IS EQUAL TO [0.0007>=X>0.0004 (inch)]
and [RTM] IS EQUAL TO [3.90>=X>3.00 (um)]
THEN [S_SPEED] IS EQUAL TO [X <= 5,386 (RPM)]
and [FEEDRATE] IS EQUAL TO [X <= 102.8 (IN/MIN)]
and [DEPTH_CUT] IS EQUAL TO [HIGH]

Rule 11:
IF [P_TOL] IS EQUAL TO [0.001>=X>0.0007 (inch)]
and [RTM] IS EQUAL TO [3.90>=X>3.00 (um)]
THEN [S_SPEED] IS EQUAL TO [X <= 5,386 (RPM)]
and [FEEDRATE] IS EQUAL TO [102.8 <= X <= 180.0 (IN/MIN)]
and [DEPTH_CUT] IS EQUAL TO [HIGH]

Rule 12:
IF [P_TOL] IS EQUAL TO [X>0.001 (inch)]
and [RTM] IS EQUAL TO [X>3.90 (um)]
THEN [S_SPEED] IS EQUAL TO [X <= 5,386 (RPM)]
and [FEEDRATE] IS EQUAL TO [X >= 180.0 (IN/MIN)]
and [DEPTH_CUT] IS EQUAL TO[HIGH]

Rule 13:
IF [P_TOL] IS EQUAL TO [0.0007>=X>0.0004 (inch)]
and [RTM] IS EQUAL TO [3.00>=X>2.10 (um)]
THEN [S_SPEED] IS EQUAL TO [5,386<=X<= 13,796 (RPM)]
and [FEEDRATE] IS EQUAL TO [X<=102.8 (IN/MIN)]
and [DEPTH_CUT] IS EQUAL TO [LOW]

Rule 14:
IF [P_TOL] IS EQUAL TO [0.0007>=X>0.0004 (inch)]
and [RTM] IS EQUAL TO [3.90>=X>3.00 (um)]
THEN [S_SPEED] IS EQUAL TO [5,386<=X<= 13,796 (RPM)]
and [FEEDRATE] IS EQUAL TO [102.8<=X<=180.0 (IN/MIN)]
and [DEPTH_CUT] IS EQUAL TO [CENTRAL]

Rule 15:
IF [P_TOL] IS EQUAL TO [0.001>=X>0.0007 (inch)]
and [RTM] [X>3.90 (um)]
THEN [S_SPEED] IS EQUAL TO [5,386 <=X<=13,796 (RPM)]
and [FEEDRATE] IS EQUAL TO [X >=180.0 (IN/MIN)]
and [DEPTH_CUT] IS EQUAL TO [HIGH]

Rule 16:
IF [P_TOL] IS EQUAL TO [0.0004>=X>0.0001 (inch)]
and [RTM] [X<1.20 (um)]
THEN [S_SPEED] IS EQUAL TO [5,940<=X<=14,080 (RPM)]
and [FEEDRATE] IS EQUAL TO [X<=70.86 (IN/MIN)]
and [DEPTH_CUT] IS EQUAL TO [LOW]

Rule 17:
IF [P_TOL] IS EQUAL TO [0.0004>=X>0.0001 (inch)]
and [RTM] [2.10>=X>=1.20 (um)]
THEN [S_SPEED] IS EQUAL TO [5,940<=X<=14,080 (RPM)]

and [FEEDRATE] IS EQUAL TO [70.86<=X<=148.06 (IN/MIN)]
and [DEPTH_CUT] IS EQUAL TO [LOW]

Rule 18:

IF [P_TOL] IS EQUAL TO [0.0004>=X>0.0001 (inch)]
and [RTM] [3.00>=X>=2.10 (um)]
THEN [S_SPEED] IS EQUAL TO [5,940<=X<=14,080 (RPM)]
and [FEEDRATE] IS EQUAL TO [X<=148.06 (IN/MIN)]
and [DEPTH_CUT] IS EQUAL TO [CENTRAL]

Rule 19:

IF [P_TOL] IS EQUAL TO [X<0.0001 (inch)]
and [RTM] [X<2.10 (um)]
THEN [S_SPEED] IS EQUAL TO [X>14,080 (RPM)]
and [FEEDRATE] IS EQUAL TO [X<70.86 (IN/MIN)]
and [DEPTH_CUT] IS EQUAL TO [LOW]

5.5 Application of the Proposed Heuristic to Different Surfaces

Six surfaces, listed in Table 5-23 and illustrated in Figure 5-25, are selected to illustrate the proposed knowledge base. Straight-taper geometry is specified in surfaces 1 through 4. Contour geometry is specified in surfaces 5 and 6. Surface 1 specifications include a position tolerance of 0.005 inches, a straightness tolerance of 0.003 inches, and a peak-to-valley height of 2.032 microns. Surface 2 specifications include a position tolerance of 0.005 inches, a parallelism tolerance of 0.003 inches, and a peak-to-valley height of 1.524 microns. Surface 3 specifications include a position tolerance of 0.005 inches, an angularity tolerance of 0.005 inches, and a peak-to-valley height of 2.032 microns. Surface 4 specifications include a position tolerance of 0.005 inches and a peak-to-valley height of 2.032 microns. Surface 5 specifications include a position tolerance of 0.005 inches, a total runout tolerance of 0.002 inches, and a peak-to-valley height of 2.032 microns. Surface 6 specifications include a position tolerance of 0.005 inches, a circularity tolerance of 0.002 inches, and a peak-to-valley height of 1.524 microns.

Operating parameters, listed as surface 6-A, are specified for surface 6. Operating parameters include a 7,000 RPM spindle speed and a 150 in./min feedrate at a low depth.

Table 5-23. User Input Specification

Surface	Geometry	P_TOL (in.)	STR_TOL (in.)	PARA_TOL (in.)	RTM (um)	DIM. (in.)
1	S_TAPER	0.005	0.003		2.032	5.62
2	S_TAPER	0.005		0.003	1.524	2.12
		P_TOL (in.)		ANG_TOL (in.)	RTM (um)	DIM. (in.)
3	S_TAPER	0.005		0.005	2.032	2.88
4	S_TAPER	0.005			2.032	2.88
		P_TOL (in.)	CIRC_TOL (in.)	T_RUN_TOL (in.)	RTM (um)	DIM. (in.)
5	CONTOUR	0.005		0.002	2.032	0.75
6	CONTOUR	0.005	0.002		1.524	0.62
User Defined Operating Parameters						
Surface	Geometry	Speed (RPM)	Feedrate (in./min)	Depth of Cut (in.)		DIM. (in.)
6-A	CONTOUR	7,000 (C)	150 (SH)	(LOW)		0.62

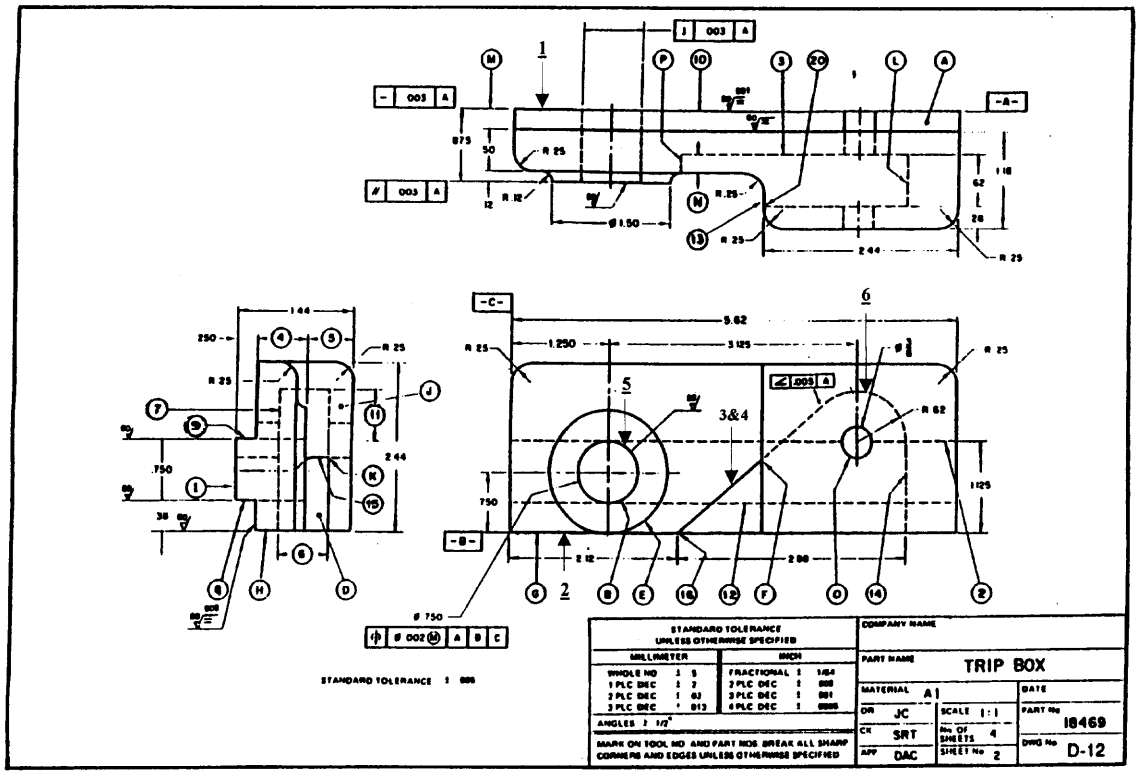

Figure 5-25. Proposed Case Study

Depth of cut, listed in Table 5-24, is determined for each surface based on the depth frequency from the rating database. The highest depth of cut for the highest frequency is selected to maximize MRR. Surface 1 is fixed at a central depth of cut since the central depth has the highest frequency for position tolerance, straightness tolerance, and peak-to-valley height. Surface 2 is fixed at a central depth since the central depth has the highest frequency for position tolerance, parallelism tolerance, and peak-to-valley height. Surface 3 is fixed at a high depth since angularity tolerance frequency provides a high depth. Position tolerance and peak-to-valley height provided a central depth of cut. Surface 4 is fixed at a central depth of cut since the central depth has the highest frequency for position tolerance and peak-to-valley height. Surface 5 is fixed at a high depth of cut since peak-to-valley height frequency provides a high depth of cut. Position tolerance provided a low depth of cut and total runout tolerance provided a central depth of cut. Surface 6 is fixed at a high depth of cut since the peak-to-valley height frequency provides a high depth. Position tolerance provided a low depth and circularity tolerance provided a central depth.

Table 5-24. Frequency of Rating for Depth Selection

SURFACE 1 [S_TAPER]						
Index	**Rating**	**L**	**C**	**H**	**Highest Freq.**	**Depth of Cut**
P_TOL	**1**	4	7	5	Central	**Central**
STR_TOL	**1**	0	4	2	Central	
RTM	**4**	5	5	4	Central	
SURFACE 2 [S_TAPER]						
P_TOL	**1**	4	7	5	Central	**Central**
PARA_TOL	**1**	0	4	2	Central	
RTM	**4**	5	5	4	Central	
SURFACE 3 [S_TAPER]						
P_TOL	**1**	4	7	5	Central	**High**
ANG_TOL	**1**	3	0	8	High	
RTM	**4**	5	5	4	Central	
SURFACE 4 [S_TAPER] ***Expert Rule***						
P_TOL	**1**	4	7	5	Central	**Central**

Table 5-24. (Continued)

RTM	**4**	5	5	4	Central	
SURFACE 5 [CONTOUR]						
P_TOL	**2**	4	4	1	Low	**High**
T_RUN_TOL	**2**	0	4	3	Central	
RTM	**1**	3	3	5	High	
SURFACE 6 [CONTOUR]						
P_TOL	**2**	4	4	1	Low	**High**
CIRC_TOL	**5**	4	2	2	Central	
RTM	**1**	3	3	5	High	

Relationship selection for determining operating parameters and performance indices based on the R-square is listed in Table 5-25. Surface 1 through 4 parameters and indices are determined by the multiple regression (MR) relationships due the high R-square values. The multiple regression function for position tolerance is selected over the simple regression (SR) relationship since the MR relationship is a direct link to determining the operating parameters. Surfaces 5 and 6 utilize the MR relationships for position tolerance, total runout tolerance and circularity tolerance but utilizes the SR relationship for determining the peak-to-valley height performance index.

Table 5-25. MR/SR Relationship Decision

SURFACE 1 (S_TAPER)			
Index	**Force-SR R-Square**	**MR R-Square**	**MR/SR Selection***
P_TOL	0.859	0.844	MR**
STR_TOL	0.735	0.962	MR
RTM	0.696	0.931	MR
SURFACE 2 (S_TAPER)			
P_TOL	0.859	0.844	MR**
PARA_TOL	0.768	0.840	MR
RTM	0.696	0.931	MR
SURFACE 3 (S_TAPER)			
P_TOL	0.811	0.811	MR**
ANG_TOL	0.927	0.930	MR
RTM	0.700	0.833	MR

Table 5-25. (Continued)

SURFACE 4 (S_TAPER)			
P_TOL	0.859	0.844	MR**
RTM	0.696	0.931	MR
SURFACE 5 (CONTOUR)			
P_TOL	0.845	0.846	MR
T_RUN_TOL	0.819	0.988	MR
RTM	0.926	0.854	SR
SURFACE 6 (CONTOUR)			
P_TOL	0.845	0.846	MR
CIRC_TOL	0.808	0.831	MR
RTM	0.926	0.854	SR

**** User May Opt For Force Relationship If The Capability Exists***
***** MR is Desirable Since it is a Direct Link to the Operating Parameters***

From the empirical relationships presented, spindle speed and feedrate, listed in Table 5-26, are determined by solving the relationships simultaneously. For the fixed depths of cut, both spindle speed and feedrate ranges from low to high. Surface 1 operating parameters are set at 9,567 RPM for spindle speed and 236.034 inches per minute for feedrate. Surface 2 operating parameters are set at 15,600 RPM for spindle speed and 241.827 inches per minute for feedrate. Surface 3 operating parameters are set at 8,635 RPM for feedrate and 120.051 inches per minute for feedrate. Surface 4 operating parameters are set at 13,950 RPM for spindle speed and 218.735 inches per minute for feedrate. Surface 5 operating parameters are set at 5,304 RPM for spindle speed and 45.543 inches per minute for feedrate. Surface 6 operating parameters are set at 6,970 RPM for spindle speed and 113.776 inches per minute for feedrate.

Table 5-26. Speed/Feedrate Selection

Surface #	Spindle Speed (RPM)	Feedrate (in./min)	Depth of Cut (in.)
1 [S_TAPER]	9,567 (C)	236.034 (H)	Central (C)
2 [S_TAPER]	15,600 (H)	241.827 (H)	Central (C)
3 [S_TAPER]	8,635 (C)	120.051 (SL)	High (H)
4 [S_TAPER]	13,950 (H)	218.735 (SH)	Central (C)
5 [CONTOUR]	5,304 (L)	45.543 (L)	High (H)
6 [CONTOUR]	6,970 (C)	113.776 (SL)	High (H)

The levels at which variability is caused for the mean, log(s) and signal/noise are listed in Table 5-27. For surface 1, the spindle speed, dual interaction of feedrate and depth of cut, and the triple interaction of [SxFxD] are significant for straightness tolerance mean. Spindle speed is significant for the peak-to-valley height signal/noise ratio. On surface 2, both the spindle speed and feedrate have a significant effect on mean parallelism tolerance. Spindle speed also has a significant effect for the peak-to-valley height signal/noise ratio. On surface 3, feedrate is significant for position tolerance variance. The spindle speed, feedrate and depth dual interaction, and [SxFxD] triple interaction have a significant effect on angularity tolerance mean and signal/noise ratio. Spindle speed is significant for peak-to-valley height signal/noise ratio on surface 4. On surface 5, the spindle speed and dual interaction of speed and depth of cut have a significant effect on mean total runout tolerance. Feedrate has a significant effect on mean peak-to-valley height. On surface 6, the feedrate is significant for position tolerance variability and spindle speed is significant for both mean circularity tolerance and mean peak-to-valley height. For the significant parameters, the optimal levels for mean, log(s), and signal-to-noise are also listed in Table 5-27.

Table 5-27. Significant Factors

Index	Significance (Y/N)	Significant Parameter(s)	Optimum Level(s)		
			Mean	Log(S)	S/N
Surface 1 (S_TAPER)					
P_TOL	N				
STR_TOL	Y	(S), (FxD), (SxFxD)	(H), (SHxH), (HxHxH)		
RTM	Y	(S)			(H)
Surface 2 (S_TAPER)					
P_TOL	N				
PARA_TOL	Y	(S), (F)	(H), (SH)		
RTM	Y	(S)			(H)
Surface 3 (S_TAPER)					

Table 5-27. (Continued)

P_TOL	Y	(F)		(L)	
ANG_TOL	Y	(S), (FxD), (SxFxD)	(L), (HxC), (HxSHxL)		(L), (HxC), (HxHxH)
RTM	N				
Surface 4 (S_TAPER)					
P_TOL	N				
RTM	Y	(S)			(H)
Surface 5 (CONTOUR)					
P_TOL	N				
T_RUN_TOL	Y	(S), (SxD)	(H), (HxC)		
RTM	Y	(F)	(H)		
SURFACE 6 (CONTOUR)					
P_TOL	Y	(F)		(SL)	
CIRC_TOL	Y	(S)	(L)		
RTM	Y	(S)	(L)		(H)

The performance index values determined through the MR/SR functions are listed in Table 5-28. Surface 1 lists the performance values at the levels before the significance database. Values for position tolerance, straightness tolerance, and peak-to-valley height are also listed as other alternatives when both spindle speed and the triple interaction [SxFxD] is changed to its significant optimum level. The dual interaction of feedrate and depth of cut is ignored since the user specifications are exceeded. The original values for all the performance indices are the closest to the user specifications. Surface 2 lists the performance values for position tolerance, parallelism tolerance, and peak-to-valley height for the original levels and when spindle speed is changed to its significant optimal level. The change in feedrate results in exceeding the user requirements. Position tolerance and peak-to-valley height are closer to the user specifications at the original levels and parallelism tolerance is closer to the user specification when spindle speed is changed. Surface 3 lists the performance values for position tolerance, angularity

tolerance, and peak-to-valley height at the original levels and the triple interaction levels. The change in spindle speed and the dual interaction of feedrate and depth of cut yield no feasible performance values. The angularity tolerance and peak-to-valley height performance values at the original levels are closer to the user specifications and the angularity tolerance triple interaction provides a closer performance value. Surface 5 provides four alternatives for position tolerance, total runout tolerance, and peak-to-valley height. Both the position tolerance and total runout tolerance performance values at the significant optimal feedrate are closer to the user specification. The original levels provide the closest performance value at for peak-to-valley height. Surface 6 provides performance values for position tolerance, circularity tolerance, and peak-to-valley height at original levels and at the optimum significant level of spindle speed. The change in spindle speed to the optimum significant level provides the best performance values. At surface 6A, the prespecified operating parameters provide a close peak-to-valley performance value to the user specification but provides no feasible second alternative when spindle speed is changed to its optimum significant level.

Table 5-28. Performance Index Values

Surface 1 (S_TAPER)						
Index	**Original Value**	**Δ (S)**	**Δ (F)**	**Δ (FxD)**	**Δ (SxD)**	**Δ (SxFxD)**
P_TOL	0.0016739	0.000587		***Exceeds User Spec(s)***		0.00029939
STR_TOL	0.0006010	0.000156				0.00059505
RTM	2.0115778	1.290188				1.69500952
Surface 2 (S_TAPER)						
P_TOL	0.0007986	0.000687	***Exceeds User Spec(s)***			
PARA_TOL	0.0010678	0.001119				
RTM	1.3613031	1.324033				
Surface 3 (S_TAPER)						
P_TOL	0.0002739	***Exceeds User Spec(s)***		***Exceeds User Spec(s)***		0.00110929
ANG_TOL	0.0035827					0.00190539
RTM	2.0158701					1.59747730

Table 5-28. (Continued)

Surface 4 (S_TAPER)						
P_TOL	0.00084597					
RTM	1.51868550					
Surface 5 (CONTOUR)						
P_TOL	0.00034327	0.0001859	0.00109420		0.0002439	
T_RUN_TOL	0.00085844	0.0003712	0.00163693		0.0005017	
RTM	1.35759799	1.2349374	1.32954790		1.3098436	
Surface 6 (CONTOUR)						
P_TOL	0.00022979	0.0003311				
CIRC_TOL	0.00052923	0.0015924				
RTM	1.35759799	1.3647235				
Surface 6A (CONTOUR) (User Specified Parameters)						
P_TOL	0.00035769	***Exceeds User Spec(s)***				
CIRC_TOL	0.00018915					
RTM	1.27884230					

For the feasible levels determined through the proposed knowledge base, the benefit/cost ratios are determined. The best (highest) benefit/cost ratio is at alternative 5-3 for contouring and alternative 1-1 for straight cutting. The worst (smallest) benefit/cost ratio is at alternative 5-4 for contouring and alternative 4-1 for straight cutting.

As an additional alternative, expert rule 10 is fired which satisfies surface 4 performance requirements. For a position tolerance greater than 0.001 inches and a peak-to-valley height between 1.20 and 2.10 microns, the user should specify the spindle speed between 5,940 RPM and 14,080 RPM, the feedrate between 70.86 in./min and 148.06 in./min, and a high depth of cut. The operating parameters and performance values for the fired expert rule is listed as alternative 4-2 in Table 5-29.

From the sequence determined through the proposed inference engine, and expert rule is fired to provide an alternative for surface 4.

IF	[P_TOL]	[X>0.001 (inch)]
and	[RTM]	[2.10>=X>1.20 (um)]
THEN	[S_SPEED]	[5940<=X<=14,080 (RPM)]
and	[FEEDRATE]	[70.86<=X<=148.06 (in./min)]
and	[DEPTH_CUT]	[HIGH]

The alternative operating parameters for each specified surface produced by the proposed knowledge base is listed in Table 5-29 and 5-30. In terms of the performance index values being closest to the user specifications for straight taper geometry, alternative 1-1 provides the overall best performance where there is a 67 percent improvement in position tolerance, a 1.0 percent improvement in peak-to-valley height, and an 80 percent improvement in straightness tolerance. For surface 2, alternative 2-1 provides the best overall performance where there is an 84 percent improvement in position tolerance, an 11 percent improvement in peak-to-valley height, and a 64 percent improvement in parallelism tolerance. For surface 3, alternative 3-1 provides the best performance where there is a 95 percent improvement in position tolerance, a 1.0 percent improvement in peak-to-valley height, and a 28 percent improvement in angularity tolerance. For surface 4, alternative 4-2 provides the best performance where there is a 97 percent improvement in position tolerance and a 10 percent improvement in peak-to-valley height. For surface 5, alternative 5-3 provides the best performance where there is a 78 percent improvement in position tolerance, a 35 percent improvement in peak-to-valley height, and an 18 percent improvement in total runout tolerance. For surface 6, alternative 6-2 provides the best performance where there is a 93 percent improvement in position tolerance, a 10 percent improvement in peak-to-valley height, and a 20 percent improvement in circularity tolerance.

In terms of benefit/cost ratio, the best alternatives are universal since the same alternatives shown where a closer performance value is desirable. Alternative 1-1 provides a 5.00 B/C ratio, alternative 2-1 provides a 2.50 B/C ratio, alternative 3-1

provides a 3.00 B/C ratio, alternative 4-2 provides a 3.00 B/C ratio, alternative 5-3 provides a 12.0 B/C ratio, and alternative 6-2 provides a 6.00 B/C ratio.

Table 5-29. Display of Alternative Operating Parameters

Surface #/Alt.	Spindle Speed	Feedrate	Depth of Cut	B/C Ratio	P_TOL	% Diff. From Spec.	RTM	% Diff. From Spec.	STR_TOL	% Diff. From Spec.	PARA_TOL	% Diff. From Spec.	ANG_TOL	% Diff. From Spec	CIRC_TOL	% Diff. From Spec	T_RUN_TOL	% Diff. From Spec
1-1 ♣	9,567 (C)	236.034 (H)	Central (C)	5.00	0.001674	67	2.011578	1	0.00060	80								
1-2*	16,000 (H)	236.034 (H)	Central (C)	2.50	0.000587	88	1.290188	37	0.00015	95								
1-3*	16,000 (H)	230.000 (H)	High (H)	3.00	0.000299	94	1.69501	17	0.00059	80								
2-1 ♣	15,600 (H)	241.827 (H)	Central (C)	2.50	0.000798	84	1.361303	11			0.001067	64						
2-2*	16,000 (H)	241.827 (H)	Central (C)	2.50	0.000687	86	1.324033	13			0.001119	63						
3-1 ♣	8,635 (C)	120.051 (SL)	High (H)	3.00	0.000273	95	2.015870	1					0.003582	28				
3-2*	16,000 (H)	170.000 (SH)	Low (H)	2.00	0.001109	78	1.597477	21					0.001905	62				
4-1	13,950 (H)	218.735 (SH)	Central (C)	1.50	0.000845	83	1.518685	25										
4-2** ♣	10,010 (C)	109.46 (SL)	High (H)	3.00	0.000172	97	1.818649	10										
5-1	5,304 (L)	45.543 (L)	High (H)	5.00	0.000343	93	1.357598	33									0.000858	57
5-2*	16,000 (H)	45.543 (L)	High (H)	1.25	0.000186	96	1.234937	39									0.000371	81
5-3* ♣	5,304 (L)	230.000 (H)	High (H)	12.0	0.001094	78	1.329548	35									0.001637	18
5-4*	16,000 (H)	45.5430 (L)	Central (C)	0.75	0.000244	95	1.309844	36									0.000502	75
6-1	6,970 (C)	113.776 (SL)	High (H)	3.00	0.000229	95	1.357597	11							0.000529	74		
6-2* ♣	3,000 (L)	113.776 (SL)	High (H)	6.00	0.000331	93	1.364723	10							0.001592	20		
6A-1***	7,000 (C)	150.000 (SH)	Low (L)	2.50	0.000357	93	1.278842	16							0.000189	91		

** Adjusted According to Optimum Significant Levels*
*** Determined By Expert Rule(s)*
**** User Prespecified Parameters*
♣ Best Surface Alternative

Table 5-30. Additional Performance Indices for Best Surface Alternatives

Index	Alternative					
	1-1	2-1	3-1	4-2	5-3	6-2
Kurtosis (Rku) (um)	2.6208	2.8517	2.9155	2.7213	2.3770	2.5736
Skewness (Rsk) (um)	0.5630	0.4321	0.0410	0.0377	0.3114	0.3321
Wavelength (Lq) (um)	0.2088	0.1705	0.1889	0.1715	0.0295	0.0273
Spacing (SM) (um)	444.6525	302.0548	394.534	360.9141	401.2577	370.5231
Flatness (FLAT_TOL) (in.)	0.000281	0.000527	1.74E-05	7.50E-06		
Runout (RUN_TOL) (in.)					0.00021	0.00084
Cylindricity (CYLN_TOL) (in.)					0.00182	0.00115

The heuristic case study provides three feasible alternatives for surface 1, two feasible alternatives for surface 2, two feasible alternatives for surface 3, two feasible alternatives for surface 4, four feasible alternatives for surface 5, and two feasible alternatives for surface 6.

Surface 1 spindle speed ranges from central to high. The increase in spindle speed provides 27 percent user specification improvement in position tolerance, a 16 percent user specification improvement in surface peak-to-valley height, and no improvement in straightness tolerance. Benefit/cost ratio is reduces from 5.00 to 3.00.

Surface 2 spindle speed is increased from 15,600 RPM to 16,000 RPM between alternatives. The slight increase provides a 2 percent user specification improvement in position tolerance, a 2 percent user improvement in surface peak-to-valley height, and a 1 percent improvement in parallelism tolerance. Benefit/cost ratio is 2.50 for both alternatives.

Surface 3 spindle speed is increased by 7,369 RPM and feedrate is increased by 50 in./min. between alternatives. There is a 17 percent user specification improvement in position tolerance alternative 1, a 4 percent user specification improvement in surface peak-to-valley height at alternative 2, and a 34 percent user specification improvement in angularity tolerance at alternative 2. Benefit/cost ratio is improved by 1.00 at alternative 2.

Surface 4 has a 3,940 RPM difference in spindle speed, a 109.3 in./min. difference in feedrate, and a level difference in depth of cut. There is a 14 percent user specification improvement in position tolerance at alternative 1 and a 15 percent user

specification improvement for surface peak-to-valley height at alternative 1. There is a 1.50 improvement in benefit/cost ratio at alternative 2.

There are four feasible alternatives at surface 5. There is a 10,696 RPM difference in spindle speed between high and low levels and a 184.46 in./min difference in feedrate between high and low levels. There is an 18 percent user specification improvement in position tolerance at alternative 2, a 6 percent user specification improvement in surface peak-to-valley height at alternative 2, and a 63 percent improvement in total runout tolerance at alternative 2.

There are three feasible alternatives at surface 6. There is a 4,000 RPM difference in spindle speed and a 37 in./min difference in feedrate. There is 2 percent user specification improvement in position tolerance at alternative 1, a 5 percent user specification improvement in surface peak-to-valley height at alternative 1, and a 71 percent user specification improvement for circularity tolerance at alternative 3. Benefit/cost ratio is improved by 3.50 at alternative 2.

5.6 CNC Retrofit Justification

A retrofit can be defined as the changing of machine components, mechanical and/or control system, for the purpose of improving machine performance and cost. The initial desire to retrofit a particular piece of equipment has certain elements to consider. The relative importance of each element of this justification is determined by various economic conditions. Incurred cost is an area that draws much attention. Areas of consideration include unit cost of retrofit components and cost of installation and maintenance (cost avoidance).

The retrofit procedure begins with an inventory and survey of all relevant machine tool components. The survey consists of the following:

1. *Types of mechanical components.* Components that improve machining performance due to physical benefits.
2. *Types of control/feedback components.* Components that improve machining performance due to high resolution feedback and controls.
3. *Capabilities of mechanical and control components.* A survey of performance specification compatibility.
4. *Benefits of mechanical and control components.* A survey of the performance and cost benefits of component replacement.

Following the inventory and survey of machine tool components, an investigation into the problem areas of the current system is required. These areas include:

5. *Define problem areas.* Problem areas include machine components that inhibit performance.
6. *Define practical solutions.* Provide solutions that are physically feasible on the current machine.
7. *Determine solution cost.* Calculate the total initial cost of all replacement components.

Following the problem area investigation, feasible alternatives are required. Feasible alternatives are determined by the following criteria:

8. *Retain/Retrofit/Replace.* An alternative to either retain the existing machine, retrofit the machine, replace the machine.
9. *Return on Investment.* Determine the alternative that provides the best investment return.

10. *Production Demands*. Generate alternatives that are feasible on production demands.
11. *Future Requirements*. Generate alternatives that will accommodate future performance, cost, and production demands.

Current CNC machine configurations consist of a DC servomotor driving gears and a leadscrew to create linear motion under digital control for the purpose of moving an XY table and spindle column. Traditional drive systems are limited for both current and future industry demands. Rotary motors have a limited maximum rotation speed, gear reducers add inertia and lower efficiency, and motor couplings produce windup distortion. Also, encoder couplings deflect during acceleration and deceleration. Drive systems rely on drive screws that provide length restrictions, mechanical backlash, friction, pitch-cyclic errors, and long vibration decay times. Such common configurations in today's high tech manufacturing facilities reveal the following problems:

- Major mechanical elements between the motor and the workpiece such as a gearbox and ballscrew introducing positioning error, friction, and high inertia. Current configurations cannot maintain accuracy levels over a long time period.
- Feedrate limitations due to mechanical components.
- High maintenance cost due to replacement of worn parts.
- Slow tool position time compared with PMBDCLM equipped CNC machines.
- Backlash due to mechanical linkages.

A conventional drive system including a DC servomotor and leadscrew is illustrated in Figure 5-26. Figure 5-27 details the ballscrew drive components that introduce wear and positioning error.

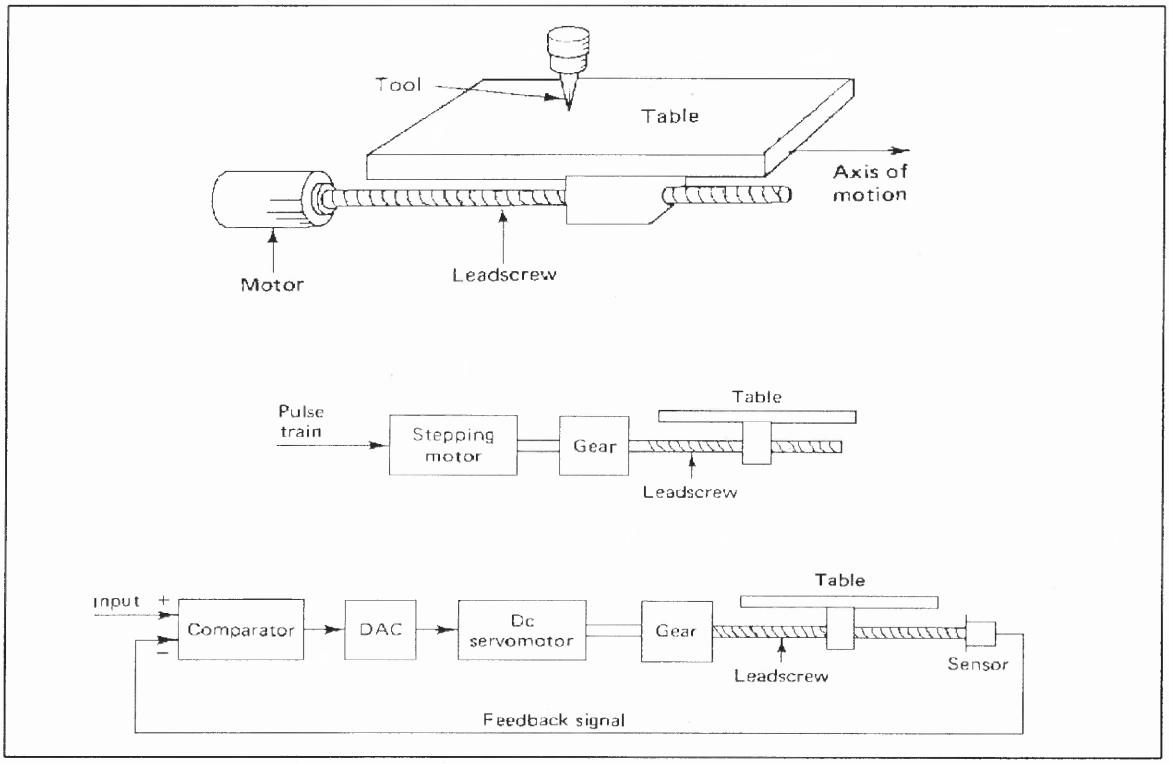

Figure 5-26. Current CNC Configuration Illustrating Drive Train

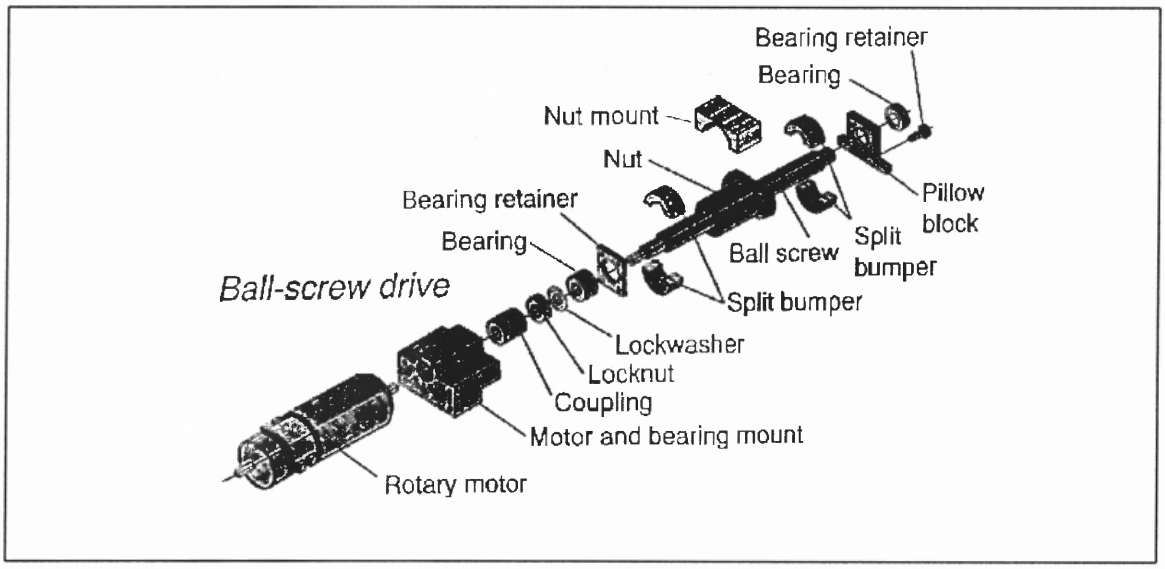

Figure 5-27. Typical Ballscrew Drive

With the conventional configuration, there is a reduction in surface finish and texture with high cutting time. The conventional configuration maximizes peaks and valleys, roughness and waviness, and irregularity heights and different spacing, and has

difficulty in performing complex surface and contouring at high resolution and at high feedrate.

Elimination of the current drive system will provide many benefits in machine performance and maintenance. As illustrated in Figure 5-28, the typical ballscrew assembly is replaced by a linear motor configuration. The linear motor configuration eliminates the entire ballscrew drive for each axis of travel.

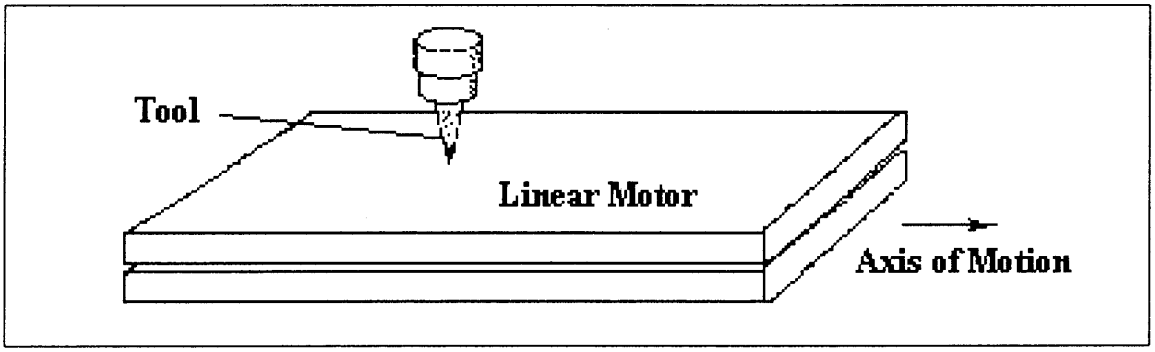

Figure 5-28. Proposed Retrofit Drive System

There are many benefits associated with using the linear motor retrofit configuration. The benefits include:

1. Linear motor technology eliminates the need for brushes, thus motor reliability is increased.
2. Linear motors provide smoother action and less ripple by the use of sinusoidal magnetic fields. As a benefit, the electric current is smoothly commutated, eliminating the high current-switching transients associated with normal square wave or trapezoidal wave commutation.
3. The use of linear motors will decrease the time of machining by reducing the time of tool positioning, thus increasing throughput.

4. Stiffness is a major benefit of linear motors. The drive force is transmitted through an air gap between the moving coil assembly and the fixed magnets. The magnets are fixed to a steel plate, which are bolted directly to the slide.
5. Non-contact linear motor design provides built-in reliability and requires minimal maintenance when compared to other drives, such as ballscrew, rack and pinion, and hydraulic cylinder.
6. No backlash since there are no mechanical linkages.
7. Unlimited travel lengths.

Linear motors have great advantages in stiffness that other motion control devices do not have. Comparing the linear motor drive to a ballscrew, for example, the ballscrew and nut contain inherent deflections of the ball, nut, and screw, as well as rotary support bearings and bearing blocks. With a ballscrew, you can increase the stiffness by increasing the size, but that increases inertia, which in turn increases the deflection. Increasing the pre-load in a ball screw and associated bearings can also add stiffness, but that increases the torque requirements of the rotary motor that results in a larger deflection. Using a rack and pinion drive, the deflection of the teeth and bearings similarly limits stiffness.

The application of PMBDCLM's to CNC metal cutting operations will provide many benefits, both in performance and cost. With current drive systems consisting of machine elements such as gear drives, spindle, slides, and the driving DC servomotors, linear motors will eliminate the need for such a system. The slide, or drive table, is the linear motor slide, thus the conventional configuration is not necessary.

Linear motors utilize the same amplifiers and controllers as rotary motors, therefore there are very few components required for retrofitting. The two types of replacement components include mechanical and feedback. Based on a FADAL VMC-20 milling machine, the mechanical components include the X, Y, and Z-axis ballscrew assembly and servomotor. Feedback components include the X, Y, and Z-axis rotary encoder and controller card.

Mechanical component replacement includes implementing high force linear motors in the X, Y, and Z-axis. Rotary encoders are replaced with a high accuracy/high repeatability linear encoder in the X, Y, and Z-axis. FADAL VMC-20 specifications, linear motor specifications, and replacement components are listed in Table 5-31.

Table 5-31. Component Specifications

Linear Motor Drive System Specifications			
Parameter	**Unit**	**Value**	
Force Constant Ph to Ph	Lbs./amp	34.0	
Back EMF Constant Ph to Ph	V/ips.	3.80	
Continuous Force	Lbs.	500	
Peak Force at 25% Duty	Lbs.	1000	
Continuous Current	Amps	14.7	
Peak Current @25% Force	Amps	29.4	
Resistance Ph to Ph	Ohms	10.0	
Inductance Ph to Ph	mh	42.0	
Electrical Time Constant	msec	4.20	
Moving Member Weight	Lbs	80.0	
Moving Member Length	Inch	25.2	
Stationary Member Weight	Lbs/inch	1.10	
Magnetic Attraction	lbs	3000	
Replacement Components			
Existing FADAL VMC 20 Components			
Mechanical			
Parameter	**Axis**	**Repeatability**	**Accuracy**
FADAL Leadscrew Assembly A-7879	X, Y, Z	+/- 0.00015"	+/- 0.0004"
GlenTek GM4050 DC Axis Motor	**Power**	**Base Speed**	**Field Voltage**
	1.5 HP	1,750 RPM	PM

Table 5-31. (Continued)

Feedback						
	Axis		**Accuracy**		**Resolution**	
GlenTek GM4050 Resolver and Tachometer	X, Y, Z		+/- 0.5 LSB		600 Counts/Rev	
Replacement Components						
Mechanical						
NORMAG BLCH-1 High Force PMBDCLM	**Axis**		**Repeatability**		**Accuracy**	
	X, Y, Z		Sub-Micron		Sub-Micron	
Feedback						
Heidenhain LF-481 Sealed Linear Encoder	**Axis**	**Max. Accel.**	**Max. Speed**	**Max Length**	**Resolution**	**Output Signal**
	X, Y, Z	80 m/s^2	120 m/min	1220 mm	+/- 0.10 um	~1VPP
Heidenhain IBV Encoder Card (Slot 1, 2, 3)	**Axis**		**Input Signal**	**Resolution**		
	X, Y, Z		~1VPP	+/- 0.05 um		

PMBDCLM Drive System

Northern Magnetics high force single sided linear permanent magnet DC brushless motors replace the FADAL VMC-20 drive system. The drive system consists of a moving single sided laminated core type coil winding assembly and a stationary magnet assembly separated by a 0.025-inch air-gap. The thrust and magnetic attraction forces are transmitted directly through the air-gap eliminating mechanical transmission devices.

The PMBDCLM requires external commutation that occurs every 0.30 inches. The three phases are switched through +, -, and 0. Three Hall Effect devices, as part of the moving coil secondary, provide position information for commutation. The linear motor configuration is illustrated in Figure 5-29.

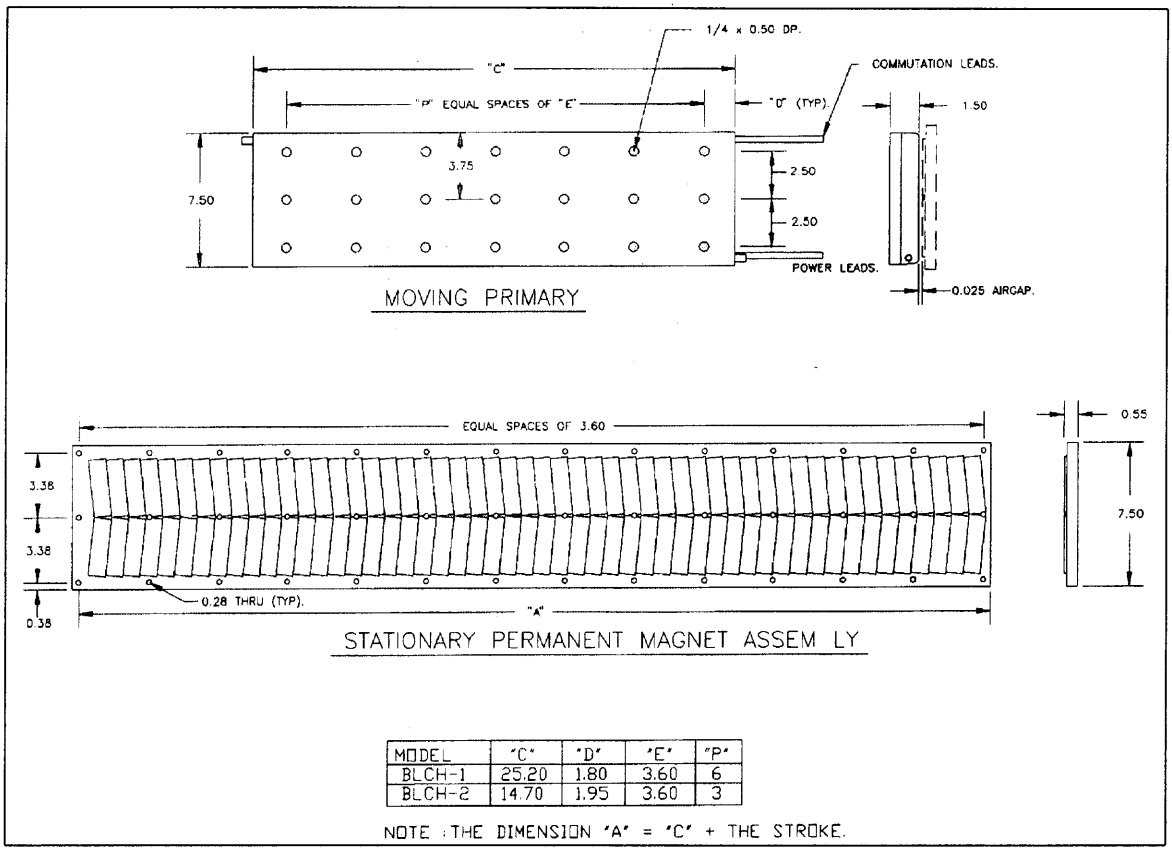

MODEL	"C"	"D"	"E"	"P"
BLCH-1	25.20	1.80	3.60	6
BLCH-2	14.70	1.95	3.60	3

Figure 5-29. Linear Motor

Total cost is divided into four areas. The first area is material and installation, the second area is the PMBDCLM effect on cost, the third area is machining cost, and the fourth area is salvage value. The cost factors are listed in Table 5-32.

Table 5-32. Cost Factors

Material and Installation Cost (C_{mi})	
PMBDCLM	C_{lm}
Linear Encoder	C_{le}
Encoder Card	C_{ec}
Installation Cost	C_i
PMBDCLM Effect on Cost (C_{lm})(P_c = *Performance Coefficient*)	
Maintenance	$(Pc_m)*C_m$
Rework	$(Pc_r)*C_r$
Power	$(Pc_p)*C_p$
Machining Cost (C_{mc}) and **Salvage** (C_s)	
DC Servo Motor	C_{sm}
Rotary Encoder	C_{re}
Encoder Card	C_{ec}
Ballscrew/Leadscrew Assembly	C_{ls}

Based on the required retrofit components and PMBDCLM performance, the following relationships are obtained:

1. Material and Installation Cost

$$C_{mi} = \sum_{m=1}^{n} C_m \tag{5-1}$$

2. PMBDCLM Effect on Cost

$$C_{lm} = \sum_{k=1}^{n} C_k \tag{5-2}$$

3. Machining Cost

Total cutting time for part geometry is;

$$T_{tc} = \sum_{t=1}^{n} \left[\frac{(l - l_c)}{Pc(v)} \right]_t \tag{5-3}$$

where, l = *Length of surface*
l_c = *Extent of cutters first contact with the surface*
v = *Feedrate*

Machining cost is;

$$C_{mc} = C_o T_{tc} \tag{5-4}$$

where, C_o = *Direct labor wage*

Tooling cost per operation is;

$$C_{tl} = C_t \left(\frac{T_{tc}}{T} \right) \tag{5-5}$$

where, C_t = *Cost of tool*

$$T = \left(\frac{K}{V} \right)^{\frac{1}{n}} = \textit{Tool life}$$

Total cost is;

$$C_{tmc} = C_o \left[\sum_{t=1}^{n} \left(\frac{l - l_c}{Pc(v)} \right)_t \right] + C_t \left[\frac{\sum_{t=1}^{n} \left(\frac{l - l_c}{Pc(v)} \right)_t}{\left(\frac{K}{V} \right)^{\frac{1}{n}}} \right] = T_{tc} \left(C_o + \frac{C_t}{T} \right) \tag{5-6}$$

4. Salvage Value

$$C_s = \sum_{l=1}^{n} C_l \tag{5-7}$$

5. Total Cost

$$TC = \sum_{m=1}^{n} C_m + \sum_{k=1}^{n} C_k + C_{tmc} - \sum_{l=1}^{n} C_l \qquad (5\text{-}8)$$

6. Total Cost Savings

$$TC_s = \sum_{m=1}^{n} C_m + \sum_{k=1}^{n} C_k + [(Pc_m)*C_m + (Pc_r)*C_r + (Pc_p)*C_p] - \sum_{l=1}^{n} C_l \qquad (5\text{-}9)$$

From the above relationships, retrofit payback period can be determined.

PMBDCLM implementation has a cost benefit effect. From the empirical data of the PMBDCLM and DC servomotor experimentation, a performance benefit coefficient is determined. Based on percentage improvement in surface finish improvement, a coefficient of 0.539 is multiplied with the rework parameter and a 1.127 coefficient of 1.127 is multiplied by the feedrate. Based on the percentage reduction in force, a 0.923 coefficient is multiplied with the power parameter. Maintenance cost is reduced by half due to PMBDCLM implementation.

Utilizing the relationships, an example involves finish-machining the presented case study surfaces (1 through 6) at the optimal operating parameters and the associated retrofit costs. The costs are listed in Table 5-33.

Table 5-33. Material Cost

Component	**# Units**	**Cost/Salvage Value**		
NORMAG BLCH-1 High Force PMBDCLM	3	$8,000		
Heidenhain LF-481 Sealed Linear Encoder		**X**	**Y**	**Z**
		$1,660	$1,445	$1,660
Heidenhain IBV Encoder Card		$550		
Components Replaced		**New**		**Salvage ***
FADAL Leadscrew Assembly A-7879	3	$2,000		$1,200
GlenTek GM4050 DC Axis Motor		$1,745		$1,047
GlenTek GM4050 Resolver and Tachometer		$395		$237
Related Costs				

Table 5-33. (Continued)

Installation	Rate/Hour	Reqd. Hrs.
	$40	30

**Based on 60% Resale Value*

Material and Installation Cost

$C_{mi} = [3(\$8,000) + [2(\$1,600) + \$1,445] + 3(\$550) + 30(\$40)] = \$31,495$

PMBDCLM Effect on Cost

$C_{lm} = [0.50(\$50/week) + 0.539(\$250/week) + 0.923(\$650/week)] = \$760/week$

Machining Cost

Qualifying the blank @ 354 in./min. + Σ(finishing 6 surfaces) = 2.10 min.

2,000 Units = [4,200 min. + (1,000 min. setup time)] = 87 hr.

Cost @ $15/hour = $1,305

Tooling Cost = $250

Total Machining Cost = $1,555/2000 units/week

Salvage Value

$C_s = [3(\$1,200) + 3(\$1,047) + 3(\$237)] = \$7,452$

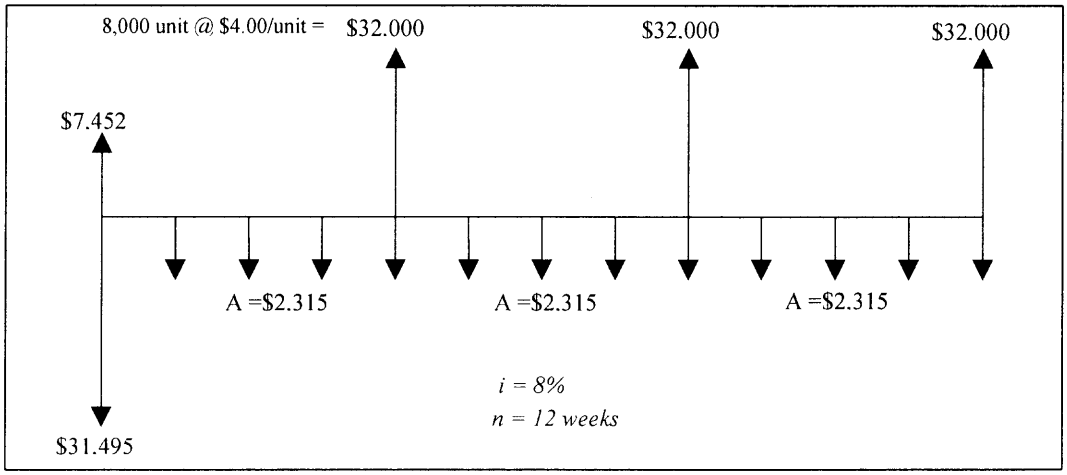

$$P.V._{cost} = \$31,495 + \$2,315\left[\frac{(1+0.154)^{12}-1}{0.154(1+0.154)^{12}}\right] = \$43,832$$

$$P.V._{benefit} = \$7,452 + \$32,000(1+0.67)^{-1} + \$32,000(1+0.67)^{-2} + \$32,000(1+0.67)^{-3} = \$44,956$$

NPV = $1,370

Payback Period

[($31,495 - $7,452)/($32,000 – $9,260)] = 1.06 months

The payback period is 1.06 months at a $1,370 net present value.

Overall Results

The research has been conducted to derive optimal operating parameters for high speed milling machines equipped with PMBDCLM feed drives. Based on the research, each of the proposed objectives are fulfilled. The finite element analysis illustrates that variant effects such as air-gap size, input voltage, and applied cutting force has a significant effect on PMBDCLM performance. Cutting force variants provide a method of determining PMBDCLM feedrate where slider velocity, both in freely moving and applied cutting force models, supply operating parameter levels for DOE. Based on the DOE, experimental results show that PMBDCLM CNC feed drives improve overall tolerance and surface finish performance, and cost. The DOE provides the performance and significant databases used in the developed heuristic. The developed heuristic provides a new method of applying a set of decisions through a knowledge base to provide a set of operating parameters which meet user specified tolerance and surface finish requirements for given surfaces. Finally, retrofitting a conventional CNC milling machine with PMBDCLM feed drives will provide not only performance benefits, but also cost benefits in terms of reduced maintenance, power requirements, and conforming parts.

CD Appendix

All force, tolerance, surface finish, and FEA data is enclosed on the CD Appendix. The CD appendix menu is activated by opening the "appendix" directory and by clicking on the "default.htm" file.

CHAPTER 6

CONCLUSIONS AND RECOMMENDATIONS

The research has been conducted to provide a general heuristic for deriving operating parameters on high speed milling machines equipped with PMBDCLM feed drives. Based on the research, each of the proposed research objectives has been fulfilled.

1. The proposed model illustrated that in order to achieve the research objectives, systematic procedures, provided in the proposed heuristic, were followed as such:
   a) By applying the FEA, slider velocity was determined to provide feedrate levels for DOE.
   b) From DOE, a knowledge base and two sets of rules have been developed, as listed in the research.

   By following the developed general heuristic, knowledge for all machine configurations, material and tool types, and coolant status can be generated.
2. An actual PMBDCLM design has been analyzed based on design and experimentation. Finite element models based on design show the following:
   a) By incorporating air-gap variants, the decrease in air-gap size, from high to low provides an increase in magnet array temperature and generated force of 7.13% and 17%, respectively.
   b) By incorporating applied voltage variants, the increase in input voltage, from low to high provides an increase in magnet-array and air-gap temperature, flux

density, electric field strength, slider velocity and acceleration by 12.5%, 86.3%, 30.3%, 40.8%, and 40.9%, respectively.

c) By incorporating applied force variants, the increase in applied force, from low to high provides an increase in magnet-array and air-gap temperature, flux density, and electric field strength by 13.2%, 10.8%, 25.8%, and 13.9%, respectively.

3. Based on experimentation using 7075-T6 aluminum and a two-flute solid carbide tool, the PMBDCLM feed drive showed significant improvement in some tolerance and surface finish performance indices. These included:

a) At a high depth of cut, position, runout, circularity, and cylindricity tolerance is improved by 44%, 42.7%, 31.4%, and 69%, respectively for contouring and position and straightness tolerance, spacing, and wavelength is improved by 64.3%, 59.1%, 11.8%, 10%, and 37%, respectively for straight/taper milling.

b) At a central depth of cut, position, runout, circularity and cylindricity tolerance, and kurtosis is improved by 24.6%, 50.6%, 52%, 66.5%, and 21.2%, respectively for contouring and position, flatness, straightness, angularity and parallelism tolerance, and peak-to-valley height is improved by 61.3%, 55.4%, 35.5%, 40.1%, 19.4%, and 23.3%, respectively for straight/taper milling.

c) At a low depth of cut, position, runout, circularity and cylindricity tolerance, and kurtosis, skewness, spacing, wavelength, and peak-to-valley height is improved by 33.1%, 40.8%, 52%, 66.8%, 83.8%, 34.1%, 17.7%, 8%, 24%, and 23.5%, respectively for contouring and position tolerance, skewness, wavelength, and peak-to-valley height is improved by 85.2%, 35.4%, 22.8%, 40.1%, and 27.3%, respectively for straight/taper milling.

4. From results of DOE, knowledge is extracted providing databases, empirical relationships, and rules. The proposed optimal operating parameters heuristic has been developed to utilize this knowledge to determine optimal operating parameters for any machine configuration, material and tool type, and coolant status.

   A case study has been used to demonstrate the application of the developed heuristic. Based on alternative solutions, the overall performance was summarized in terms of high tolerance, high surface finish, and a higher material removal rate.

5. Savings in terms of material removal rate, maintenance, rework, and power by 12%, 53%, 50%, and 7.7%, respectively were illustrated both in terms of machine components and cost. The developed cost model accounts for these savings, as demonstrated in the research.

Recommendations

This dissertation provides a foundation for which future research can grow. Although the proposed heuristic has developed a method for optimal operating parameter selection on PMBDCLM equipped high speed vertical CNC machines, further studies are needed. Listed are the areas of interest that that emerged during the course of this research.

- Modify existing finite element models by adding new boundary conditions based on experimental results.
- Conduct new experiments for complex/contour surfaces.
- Develop new performance indices for tolerance and surface finish.
- Develop an expert system to incorporate additional knowledge.
- Validate existing models by conducting DOE for alternative operating parameters.
- Implement PMBDCLM retrofit components to an existing machine.

REFERENCES

Abdou G., Sherif, S. 1991. "Theoretical and Experimental Design of LIM in Automated Manufacturing Systems". *IEEE Transactions on Industry Applications*. 72: 286-293.

Akmease R., Eastham, J.F. 1992. "Design of Permanent Magnet Flat Linear Motors for Standstill Applications". *IEEE Transactions on Magnetics*. 28: 3042-3044.

Alter, David., Tsao, Tsu-Chin. 1994. "Stability of Turning Processes with Actively Controlled Linear Motor Feed Drives". *Journal of Engineering for Industry – Transactions of the ASME*. 116: 298-307.

Basak, Amitava. 1996. *Permanent Magnet DC Linear Motors.* Oxford Science Publications, Clarendon Press.

Basak, A., Anayi, F.J. 1995. "A DC Linear Motor with a Square Armature". *IEEE Transactions on Energy Conversion*. 10: 462-468.

Basak, A.; Anayi F.J. 1992 "Construction of a NdFeB Magnet Brushless DC Linear Motor and its Static and Dynamic Characteristics". *Journal of Magnetism and Magnetic Materials*. 112: 426-428.

Basak, A.;Demirci, R. 1996. "Real-Time Model Reference Adaptive (MRAC) Velocity Controller for a PMDC Linear Motor". *Proceedings of the Universities Power Engineering Conference Proceedings of the 1996 31st Universities Power Engineering Conference*. Part 1 (of 3).

Basak, A., Filho, F., Nakata, T. and N. Takahahi. 1997. "Three Dimensional Computation of Force in a Novel Brushless DC Linear Motor". *IEEE Transactions on Magnetics*. 33: 69-71.

Basak. A; Shirkoohi, 1990. G.H. "Computation of Magnetic Field in D.C. Brushless Linear Motors Built with NdFeB Magnets". *IEEE Transactions of Magnetics*. 26: 948-951.

Casadei, D., Cecati, C., Grandi, G., and G. Serra. 1994. "Adaptive Control of a Slotless PM Linear DC Actuator". *IEEE Transactions*. 2086-2090.

Dapeng, Fan; Ziqiang, Yin. 1997. "Precision Grinding of the High Speed Bearing's Non Circular Inner Race". *Gaojisu Tongxin/High Technology Letters*, Institute of Science and Technology Information. Beijing, China.

REFERENCES
(Continued)

EMRC NISA Users Manual, Version 93.0. Volume 1 and 2. Engineering Mechanics Research Corporation. Troy, MI.

Evers, W. Henneberger, G., Wunderlich, H., and A. Seelig. 1998. "A Linear Homopolar Motor for a Transportation System". *The Second International Symposium on Linear Drives for Industry Applications*. 46-49.

Filho, Flores; Basak A. 1997. "Improvement of the Force Produced by a Homopolar Brushless DC Linear Motor". *Proceedings of the 1997 IEEE International Electric Machines and Drives Conference*. May 18-21, Milwaukee WI. Pp. MC1 12.1-12.3.

Groning, I., Henneberger, G., Wunderlich, H. and A. Seelig. 1998. "Optimization of a Magnetic Levitation System for a Linear Drive". *The Second International Symposium on Linear Drives for Industry Applications*. 102-105.

Hanaoka, Motoyasu; Miyaji, Hiroshi; Kano, Yoshio; and Shinya Hasebe. 1992. "Analysis of Moving Magnet Linear DC Motor with Two Straight Stators". *Electrical Engineering in Japan*. 112: 708-713.

Hur, J.; Yoon, Sang-Baeck; and Dong-Seok Hyun. 1997. "Fast and Precise Position Control of Linear DC Motor for Carrier using Seek Control and Neural Network". *IEEE International Electric Machines and Drives Conference*. 25-27.

In-Soung jung, Sng-Baeck Yoon, Jang-Ho Shim, and Dong-Seok Hyun. 1997. "Analysis of Forces in a Short Primary Type and a Short Secondary Type Permanent Magnet Linear Synchronous Motor". *IEEE International Electric Machines and Drives Conference Record Proceedings*. MCI-8.1-8.3.

Kwon, B., Woo, K, Rhyu, S., and S. Park. 1998. Analysis of Direct Thrust Control in Permanent Magnet Type Linear Synchronous Motor by FEM". *The Second International Symposium on Linear Drives for Industry Applications*. 404-407.

Laithwaite, E.R. 1995. "Adapting a Linear Induction Motor for the Acceleration of Large Masses to High Velocities". *IEE Proceedings of Electric and Power Applications*. 142: 262-268.

Lequesne, Bruno. 1996. "Permanent Magnet Linear Motors for Short Strokes". *IEEE Transactions on Industry Applications*. 32: 161-168.

REFERENCES
(Continued)

Moghani, J., Eastham, J. 1996. "The Dynamic Response of a Linear Brushless D.C. Motor". *PEDES Proceedings of the 1996 International Conference on Power Electronics, Drives, and Energy Systems for Industrial Growth.* 1: 599-602.

Muraguchi, Y., Karita, M., Nakagawa, H., Shinya, T., and M. Maeda. 1998. "Method of Measuring Dynamic Characteristics for Linear Servo Motor and Comparison of their Performance". *The Second International Symposium on Linear Drives for Industry Applications.* 204-207.

Sato, Yasuo; Iga, Motoichi; and Hajime Yamada. 1992. "Single-sided Linear Motor Controlling the Surface Shape of Molten Tin". *IEEE Transactions on Magnetics.* 28: 3333-3335.

Shirkoohi, G.H.; Basak, A. 1990. "Three Dimensional Computation of Field in a NdFeB Magnet DC Linear Stepping Motor". *The International Journal for Computation and Mathematics in Electrical and Electronic Engineering.* 9: Supplement A, 163-166.

Trumper, David; Kim, Wong-Jong; and Mark Williams. 1996. "Design and Analysis Framework for Linear Permanent Magnet Machines". *IEEE Transactions on Industry Applications.* 32: 371-379.

Wang R. and Gierras J.F. 1998. "Performance Calculations for a PM Hybrid Linear Stepping Motor by the Finite Element and Reluctance Network Approach". *The Second International Symposium on Linear Drives for Industry Applications.* 400-403.